รายงานวิจัยฉบับสมบูรณ์

แบบจำลองทางคณิตศาสตร์สำหรับคำนวณการเคลื่อนที่ของตะกอนและการเปลี่ยนแปลงของพื้นท้องทะเลภายใต้การกระทำของคลื่นแบบไม่สม่ำเสมอ (ส่วนที่ 1 แบบจำลองคลื่น)

โดย นายวิญญู รัตนปิติกรณ์

กรกฎาคม 2551

สัญญาเลขที่ RMU4880020

รายงานวิจัยฉบับสมบูรณ์

แบบจำลองทางคณิตศาสตร์สำหรับคำนวณการเคลื่อนที่ของตะกอนและการเปลี่ยนแปลงของพื้นท้องทะเลภายใต้การกระทำของคลื่นแบบไม่สม่ำเสมอ (ส่วนที่ 1 แบบจำลองคลื่น)

นายวิญญู รัตนปิติกรณ์
สาขาวิชาวิศวกรรมโยธา สถาบันเทคโนโลยีนานาชาติสิรินธร
มหาวิทยาลัยธรรมศาสตร์

สนับสนุนโดยสำนักงานคณะกรรมการการอุดมศึกษา
และสำนักงานกองทุนสนับสนุนการวิจัย

(ความเห็นในรายงานนี้เป็นของผู้วิจัย สกอ. และ สกว. ไม่จำเป็นต้องเห็นด้วยเสมอไป)

Acknowledgments

The author is thankful to the Thailand Research Fund and the Commission on Higher Education, Ministry of Education for providing the financial support of this study.

Sincere appreciation is expressed to the previous researchers for supplying the valuable experimental results to the public, which enabled him to perform this research.

To his wife, for her patience and understanding.

Abstract

The goal of this study is to develop the mathematical model for computing beach deformation under the action of irregular waves. The beach deformation model consists of 5 sub-models i.e., wave model, undertow model, sediment concentration model, sediment transport model, and beach deformation model. Due to the time constrain, the present study concentrates only on the wave models for computing the representative wave heights, i.e. root mean square wave height (H_{rms}), significant wave height ($H_{1/3}$), and maximum wave height ($H_{\max}$). Common methods to model the representative wave heights transformation may be classified into four main approaches, i.e. representative wave approach, probabilistic approach, spectral approach, and conversion approach. For computing beach deformation, the wave model should be kept as simple as possible because of the frequent updating of wave field to account for the change of bottom profiles. The present study focuses on the representative wave approach and the conversion approach, as these appear to be the simple methods.

The representative wave approach relies on the macroscopic features of breaking waves and predicts only the transformation of representative wave heights. Many researchers have pointed out that the use of representative wave approach can give erroneous results in the computation of representative wave heights transformation. This study is carried out to investigate the possibility of simulating representative wave height transformation by using representative wave approach. A large amount and wide range of experimental conditions, covering small-scale, large-scale, and field experimental conditions, are used to calibrate and examine the model. The transformations of representative wave heights are computed from the energy flux conservation law. Various energy dissipation models of regular wave breaking are directly applied to the irregular wave model and test their applicability. Surprisingly, it is found that by using an appropriate energy dissipation model with new coefficients, the representative wave approach can be used to compute the representative wave heights with very good accuracy.

The conversion approach is used to convert the representative wave heights from one to another through the known relationships. The root mean square wave height (H_{rms}) is usually used as a reference wave height of the conversion because it is the output of many wave models. The well-known relationships are derived based on the Rayleigh distribution of wave heights. In shallow water, it has been pointed out by many researchers that the wave height distribution deviates from the Rayleigh distribution. However, it is not clear whether this deviation can lead to significant errors on the estimation of representative wave heights or not. Experimental data from small-scale, large-scale, and field experiments were used to examine the errors of the relationships derived from the Rayleigh distribution on estimating representative wave heights. The examination indicates that if H_{rms} is given, the relationships give overall very good estimations on $H_{1/3}$ but fair estimation on $H_{\max}$. The effect of wave breaking was empirically incorporated into the relationships. The new relationships give better estimation than the relationships derived from the Rayleigh distribution.

บทคัดย่อ

วัตถุประสงค์หลักของโครงการคือ พัฒนาแบบจำลองทางคณิตศาสตร์สำหรับคำนวณการเปลี่ยนแปลงของพื้นท้องทะเลภายใต้การกระทำของคลื่นแบบไม่สม่ำเสมอ แบบจำลองการเปลี่ยนแปลงของพื้นท้องทะเลนี้ ประกอบขึ้นจากแบบจำลองแบบจำลองย่อย ห้าแบบจำลองคือ wave model, undertow model, sediment concentration model, sediment transport model และ beach deformation model แต่เนื่องจาก แบบจำลองการเปลี่ยนแปลงของพื้นท้องทะเล ครอบคลุมเนื้อหาค่อนข้างกว้าง และระยะเวลาของโครงการนี้ค่อนข้างจำกัด ดังนั้นรายงานนี้จะเน้นเฉพาะส่วนของ wave model สำหรับคำนวณการเปลี่ยนแปลงความสูงคลื่นตัวแทน ได้แก่ root mean square wave height (H_{rms}), significant wave height ($H_{1/3}$), และ maximum wave height ($H_{\max}$) ซึ่งเป็นตัวแปรสำคัญ ที่ในการคำนวณแบบจำลองอื่นๆ วิธีการจำลองการเปลี่ยนแปลงความสูงคลื่นตัวแทน สามารถแบ่งได้เป็น สี่วิธีหลักๆ คือ representative wave approach, probabilistic approach, spectral approach, และ conversion approach ในการคำนวณการเปลี่ยนแปลงของพื้นท้องทะเล แบบจำลองคลื่นควรจะเป็นแบบจำลองที่ง่ายและคำนวณได้เร็ว เพราะจะต้องมีการคำนวณหลายครั้งมาก เนื่องจากพื้นท้องทะเลจะเปลี่ยนแปลงตลอดเวลา การศึกษาครั้งนี้จึงมุ่งเน้นไปที่ representative wave approach และ conversion approach เนื่องจากเป็นวิธีที่ง่ายและคำนวณได้เร็ว เหมาะสมสำหรับการใช้ในการคำนวณการเปลี่ยนแปลงของพื้นท้องทะเล

วิธี representative wave approach จะสนใจที่ภาพรวมของคลื่นแตกและคำนวณเฉพาะการเปลี่ยนแปลงของคลื่นตัวแทน นักวิจัยหลายท่านเชื่อว่าวิธีนี้ให้ผลการคำนวณที่ไม่ดีนัก ดังนั้นการศึกษานี้ทำขึ้นเพื่อทดสอบหาความเป็นไปได้ที่จะใช้วิธีนี้ในการคำนวณการเปลี่ยนแปลงของคลื่นตัวแทน โดยทดลองใช้แบบจำลองการสูญเสียพลังงานหลายๆแบบ จากการศึกษาพบว่าวิธี representative wave approach จะให้ผลการคำนวณที่ค่อนข้างดีมากเมื่อใช้แบบจำลองการสูญเสียพลังงานที่เหมาะสม

วิธี conversion approach เป็นการแปลงค่าจากคลื่นตัวแทนหนึ่ง ไปเป็นอีกค่าหนึ่งโดยใช้สมการความสัมพันธ์ระหว่างคลื่นตัวแทน สมการความสัมพันธ์ที่ใช้กันได้มาจากการสมมุติว่าความสูงคลื่นมีการกระจายแบบ Rayleigh แต่มีนักวิจัยหลายท่านชี้ว่า การกระจายของความสูงคลื่นในช่วงน้ำตื้นค่อนข้างที่จะแตกต่างจากการกระจายแบบ Rayleigh ดังนั้นจึงไม่เป็นที่แน่ชัดว่าความสัมพันธ์ระหว่างคลื่นตัวแทนโดยสมมุติว่าความสูงคลื่นมีการกระจายแบบ Rayleigh จะสามารถใช้ได้หรือไม่ในช่วงน้ำตื้น การศึกษานี้พบว่าสมการความสัมพันธ์นี้ ใช้ได้ดีมากในการคำนวณหา $H_{1/3}$ แต่ใช้ไม่ดีในการคำนวณหา $H_{\max}$ ในการศึกษานี้ได้มีการเพิ่มตัวแปรซึ่งแสดงผลกระทบของคลื่นแตกเข้าไปในสมการความสัมพันธ์ ทำให้สมการความสัมพันธ์ตัวใหม่ให้ผลการคำนวณที่ดีขึ้น

Executive Summary

Project Code: RMU4880020
Project Title: Mathematical Modeling for Cross Shore Sediment Transport and Beach Deformation under Irregular Waves
Investigator: Mr. Winyu Rattanapitikon, D.Eng., Assoc. Prof., Civil Engineering Program, Sirindhorn International Institute of Technology, Thammasat University,
E-mail Address: winyu@siit.tu.ac.th
Project Period: 3 years (29 Jul. 2005 – 28 Jul. 2008)

Objectives: The main objective of this study is to develop a mathematical model for computing beach deformation under the action of regular and irregular waves. The beach deformation model consists of 5 sub-models i.e., wave model, undertow model, sediment concentration model, sediment transport model, and beach deformation model. Due to the time constrain, the present report concentrates only on the wave model for computing the representative wave heights, which are the essential required factors for the study of beach deformation and the design of coastal structures.

Methodology: The wave models are developed based on the analysis of the related existing models. To make the models reliable, wide range and large amount of published experimental results are used to calibrate and verify the models.

Results: Reliable mathematical models for computing the representative wave heights, i.e. root mean square wave height (H_{rms}), significant wave height ($H_{1/3}$), and maximum wave height ($H_{\max}$). The outputs of this project are as follows:

International journals:

1) Rattanapitikon, W. and Shibayama, T. (2006). Breaking wave formulas for breaking depth and orbital to phase velocity ratio, Coastal Engineering Journal, 48, 4, 395-416.
2) Rattanapitikon, W. (2007). Calibration and modification of energy dissipation models for irregular waves breaking, Ocean Engineering, 34, 1592-1601.
3) Rattanapitikon, W. and Shibayama, T. (2007). Estimation of shallow water representative wave heights, Coastal Engineering Journal, 49, 3, 291-310.
4) Rattanapitikon, W. (2008). Transformation of significant wave height using representative wave approach, Ocean Engineering, 35, 1259-1270.
5) Rattanapitikon, W. and Sawanggun, S. (2008). Energy dissipation model for a parametric wave approach based on laboratory and field experiments, Songklanakarin J. of Science and Technology (accepted).

International conference:

1) Rattanapitikon, W. and Sawanggun, S. (2007). Modification of a parametric model, The 4th International Conference on Asian and Pacific Coasts [CD-ROM], September 21-24, Nanjing, China, pp. 346-357.

Discussion Conclusion: Based on a wide range and large amount of published experimental results, reliable models are developed for computing breaking wave height, and transformation of representative wave heights. The accuracy of the present models and some existing models are also compared. The comparisons show that the present models give better agreement than those of existing models.

CONTENTS

Acknowledgments ii
Abstract
iii
Executive Summary v
List of Symbols
viii
List of Figures x
List of Tables
xi

1 INTRODUCTION 1
1.1 General 1
1.2 Scope and Objective of Study 4
1.3 Organization of Report 4

2 BREAKING WAVE FORMULAS 5
2.1 Introduction 5
2.2 Breaker Height Formulas 7
2.2.1 Examination of existing formulas 9
2.3 Breaker Depth 13
2.3.1 Examination of existing formulas 13
2.3.2 Formula development 15
2.4 Orbital to Phase Velocity Ratio 19
2.4.1 Examination of existing formulas 19
2.4.2 Formula modification 21
2.4.3 Formula development 22

3 TRANSFORMATION OF REPRESENTATIVE WAVE HEIGHTS USING REPRESENTATIVE WAVE APPROACH 28
3.1 Introduction 28
3.2 Transformation of Root Mean Square Wave Heights 29
3.2.1 Collected laboratory data 30
3.2.2 Existing energy dissipation models 31
3.2.3 Examination of existing models 35
3.2.4 Model calibration and comparison 36
3.2.5 Model modification 37
3.2.6 Model development 41
3.3 Transformation of Significant Wave Heights 50
3.3.1 Collected laboratory data 51
3.3.2 Regular wave models 54
3.3.3 Irregular wave model 55
3.3.4 Model modification 61
3.4 Transformation of Maximum Wave Heights 68
3.4.1 Regular wave models 69
3.4.2 Highest wave representation approach 70

4 TRANSFORMATION OF REPRESENTATIVE WAVE HEIGHTS USING CONVERSION APPROACH 75
4.1 Introduction 75
4.2 Estimation of Shallow Water Representative Wave Heights 75
4.2.1 Representative wave heights derived from the Rayleigh distribution 78
4.2.2 Formula development 82

5 CONCLUSIONS 91

REFERENCES 94

OUTPUTS 100

APPENDIX: PAPER REPRINTS 101
A.1 Breaking wave formulas for breaking depth and orbital to phase velocity ratio 101
A.2 Calibration and modification of energy dissipation models for irregular waves breaking 124
A.3 Estimation of shallow water representative wave heights 135
A.4 Verification of significant wave representation approach 156
A.5 Energy dissipation model for a parametric wave approach based on laboratory and field experiment 169
A.6 Modification of a parametric model 179

List of Symbols

c phase velocity
c_g group velocity
c_o deepwater phase velocity
D_B rate of energy dissipation due wave breaking
E wave energy density
E_s stable energy density
ER_g root mean square relative error of the data group
ER_{avg} average root mean square relative error
f_n function
g acceleration due to gravity
H wave height
H_b wave height at breaking point
H_b' assumed breaker height
H_i incident wave height
H_o deepwater wave height
$\overline{H}$ mean wave height
H_{rms} root mean square wave height
$H_{1/3}$ highest one third wave height
H_s significant wave height
$H_{1/10}$ highest one tenth wave height
$H_{\max}$ maximum wave height
$\frac{H_o}{L_o}$ deepwater wave steepness
h water depth
h_b water depth at breaking
K_n coefficient ($n = 1, 2, 3, \ldots$)
k wave number
k_b wave number at breaking
L wavelength
L_o deepwater wavelength
L_b wavelength at breaking
m local bottom slope
pdf probability density function
Q_b fraction of breaking waves
rms root mean square

S_n bottom-slope-effect coefficient
T wave period
T_p peak spectral wave period
$\hat{u}_b$ orbital velocity at the breaking
V variable
x distance in cross-shore direction
θ mean wave angle
ρ water density
Γ stable wave factor
β_n proportionality constant

List of Figures

Figure		Page
1.1	Basic structure of the beach deformation model	1
2.1	Relationship between h_b/H_o and H_o/L_o	16
2.2	Relationship between slope effect coefficient S_1 and bottom slope m when $K_1 = -0.16$ (laboratory data from 26 sources shown in Table 1 excluding the data that $H_o/L_o > 0.1$). Solid line is the computed S_1 from Eq. (2.16).	17
2.3	The plots of Eq. (2.17) for 4 bottom slopes (m = 0.01, m = 0.05, m = 0.10, and m = 0.20).	18
2.4	Relationship between h_b/L_o and H_o/L_o (laboratory data from 26 sources shown in Table 2.1)	19
2.5	Relationships between $\hat{u}_b/c_b$ and (a) h_b/L_b, (b) h_b/L_o, (c) H_o/L_o for the case of breaking wave on step beach (laboratory data from Hattori and Aono, 1985; Horikawa and Kuo, 1966; and Nagayama, 1983)	25
2.6	Relationships between H_b'/L_o and (a) h_b/L_b, (b) h_b/L_o, (c) H_o/L_o for the case of breaking wave on step beach (laboratory data from Hattori and Aono, 1985; Horikawa and Kuo, 1966; and Nagayama, 1983). Solid line in figure (c) is the fitted line	26
2.7	Relationship between slope effect coefficient S_2 and bottom slope m when $K_{12} = 0.83$ (laboratory data from 26 sources shown in Table 2.1). Solid line is the computed S_2 from Eq. (2.32)	27
3.1	Relationship between measured Q_b versus H_{rms}/H_b by using Eqs. (3.35) and (3.37) for computing D_s and H_b	45
3.2	Relationship between f and H_{sb}/H_s (measured data from Dette et al., 1998)	62
3.3	Comparison between measured and computed significant wave height by using the model MD7 (measured data from Table 3.18)	64
3.4	Examples of measured and computed significant wave height transformation by using the model MD7 (measured data from small-scale experiments)	65
3.5	Examples of measured and computed significant wave height transformation by using the model MD7 (measured data from large-scale experiments)	66
4.1	Relationships between H_{rms}/h versus a) β_m, b) $\beta_{1/3}$, c) $\beta_{1/10}$, and d) $\beta_{\max}$	84
4.2	Relationships between H_{rms}/H_{tr} versus a) β_m, b) $\beta_{1/3}$, c) $\beta_{1/10}$, and d) $\beta_{\max}$	85

4.3 Relationships between H_{rms}/H_b versus a) β_m, b) $\beta_{1/3}$, c) $\beta_{1/10}$, and d) $\beta_{\max}$ 86

List of Tables

Table		Page
2.1	Summary of collected experimental data	6
2.2	Existing breaker height formulas	8
2.3	The root mean square relative error (ER) of each formula comparing with small-scale experimental data (measured data from 24 sources shown in Table 2.1)	11
2.4	The root mean square relative error (ER) of each formula comparing with large-scale experimental data (measured data from 2 sources shown in Table 2.1)	12
2.5	The root mean square relative error (ER_g) of the formulas for computing the breaker depth (laboratory data from 26 sources shown in Table 2.1)	15
2.6	The root mean square relative error (ER_g) of the formulas for computing $\hat{u}_b$ and H_b' (laboratory data from 26 sources shown in Table 2.1)	21
3.1	Summary of collected experimental data	31
3.2	The errors ER_g and ER_{avg} of the existing models for three groups of experiment scale (using the default coefficients)	36
3.3	Default and calibrated coefficients of the existing models	36
3.4	The errors ER_g and ER_{avg} of the existing models for three groups of experiment scale (using the calibrated coefficients)	37
3.5	Calibrated coefficients and average errors ER_{avg} of all 42 possible dissipation models	38
3.6	The errors ER_g and ER_{avg} of the six suitable models for three groups of experiment scale	41
3.7	The errors ER_g of the six suitable models for each source of data	41
3.8	Calibrated constants (K_1 to K_4) and correlation coefficients (R^2) of Q_b formula [Eq. (3.55)] for difference D_s and H_b formulas	46
3.9	Errors (ER) of present D_B models [Eq. (3.56)] with different D_s and H_b formulas for 3 experiment-scales and all collected data (using the calibrated constants from Table 3.8 and measured data from Table 3.1)	48
3.10	Errors (ER) of existing D_B models for 3 experiment-scales and all collected data (measured data from Table 3.1)	49
3.11	Summary of collected experimental data used to calibrate and verify the regular wave models	51
3.12	Summary of collected experimental data used to calibrate and verify the irregular wave models	52
3.13	The errors (ER_g and ER_{avg}) of the models MD1-MD6 (using the coefficients of regular waves) for 2 groups of experiment-scales	58

(measured data from Table 3.12)
3.14 The errors (ER_g and ER_{avg}) of the models MD1-MD6 (using the calibrated coefficients) and the modified model (MD7) for 2 groups of experiment-scales (measured data from Table 3.12) 59
3.15 The errors (ER_g and ER_{avg}) of the models MD5-MD6 (using the calibrated coefficients) and the modified model (MD7) for 36 groups of test series 60
3.16 The errors (ER_g and ER_{avg}) of the six existing regular wave and the modified model (MD8) for 2 groups of experiment-scales (measured data from Table 3.11) 67
3.17 Summary of collected experimental data used to calibrate and verify the irregular wave models 72
3.18 The errors (ER_g and ER_{avg}) of the models MD1-MD7 (using the coefficients of regular waves) for 2 groups of experiment-scales (measured data from Table 3.17) 73
3.19 The errors (ER_g and ER_{avg}) of the models MD1-MD7 (using the calibrated coefficients) for 2 groups of experiment-scales (measured data from Table 3.17) 73
4.1 Summary of collected experimental data used to verify the formulas 77
4.2 The errors (ER_g and ER_{avg}) of Rayleigh distribution (Eqs. (4.3) to (4.6)) on the estimation of $\overline{H}$, $H_{1/3}$, $H_{1/10}$, and $H_{\max}$ for three groups of experiment scale 81
4.3 The errors (ER_g) of Rayleigh distribution (Eqs. (4.3) to (4.6)) on the estimation of $\overline{H}$, $H_{1/3}$, $H_{1/10}$, and $H_{\max}$ for all groups of major test 81
4.4 Best fitted constants K_1 and K_2 for the coefficients β_m, $\beta_{1/3}$, $\beta_{1/10}$ and $\beta_{\max}$ 88
4.5 The errors (ER_g and ER_{avg}) of present formulas (Eqs. (4.19) to (4.21)) on the estimation of $\overline{H}$, $H_{1/3}$, $H_{1/10}$, and $H_{\max}$ for three groups of experiment scale 89
4.6 The errors (ER_g) of present formulas (Eq. (4.19) to (4.21)) on the estimation of $\overline{H}$, $H_{1/3}$, $H_{1/10}$, and $H_{\max}$ for all groups of major test 89

I. INTRODUCTION

1.1. General

In recent years, the coastal region has become an area of intense human activity for industry and recreation. It is also an important area for tsunami and storm surge protection. The need for reliable predictions of beach response to the changes in hydrodynamic conditions, or to the construction of man-made structures, is increasing due to an increase of human activities on the coast.

Figure 1.1 shows the typical structure of beach deformation model. The calculation of beach deformation is composed of six main parts, i.e., input data, wave, undertow velocity, sediment concentration, sediment transport, and profile change. The wave model is used to compute wave height transformation across beach. From the computed wave height, undertow velocity, sediment concentration and sediment transport rate can be computed. Then new beach profile can be computed from the mass conservation equation. The new beach profile will feed-back into the wave model and causes wave height changes. This yields the loop of dynamic beach deformation. The present study concentrates only on the wave models for computing the transformation of representative wave heights, which are the essential required factors for the study of beach deformation and the design of coastal structures.

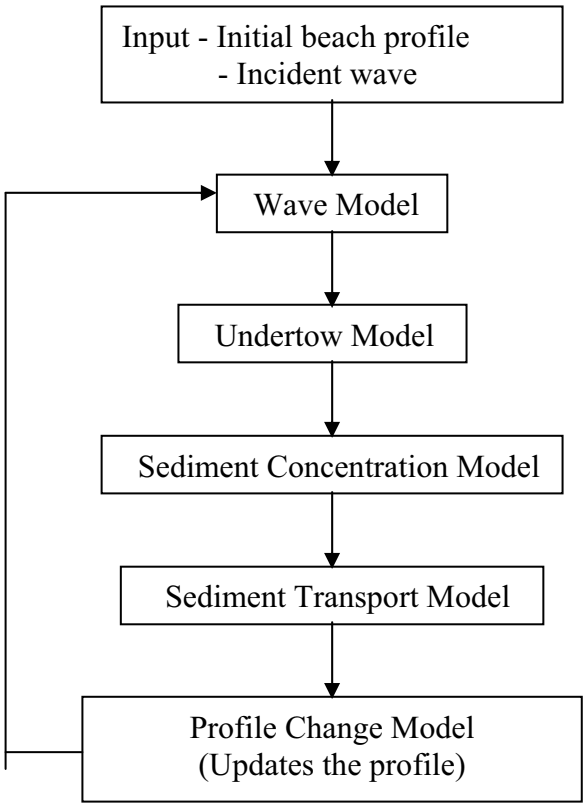

Figure 1.1: Basic structure of the beach deformation model.

The representative wave heights [e.g. root mean square wave height (H_{rms}), significant wave height ($H_{1/3}$), and maximum wave height ($H_{\max}$)] are the essential required factors for the study of beach deformation and the design of coastal structures. The wave heights are usually available in deepwater but not available at the depths required in shallow water. The wave heights in shallow water can be determined from wave models. Common methods to model the representative wave heights transformation may be classified into four main approaches, i.e. representative wave approach, probabilistic approach, spectral approach, and conversion approach.

The representative wave approach is the simplest approach to compute the representative wave heights transformation. It seeks to reduce the computational effort by describing the energy dissipation rate in term of time-averaged parameter. As this approach relies on the macroscopic features of breaking waves and predicts only the transformation of representative wave heights, it is suitable when a detail wave height distribution is not needed. The works on this approach can be separated into three classes based on the assumption about the *pdf* of wave height in the surf zone. The first class assumes that the Rayleigh *pdf* (or modified Rayleigh *pdf*) is valid in the surf zone. The average rate of energy dissipation is described by integrating the product of energy dissipation of a single broken wave and the probability of occurrence of breaking waves. Various semi-analytical models have been developed based on this class (e.g. Battjes and Janssen, 1978; Thornton and Guza, 1983; Baldock et al., 1998; and Rattanapitikon and Shibayama, 1998). The significant differences of those models are the formulation of energy dissipation of a single broken wave and the assumption on probability of occurrence of breaking waves. The weak point of this class is the assumption on Rayleigh *pdf* in the surf zone, because this assumption is not supported by some experiments (Dally, 1990). The second class was proposed, by Larson (1995), to overcome the weakness of the first class. Larson (1995) proposed a semi-analytic model without making any assumptions about the *pdf* in the surf zone. The average rate of energy dissipation is described by adding up the dissipation of each broken wave component and dividing by the total number of waves (including broken and unbroken waves). The semi-analytic model reproduces macroscopic features of wave height and energy flux transformation, including breaking and reforming, in agreement with the individual wave approach that involves transformation of many individual waves. The third class does not assume any *pdf* of wave height. The formulas of regular waves have been directly applied to irregular waves by using the representative waves. Since the highest wave in irregular wave train tends to break at the greatest distance from shore, the initiation of surf zone of irregular waves tend to occur at greater distance from shore than that of regular waves. Therefore, the use of regular wave model may give considerable errors in the surf zone. To overcome this problem, the coefficient of breaker height formula for regular waves may have to be reduced when applying to model irregular waves.

Probabilistic (or individual wave) approach considers the propagation of individual waves in the time domain. The incident individual waves may be determined from the irregular wave records or from probability density function (*pdf*) of wave height. These individual waves are then propagated shoreward independently using an appropriate regular wave model, assuming no wave-to-wave interaction. A new *pdf* at the required location can be constructed from the simulation results of all individual waves. This method is particularly useful if a detailed wave height distribution is required. However, because of the time-consumed, this approach may not be well suited to incorporate into beach deformation model. Over the past few decades, many research works have been

performed in this approach (e.g. Mase and Iwagaki, 1982; Mizuguchi, 1982; Dally, 1990 and 1992; and Kuriyama, 1996). The main difference of those research works is the formulation of regular wave model that used to simulate the propagation of individual wave.

Spectral approach assumes that irregular wave trains consist of numerous wave heights with different frequencies. The distribution of the energy of these wave heights when plotted against the frequency (and direction) is called wave spectrum. In the modeling, the incident spectrum is decomposed into a number of component waves. The propagation of each wave component is computed by using an appropriate regular wave model. The wave spectrum at the required location is obtained by assembling the simulation results from all the wave components by linear superposition. Several models have been proposed based on this approach, differing mainly in the regular wave model used to simulate the propagation of wave components (e.g. Izumiya and Horikawa, 1987; Isobe, 1987; Panchang et al., 1990; and Grassa, 1990). The application of this approach may be restricted when applying in the surf zone, i.e. the component waves in frequency domain do not break, but real waves or individual waves in the time domain do break. To overcome this problem, the energy dissipation model developed based on parametric approach may be incorporated to predict the energy losses due to wave breaking (e.g. Mase and Kirby, 1992; Chawla et al., 1998; and Mase and Kitano, 2000). However, the spectrum approach requires large computation times. It may not be appropriate to incorporate into the beach deformation model.

The conversion approach is used to convert the representative wave heights from one to another through the known relationships. The root mean square wave height (H_{rms}) is usually used as a reference wave height of the conversion because it is the output of many wave models (e.g. the models of Battjes and Janssen, 1978; Thornton and Guza, 1983; Larson, 1995; and Rattanapitikon, 2007). Therefore, the other representative wave heights ($H_{1/3}$, and $H_{\max}$) can be determined from the known relationships between the representative wave heights (e.g. the relationships of Longuet-Higgins, 1952; Battjes and Groenendijk, 2000; and Rattanapitikon and Shibayama, 2007).

For computing beach deformation, the wave model should be kept as simple as possible because of the frequent updating of wave field to account for the change of bottom profiles. The present study focuses on the representative wave approach and the conversion approach, as these appear to be the simple method.

During the last few decades, many theories have been developed and experimental studies, both in laboratory and in the field, have been carried out to draw a clearer picture of wave height transformation. Considerable amount of knowledge on the mechanism of wave has been accumulated so far. However, it has not reached to a satisfactory level. Owing to the complexity of the wave breaking mechanism, full description of the mechanism of the wave breaking has not yet been developed. At the present state of knowledge, clearly any type of numerical model for computing wave breaking has to be based on empirical or semi-empirical formulas calibrated with the experimental results. However, most of the models were developed with the limited experimental conditions. Therefore, their validity is limited according to the range of experimental conditions, which were employed in the calibration. The evidence is that there are so many models exist.

In the past, we could not develop a model based on a large amount of experimental results covering a wide range of test conditions, because they did not exist. However, at present, the experimental results obtained by many researchers have been accumulated and a large amount of experimental results have become available. It is a good time to develop

models based on the large amount and wide range of experimental results. In addition, it is logical to expect that a relatively new models based on more experimental results than the previous ones should be the most reliable ones if the accuracy is in the acceptable range.

1.2. Scope and Objective of Study

The scope and objectives of the present study can be described as follows:

1. This study focuses mainly on the two-dimensional (cross-shore) irregular wave models.
2. Published experimental results are collected for calibration and verification of the models.
3. The main purpose of the present study is to develop simple models for predicting the transformation of representative wave heights (H_{rms} , $H_{1/3}$, and $H_{\max}$) based on a wide range of published experimental results.
4. To confirm the ability of the models, the present models are compared with some existing models.

1.3. Organization of Report

The contents of some parts of this report are substantially the same as a series of papers published in the international conference and journals shown in appendix. The report updates and extends some material in the papers. The present report is written in the following stages:

Chapter 1 is an introduction and gives a statement of problem and objective and scope of study.

Chapter 2 describes the breaking wave formulas

Chapter 3 describes the transformation of representative wave heights using representative wave approach.

Chapter 4 presents the formulas for computing representative wave heights using conversion method.

Chapter 5 gives conclusions of the study.

Appendix presents the paper reprints of this research.

II. BREAKING WAVE FORMULAS

2.1. Introduction

When waves propagate from offshore to the near shore zone, wave profiles become steep. The increase in wave steepness continues until the wave breaks. To analyze the coastal processes, breaking point is one of the most essentially required factors. In the wave model (or beach deformation model), it is necessary to determine the breaking point accurately because the breaking point is the point at which to start including the energy dissipation rate or surface roller into the wave model. Unless the breaking point is accurately predicted (no matter how exact the equations governing wave deformation in and outside the surf zone be), an accurate computation of the wave field or other wave-induced phenomena cannot be expected.

In the wave model, the breaker height is commonly used to indicate the location of wave breaking. Many breaker height formulas have been proposed over the past century (see Rattanapitikon et al., 2003). These formulas can be used to determine the breaking point if wave shoaling is computed accurately. However, it is well known that the linear wave theory gives underestimation of wave height just before the breaking point. Therefore, if the breaker height formula is used together with the linear wave shoaling, the predicted breaking point will shift on shoreward of the real one (Isobe, 1987). This will cause certain error on the computation of wave height transformation and other wave-induced phenomena, e.g. undertow, suspended sediment concentration, sediment transport, and beach deformation.

There are two methods for dealing with the problem of underestimation of the linear wave shoaling. The first method uses nonlinear wave theories for computing wave shoaling (e.g. Stokes, 1847; Dean, 1965; Shuto, 1974; and Isobe, 1985). The second one uses linear wave theory to compute wave shoaling and uses other variables, instead of breaker height, to compute the breaking point (e.g. Watanabe et al., 1984; Isobe, 1987; and Rattanapitikon, 1995). Since the linear wave theory is the most widely used in practice, the present study concentrates on the second method of using other variables to determine the breaking point. The variables that may be used to determine the breaking point are breaker depth, orbital to phase velocity ratio at the breaking point based on linear wave shoaling (hereafter referred to as assumed orbital to phase velocity ratio), and breaker height based on linear wave shoaling (hereafter referred to as assumed breaker height). Various formulas have been proposed to compute these three variables (e.g. Ogawa and Shuto, 1984; Dean and Dalrymple, 1984; Isobe, 1987; and Rattanapitikon, 1995).

The objective of this study is to find out the reliable breaking wave formulas for computing the breaker height, breaker depth, assumed orbital to phase velocity ratio and assumed breaker height. All of the existing breaking wave formulas are empirically determined from the laboratory data. It is known that the validity of empirical formula may be limited according to the range of wave and bottom slope conditions that were employed in calibration or verification. To make an empirical formula reliable, it is necessary to calibrate or verify the formula with a large amount and wide range of laboratory data.

As it is difficult to measure the breaking point of each individual wave in the field, small-scale and large-scale laboratory experiments are the sources of quantitative information for examination of the breaking point formulas. Laboratory data of the breaking point from 26 sources, covering 695 cases, have been collected for the examination of the breaking wave formulas. The data cover a wide range of wave and bottom slope conditions: the deepwater wave steepness (H_o / L_o) ranging between 0.001 and 0.112, and the bottom slope (m) ranging between 0 and 0.38. The data include four

types of beach conditions, i.e. plane beach, barred beach, stepped beach and movable (sandy) beach. All experiments were performed for regular waves in both small-scale and large-scale wave flumes. The experiments of Kajima et al. (1982) and Kraus and Smith (1994) were performed in large-scale wave flumes and other experiments were performed in small-scale wave flumes. The small-scale experiments were conducted under fixed beach conditions whereas the large-scale experiments were carried out under movable beach conditions. A summary of the collected laboratory data is given in Table 2.1.

This chapter is divided into three main sections. The first section is the examination of some existing breaker height formulas. The second section describes the development of breaker depth formulas while the third section describes the development of formulas for computing assumed orbital to phase velocity ratio and assumed breaker height.

Table 2.1. Summary of collected experimental data.

No	Sources	No. of cases	Beach conditions	m **	H_o / L_o
1	Cox et al. (1994)	1	Plane beach	0.03	0.016
2	Galvin (1969)*	19	Plane beach	0.05-0.20	0.001-0.051
3	Hansen and Svendsen (1979)	17	Plane beach	0.03	0.002-0.069
4	Hattori and Aono (1985)	3	stepped beach	0.00	0.006-0.021
5	Horikawa and Kuo (1966)	98 60	Plane beach stepped beach	0.01-0.05 0.00	0.006-0.073 0.007-0.100
6	Hwung et al. (1992)	2	Plane beach	0.07	0.026-0.048
7	Iversen (1952)*	63	Plane beach	0.02-0.10	0.003-0.080
8	Iwagaki et al. (1974)	39	Plane beach	0.03-0.10	0.005-0.074
9	Kajima et al. (1982)***	98	movable beach	0.00-0.29	0.003-0.112
10	Kraus and Smith (1994)***	23	movable beach	0.01-0.13	0.003-0.066
11	Mizuguchi (1980)*	1	Plane beach	0.10	0.045
12	Nadaoka et al. (1982)	12	Plane beach	0.05	0.013-0.080
13	Nagayama (1983)	1 5 6	Plane beach barred beach stepped beach	0.05 0.05 0.00-0.05	0.027 0.025-0.051 0.025-0.055
14	Okayasu et al. (1986)	2	Plane beach	0.05	0.023-0.025
15	Okayasu et al. (1988)	10	Plane beach	0.03-0.05	0.009-0.054
16	Ozaki et al. (1977)	20	Plane beach	0.10	0.005-0.060
17	Saeki and Sasaki (1973)*	2	Plane beach	0.02	0.005-0.039
18	Sato et al. (1988)	3	Plane beach	0.05	0.031-0.050
19	Sato et al. (1989)	2	Plane beach	0.03	0.019-0.036
20	Sato et al. (1990)	7	Plane beach	0.05	0.003-0.073
21	Singamsetti and Wind (1980)*	95	Plane beach	0.03-0.20	0.018-0.079
22	Smith and Kraus (1990)*	5 75	Plane beach barred beach	0.03 0.03-0.38	0.009-0.092 0.008-0.096
23	Stive (1984)	2	Plane beach	0.03	0.010-0.032
24	Ting and Kirby (1994)	2	Plane beach	0.03	0.002-0.020
25	Visser (1982)*	7	Plane beach	0.05-0.10	0.014-0.079
26	Walker (1974)*	15	Plane beach	0.03	0.001-0.037
	Total	695		0.00-0.38	0.001-0.112

* data from Smith and Kraus (1990)
** measured seaward of the breaking point
*** large-scale laboratory

2.2. Breaker Height Formulas

The initiation of breaking wave height (or breaker height) has been a subject of study for a century due to its importance in design of coastal structures, as well as for the prediction of wave height transformation and beach deformation. During the past century, a number of studies and experiments have been carried out to develop the breaker height formulas. Because of the complexity of wave breaking mechanism, it is difficult to describe a breaking wave mechanism by using available wave theories. Hence, most predictions of the breaker heights are based on empirical or semi-empirical formulas calibrated from experimental data.

Possibly because of its importance, many different breaker height formulas have been proposed during the past century. This often causes confusion in the profession in the selection of the formula.

Most of the existing formulas were developed based on empirical approach. The majority of the existing formulas represent a relationship between the breaking wave height (H_b) and the variables at the breaking or deepwater conditions, i.e. still water depth at breaking (h_b), wavelength at breaking (L_b), local bottom slope (m), deepwater wavelength (L_o), and deepwater wave height (H_o). The term "breaker index" is used to describe non-dimensional breaker height. The existing breaker height formulas can be classified into three common breaker indices, i.e. wave height to depth ratio (H_b / h_b), wave steepness (H_b / L_b), and wave height to deepwater wave height ratio (H_b / H_o). The example of existing formulas that proposed in the form of each breaker indices are as follows.

The formulas that proposed in the form of H_b / h_b are McCowan (1894), Galvin (1969), Collins and Weir (1969), Goda (1970), Weggel (1972), Madsen (1976), Sunamura (1980), Singamsetti and Wind (1980), Seyama and Kimura (1988), Larson and Kraus (1989), Hansen (1990), Smith and Kraus (1990), and Rattanapitikon and Shibayama (2000b). This breaker index seems to be the most frequently re-analyzed topics.

The formulas that proposed in the form of H_b / L_b are Miche (1944), Battjes and Janssen (1978), Ostendorf and Madsen (1979), Battjes and Stive (1985), Kamphuis (1991), Rattanapitikon and Shibayama (2000b), and Rattanapitikon et al. (2003). Most of the formulas in this group were developed based on the formula of Miche (1944).

The formulas that proposed in the form of H_b / H_o are Le Mehaute and Koh (1967), Komar and Gaughan (1972), Sunamura and Horikawa (1974), Singamsetti and Wind (1980), Ogawa and Shuto (1984), Larson and Kraus (1989), Smith and Kraus (1990), Gourlay (1992), and Rattanapitikon and Shibayama (2000b).

Either local or deepwater conditions are used to express the breaker indices. There are four dimensionless parameters that often used to express the breaker indices, i.e. m, h_b / L_b, h_b / L_o, and H_o / L_o. The existing breaker indices, therefore, can be categorized into three general functions as

$$\frac{H_b}{h_b} = f_1\left\{m, \frac{h_b}{L_b}, \frac{h_b}{L_o}, \frac{H_o}{L_o}\right\} \tag{2.1}$$

$$\frac{H_b}{L_b} = f_2\left\{m, \frac{h_b}{L_b}, \frac{h_b}{L_o}, \frac{H_o}{L_o}\right\} \tag{2.2}$$

$$\frac{H_b}{H_o} = f_3\left\{m, \frac{h_b}{L_b}, \frac{h_b}{L_o}, \frac{H_o}{L_o}\right\} \tag{2.3}$$

where f_1, f_2 and f_3 are functions.

The existing breaker height formulas are summarized in Table 2.2.

Table 2.2. Existing breaker height formulas.

Researchers	Abbreviation	Formulas
McCowan (1894)	MC94	$H_b = 0.78h_b$
Miche (1944)	MI44	$H_b = 0.142L_b \tanh\left(\frac{2\pi h_b}{L_b}\right)$
Le Mehaute and Koh (1967)	MK67	$H_b = 0.76H_o\left(\frac{H_o}{L_o}\right)^{-1/4} m^{1/7}$
Galvin (1969)	GA69	$H_b = h_b \frac{1}{1.40 - 6.85m}$ for $m \le 0.07$ $H_b = \frac{h_b}{0.92}$ for $m > 0.07$
Collins and Weir (1969)	CW69	$H_b = h_b(0.72 + 5.6m)$
Goda (1970)	GO70	$H_b = 0.17L_o\left\{1 - \exp\left[-1.5\frac{\pi h_b}{L_o}\left(1 + 15m^{4/3}\right)\right]\right\}$
Weggel (1972)	WE72	$H_b = \frac{h_b g T^2 1.56/[1 + \exp(-19.5m)]}{gT^2 + h_b 43.75[1 - \exp(-19m)]}$
Komar and Gaughan (1972)	KG72	$H_b = 0.56H_o\left(\frac{H_o}{L_o}\right)^{-1/5}$
Sunamura and Horikawa (1974)	SH74	$H_b = H_o m^{0.2}\left(\frac{H_o}{L_o}\right)^{-0.25}$
Madsen (1976)	MA76	$H_b = 0.72h_b(1 + 6.4m)$ for $m < 0.10$
Ostendorf and Madsen (1979)	OM79	$H_b = 0.14L_b \tanh\left[(0.8 + 5m)\frac{2\pi h_b}{L_b}\right]$ for $m \le 0.1$ $H_b = 0.14L_b \tanh\left[(0.8 + 5(0.1))\frac{2\pi h_b}{L_b}\right]$ for $m > 0.1$
Sunamura (1980)	SU80	$H_b = 1.1h_b\left(\frac{m}{\sqrt{H_o / L_o}}\right)^{1/6}$
Singamsetti and Wind (1980), A	SW80A	$H_b = 0.575H_o m^{0.031}\left(\frac{H_o}{L_o}\right)^{-0.254}$
Singamsetti and Wind (1980), B	SW80B	$H_b = 0.937h_b m^{0.155}\left(\frac{H_o}{L_o}\right)^{-0.13}$

Table 2.2 (continue). Existing breaker height formulas.

Researchers	Abbreviation	Formulas
Ogawa and Shuto (1984)	OS84	$H_b = 0.68 H_o m^{0.09} \left(\frac{H_o}{L_o} \right)^{-0.25}$
Larson and Kraus (1989)	LK89	$H_b = 1.14 h_b \left(\frac{m}{\sqrt{H_o / L_o}} \right)^{0.21}$
Hansen (1990)	HA90	$H_b = 1.05 h_b \left(m \frac{L_b}{h_b} \right)^{0.2}$
Smith and Kraus (1990),A	SK90A	$H_b = h_b \left\{ \frac{1.12}{1+\exp(-60m)} - 5.0[1-\exp(-43m)] \frac{H_o}{L_o} \right\}$
Smith and Kraus (1990),B	SK90B	$H_b = H_o (0.34 + 2.47m) \left(\frac{H_o}{L_o} \right)^{-0.30+0.88m}$
Gourlay (1992)	GL92	$H_b = 0.478 H_o \left(\frac{H_o}{L_o} \right)^{-0.28}$
Rattanapitikon and Shibayama (2000b)	RS00a	$H_b = (10.02m^3 - 7.46m^2 + 1.32m + 0.55) H_o \left(\frac{H_o}{L_o} \right)^{-1/5}$
Rattanapitikon and Shibayama (2000b)	RS00b	$H_b = 0.17 L_o \left\{ 1 - \exp\left[\frac{\pi h_b}{L_o} (16.21m^2 - 7.07m - 1.55) \right] \right\}$
Rattanapitikon and Shibayama (2000b)	RS00c	$H_b = 0.14 L_b \tanh\left[(-11.21m^2 + 5.01m + 0.91) \frac{2\pi h_b}{L_b} \right]$
Rattanapitikon et al, (2003)	RS03	$H_b = (-1.40m^2 + 0.57m + 0.23) L_b \left(\frac{H_o}{L_o} \right)^{0.35}$

2.2.1. Examination of existing formulas

A straightforward way to examine the accuracy of a formula is to compare the computed breaker depth data with the laboratory data. The basic parameter for determination of the overall accuracy of the formula is the average root mean square relative error (ER_{avg}), which is defined as

$$ER_{avg} = \frac{\sum_{j=1}^{tn} ER_{gj}}{tn} \tag{2.4}$$

where ER_{gj} is the root mean square relative error of the data group j (the group number), and tn is the total number of groups. The small value of ER_{avg} indicates good overall accuracy of the formula.

The group *rms* relative error (ER_g) is defined as

$$ER_g = 100\sqrt{\frac{\sum_{i=1}^{ng}(V_{ci} - V_{mi})^2}{\sum_{i=1}^{ng} V_{mi}^2}} \tag{2.5}$$

where i is the data number, V_{ci} is the computed variable of number i, V_{mi} is the measured variable of number i, and ng is the total number of measured data in each data group.

In accordance with Rattanapitikon and Shibayama (2000), the bottom slope of the collected experimental data is classified into four groups, i.e., horizontal ($m = 0$), gentle ($0 < m \le 0.07$), intermediate ($0.07 < m \le 0.10$), and steep ($m > 0.10$).

The computations of the present formula and the existing formulas are carried out with 26 sources of collected data shown in Table 2.1. Tables 2.3 and 2.4 show the *rms* relative error of the existing formulas for 4 groups of bottom slope for small-scale and large-scale wave flumes. The formulas that give very good predictions ($ER < 12$) are marked in the Table. The examination results from Tables 2.3 and 2.4 can be summarized as follows:

(a) The formulas that give very good predictions ($ER < 12$) for all cases in both of small-scale and large-scale experiments are the formulas of RS00b, RS00c, and RS03.

(b) The formula that gives very good prediction for all bottom slope conditions is the formula of RS03. Overall, the formula of RS03 gives the best prediction over a wide range of experimental conditions. However, the RS03 formula depends on deepwater wave height. It might not be capable of modeling multiple breaking and reformation in a wave model.

Table 2.3. The root mean square relative error (ER) of each formula comparing with small-scale experimental data (measured data from 24 sources shown in Table 2.1).

Formulas	$m = 0$ (64 cases)	$0 < m \leq 0.07$ (338 cases)	$0.07 < m \leq 0.10$ (102 cases)	$0.1 < m \leq 0.38$ (70 cases)	All 574 cases
MC94	14.8	15.3	21.8	27.9	18.9
MI44	13.9	12.8	18	25.4	16.4
MK67	N.A.*	13	17.3	28	17.3**
GA69	15.8	14.8	25.5	17.6	17.3
CW69	15.6	17.7	41.3	110.3	49.2
GO70	13.9	11.3	23	81.6	35.3
WE72	14.8	13.7	18.2	19	15.5
KG72	10.9	12.2	12.4	12.6	12.2
SH74	N.A.*	14.5	32	52.9	28.3**
MA76	15.6	15.3	32	87	39.2
BJ78	13	15.7	23.3	30.5	19.8
OM79	18.9	12.9	11.7	14.4	13.7
SU80	N.A.*	12.7	14.5	20.2	14.6**
SW80a	N.A.*	14.8	17.2	17.3	15.6**
SW80b	N.A.*	15.1	15.5	20.7	16.3**
OS84	N.A.*	12.2	18.4	24.1	16.0**
BS85	20.7	21.3	28.4	29.7	23.9
SK88	14.4	14.5	13.4	35.6	19.4
LK89a	N.A.*	13.9	14.4	23.5	16.1**
LK89b	16.2	13.5	13.2	12.3	13.6
HA90	N.A.*	13.3	20.3	29.8	18.5**
SK90a	30	12.8	11.8	21.1	16.6
SK90b	13.9	13.2	12.9	20.8	14.8
KA91	13.8	11.4	19.1	106.4	44.6
GL92	21.2	16.8	16.4	13.2	16.7
RS00a	10.6	11.7	14.1	11.7	12
RS00b	13	11.3	11.9	12	11.7
RS00c	13.3	11.3	11.9	12.2	11.7
RS03	9.7	10.5	10.6	10.4	10.5

*N.A. = Not Applicable

** = Exclude $m = 0$

= Very Good Prediction ($ER < 12$)

Table 2.4. The root mean square relative error (ER) of each formula comparing with large-scale experimental data (measured data from 2 sources shown in Table 2.1).

Formulas	$m = 0$ (3 cases)	$0 < m \le 0.07$ (41 cases)	$0.07 < m \le 0.10$ (24 cases)	$0.1 < m \le 0.29$ (53 cases)	All 121 cases
MC94	14.3	28.5	28.7	32.2	30.6
MI44	8.8	12.4	20.3	27.7	23.1
MK67	N.A.*	19.7	8.4	18.2	17.5**
GA69	15	38.4	38.3	23.9	31
CW69	14.7	43.7	49.6	78.7	66.1
GO70	12.8	9.6	13.3	40.2	30.9
WE72	14.3	12.5	11.8	12.9	12.6
KG72	16.3	17.7	16.8	11.1	14.2
SH74	N.A.*	18.1	16.7	38.4	31.1**
MA76	14.7	39.1	41.9	62.6	53.7
BJ78	11.1	16.3	25.8	33	28
OM79	19	12.4	10.5	14.2	13.2
SU80	N.A.*	26	22.4	20.7	22.6**
SW80a	N.A.*	8.5	8.9	13	11.3**
SW80b	N.A.*	24.7	22.5	20.2	21.9**
OS84	N.A.*	13.6	8.7	16.7	14.9**
BS85	22.2	28.6	38.8	38	35.6
SK88	13.5	18.3	18.8	16.1	17.2
LK89a	N.A.*	23.7	21.3	21.8	22.3**
LK89b	8.5	9.9	9.5	8.9	9.2
HA90	N.A.*	24.6	23.8	24	24.1**
SK90a	29.2	14.1	10.1	19.3	16.9
SK90b	26.4	18	10.4	10.8	13.4
KA91	12.7	11	14.9	49.9	38.2
GL92	4.2	7.5	11.1	12.4	11
RS00a	17.7	14.6	10.7	8.9	11.2
RS00b	10.9	9.6	10.4	11.8	11
RS00c	11.7	9.4	9.5	11.1	10.4
RS03	10.7	7.6	7	7.5	7.5

*N.A. = Not Applicable

** = Exclude $m = 0$

= Very Good Prediction ($ER < 12$)

2.3. Breaker Depth Formulas

It is known that the limitation of empirical formulas depends on the range of laboratory data. As the previous formulas were developed based on a limited range of laboratory data, it is expected that errors of the existing formulas are large when comparing with a wide range of laboratory data. However, some existing formulas may give good predictions for a wide range of laboratory data. Therefore, it is necessary to examine the accuracy of existing formulas before developing new formulas.

2.3.1. Examination of existing formulas

Brief reviews of selected breaker depth formulas are described below.

a) Goda (1970) analyzed several sets of laboratory data of breaking waves on slopes obtained by several researchers (Iversen, 1952; Mitsuyasu, 1962; and Goda, 1964). The experiments cover a range of $0.01 < m < 0.1$ and $0.003 < H_o / L_o < 0.07$. He proposed a diagram presenting criteria for predicting breaker depth. The diagram is expressed in terms of the ratio of breaker depth to deepwater wave height (h_b / H_o) as a function of deepwater wave steepness (H_o / L_o) and bottom slope (m). As it is not convenient to use this diagram in the wave model, it is not considered in the present study.

b) Ogawa and Shuto (1984) reanalyzed the same data set as used by Goda (1970) and obtained the following formula:

$$h_b = 0.46 H_o m^{-0.12} \left(\frac{H_o}{L_o} \right)^{-0.2} \tag{2.6}$$

where h_b is the breaker depth, m is the bottom slope, H_o is the deepwater wave height, and L_o is the deepwater wavelength. This formula is referred to as OS84 hereafter.

c) Dean and Dalrymple (1984) used linear wave theory to derive a breaker depth formula from energy flux conservation together with the breaker height formula of McCowan (1894).

$$h_b = \frac{1}{g^{1/5} \kappa^{4/5}} \left(\frac{H_o^2 c_o}{2} \right)^{2/5} \tag{2.7}$$

where $\kappa = 0.78$ is a constant in the formula of McCowan (1984), g is the gravity acceleration, and c_o is the deepwater phase velocity. Using linear wave theory, Eq. (2.7) is re-written in the similar form as Eq. (2.6) as

$$h_b = 0.64 H_o \left(\frac{H_o}{L_o} \right)^{-0.2} \tag{2.8}$$

This formula is referred to as DD84 hereafter. It should be noted that Eq. (2.7) (or Eq. (2.8)) was not calibrated with any laboratory data.

d) Gourlay (1992) proposed an empirical formula based on seven sources of laboratory data (Bowen et al., 1968; Smith, 1974; Visser, 1977; Gourlay, 1978; Van Dorn, 1978; Stive, 1984; and Hansen and Svendsen, 1979). The experiments cover a range of $0.022 < m < 0.1$ and $0.001 < H_o / L_o < 0.066$. The data were used to plot the relationship between h_b / H_o and $m^2 H_o / L_o$. The curve fitting yields

$$h_b = 0.259 H_o m^{-0.34} \left(\frac{H_o}{L_o} \right)^{-0.17} \tag{2.9}$$

This formula is referred to as GL92 hereafter.

e) The breaker depth formula can also be derived from the existing breaker height formulas. In the present study, the breaker depth formula is derived from the breaker height formulas of Rattanapitikon and Shibayama (2000), which were modified from the breaker height formulas of Komar and Gaughan (1972) and Goda (1970). The breaker height formulas are expressed as follows:

$$H_b = \left(10.02m^3 - 7.46m^2 + 1.32m + 0.55\right)H_o\left(\frac{H_o}{L_o}\right)^{-0.2} \tag{2.10}$$

$$H_b = 0.17L_o\left[1 - \exp\left(\frac{\pi h_b}{L_o}(16.21m^2 - 7.07m - 1.55)\right)\right] \tag{2.11}$$

where H_b is the breaker height.

Substituting H_b from Eq. (2.9) into Eq. (2.10), yields

$$h_b = \frac{L_o}{\pi(16.21m^2 - 7.07m - 1.55)}\ln\left[1 - \left(58.94m^3 - 43.88m^2 + 7.76m + 3.24\right)\left(\frac{H_o}{L_o}\right)^{0.8}\right] \tag{2.12}$$

This formula is referred to as RS00 hereafter.

The laboratory data from 26 sources are used to examine the validity of each formula. The laboratory data cover a wide range of wave and bottom conditions ($0.001 \le H_o / L_o \le 0.112$, and $0 \le m \le 0.38$). In order to see the performance of each formula clearly, the experimental conditions are divided into various groups of deepwater wave steepness (H_o/L_o), bottom slope (m) and experiment scale.

As the breaker depth diagram of Goda (1970) shows that h_b/H_o increases rapidly when $H_o/L_o > 0.1$, the laboratory data are divided into two groups of deepwater wave steepness, i.e. $H_o/L_o \le 0.1$, and $H_o/L_o > 0.1$. Following the classification of Rattanapitikon and Shibayama (2000), the bottom slope of the collected data is divided into four groups, i.e. horizontal ($m = 0$), gentle ($0 < m \le 0.07$), intermediate ($0.07 < m \le 0.10$), and steep ($0.1 < m \le 0.38$). The experiment scale is separated into 2 groups, i.e. small-scale and large-scale experiments. The collected data shown in Table 2.1 are separated into 11 groups of deepwater wave steepness, bottom slope and experiment scale (see Table 2.5). The total number of cases for each group is shown in the fourth column of Table 2.5.

The computations of the breaker depth formulas are carried out with 26 sources of collected data (see Table 2.1). The variables required for the examinations are h_b, H_o, L_o, and m. The bottom slope (m) used in the computation is the local bottom slope seaward of the breaking point and the negative slope is set to be zero. The errors (ER_g) of OS84, DD84, GL92 and RS00 for each group are shown in the fifth to eighth columns of Table 2.5. The examination results from Table 2.5 are summarized as follows:

a) The overall accuracy of each existing formula for small-scale and large-scale experiments is nearly the same.
b) The formulas of OS84 and RS00 give good prediction for the cases of $H_o/L_o \le 0.1$ but fair prediction for the case of $H_o/L_o > 0.1$, while the formulas of DD84 and GL92 give fair prediction for most conditions.
c) The formula of OS84 is better than that of DD84 because of the term of bottom-slope-effect.

d) The formula of OS84 gives good prediction for the cases of $H_o/L_o \le 0.1$ but it is not valid for the breaking wave on the horizontal bed ($m = 0$) and should not be used for the cases of $H_o/L_o > 0.1$.
e) For the cases of $H_o/L_o > 0.1$, only the formula of RS00 predicts increase of h_b/H_o at $H_o/L_o > 0.1$ while other existing formulas do not have this property.
f) Considering the simplicity and accuracy of the formula, the formula of OS84 is more attractive than that of RS00 for the cases of $H_o/L_o \le 0.1$.
g) The formula of RS00 seems to be the best but it is the longest one. Moreover, it should be used with care for the cases of $H_o/L_o > 0.1$.
h) Overall, the predictions of all existing formulas are unsatisfactory for the cases of $H_o/L_o > 0.1$.

Table 2.5. The root mean square relative error (ER_g) of the formulas for computing the breaker depth (laboratory data from 26 sources shown in Table 2.1).

Experiment	H_o/L_o	Bottom Slope	No. of Cases	OS84	DD84	GL92	RS00	Eq. (2.17)
Small scale	≤ 0.1	$m = 0$	64	N.A.*	17.7	N.A.*	19.2	17.1
		$0 < m \le 0.07$	338	13.7	16.0	26.1	11.6	12.7
		$0.07 < m \le 0.10$	102	14.8	15.0	21.4	13.5	12.8
		$0.1 < m \le 0.38$	70	13.8	19.2	33.2	16.0	12.5
		ER_{avg} (for 4 groups)		14.1	17.0	26.9	15.0	13.8
Large scale	≤ 0.1	$m = 0$	3	N.A.*	26.1	N.A.*	11.1	11.1
		$0 < m \le 0.07$	33	13.9	20.1	43.3	14.6	13.7
		$0.07 < m \le 0.10$	21	11.9	12.2	18.9	10.5	10.3
		$0.1 < m \le 0.38$	46	18.3	27.5	21.2	17.4	18.1
		ER_{avg} (for 4 groups)		14.7	21.5	27.8	13.4	13.3
Large scale	> 0.1	$m = 0$	0	-	-	-	-	-
		$0 < m \le 0.07$	8	40.2	43.4	36.5	19.0	6.0
		$0.07 < m \le 0.10$	3	39.9	37.5	46.1	16.0	5.9
		$0.1 < m \le 0.38$	7	37.2	28.2	52.5	20.6	10.4
		ER_{avg} (for 3 groups)		39.1	36.4	45.0	18.5	7.5
ER_{avg} (for 11 groups)				22.6	23.9	33.2	15.4	11.9

*N.A. = Not Applicable

2.3.2. Formula development

From the existing breaker depth formulas, the breaker depth may depend on the deepwater wave height (H_o), the deepwater wavelength (L_o), and the bottom slope at the breaking location (m). Therefore, the possible breaker depth formula can be expressed as the following functions.

$$\frac{h_b}{H_o} = f_1\left\{m, \frac{H_o}{L_o}\right\} \tag{2.13}$$

$$\frac{h_b}{L_o} = f_2\left\{m, \frac{H_o}{L_o}\right\} \tag{2.14}$$

where f_1 and f_2 are functions proposed for each formula.

The laboratory data from 26 sources (shown in Table 2.1) are used to develop a new breaker depth formula. The required data for the development are h_b, H_o, m, and L_o. The data of h_b, m, and T were measured directly from the experiments, while the data of H_o and L_o are computed by using linear wave theory. The development of a new formula is separated into two stages. The first stage is determination of the general relationship between h_b/H_o versus H_o/L_o (or h_b/L_o versus H_o/L_o). After that, the bottom-slope-effect is included explicitly into the general formula obtained from the first stage.

2.3.2.1. Relationship between h_b/H_o and H_o/L_o

The relationship between h_b/H_o and H_o/L_o is plotted to determine the possible form of fitting equation (see Fig. 2.1).

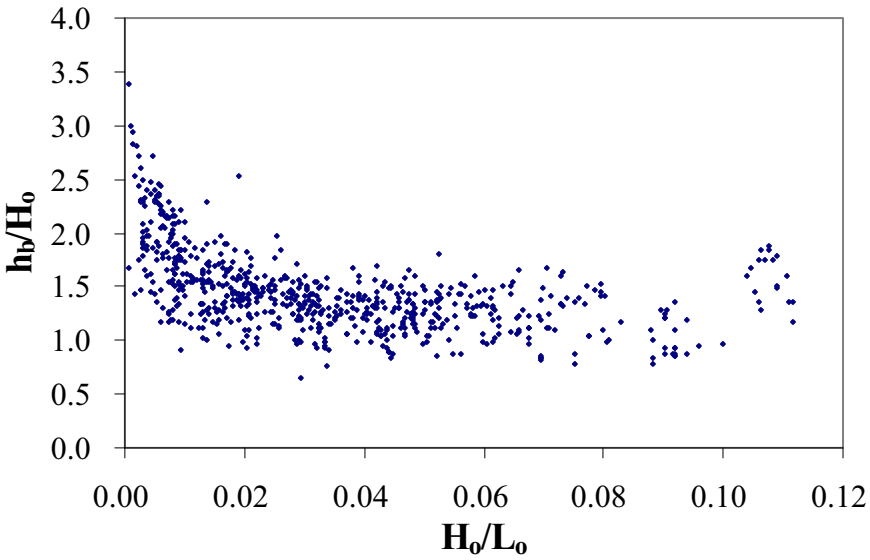

Figure 2.1. Relationship between h_b/H_o and H_o/L_o (laboratory data from 26 sources shown in Table 2.1).

The relationship in Fig. 2.1 can be fitted with a power function. However, the parameter h_b/H_o tends to increase rapidly when $H_o/L_o > 0.1$. It is better to separate the formula into two parts, i.e. for $H_o/L_o \le 0.1$ and for $H_o/L_o > 0.1$. The general formula can be expressed in form of step function as

$$\frac{h_b}{H_o} = S_1\left(\frac{H_o}{L_o}\right)^{K_1} \qquad \text{for} \quad \frac{H_o}{L_o} \le 0.1 \tag{2.15a}$$

$$\frac{h_b}{H_o} = S_1\left(\frac{H_o}{L_o}\right)^{K_2} \qquad \text{for} \quad \frac{H_o}{L_o} > 0.1 \tag{2.15b}$$

where S_1 is the slope effect coefficient, and K_1 and K_2 are constants.

Using the laboratory data of h_b, H_o, and L_o for the cases that $H_o/L_o \le 0.1$, the data of S_1 can be determined from Eq. (2.15a), if the constant K_1 is given. For a given constant K_1, the relationship between S_1 versus m is plotted to determine the correlation. Then the

constant K_1 is gradually adjusted until it gives the best correlation. The relationship shows the best correlation when $K_1 = -0.16$ (see Fig. 2.2).

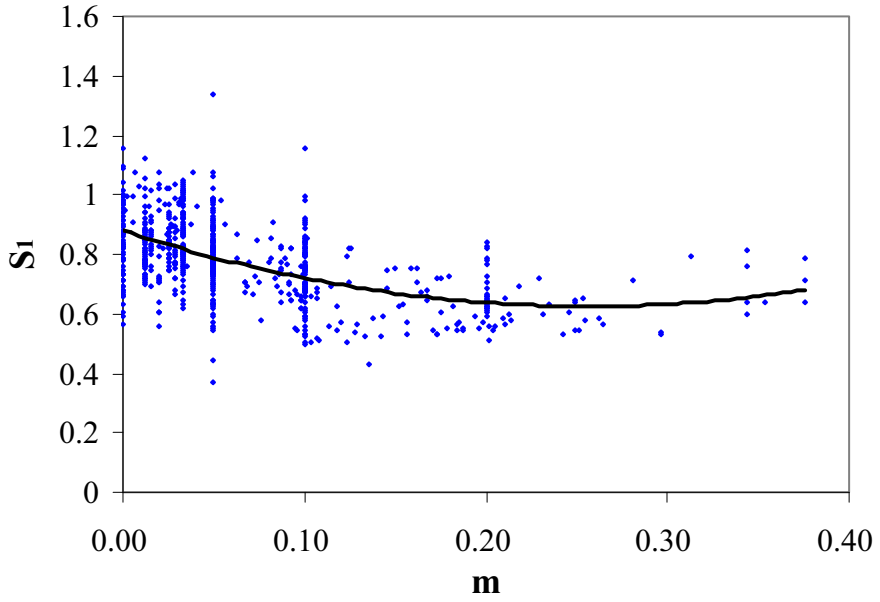

Figure 2.2. Relationship between slope effect coefficient S_1 and bottom slope m when $K_1 = -0.16$ (laboratory data from 26 sources shown in Table 2.1 excluding the data that $H_o/L_o > 0.1$). Solid line is the computed S_1 from Eq. (2.16).

The scatter in Fig. 2.2 is caused by Eq. (2.15). The scatter shows a weak correlation between S_1 and m. However, it still has some correlation. The relationship in Fig. 2.2 can be fitted with a parabolic function. The coefficients in the parabolic function are determined from multi-regression analysis. After the analysis, it is found that the best-fit formula for S_1 can be expressed as

$$S_1 = 3.86m^2 - 1.98m + 0.88 \tag{2.16}$$

Using the laboratory data for the cases that $H_o/L_o > 0.1$, the constant K_2 can be determined from regression analysis. The regression analysis between $\ln(h_b/(S_1 H_o))$ and $\ln(H_o/L_o)$ yields $K_2 = -0.34$.

Substituting Eq. (2.16) and $K_1 = -0.16$, $K_2 = -0.34$ into Eq. (2.15), yields

$$h_b = (3.86m^2 - 1.98m + 0.88)H_o\left(\frac{H_o}{L_o}\right)^{-0.16} \quad \text{for} \quad \frac{H_o}{L_o} \le 0.1 \tag{2.17a}$$

$$h_b = (3.86m^2 - 1.98m + 0.88)H_o\left(\frac{H_o}{L_o}\right)^{-0.34} \quad \text{for} \quad \frac{H_o}{L_o} > 0.1 \tag{2.17b}$$

The plots of Eq. (2.17) for 4 bottom slopes ($m = 0.01$, $m = 0.05$, $m = 0.10$, and $m = 0.20$) are shown as the lines in Fig. 2.3. The computations of the breaker depth from Eq. (2.17) are carried out with 26 sources of collected data (see Table 2.1). The verification results are shown in the last column of Table 2.5. The verification results are summarized as follows:

a) Eq. (2.17) gives better predictions than the existing formulas (except RS00) for all conditions while gives better predictions than the formula of RS00 for most conditions.
b) Although Eq. (2.17) is more complicate than the formula of RS00 (which is the longest and the best existing formula), the accuracy of Eq. (2.17) for the cases of $H_o/L_o > 0.1$ is significantly better than that of RS00 (ER_{avg} of RS00 is 18.5% while ER_{avg} of Eq. (2.17) is 7.5%).
c) In comparison with the existing formulas, overall accuracy of Eq. (2.17) is slightly better for the cases of $H_o/L_o \le 0.1$, but much better for the cases of $H_o/L_o > 0.1$.
d) The overall accuracy of Eq. (2.17) is significantly better than that of existing formulas, and its use is recommended for computing the breaker depth. However, since the formula is based on deepwater wave height, it is not possible to model the multiple breaking and reformation in a wave model.

The validity of empirical formulas may be limited according to the range of experimental conditions used in the calibrations or verifications. Therefore, the use of Eq. (2.17) becomes questionable for the beaches having slope greater than 0.38 and for the deepwater wave steepness (H_o / L_o) greater than 0.112. Moreover, since the experimental data is not available for the range of $0.100 < H_o/L_o < 0.104$ (see Fig. 2.1), caution should be taken when using Eq. (2.17b) for this narrow range. The step function in Eq. (2.17) can be avoided by adding the equation for the transition zone ($0.100 < H_o/L_o < 0.104$) but Eq. (2.17) will become quite complicate. Because of the complexity of equation, unavailability of experimental data, and the narrow range of transition zone, the transition zone is not considered in this study.

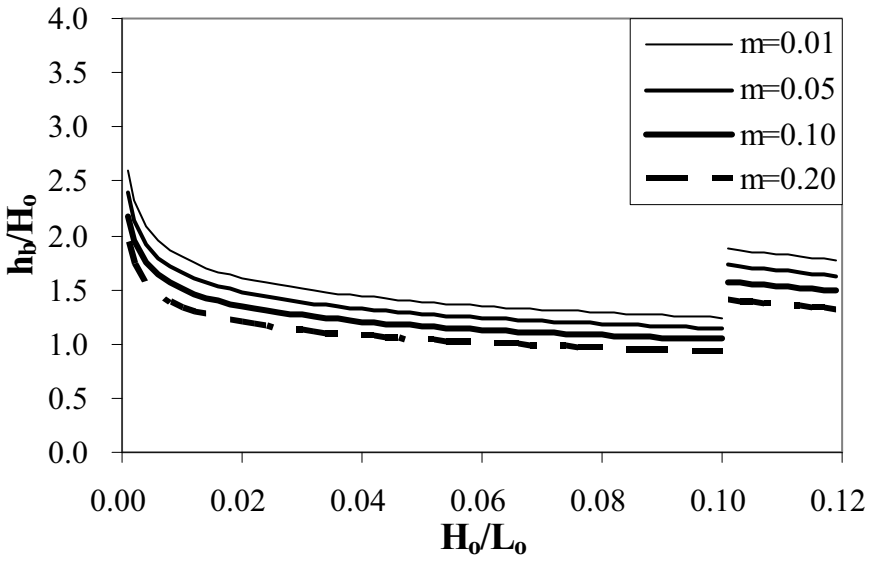

Figure 2.3. The plots of Eq. (2.17) for 4 bottom slopes (m = 0.01, m = 0.05, m = 0.10, and m = 0.20).

2.3.2.2. Relationship between h_b / L_o and H_o / L_o

The relationships between h_b / L_o and H_o / L_o is plotted to determine the possible form of fitting equation (see Fig. 2.4). Figure 2.4 shows that the relationship can also be fitted with a power function as in Fig. 2.1. Therefore, the general formula can be expressed in the same form as in Eq. (2.15). Following the same procedure as in sub-section 2.3.2.1, the final formula is the same as shown in Eq. (2.17).

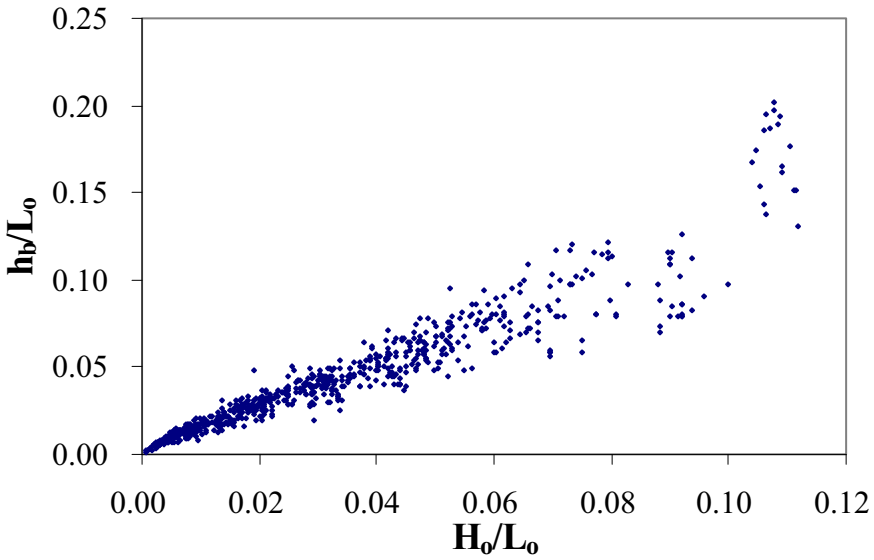

Figure 2.4. Relationship between h_b / L_o and H_o / L_o (laboratory data from 26 sources shown in Table 2.1).

2.4. Assumed Orbital to Phase Velocity Ratio and Assumed Breaker Height

The objective of this section is to find out the reliable formulas for computing the assumed orbital to phase velocity ratio at the breaking ($\hat{u}_b / c_b$) and assumed breaker height (H'_b). These two variables are considered at the same time because one variable can be converted into the other by using linear wave theory. Similar to the previous section, examination of existing formulas is performed before development of the new formulas.

2.4.1. Examination of existing formulas

Only two formulas have been proposed to compute $\hat{u}_b / c_b$ and H'_b. A brief review of the formulas is described below.

Watanabe et al. (1984) pointed out that the assumed orbital to phase velocity ratio is more suitable for the computation of composite waves breaking. They employed the linear wave theory to determine the assumed breaker height (H'_b) from the known deepwater wave height (H_o), water depth at breaking (h_b) and wave period (T).

$$H'_b = H_o \sqrt{\frac{c_o}{2c_{gb}}} \tag{2.18}$$

where c_{gb} is the group velocity at the breaking point.

Then the assumed orbital velocity ($\hat{u}_b$) at the mean water level is computed from H'_b, h_b, and T by using linear wave theory as

$$\hat{u}_b = \frac{H'_b c_b k_b}{2\tanh(k_b h_b)} = \frac{\pi c_b H'_b}{L_o \tanh^2(k_b h_b)} \tag{2.19}$$

where c_b is the phase velocity at the breaking point, and k_b is the wave number at the breaking point.

By reanalyzing the same data set as used by Goda (1970), the breaker depth diagram of Goda (1970) was converted into a diagram, which shows the relationship between assumed orbital to phase velocity ratio ($\hat{u}_b / c_b$) versus relative water depth (h_b / L_o), and bottom slope (m). For convenience in numerical calculation, the diagram of Watanabe et al. (1984) was approximated by Isobe (1987) as

$$\hat{u}_b = c_b \left\{ 0.53 - 0.3\exp\left[-3\sqrt{\frac{h_b}{L_o}} \right] + 5m_b^{3/2} \exp\left[-45\left(\sqrt{\frac{h_b}{L_o}} - 0.1 \right)^2 \right] \right\} \tag{2.20}$$

This formula is referred to as WI87a hereafter.

Since wave height is the convenient variable for many wave models, Rattanapitikon (1995) converted Eq. (2.20) to be expressed in terms of assumed breaker height (H'_b) by using linear wave theory.

$$H'_b = \frac{L_o \tanh^2(k_b h_b)}{\pi} \left\{ 0.53 - 0.3\exp\left[-3\sqrt{\frac{h_b}{L_o}} \right] + 5m_b^{3/2} \exp\left[-45\left(\sqrt{\frac{h_b}{L_o}} - 0.1 \right)^2 \right] \right\} \tag{2.21}$$

This formula is referred to as WI87b hereafter. It should be noted that Eqs. (2.20) and (2.21) are identical in terms of linear wave theory.

The collected data shown in Table 2.1 are used to examine the formulas of WI87a and WI87b. The required data in the examination are $\hat{u}_b$, H'_b, h_b, L_o, c_b, m, and k_b. The water depth (h_b) and the bottom slope (m) were measured directly from the experiments. The data of H'_b and $\hat{u}_b$ are determined by using Eqs. (2.18) and (2.19) respectively. Other variables are computed based on the linear wave theory from the known h_b and T.

As the variation of $\hat{u}_b / c_b$ for the cases of $H_o / L_o > 0.1$ shows the same trend as that of $H_o / L_o \le 0.1$ (see Fig. 4 in the paper of Watanabe et al., 1984), the collected laboratory data are divided on the basis of bottom slope and experiment scale. The computations of $\hat{u}_b$ and H'_b from Eqs. (2.20) and (2.21) are carried out with 26 sources of collected data (see Table 2.1). The errors ER_g of WI87a and WI87b for 8 groups of bottom slope and experiment scale are shown in the fourth and seventh columns of Table 2.6. The examination results from Table 2.6 are summarized as follows:

a) As formulas of WI87a and WI87b are identical in terms of linear wave theory, it is not surprising to see that the accuracy of both formulas is nearly the same.
b) Although the development of formulas WI87a and WI87b were based on small-scale experiments, they surprisingly give good prediction for the large-scale experiments but fair prediction for the small-scale experiments. However, what is considered a good formula should give good predictions for both small-scale and large-scale experimental conditions. The formulas of WI87a and WI87b should be modified for better predictions.

c) The errors of WI87a and WI87b tend to vary with the bottom slope. The error is pronounced for the breaking wave on the steep slope.

Table 2.6. The root mean square relative error (ER_g) of the formulas for computing $\hat{u}_b$ and H_b' (laboratory data from 26 sources shown in Table 2.1).

Experiment	Bottom Slope	No. of Cases	Formulas for computing $\hat{u}_b$			Formulas for computing H_b'		
			WI87a	Eq. (2.23)	Eq. (2.34)	WI87b	Eq. (2.24)	Eq. (2.33)
Small scale	$m = 0$	64	21.9	20.2	4.1	21.0	19.3	4.0
	$0 < m \le 0.07$	338	16.7	15.0	2.7	15.4	13.6	2.4
	$0.07 < m \le 0.10$	102	17.6	15.8	3.7	16.2	14.4	3.4
	$0.1 < m \le 0.38$	70	37.4	19.4	2.6	41.7	20.9	2.7
	ER_{avg} (for 4 groups)		23.4	17.6	3.3	23.5	17.1	3.1
Large scale	$m = 0$	3	12.8	11.5	1.5	13.2	11.8	1.5
	$0 < m \le 0.07$	41	11.8	15.6	4.2	11.7	15.5	4.4
	$0.07 < m \le 0.10$	24	14.1	12.5	3.1	13.0	12.0	3.1
	$0.1 < m \le 0.38$	53	19.9	17.4	3.3	19.3	16.4	3.0
	ER_{avg} (for 4 groups)		14.6	14.3	3.0	14.3	13.9	3.0
ER_{avg} (for 8 groups)			19.0	15.9	3.2	18.9	15.5	3.1

2.4.2. Formula modification

Since WI87a and WI87b give fair predictions for the small-scale experiments and the error of predictions tend to vary with the bottom slope, it is expected that reformulating the term of bottom-slope-effect and changing the constants in the formula can improve the accuracy. Eq. (2.20) can be written in a general form as

$$\frac{\hat{u}_b}{c_b} = K_3 + K_4 \exp\left[-K_5\sqrt{\frac{h_b}{L_o}}\right] + K_6\left(m_b^{K_7} + K_8\right)\exp\left[-K_9\left(\sqrt{\frac{h_b}{L_o}} - K_{10}\right)^2\right] \qquad (2.22)$$

where K_3 to K_{10} are constants. The constants K_3, K_4 and K_6 can be determined from multi-regression analysis, if the constants K_5, K_7, K_8, K_9, and K_{10} are given. The constants K_5, K_7, K_8, K_9, and K_{10} are gradually adjusted until they give the minimum error. The best fitted K_3 to K_{10} are 0.46, 0.0, 3.0, 1.0, 0.95, -0.1, 13.0, and 0.1 respectively. As K_4 is equal to zero, the second term on the right hand side of Eq. (2.22) is not significant. Substituting all the constants into Eq. (2.22), yields

$$\hat{u}_b = c_b\left\{0.46 + \left(m_b^{0.95} - 0.1\right)\exp\left[-13\left(\sqrt{\frac{h_b}{L_o}} - 0.1\right)^2\right]\right\} \qquad (2.23)$$

Various functions of bottom-slope-effect have been tried to replace the term "$m_b^{0.95} - 0.1$" in Eq. (2.23), i.e. power, linear, quadratic, and cubic models. It is found that the accuracy of those functions is not better than that of "$m_b^{0.95} - 0.1$".

Similar to Rattanapitikon (1995), Eq. (2.23) is converted to express in term of the assumed breaker height (H_b') by using linear wave theory.

$$H_b' = \frac{L_o \tanh^2(k_b h_b)}{\pi}\left\{0.46 + \left(m_b^{0.95} - 0.1\right)\exp\left[-13\left(\sqrt{\frac{h_b}{L_o}} - 0.1\right)^2\right]\right\} \tag{2.24}$$

The errors (ER_g) of Eqs. (2.23) and (2.24) for 8 groups of bottom slope and experiment scale are shown in the fifth and eighth columns of Table 2.6. It can be seen that although Eqs. (2.23) and (2.24) are slightly simpler than those of WI87a and WI87b, they seem to give better predictions for a wide range of experimental conditions. The overall accuracy of Eqs. (2.23) and (2.24) for large-scale experiments is nearly the same as that of WI87a and WI87b. For small-scale experiments, the accuracy of Eqs. (2.23) and (2.24) is significantly better than that of WI87a and WI87b.

2.4.3. Formula development

Although Eqs. (2.23) and (2.24) give good predictions, it may be possible to develop new formulas which give better predictions than Eqs. (2.23) and (2.24). As the formulas for computing $\hat{u}_b / c_b$ and H_b' are considered to be identical, it is better to analyze them at the same time. The assumed breaker height (H_b') and assumed orbital to phase velocity ratio ($\hat{u}_b / c_b$) may depend on the variables at the deepwater or breaking conditions, i.e. deepwater wavelength (L_o), deepwater wave height (H_o), still water depth at the breaking location (h_b), wavelength at the breaking location (L_b), and bottom slope at the breaking location (m). The possible breaker index can be expressed as the following functions.

$$\frac{\hat{u}_b}{c_b} = f_3\left\{m, \frac{h_b}{L_b}, \frac{h_b}{L_o}, \frac{H_o}{L_o}\right\} \tag{2.25}$$

$$\frac{H_b'}{h_b} = f_4\left\{m, \frac{h_b}{L_b}, \frac{h_b}{L_o}, \frac{H_o}{L_o}\right\} \tag{2.26}$$

$$\frac{H_b'}{L_b} = f_5\left\{m, \frac{h_b}{L_b}, \frac{h_b}{L_o}, \frac{H_o}{L_o}\right\} \tag{2.27}$$

$$\frac{H_b'}{H_o} = f_6\left\{m, \frac{h_b}{L_b}, \frac{h_b}{L_o}, \frac{H_o}{L_o}\right\} \tag{2.28}$$

$$\frac{H_b'}{L_o} = f_7\left\{m, \frac{h_b}{L_b}, \frac{h_b}{L_o}, \frac{H_o}{L_o}\right\} \tag{2.29}$$

where f_3 to f_7 are functions proposed in each formula.

The laboratory data from 26 sources (shown in Table 2.1) are used to develop the new formulas for computing H_b' and $\hat{u}_b / c_b$. The required data for the development are h_b, H_o, m, L_o, c_b, L_b, H_b', and $\hat{u}_b$. The data of h_b, m, and T were measured directly from the experiments. The data of H_o, L_o, c_b, and L_b are computed by using linear wave theory. The data of H_b' and $\hat{u}_b$ are computed from Eqs. (2.18) and (2.19) respectively.

Each breaker index may be a function of four dimensionless parameters as shown in Eqs. (2.25) to (2.29). However, not all of the dimensionless parameters are contained in each existing breaker index and it is difficult to consider all these dimensionless parameters simultaneously. A common way to do is to select only one dimensionless parameter as a dominant parameter governing each breaker index. The selection of dominant parameter is performed by plotting the relationship between each breaker index and each dimensionless parameter. A much simpler relationship is expected for the

breaking wave on step beach ($m = 0$) because the parameter m can be excluded from the formula. Therefore, the development of a new formula is separated into two stages. For the first stage, the breaking waves on step beach ($m = 0$) are analyzed to identify a "basic form" of breaker index. After that, the bottom-slope-effect is included explicitly into the basic formula obtained from the first stage.

The laboratory data of the breaking waves on step beach (i.e. the experiments from Hattori and Aono, 1985; Horikawa and Kuo, 1966; and Nagayama, 1983) are used to determine a basic form of breaker index. An attempt is made to correlate the breaking indices ($\hat{u}_b / c_b$, H'_b / h_b, H'_b / L_b, H'_b / H_o, and H'_b / L_o) with the possible dimensionless parameters (h_b / L_b, h_b / L_o, and H_o / L_o). A total of fifteen possible relations is plotted to identify the best correlation. It is found that the relationship between H'_b / L_o and H_o / L_o shows the best correlation and it is selected as a basic form of breaking index. Examples of relationships between $\hat{u}_b / c_b$ and H'_b / L_o versus h_b / L_b, h_b / L_o, and H_o / L_o are shown in Figs. 2.5 and 2.6.

The relationship between H'_b / L_o and H_o / L_o (in Fig. 2.6c) can be fitted with a power function as

$$\frac{H'_b}{L_o} = K_{11}\left(\frac{H_o}{L_o}\right)^{K_{12}} \tag{2.30}$$

where K_{11} and K_{12} are constants. From the regression analysis between $\log(H'_b / L_o)$ and $\log(H_o / L_o)$, the values of K_{11}, K_{12}, and the correlation coefficient (R^2) are 0.64, 0.85, and 0.99 respectively. The best-fitted line is shown as the solid line in Fig. 2.6c. However, the values of K_{11} and K_{12} are not used in the next analysis because they may change slightly when the bottom-slope-effect and all collected laboratory data are included in the analysis.

The analysis is extended by incorporating the laboratory data of the breaking waves on various bottom slopes. All the laboratory data shown in Table 2.1 are used in the analysis. This revised analysis is based entirely on the basic formula obtained from the first stage of development (Eq. (2.30)). The slope effect coefficient is included in Eq. (2.30) by replacing the constant K_{11} as

$$\frac{H'_b}{L_o} = S_2\left(\frac{H_o}{L_o}\right)^{K_{12}} \tag{2.31}$$

where S_2 is the bottom-slope-effect coefficient.

Using the data of H_o, L_o, and H'_b, the data of S_2 can be determined from Eq. (2.31), if the constant K_{12} is given. For a given constant K_{12}, the relationship between S_2 and m is plotted to determine the correlation. Then the constant K_{12} is gradually adjusted until it gives the best correlation. The relationship between S_2 and m shows the best correlation when $K_{12} = 0.83$ (see Fig. 2.7). Using regression analysis, the best-fit formula for S_2 can be expressed as

$$S_2 = -0.57m^2 + 0.31m + 0.58 \tag{2.32}$$

Substituting Eq. (2.32) and $K_{12} = 0.83$ into Eq. (2.31), yields

$$H'_b = \left(-0.57m^2 + 0.31m + 0.58\right)L_o\left(\frac{H_o}{L_o}\right)^{0.83} \tag{2.33}$$

It can be seen from Fig. 2.7 that S_2 (y-axis) varies between 0.55 and 0.65. This narrow band of variation indicates that the effect of bottom slope (m) on Eq. (2.33) is limited.

Eq. (2.33) can be converted to express in term of the assumed orbital velocity ($\hat{u}_b$), by using linear wave theory, as

$$\hat{u}_b = \frac{\left(-0.57m^2 + 0.31m + 0.58\right)\pi c_b}{\tanh^2(k_b h_b)} \left(\frac{H_o}{L_o}\right)^{0.83} \tag{2.34}$$

The errors (ER_g) of Eqs. (2.33) and (2.34) for 8 groups of bottom slope and experiment scale are shown in the last and the sixth columns of Table 2.6. Table 2.6 shows that Eqs. (3.33) and (2.34) give surprisingly excellent predictions for both small-scale and large-scale experiments. The formulas give the best prediction for all conditions. However, they cannot be used in modeling the multiple breaking and reformation in a wave model because the formulas depend on deepwater wave height.

As the proposed formulas are empirical formulas, they are applicable in the limited range of experimental conditions that are used in the calibrations or verifications. Therefore, the use of Eqs. (2.33) and (2.34) becomes questionable for the beaches having slope greater than 0.38 and for the deepwater wave steepness greater than 0.112.

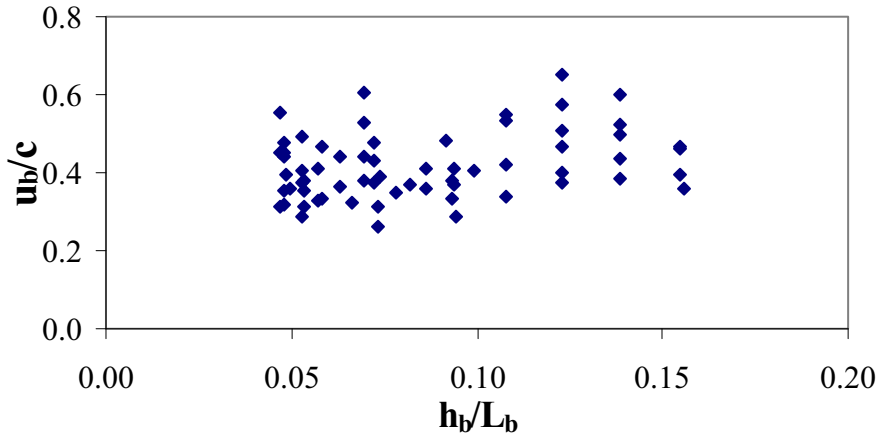

(a)

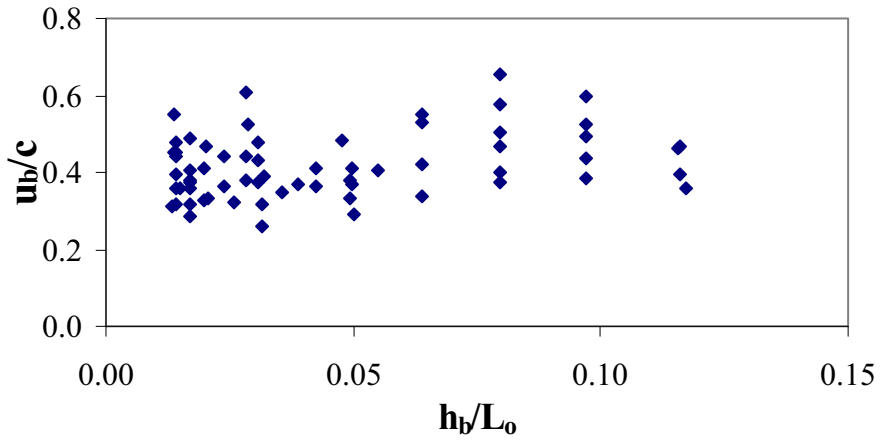

(b)

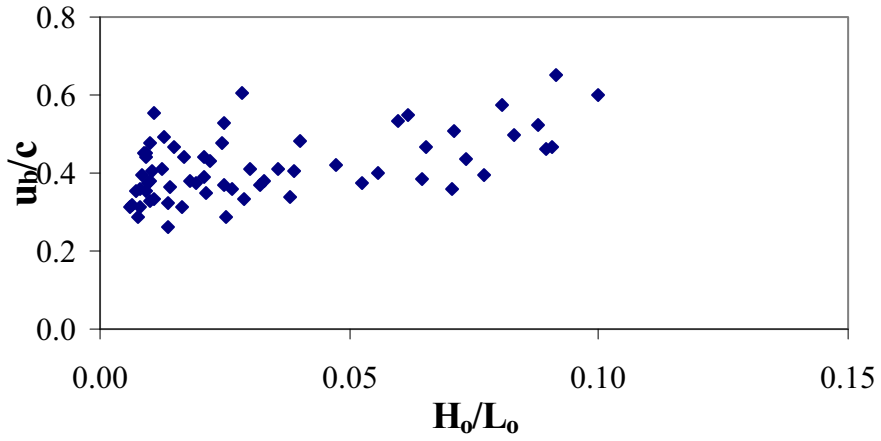

(c)

Figure 2.5. Relationships between $\hat{u}_b / c_b$ and (a) h_b / L_b, (b) h_b / L_o, (c) H_o / L_o for the case of breaking wave on step beach (laboratory data from Hattori and Aono, 1985; Horikawa and Kuo, 1966; and Nagayama, 1983).

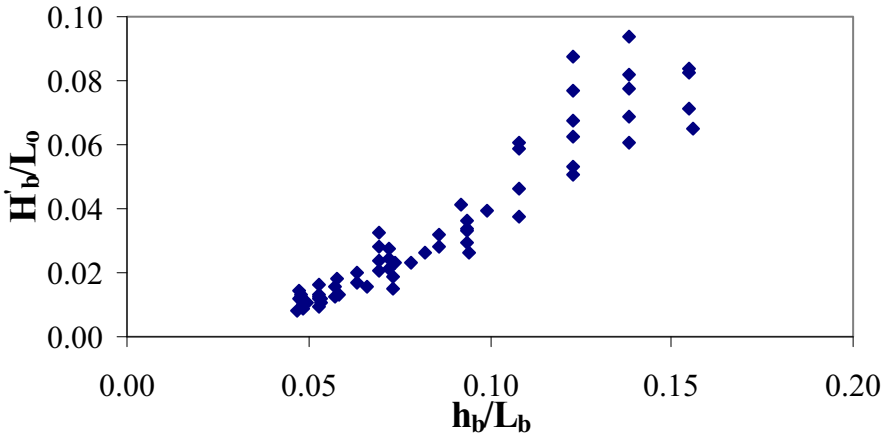

(a)

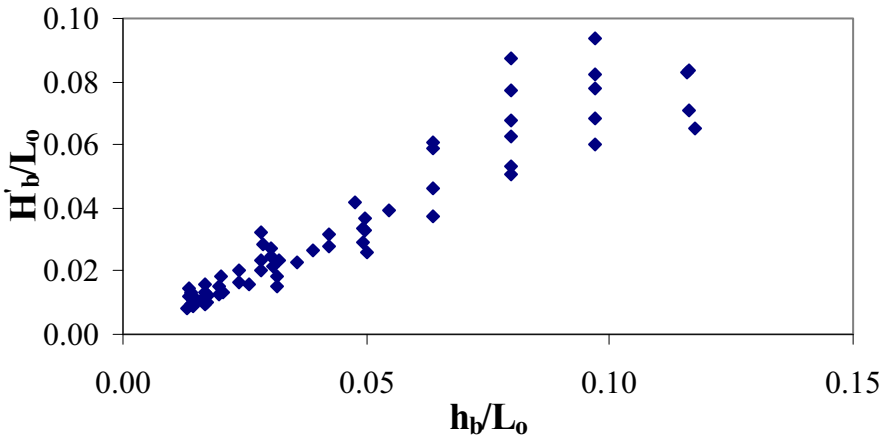

(b)

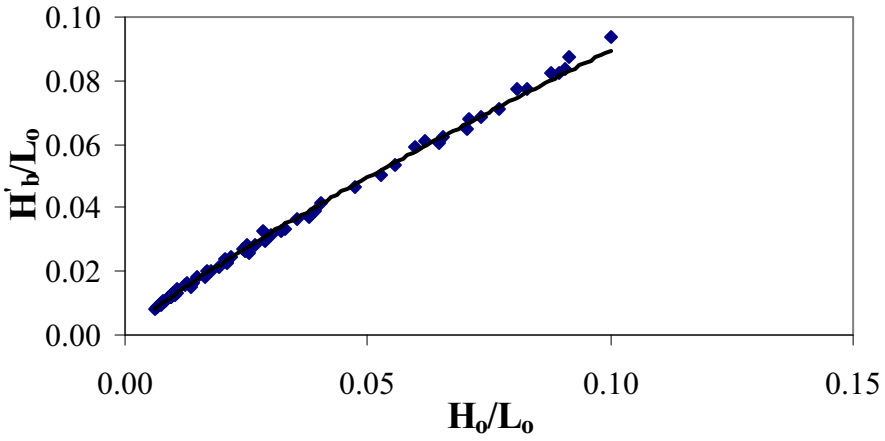

(c)

Figure 2.6. Relationships between H_b' / L_o and (a) h_b / L_b, (b) h_b / L_o, (c) H_o / L_o for the case of breaking wave on step beach (laboratory data from Hattori and Aono, 1985; Horikawa and Kuo, 1966; and Nagayama, 1983). Solid line in figure (c) is the fitted line.

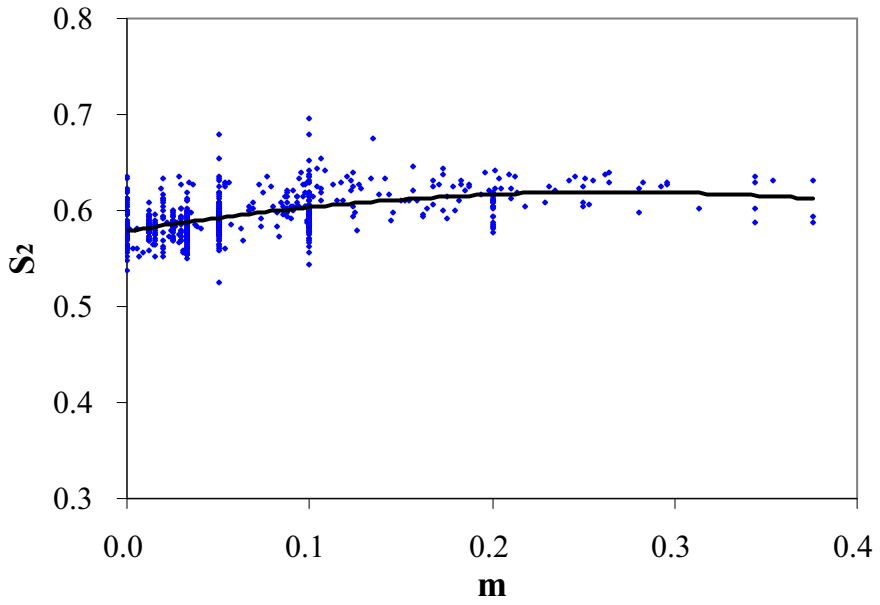

Figure 2.7. Relationship between slope effect coefficient S_2 and bottom slope m when $K_{12} = 0.83$ (laboratory data from 26 sources shown in Table 2.1). Solid line is the computed S_2 from Eq. (2.32).

III. TRANSFORMATION OF REPRESENTATIVE WAVE HEIGHTS USING REPRESENTATIVE WAVE APPROACH

3.1. Introduction

The present section concentrates the determination of three common representative wave heights, i.e. root mean square wave height (H_{rms}), significant wave height ($H_{1/3}$), and maximum wave height ($H_{\max}$). The representative wave heights (H_{rms}, $H_{1/3}$, and $H_{\max}$) are the essential required factors for the study of beach deformation and the design of coastal structures. Wave data are usually available in deepwater but not available in the shallow water at the depths required. When waves propagate to the nearshore zone, wave profiles steepen and eventually waves break. Once the waves start to break, a part of wave energy is transformed into turbulence and heat, and wave height decreases towards the shore. Irregular wave breaking is more complex than regular wave breaking. In contrast to regular waves, there is no well-defined breaking position for irregular waves. The higher wave tends to break at the greater distance from the shore. Closer to the shore, more and more waves are breaking, until in the inner surf zone almost all the waves are breaking. The representative wave heights (H_{rms}, $H_{1/3}$, and $H_{\max}$) in shallow water can be determined from a wave height transformation model. Common methods to model H_{rms}, $H_{1/3}$, and $H_{\max}$ may be classified into three approaches, i.e. individual wave approach, conversion approach, and representative wave approach.

The individual wave approach considers the propagation of individual waves in the irregular wave train. The incident individual waves may be determined from the irregular wave records or from probability density function (pdf) of wave height. The propagation of each individual wave is computed by using an appropriate regular wave model. Recombining the individual wave heights at the required depth yields the irregular wave train, which used to determine the representative wave heights (H_{rms}, $H_{1/3}$, and $H_{\max}$). Several models have been proposed based on this approach, differing mainly in the regular wave model used to simulate the propagation of the individual waves (e.g. the models of Goda, 1975; Mase and Iwagaki, 1982; Mizuguchi, 1982; Dally, 1990 and 1992; Kuriyama, 1996; and Goda, 2004). This method is particularly useful if a detailed wave height distribution is required. However, it has a demerit in time-consuming, which may not suite for the practical works.

The conversion approach is used to convert the representative wave heights from one to another through the known relationships. The root mean square wave height (H_{rms}) is usually used as a reference wave height of the conversion because it is the output of many wave models (e.g. the models of Battjes and Janssen, 1978; Thornton and Guza, 1983; Larson, 1995; and Rattanapitikon, 2007). Therefore, the other representative wave heights ($H_{1/3}$ and $H_{\max}$) can be determined from the known relationships between the representative wave heights (e.g. the relationships of Longuet-Higgins, 1952; Battjes and Groenendijk, 2000; and Rattanapitikon and Shibayama, 2007).

The representative wave approach considers only the propagation of the representative wave height. This method has a merit of simple calculation, but it may have the demerit of containing a possible large estimate error when applying to compute H_{rms}, $H_{1/3}$, and $H_{\max}$. However, Rattanapitikon et al. (2003) showed that by using an appropriate energy

dissipation model with new coefficients, the representative wave approach can be used to compute the *rms* wave height (H_{rms}) transformation with good accuracy. Therefore, it may be possible to use the representative wave approach to predict the transformation of $H_{1/3}$, and $H_{\max}$. This chapter is carried out to investigate the possibility of using the representative wave approach and find out a suitable dissipation model that can be used to compute H_{rms}, $H_{1/3}$, and $H_{\max}$.

3.2. Transformation of Root Mean Square Wave Height

The transformation of root mean square (*rms*) wave heights has been a subject of study for decades because of its importance in studying beach deformations and the design of coastal structures. When waves propagate to the nearshore zone, wave profiles steepen and eventually waves break. The higher waves tend to break at the greater distance from the shore. Closer to the shore, more and more waves are breaking, until in the inner surf zone almost all the waves are breaking. Once the waves start to break, a part of the wave energy is transformed into turbulence and heat, and wave height decreases towards the shore.

Common methods to model irregular wave height transformation can be classified into three main approaches, i.e. representative wave approach, spectral approach, and probabilistic approach. For computing beach deformation, the wave model should be kept as simple as possible because of the frequent updating of wave field to account for the change of bottom profiles. The representative wave approach seems to be suitable for the beach deformation models. The approach relies on the macroscopic features of breaking waves and predict only the transformation of *rms* wave height. The *rms* wave height transformation is computed from the energy flux conservation law as:

$$\frac{\partial\left(Ec_g \cos\theta\right)}{\partial x} = -D_B \tag{3.1}$$

where E is the wave energy density, c_g is the group velocity, θ is the mean wave angle, x is the distance in cross shore direction, and D_B is the energy dissipation rate due to wave breaking which is zero outside the surf zone. The energy dissipation rate due to bottom friction is neglected. In the present study, all variables are based on the linear wave theory.

Snell's law is employed to describe wave refraction.

$$\frac{\sin\theta}{c} = \text{constant} \tag{3.2}$$

where c is the phase velocity.

From the linear wave theory, the wave energy density (E) is equal to $\rho g H_{rms}^2 / 8$. Therefore, Eq. (3.1) can be written in terms of *rms* wave height as:

$$\frac{\rho g}{8}\frac{\partial\left(H_{rms}^2 c_g \cos\theta\right)}{\partial x} = -D_B \tag{3.3}$$

where H_{rms} is the *rms* wave height.

The *rms* wave height transformation can be computed from the energy flux balance equation [Eq. (3.3)] by substituting the model of energy dissipation rate (D_B) and numerically integrating from offshore to shoreline. In the offshore zone, the energy dissipation rate is set to zero. The main difficulty of Eq. (3.3) is how to formulate the energy dissipation rate caused by the breaking waves.

During the past decades, various energy dissipation models have been proposed for computing H_{rms} in the surf zone. Because of the complexity of the wave breaking

mechanism, most of the energy dissipation models were developed based on the empirical or semi-empirical approach. To make an empirical formula reliable, it has to be calibrated or verified with a wide range of experimental conditions. However, most of the previous models were developed with limited experimental conditions. Therefore, their validity may be limited according to the range of experimental conditions that were employed in calibration or verification. Moreover, since the models are different, the computed results from various models should differ from each other and from the measured data. No direct study has been made to describe clearly the accuracy of each model on the estimation of H_{rms} for a wide range of experimental conditions. It is not clear which model is suitable for computing the transformation of H_{rms}. The main objective of this study is to find out the suitable models that predict well for a wide range of experimental conditions.

This section is divided into six main parts. The first part describes the collected data. The second part briefly reviews the existing dissipation models. The third part is examination of existing models. The fourth part is recalibration and comparison of the existing models for identifying the suitable models. The fifth part describes the modification of the existing models. The last part describes the development of the new model.

3.2.1. Collected experimental data

The experimental data of *rms* wave height transformation from 13 sources, covering 1723 cases of wave and bottom conditions, have been collected for examination of the dissipation models. The experiments cover a wide range of wave and bottom topography conditions, including small-scale, large-scale and field experiments. The experiments cover a variety of beach conditions and cover a range of deepwater wave steepness (H_{rmso}/L_o) from 0.0007 to 0.0588. A summary of the collected laboratory data is given in Table 3.1. Most of the data sources are the same as that used by Rattanapitikon et al. (2003). The additional data are from the DELILAH project (Birkemeier et al., 1997) and DUCK94 project (Herbers et al. 2006). A brief summary of the DELILAH and DUCK94 projects are summarized below.

DELILAH (Duck Experiment on Low-frequency and Incident-band Longshore and Across-shore Hydrodynamics) project was conducted on the barred beach in Duck, North Carolina, USA in October 1990. The objective of the project is to improve fundamental understanding and modeling of surf zone physics. The experiment emphasized surf zone hydrodynamics in the presence of a changing barred bathymetry. Nine pressure gauges were installed to measure the nearshore wave heights across-shore and one of them was in the swash zone. Tidal elevations were measured at the FRF pier. The measured wave heights are available at http://dksrv.usace.army.mi/jg/del90dir. The data of wave heights and water depths measured during Oct 2-21, 1990 are available. The wave heights and water depths data are available at approximately every 34 min. A total of 776 sets of measured wave heights and water depths are available on the data server. A data set that has only a few points of measurements is not suitable to use for verifying the models. A total of 745 data sets are considered in this study.

DUCK94 project was conducted on the barred beach in Duck, North Carolina, USA during Aug - Oct 1994. The project objective is the same as that of DELILAH. The experiment emphasized surf zone hydrodynamics, sediment transport and morphological evolution. Thirteen experiments were carried out by 19 organizations. The experiment of wave height transformation was performed by Herbers, T. H. C., Elgar, S., Guza, R. T., and O'Reilly, W. C. Thirteen pressure gauges were installed to measure the nearshore wave heights across-shore and one of them was in the swash zone. Tidal elevations were

measured at the FRF pier. The measured wave heights, and water depths are available at http://dksrv.usace.army.mi/jg/dk94dir. The wave heights data are available at approximately every 17 min while the water depths data are available at every 3 h. The wave heights and water depths at every 3 h that were measured during Aug 15 – Oct 31, 1994 are used in the present study. Excluding the data sets that have only a few points of measurements, a total of 587 data sets are considered in the present study.

Table 3.1. Summary of collected experimental data.

Sources	No of cases	No of points	Beach conditions	H_{rmso}/L_o	Apparatus
Hurue (1990)	1	7	plane beach	0.0259	Small-scale
Smith and Kraus (1990)	12	96	plane and barred beach	0.0214-0.0588	Small-scale
Sultan (1995)	1	12	plane beach	0.0042	Small-scale
Grasmeijer and Rijn (1999)	2	20	sandy beach	0.0142-0.0168	Small-scale
Hamilton and Ebersole (2001)	1	10	plane beach	0.0165	Small-scale
Ting (2001)	1	7	plane beach	0.0161	Small-scale
Kraus and Smith (1994): SUPERTANK project	128	2,223	sandy beach	0.0011-0.0452	Large-scale
Roelvink and Reniers (1995): LIP 11D project	95	923	sandy beach	0.0039-0.0279	Large-scale
Dette et al. (1998): MAST III – SAFE project	138	3,559	sandy beach	0.0061-0.0147	Large-scale
Thornton and Guza (1986)	4	60	sandy beach	0.0012-0.0013	field
Kraus et al. (1989): DUCK85 project	8	90	sandy beach	0.0007-0.0018	field
Birkemeier et al. (1997): DELILAH project	745	5,049	sandy beach	0.0007-0.0254	field
Herbers et al. (2006): DUCK94 project	587	6,104	sandy beach	0.0009-0.0290	field
Total	1,723	18,160		0.0007-0.0588	

3.2.2. Existing energy dissipation models

During the past decades, various energy dissipation models have been developed based on the parametric approach and the representative wave approach. Brief reviews of some existing dissipation models are described below.

a) Battjes and Janssen (1978), hereafter referred to as BJ78, proposed to compute D_B by multiplying the fraction of irregular breaking waves (Q_b) by the energy dissipation of a single broken wave. The energy dissipation of a broken wave is described by the bore analogy and assuming that all broken waves have a height equal to breaking wave height (H_b) as:

$$D_B = K_1 Q_b \frac{\rho g H_b^2}{4T_p} \tag{3.4}$$

where T_p is the spectral peak period, and K_1 is the coefficient introduced to account for the difference between breaking wave and hydraulic jump. The published value of K_1 is 1.0. The fraction of breaking waves (Q_b) was derived based on the assumption that the probability density function (pdf) of wave height could be modeled with a Rayleigh

distribution truncated at the breaking wave height (H_b) and all broken waves have a height equal to the breaking wave height. The result is

$$\frac{1-Q_b}{-\ln Q_b}=\left(\frac{H_{rms}}{H_b}\right)^2 \tag{3.5}$$

in which the breaking wave height (H_b) is determined from the formula of Miche (1944) with additional constant (K_3).

$$H_b = K_2 L \tanh\left(K_3 kh\right) \tag{3.6}$$

where L is the wavelength related to T_p, k is the wave number, h is the water depth, and K_2 and K_3 are the coefficients. Based on their laboratory data, the coefficients K_2 and K_3 are determined at 0.14 and 0.91 respectively. This model is widely used for computing D_B. However the additional constant K_3 may be changed slightly for the best fit with other experimental data, e.g. it is determined at 0.89 for Oliveira (2007).

Since Eq. (3.5) is an implicit equation, an iteration process is necessary to compute the fraction of breaking waves (Q_b). It will be more convenient if we can compute Q_b from the explicit form of Eq. (3.5). Rattanapitikon and Shibayama (1998) proposed the explicit form of Q_b based on multiple regression analysis (with correlation coefficient $R^2 = 0.999$) as:

$$Q_b = \begin{cases} 0 & for \quad \dfrac{H_{rms}}{H_b} \le 0.43 \\ 1.785\left(\dfrac{H_{rms}}{H_b}\right)^3 - 0.280\left(\dfrac{H_{rms}}{H_b}\right)^2 - 0.738\left(\dfrac{H_{rms}}{H_b}\right) + 0.235 & for \quad 0.43 < \dfrac{H_{rms}}{H_b} < 1.0 \\ 1 & for \quad \dfrac{H_{rms}}{H_b} \ge 1.0 \end{cases} \tag{3.7}$$

As Eqs. (3.5) and (3.7) give almost identical results ($R^2 = 0.999$), for convenience, Eq. (3.7) is used in this study.

b) Thornton and Guza (1983), hereafter referred to as TG83, proposed to compute D_B by integrating from 0 to ∞ the product of the dissipation for a single broken wave and the pdf of the breaking wave height. The energy dissipation of a single broken wave is described by the bore model, which is slightly different from the bore model of BJ78. The pdf of breaking wave height is expressed as a weighting of the Rayleigh distribution. By introducing the formula of the weighting, a model of D_B was proposed.

$$D_B = K_4 \frac{3\sqrt{\pi}}{4}\left(\frac{H_{rms}}{H_b}\right)^2 \left\{1-\frac{1}{\left[1+\left(H_{rms}/H_b\right)^2\right]^{2.5}}\right\}\frac{\rho g H_{rms}^3}{4T_p h} \tag{3.8}$$

where K_4 is the coefficient introduced to account for the difference between breaking wave and hydraulic jump. The published value of K_4 is 0.51 for laboratory data. The breaker height (H_b) is determined from the following formula.

$$H_b = K_5 h \tag{3.9}$$

where K_5 is the coefficient of depth limit breaker height. The published value of K_5 is 0.42.

c) Battjes and Stive (1985), hereafter referred to as BS85, used the same energy dissipation model as that of BJ78.

$$D_B = K_6 Q_b \frac{\rho g H_b^2}{4T_p} \tag{3.10}$$

where K_6 is the coefficient. The published value of K_6 is 1.0, and Q_b is computed from Eq. (3.7). They modified the model of BJ78 by recalibrating the coefficient K_3 in the breaker height formula [Eq. (3.6)]. The coefficient K_3 was related to the deepwater wave steepness (H_{rmso} / L_o). After calibration, the breaking wave height was modified to be:

$$H_b = K_7 L \tanh\left\{\left[K_8 + K_9 \tanh\left(K_{10} \frac{H_{rmso}}{L_o}\right)\right] kh\right\} \tag{3.11}$$

where H_{rmso} is the deepwater *rms* wave height, L_o is the deepwater wavelength and K_7 to K_{10} are the coefficients. The published values of K_7 to K_{10} are 0.140, 0.57, 0.45, and 33 respectively. Hence, the model of BS85 is similar to that of BJ78 except for the formula of H_b.

d) Southgate and Nairn (1993), hereafter referred to as SN93, modified the model of BJ78 by changing the expression of energy dissipation of a single broken wave from the bore model of BJ78 to be the bore model of TG83 as:

$$D_B = K_{11} Q_b \frac{\rho g H_b^3}{4T_p h} \tag{3.12}$$

where K_{11} is the coefficient. The published value of K_{11} is 1.0 and Q_b is computed from Eq. (3.7). The breaker height (H_b) is determined from the formula of Nairn (1990) as:

$$H_b = h\left[K_{12} + K_{13} \tanh\left(K_{14} \frac{H_{rmso}}{L_o}\right)\right] \tag{3.13}$$

where K_{12} to K_{14} are the coefficients. The published values of K_{12} to K_{14} are 0.39, 0.56, and 33 respectively**.**

e) Baldock et al. (1998), hereafter referred to as BHV98, proposed to compute D_B by integrating from H_b to ∞ the product of the dissipation for a single broken wave and the *pdf* of the wave height. The energy dissipation of a single broken wave is described by the bore analogy of BJ78. The *pdf* of wave height inside the surf zone was assumed to be the Rayleigh distribution.

$$D_B = K_{15} \exp\left[-\left(\frac{H_b}{H_{rms}}\right)^2\right] \frac{\rho g\left(H_b^2 + H_{rms}^2\right)}{4T_p} \qquad \text{for } H_{rms} < H_b \tag{3.14a}$$

$$D_B = K_{15} \exp[-1] \frac{\rho g 2H_b^2}{4T_p} \qquad \text{for } H_{rms} \geq H_b \tag{3.14b}$$

The published coefficient K_{15} is 1.0. The breaker height (H_b) is determined from the formula of Nairn (1990) as:

$$H_b = h\left[K_{16} + K_{17} \tanh\left(K_{18} \frac{H_{rmso}}{L_o}\right)\right] \tag{3.15}$$

where K_{16} to K_{18} are the coefficients. The published values of K_{16} to K_{18} are 0.39, 0.56, and 33 respectively**.**

f) Rattanapitikon and Shibayama (1998), hereafter referred to as RS98, modified the model of BJ78 by changing the expression of energy dissipation of a single broken wave from the bore concept to the stable energy concept,

$$D_B = K_{19} Q_b \frac{c_g \rho g}{8h}\left[H_{rms}^2 - \left(h \exp(-K_{20} - K_{21}\frac{h}{\sqrt{LH_{rms}}}) \right)^2 \right] \tag{3.16}$$

where K_{19} to K_{21} are the coefficients. The published values of K_{19} to K_{21} are 0.10, 0.58, and 2.0 respectively. The fraction of breaking wave (Q_b) is computed from Eq. (3.7). The breaking wave height (H_b) is computed by using the breaking criteria of Goda (1970) as:

$$H_b = K_{22} L_o \left\{ 1 - \exp\left[-1.5\frac{\pi h}{L_o}\left(1 + 15m^{4/3}\right) \right] \right\} \tag{3.17}$$

where m is the average bottom slope and K_{22} is the coefficient. The published value of K_{22} is 0.10.

g) Ruessink et al. (2003) hereafter referred to as RWS03, used the same energy dissipation model as that of BHV98.

$$D_B = K_{23} \exp\left[-\left(\frac{H_b}{H_{rms}} \right)^2 \right] \frac{\rho g\left(H_b^2 + H_{rms}^2\right)}{4T_p} \qquad \text{for } H_{rms} < H_b \tag{3.18a}$$

$$D_B = K_{23} \exp[-1] \frac{\rho g 2H_b^2}{4T_p} \qquad \text{for } H_{rms} \geq H_b \tag{3.18b}$$

where K_{23} is the coefficient and the published value of K_{23} is 1.0. The breaker height formula of BJ78 [Eq. (3.6)] is used to determine H_b. The coefficient K_3 in Eq. (3.6) was related to the product of wave number and water depth (kh). After calibration, the breaker height formula was modified to be:

$$H_b = K_{24} L \tanh\left[\left(K_{25} kh + K_{26} \right) kh \right] \tag{3.19}$$

where K_{24} to K_{26} are the coefficients. The published values of K_{24} to K_{26} are 0.14, 0.86, and 0.33 respectively. Hence, the model of RWS03 is similar to that of BHV98 except for the formula of H_b.

h) Rattanapitikon et al. (2003) hereafter referred to as RKS03, applied the dissipation model for regular wave for computing the dissipation for irregular waves.

$$D_B = K_{27} \frac{\rho g c_g}{8h}\left[H_{rms}^2 - \left(K_{28} H_b \right)^2 \right] \tag{3.20}$$

where K_{27} and K_{28} are the coefficients. The published values of K_{27} and K_{28} are 0.12 and 0.42. The breaker height (H_b) is computed by using the breaking criteria of Miche (1944) as

$$H_b = K_{29} L \tanh(kh) \tag{3.21}$$

where K_{29} is the coefficient. The published value of K_{29} is 0.14. The greatest asset of RKS03's model is its simplicity and ease of application. The model was developed based on the representative wave approach while other models were developed based on the parametric approach.

3.2.3. Examination of existing models

The objective of this section is to examine the applicability of the eight existing dissipation models on simulating H_{rms}. The measured *rms* wave heights from 13 sources (total 1723 cases) of published experimental results (shown in Table 3.1) are used to examine the existing models.

The *rms* wave height transformation is computed by numerical integration of the energy flux balance equation [Eq. (3.3)] with the energy dissipation rate of the existing models [Eqs. (3.4), (3.8), (3.10), (3.12), (3.14), (3.16), (3.18), and (3.20)]. A backward finite difference scheme is used to solve the energy flux balance equation [Eq. (3.3)].

The basic parameter for determination of the overall accuracy of a model is the average *rms* relative error (ER_{avg}), which is defined as:

$$ER_{avg} = \frac{\sum_{j=1}^{tn} ER_{gj}}{tn} \tag{3.22}$$

where ER_{gj} is the *rms* relative error of the data group j (the group number), and tn is the total number of groups. The small value of ER_{avg} indicates good overall accuracy of the model.

The group *rms* relative error (ER_g) is defined as:

$$ER_g = 100\sqrt{\frac{\sum_{i=1}^{ng}(H_{ci} - H_{mi})^2}{\sum_{i=1}^{ng} H_{mi}^2}} \tag{3.23}$$

where i is the wave height number, H_{ci} is the computed wave height of number i, H_{mi} is the measured wave height of number i, and ng is the total number of measured wave heights in each data group.

The collected experiments are separated into three groups according to the experiment scale, i.e. small-scale, large-scale, and field experiments. It is expected that a good model should be able to predict well for the three groups of experiment scale. Therefore, the average error (ER_{avg}) from the three groups of experiment scale are used as a main criteria to verify the models.

Using the default coefficients ($K_1 - K_{29}$) in the computations, the errors (ER_g and ER_{avg}) of each dissipation model for three groups of experiment scale have been computed and shown in Table 3.2.

It can be seen from Table 3.2 that the model of BS85 is the best. The overall accuracy of models in descending order are the models of BS85, RS98, RKS03, RWS03, BHV98, SN93, BJ78, and TG83. Because most models were developed based on the limited experimental conditions, the coefficients in the models may not be the optimal values. Therefore, the errors in Table 3.2 should not be used to judge the applicability of the selected models. The coefficients in all models should be recalibrated before comparing the applicability of the models.

Table 3.2. The errors ER_g and ER_{avg} of the existing models for three groups of experiment scale (using the default coefficients).

Apparatus	Models							
	BJ78 (Eq. 3.4)	TG83 (Eq.3.8)	BS85 (Eq. 3.10)	SN93 (Eq. 3.12)	BHV98 (Eq. 3.14)	RS98 (Eq.3.16)	RWS03 (Eq.3.18)	RKS03 (Eq.3.20)
Small-scale	9.1	21.2	7.4	11.9	10.6	9.4	11.7	8.0
Large-scale	11.0	8.8	7.3	10.1	6.8	7.3	8.2	8.9
Field	18.0	11.3	10.4	14.7	13.5	10.1	10.1	12.9
ER_{avg}	12.7	13.8	8.3	12.3	10.3	8.9	10.0	9.9

3.2.4. Model calibration and comparison

The measured data shown in Table 3.1 are used to calibrate the coefficients ($K_1 - K_{29}$) in the dissipation models. The calibrations are conducted by gradually adjusting the coefficients $K_1 - K_{29}$ until the minimum error (ER_{avg}) of each model is obtained. The optimum values of $K_1 - K_{29}$ are shown in the third column of Table 3.3.

Table 3.3. Default and calibrated coefficients of the existing models.

Models	Default Coefficients	Calibrated Coefficients
BJ78 (Eq. 3.4)	$K_1 = 1.0,\ K_2 = 0.14,\ K_3 = 0.91$	$K_1 = 0.92,\ K_2 = 0.14,\ K_3 = 0.76$
TG83 (Eq. 3.8)	$K_4 = 1.0,\ K_5 = 0.42$	$K_4 = 0.10,\ K_5 = 0.168$
BS85 (Eq. 3.10)	$K_6 = 1.0,\ K_7 = 0.14,\ K_8 = 0.57,$ $K_9 = 0.45,\ K_{10} = 33$	$K_6 = 1.0,\ K_7 = 0.14,\ K_8 = 0.57,$ $K_9 = 0.51,\ K_{10} = 28$
SN93 (Eq. 3.12)	$K_{11} = 1.0,\ K_{12} = 0.39,\ K_{13} = 0.56,$ $K_{14} = 33$	$K_{11} = 1.40,\ K_{12} = 0.46,\ K_{13} = 0.55,$ $K_{14} = 21$
BHV98 (Eq.3.14)	$K_{15} = 1.0,\ K_{16} = 0.39,\ K_{17} = 0.56,$ $K_{18} = 33$	$K_{15} = 1.06,\ K_{16} = 0.50,\ K_{17} = 0.28,$ $K_{18} = 43$
RS98 (Eq. 3.16)	$K_{19} = 0.10,\ K_{20} = 0.58,\ K_{21} = 2.0,$ $K_{22} = 0.10$	$K_{19} = 0.08,\ K_{20} = 0,\ K_{21} = 7.3,$ $K_{22} = 0.105$
RWS03 (Eq. 3.18)	$K_{23} = 1.0,\ K_{24} = 0.14,\ K_{25} = 0.86,$ $K_{26} = 0.33$	$K_{23} = 1.05,\ K_{24} = 0.14,\ K_{25} = 0.70,$ $K_{26} = 0.45$
RKS03 (Eq.3.20)	$K_{27} = 0.12,\ K_{28} * K_{29} = 0.0588$	$K_{27} = 0.07,\ K_{28} * K_{29} = 0.047$

Using the calibrated coefficients in the computations, the errors (ER_g and ER_{avg}) of each dissipation model for three groups of experiment scale have been computed and shown in Table 3.4. The results can be summarized as follows:

(a) After calibrations, the accuracy of most models (except BS85) are improved significantly, while the accuracy of BS85 is slightly improved. This shows that the coefficients in the existing models are not the optimal values.
(b) The errors of the existing models for three groups of experiment scale are not much different. It means that those models may not have scale effect.
(c) The overall accuracy of models in descending order are the models of BS85, RS98, RKS03, BHV98, RWS03, SN93, BJ78, and TG83.

(d) Considering the overall accuracy of all models in Table 3.4, it can be concluded that all selected models can be used for practical work ($8.2 \le ER_{avg} \le 11.4$). However, lesser error is better. The model that gives very good prediction (with ER_{avg} of 8.2%) is the model of BS85. The model gives very good predictions on the laboratory experiments and good predictions on the field experiments.

Table 3.4. The errors ER_g and ER_{avg} of the existing models for three groups of experiment scale (using the calibrated coefficients).

Apparatus	Models							
	BJ78 (Eq. 3.4)	TG83 (Eq.3.8)	BS85 (Eq. 3.10)	SN93 (Eq. 3.12)	BHV98 (Eq. 3.14)	RS98 (Eq.3.16)	RWS03 (Eq.3.18)	RKS03 (Eq.3.20)
Small-scale	11.3	13.0	7.1	9.7	9.3	8.7	10.6	8.7
Large-scale	8.1	8.0	7.2	7.9	6.6	7.2	7.8	7.4
Field	12.4	13.2	10.4	10.9	10.3	9.3	9.7	9.7
ER_{avg}	10.6	11.4	8.2	9.5	8.7	8.4	9.4	8.6

3.2.5. Model modification

Although the existing models give overall good predictions, they may be modified for better predictions. Following the works of BS85 and RWS03, the modification is carry out by changing the breaker height (H_b) formula in each dissipation model. All of the H_b and D_B formulas shown in section 3 will be used in this section. It can be seen from section 3 that there are seven formulas for H_b [Eqs. (3.6), (3.9), (3.11), (3.13), (3.17), (3.19), and (3.21)] and six formulas for D_B [Eqs. (3.4), (3.8), (3.12), (3.14), (3.16), and (3.20)]. Equations (3.10), (3.15), and (3.18) have been left out of the lists because they are the same as Eqs. (3.4), (3.13), and (3.14), respectively.

Substituting the seven formulas of H_b into the six existing dissipation models, 42 possible models are considered in this section. Table 3.5 shows the combination of H_b and D_B formulas for the 42 possible dissipation models and 8 of which are the existing models (M1, M3, M9, M18, M25, M27, M33, and M42). The calibration of possible dissipation models are performed by using the measured data shown in Table 3.1. The calibrations are conducted by gradually adjusting the coefficients until the minimum error (ER_{avg}) of each model is obtained. The calibrated coefficients and average errors (ER_{avg}) from three groups of experiment scale are shown in the fourth and fifth columns of Table 3.5. The results can be summarized as follows:

(a) The accuracy of most existing models (except BS85) can be improved by changing the breaker height (H_b) formula. The model of BS85 (M3) already has a suitable combination of the formulas for H_b and D_B.

(b) The H_b formula of BS85 [Eq. (3.11)] is suitable for all D_B formulas while the H_b formulas of BJ78 [Eq. (3.6)] and BHV98 [Eq. (3.19)] are suitable for the D_B formula of RKS03 [Eq. (3.20)].

(c) There are six models (M3, M24, M31, M36, M38, and M41) that give very good accuracy (with ER_{avg} of about 8.1-8.2%) and three of them are from the D_B formula of the representative wave approach [Eq. (3.20)].

Table 3.5. Calibrated coefficients and average errors ER_{avg} of all 42 possible dissipation models.

Model No.	D_B formulas	H_b formulas	Calibrated coefficients	ER_{avg}
M1	Eq. (3.4)	Eq. (3.6)	$K_1 = 0.92,\ K_2 = 0.14,\ K_3 = 0.76$	10.6
M2		Eq. (3.9)	$K_1 = 0.94,\ K_5 = 0.63$	10.6
M3		Eq. (3.11)	$K_1 = 1.0,\ K_7 = 0.14,\ K_8 = 0.57,\ K_9 = 0.51,\ K_{10} = 28$	8.2
M4		Eq. (3.13)	$K_1 = 1.0,\ K_{12} = 0.48,\ K_{13} = 0.33,\ K_{14} = 36$	9.0
M5		Eq. (3.17)	$K_1 = 0.92,\ K_{22} = 0.14$	10.6
M6		Eq. (3.19)	$K_1 = 1.0,\ K_{24} = 0.14,\ K_{25} = 0.78,\ K_{26} = 0.40$	9.7
M7		Eq. (3.21)	$K_1 = 1.0,\ K_{29} = 0.12$	11.7
M8	Eq. (3.8)	Eq. (3.6)	$K_4 = 0.24,\ K_2 = 0.049,\ K_3 = 0.86$	11.5
M9		Eq. (3.9)	$K_4 = 0.1,\ K_5 = 0.168$	11.4
M10		Eq. (3.11)	$K_4 = 0.38,\ K_7 = 0.065,\ K_8 = 0.45,\ K_9 = 1.10,\ K_{10} = 20$	8.4
M11		Eq. (3.13)	$K_4 = 0.21,\ K_{12} = 0.14,\ K_{13} = 0.31,\ K_{14} = 19$	8.7
M12		Eq. (3.17)	$K_4 = 0.43,\ K_{22} = 0.069$	11.2
M13		Eq. (3.19)	$K_4 = 0.22,\ K_{24} = 0.04,\ K_{25} = 0.80,\ K_{26} = 0.70$	11.2
M14		Eq. (3.21)	$K_4 = 0.25,\ K_{29} = 0.044$	11.7
M15	Eq. (3.12)	Eq. (3.6)	$K_{11} = 1.40,\ K_2 = 0.13,\ K_3 = 0.82$	10.5
M16		Eq. (3.9)	$K_{11} = 1.31,\ K_5 = 0.62$	10.1
M17		Eq. (3.11)	$K_{11} = 1.43,\ K_7 = 0.14,\ K_8 = 0.55,\ K_9 = 0.47,\ K_{10} = 32$	8.7
M18		Eq. (3.13)	$K_{11} = 1.40,\ K_{12} = 0.46,\ K_{13} = 0.55,\ K_{14} = 21$	9.5
M19		Eq. (3.17)	$K_{11} = 1.36,\ K_{22} = 0.137$	10.3
M20		Eq. (3.19)	$K_{11} = 1.52,\ K_{24} = 0.14,\ K_{25} = 0.84,\ K_{26} = 0.36$	10.0
M21		Eq. (3.21)	$K_{11} = 1.48,\ K_{29} = 0.11$	10.8
M22	Eq. (3.14)	Eq. (3.6)	$K_{15} = 1.15,\ K_2 = 0.15,\ K_3 = 0.76$	10.5
M23		Eq. (3.9)	$K_{15} = 1.05,\ K_5 = 0.66$	10.0
M24		Eq. (3.11)	$K_{15} = 1.24,\ K_7 = 0.15,\ K_8 = 0.59,\ K_9 = 0.51,\ K_{10} = 25$	8.1
M25		Eq. (3.13)	$K_{15} = 1.06,\ K_{12} = 0.50,\ K_{13} = 0.28,\ K_{14} = 43$	8.7
M26		Eq. (3.17)	$K_{15} = 1.22,\ K_{22} = 0.15$	10.6
M27		Eq. (3.19)	$K_{15} = 1.05,\ K_{24} = 0.14,\ K_{25} = 0.70,\ K_{26} = 0.45$	9.4
M28		Eq. (3.21)	$K_{15} = 1.43,\ K_{29} = 0.13$	11.7

Table 3.5 (cont.). Calibrated coefficients and average errors ER_{avg} of all 42 possible dissipation models.

Model No.	D_B formulas	H_b formulas	Calibrated coefficients	ER_{avg}
M29	Eq. (3.16)	Eq. (3.6)	$K_{19}=0.07,\ K_{20}=1.0,\ K_{21}=3.6,\ K_2=0.09,\ K_3=0.88$	8.8
M30		Eq. (3.9)	$K_{19}=0.08,\ K_{20}=0.36,\ K_{21}=3.9,\ K_5=0.47$	8.9
M31		Eq. (3.11)	$K_{19}=0.10,\ K_{20}=0.55,\ K_{21}=2.1,\ K_7=0.10,\ K_8=0.56,\ K_9=0.45,\ K_{10}=33$	8.2
M32		Eq. (3.13)	$K_{19}=0.10,\ K_{20}=0.37,\ K_{21}=2.3,\ K_{12}=0.25,\ K_{13}=0.24,\ K_{14}=80$	8.8
M33		Eq. (3.17)	$K_{19}=0.08,\ K_{20}=0,\ K_{21}=7.3,\ K_{22}=0.105$	8.4
M34		Eq. (3.19)	$K_{19}=0.07,\ K_{20}=0.66,\ K_{21}=1.9,\ K_{24}=0.09,\ K_{25}=0.65,\ K_{26}=0.44$	8.4
M35		Eq. (3.21)	$K_{19}=0.06,\ K_{20}=2.6,\ K_{21}=2.2,\ K_{29}=0.079$	8.8
M36	Eq. (3.20)	Eq. (3.6)	$K_{27}=0.07,\ K_{28}*K_2=0.066,\ K_3=0.68$	8.2
M37		Eq. (3.9)	$K_{27}=0.07,\ K_{28}*K_5=0.266$	8.4
M38		Eq. (3.11)	$K_{27}=0.07,\ K_{28}*K_7=0.061,\ K_8=0.63,\ K_9=0.21,\ K_{10}=39$	8.2
M39		Eq. (3.13)	$K_{27}=0.07,\ K_{28}*K_{12}=0.266,\ K_{13}=0,\ K_{14}=33$	8.4
M40		Eq. (3.17)	$K_{27}=0.08,\ K_{28}*K_{22}=0.061$	8.4
M41		Eq. (3.19)	$K_{27}=0.07,\ K_{28}*K_{24}=0.047,\ K_{25}=0.44,\ K_{26}=0.78$	8.2
M42		Eq. (3.21)	$K_{27}=0.07,\ K_{28}*K_{29}=0.047$	8.6

Substituting the calibrated coefficients into the formulas of D_B and H_b, the top six models that give very good prediction (with ER_{avg} of about 8.1-8.2%) can be written as:

M3 (BS85):
$$D_B = Q_b \frac{\rho g H_b^2}{4T_p} \tag{3.24}$$

in which the fraction of breaking wave (Q_b) is computed from Eq. (3.7). The breaker height (H_b) is computed by using the breaker height formula of BS85 as:

$$H_b = 0.14L\tanh\left\{\left[0.57+0.51\tanh\left(28\frac{H_{rmso}}{L_o}\right)\right]kh\right\} \tag{3.25}$$

M24:
$$D_B = 1.24\exp\left[-\left(\frac{H_b}{H_{rms}}\right)^2\right]\frac{\rho g\left(H_b^2+H_{rms}^2\right)}{4T_p} \quad \text{for } H_{rms} < H_b \tag{3.26a}$$

$$D_B = 1.24\exp[-1]\frac{\rho g 2H_b^2}{4T_p} \quad \text{for } H_{rms} \geq H_b \tag{3.26b}$$

in which the breaker height (H_b) is determined from the breaker height formula of BS85 as:

$$H_b = 0.15L\tanh\left\{\left[0.59 + 0.51\tanh\left(25\frac{H_{rmso}}{L_o}\right)\right]kh\right\} \tag{3.27}$$

M31:
$$D_B = 0.1Q_b\frac{c_g\rho g}{8h}\left[H_{rms}^2 - \left(h\exp(-0.55 - 2.1\frac{h}{\sqrt{LH_{rms}}})\right)^2\right] \tag{3.28}$$

in which the fraction of breaking wave (Q_b) is computed from Eq. (3.7). The breaker height (H_b) is computed by using the breaker height formula of BS85 as:

$$H_b = 0.1L\tanh\left\{\left[0.56 + 0.45\tanh\left(33\frac{H_{rmso}}{L_o}\right)\right]kh\right\} \tag{3.29}$$

M36:
$$D_B = 0.07\frac{\rho g c_g}{8h}\left[H_{rms}^2 - \left(0.066L\tanh\left(0.68kh\right)\right)^2\right] \tag{3.30}$$

M38:
$$D_B = 0.07\frac{\rho g c_g}{8h}\left[H_{rms}^2 - \left(0.061L\tanh\left(0.63kh + 0.21kh\tanh\left(39\frac{H_{rmso}}{L_o}\right)\right)\right)^2\right] \tag{3.31}$$

M41:
$$D_B = 0.07\frac{\rho g c_g}{8h}\left[H_{rms}^2 - \left(0.047L\tanh\left(0.44\left(kh\right)^2 + 0.78kh\right)\right)^2\right] \tag{3.32}$$

Overall, the six models (M3, M24, M31, M36, M38, and M41) give nearly the same accuracy. It may be interesting to see the comparison in more detail. Table 3.6 shows the errors of the six models for three groups of experiment scale while Table 3.7 shows the errors for 13 groups of data sources. The results can be summarized as follows:

(a) It can be seen from Tables 3.6 and 3.7 that no model gives significantly better results than the others. However, considering the consistency of the models through the variance of errors in Table 3.7, the model M36 seem to be slightly better than the others.

(b) Although overall errors (ER_{avg}) of all models are very good, the models do not predict very well for all sources of data.

(c) Because of the simplicity of the representative wave approach, it is expected that this approach will give lesser accuracy than that of the parametric approach. However, the results show that the accuracy of the models of the representative approach (M36, M38, and M41) are almost the same as those of the parametric wave approach (M3, M24, and M31). This may lead to the conclusion that the concept of representative wave approach can be used for computing the irregular wave height transformation.

(d) The greatest asset of the representative approach is its simplicity and ease of application, i.e. the *rms* wave height transformation in the nearshore zone can be computed by using only one equation [e.g. Eq. (3.30)]. Therefore, the dissipation models from the representative wave approach (M36, M38, and M41) are suitable to use in the computation of irregular wave height transformation.

(e) Considering accuracy, variance of errors, and simplicity of the possible models, the model M36 [Eq. (3.30)] seems to be the most attractive model.

Table 3.6. The errors ER_g and ER_{avg} of the six suitable models for three groups of experiment scale.

Apparatus	Models					
	M3 Eq. (3.24)	M24 Eq. (3.26)	M31 Eq. (3.28)	M36 Eq. (3.30)	M38 Eq. (3.31)	M41 Eq. (3.32)
Small-scale	7.1	7.1	8.8	8.0	8.1	8.0
Large-scale	7.2	6.6	6.1	7.3	6.9	7.3
Field	10.4	10.4	9.7	9.4	9.7	9.2
ER_{avg}	8.2	8.1	8.2	8.2	8.2	8.2

Table 3.7. The errors ER_g of the six suitable models for each source of data.

Sources	Models					
	M3 Eq. (3.24)	M24 Eq. (3.26)	M31 Eq. (3.28)	M36 Eq. (3.30)	M38 Eq. (3.31)	M41 Eq. (3.32)
Hurue (1990)	4.6	4.3	5.4	9.7	10.7	9.9
Smith and Kraus (1990)	8.1	8.3	10.4	9.8	9.7	9.7
Sultan (1995)	13.9	12.8	14.9	11.4	14.4	13.0
Grasmeijer and Rijn (1999)	3.9	3.9	3.7	3.8	3.7	3.6
Hamilton and Ebersole (2001)	2.1	2.1	5.3	3.5	3.9	3.5
Ting (2001)	8.6	8.7	10.1	5.5	5.3	5.4
SUPERTANK project	13.6	11.3	9.7	10.5	11.0	10.7
LIP11D project	6.1	5.6	6.9	9.5	7.7	8.9
SAFE project	5.5	5.6	5.0	6.1	5.7	6.1
Thornton and Guza (1986)	14.7	16.0	9.6	9.2	9.1	8.7
DUCK85 project	12.6	11.6	12.0	13.4	18.2	17.1
DELILAH project	9.1	9.0	8.8	8.7	9.5	8.7
DUCK94 project	11.4	11.5	10.3	9.9	9.7	9.7
Variance of ER_g	16.3	15.4	9.4	8.1	15.6	12.8

3.2.6. Model development

Although the original form of existing D_B models (shown in Sec. 3.2.2) look quite different from each other and were derived based on different assumptions, most of them (except RS98) can be expressed in the same general form as the product of fraction of breaking waves (Q_b) and energy dissipation of a breaker height (D_s) as

$$D_B = Q_b D_s \tag{3.33}$$

in which Q_b is a function of H_{rms}/H_b. The existing D_B models can be summarized as follows.

a) BJ78: $D_B = Q_{b1} D_{s1}$ (3.34)

where $D_{s1} = \dfrac{\rho g H_b^2}{4T_p}$ (3.35)

$$\frac{1-Q_{b1}}{-\ln Q_{b1}} = \left(\frac{H_{rms}}{H_b}\right)^2 \tag{3.36}$$

$$H_b = 0.14 L \tanh(\gamma kh) \tag{3.37}$$

b) TG83: $D_B = Q_{b2} D_{s2}$ (3.38)

where $D_{s2} = \dfrac{\rho g H_b^3}{4 T_p h}$ (3.39)

$$Q_{b2} = 0.51 \frac{3\sqrt{\pi}}{4} \left(\frac{H_{rms}}{H_b} \right)^5 \left\{ 1 - \frac{1}{\left[1 + \left(H_{rms} / H_b \right)^2 \right]^{2.5}} \right\} \tag{3.40}$$

$$H_b = 0.42 h \tag{3.41}$$

c) BS85: $D_B = Q_{b1} D_{s1}$ (3.34)

where $D_{s1} = \dfrac{\rho g H_b^2}{4 T_p}$ (3.35)

$$\frac{1 - Q_{b1}}{-\ln Q_{b1}} = \left(\frac{H_{rms}}{H_b} \right)^2 \tag{3.36}$$

$$H_b = 0.14 L \tanh \left\{ \left[0.57 + 0.45 \tanh \left(33 \frac{H_{rmso}}{L_o} \right) \right] kh \right\} \tag{3.42}$$

d) SN93: $D_B = Q_{b1} D_{s2}$ (3.43)

where $D_{s2} = \dfrac{\rho g H_b^3}{4 T_p h}$ (3.39)

$$\frac{1 - Q_{b1}}{-\ln Q_{b1}} = \left(\frac{H_{rms}}{H_b} \right)^2 \tag{3.36}$$

$$H_b = h \left[0.39 + 0.56 \tanh \left(33 \frac{H_{rmso}}{L_o} \right) \right] \tag{3.44}$$

e) BHV98: $D_B = Q_{b3} D_{s1}$ (3.45)

where $D_{s1} = \dfrac{\rho g H_b^2}{4 T_p}$ (3.35)

$$Q_{b3} = \begin{cases} \left[1 + \left(\dfrac{H_{rms}}{H_b} \right)^2 \right] \exp \left[- \left(\dfrac{H_{rms}}{H_b} \right)^{-2} \right] & for \quad \dfrac{H_{rms}}{H_b} < 1 \\ 2 \exp[-1] & for \quad \dfrac{H_{rms}}{H_b} \geq 1 \end{cases} \tag{3.46}$$

$$H_b = h \left[0.39 + 0.56 \tanh \left(33 \frac{H_{rmso}}{L_o} \right) \right] \tag{3.44}$$

f) RS98: $D_B = 0.1 Q_{b1} \dfrac{c \rho g}{8h} \left[H_{rms}^2 - \left(h \exp(-0.58 - 2.0 \dfrac{h}{\sqrt{L H_{rms}}}) \right)^2 \right]$ (3.47)

where $\dfrac{1 - Q_{b1}}{-\ln Q_{b1}} = \left(\dfrac{H_{rms}}{H_b} \right)^2$ (3.36)

$$H_b = 0.1 L_o \left\{ 1 - \exp \left[-1.5 \frac{\pi h}{L_o} \left(1 + 15 m^{4/3} \right) \right] \right\} \tag{3.48}$$

g) RWS03: $D_B = Q_{b3} D_{s1}$ (3.45)

where $D_{s1} = \dfrac{\rho g H_b^2}{4T_p}$ (3.35)

$$Q_{b3} = \begin{cases} \left[1 + \left(\dfrac{H_{rms}}{H_b}\right)^2\right] \exp\left[-\left(\dfrac{H_{rms}}{H_b}\right)^{-2}\right] & for \quad \dfrac{H_{rms}}{H_b} < 1 \\ 2\exp[-1] & for \quad \dfrac{H_{rms}}{H_b} \geq 1 \end{cases} \quad (3.46)$$

$$H_b = 0.14 L \tanh\left[(0.86kh + 0.33)kh\right] \quad (3.49)$$

h) RKS03: $D_B = Q_{b4} D_{s3}$ (3.50)

where $D_{s3} = \dfrac{\rho g c_g H_b^2}{8h}$ (3.51)

$$Q_{b4} = 0.12\left[\left(\frac{H_{rms}}{H_b}\right)^2 - 0.42^2\right] \quad (3.52)$$

$$H_b = 0.14 L \tanh(kh) \quad (3.53)$$

Since the energy dissipation of a breaker height (D_s) is the energy dissipation of a possible maximum wave height, it may also be considered as a maximum energy dissipation or a potential energy dissipation. The fraction of breaking waves (Q_b) may also be considered as a fraction of energy dissipation. Therefore, the general form of the existing dissipation models [Eq. (3.33)] may be re-explained as a product of a fraction of energy dissipation (Q_b) and the potential energy dissipation (D_s).

As most of the existing D_B models can be expressed in the same general form [Eq. (3.33)], the model [Eq. (3.33)] is used as a starting point to develop the present model. The model of D_B consists of 3 main formulas, i.e. the formula of H_b, Q_b, and D_s. It can be seen from Sec. 2 that various formulas have been proposed for computing the three variables (H_b, Q_b, and D_s), i.e. seven formulas for H_b [Eqs. (3.37), (3.41), (3.42), (3.44), (3.48), (3.49), and (3.53)], four formulas for Q_b [Eqs. (3.36), (3.40), (3.46), and (3.52)], and three formulas for D_s [Eqs. (3.35), (3.39), and (3.51)]. It is not clear which formulas of H_b, Q_b, and D_s are suitable for modeling D_B (or computing H_{rms}). The objective of this section is to determine suitable formulas of H_b, Q_b, and D_s for computing D_B and the *rms* wave height transformation.

The existing formulas of Q_b were generally derived based on the assumptions of *pdf* of wave heights in the surf zone or the probability of occurrence of breaking waves which may not be supported by the experimental data. Since the acceptable *pdf* of wave heights inside the surf zone is not available (Demerbilek and Vincent, 2006), it may not be suitable to derive the formula of Q_b from the assumed *pdf* of wave heights. Alternatively, the formula of Q_b can be derived directly from the measured wave heights by inverting the energy dissipation model [Eq. (3.33)] and the wave model [Eq. (3.3)]. Therefore, in the present study, the formula of Q_b will be newly derived from the measured wave heights.

As Q_b is the function of H_{rms}/H_b, the formula of Q_b can be determined by plotting a relationship between measured Q_b versus H_{rms}/H_b. The required data for determining the

formula are the measured data of Q_b and H_{rms}/H_b. The measured Q_b can be determined from the measured wave heights as follows.

Substituting Eq. (3.3) into Eq. (3.33), and using a backward finite difference scheme to describe the differential equation, the formula for determining measured Q_b is expressed as

$$Q_{bi} = \frac{\rho g}{8D_s} \frac{\left(H_{rmsi-1}^2 c_{gi-1} \cos\theta_{i-1} - H_{rmsi}^2 c_{gi} \cos\theta_i\right)}{x_i - x_{i-1}} \tag{3.54}$$

where i is the grid number. Hereafter, the variable Q_b determined from Eq. (3.54) is referred to as the measured Q_b.

For determining Q_b from Eq. (3.54), the formulas of D_s and H_b must be given. As there are three existing formulas for D_s [Eqs. (3.35), (3.39), and (3.51)] and seven existing formulas for H_b [Eqs. (3.37), (3.41), (3.42), (3.44), (3.48), (3.49), and (3.53)], twenty-one Q_b can be determined and consequently twenty-one relationships between measured Q_b versus H_{rms}/H_b are considered in this study. The required data set for deriving the formula of Q_b are the measured data of h, T, H_{rms}, θ, and x. Other related variables (e.g. H_{rmso}, L_o, L, k, and c_g) are computed based on linear wave theory. To avoid a large fluctuation in the relationships, the data of wave height variation across shore should have a small fluctuation.

Because of a variety of wave conditions and a small fluctuation of wave height variation across shore, the data from Dette et al. (1998) are used for deriving the formulas of Q_b. However, all collected data shown in Table 3.1 are used to verify the models for identifying the best one.

The twenty-one relationships between measured Q_b versus H_{rms}/H_b have been plotted to identify a suitable equation of each relationship. An example of a relationship between measured Q_b versus H_{rms}/H_b by using Eqs. (3.35) and (3.37) for computing D_s and H_b is shown in Fig. 3.1. It is found that all relationships can be fitted well with a quadratic equation as

$$Q_b = K_1 + K_2\left(\frac{H_{rms}}{H_b}\right) + K_3\left(\frac{H_{rms}}{H_b}\right)^2 \qquad \text{for} \quad \frac{H_{rms}}{H_b} > K_4 \tag{3.55}$$

where K_1 to K_4 are constants. The fraction of energy dissipation (Q_b) is set to be zero when $H_{rms}/H_b \le K_4$ (offshore zone). The constants K_1 to K_3 are determined from multi-regression analysis between measured Q_b and H_{rms}/H_b. As the constant K_4 is the point that $Q_b = 0$ (x-intercept), it can be determined from the known constants K_1 to K_3 by solving the quadratic equation. The constants K_1 to K_4 and correlation coefficients (R^2) of the twenty-one relationships (21 formulas of Q_b) are shown in Table 3.8. The correlation coefficients (R^2) of the fitting vary between 0.67 to 0.83. Most formulas (except F18 – see Table 3.8) have R^2 greater than or equal to 0.70, which indicate a reasonably good fit.

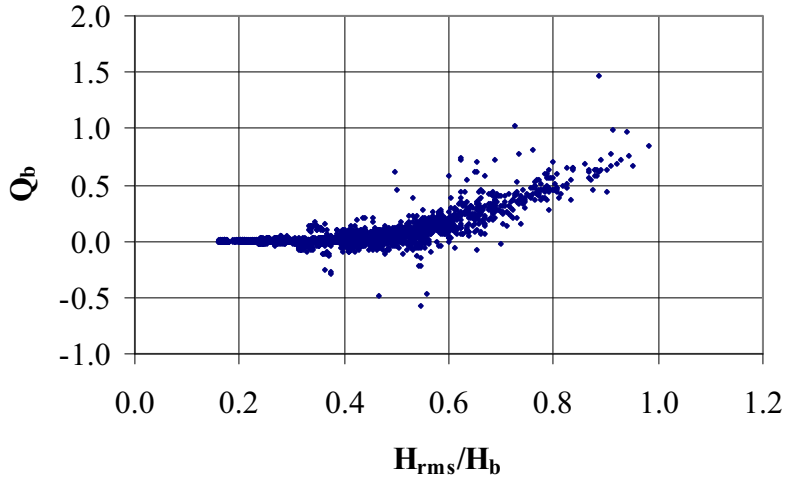

Fig. 3.1. Relationship between measured Q_b versus H_{rms}/H_b by using Eqs. (3.35) and (3.37) for computing D_s and H_b.

It should be noted that an attempt is also made to fit measured Q_b with a cubic equation. However, it is found that the correlation coefficients (R^2) of all models are not significantly improved. Therefore, a quadratic equation is used in this study.

Substituting general form of Q_b [Eq. (3.55)] into Eq. (3.33), the general form of D_B can be expressed as

$$D_B = D_s\left[K_1 + K_2\left(\frac{H_{rms}}{H_b}\right) + K_3\left(\frac{H_{rms}}{H_b}\right)^2\right] \quad \text{for} \quad \frac{H_{rms}}{H_b} > K_4 \tag{3.56}$$

As there are twenty-one formulas of Q_b (F1-F21), there are twenty-one corresponding D_B models (MD1-MD21). The constants K_1 to K_4 for each D_B model are determined from Table 3.8. The selection of the best model is described in the next section.

Table 3.8. Calibrated constants (K_1 to K_4) and correlation coefficients (R^2) of Q_b formula [Eq. (3.55)] for difference D_s and H_b formulas.

Formula No.	D_s Formulas	H_b Formulas	Calibrated constants				R^2
			K_1	K_2	K_3	K_4	
F1	Eq. (3.35)	Eq. (3.37)	0.189	-1.282	2.073	0.37	0.77
F2		Eq. (3.41)	0.582	-2.216	1.998	0.68	0.78
F3		Eq. (3.42)	0.293	-1.601	2.096	0.46	0.75
F4		Eq. (3.44)	0.309	-1.614	2.013	0.49	0.73
F5		Eq. (3.48)	0.488	-2.079	2.122	0.59	0.77
F6		Eq. (3.49)	0.342	-1.776	2.087	0.56	0.83
F7		Eq. (3.53)	0.162	-1.189	2.088	0.34	0.77
F8	Eq. (3.39)	Eq. (3.37)	0.240	-1.627	2.640	0.37	0.77
F9		Eq. (3.41)	1.386	-5.276	4.756	0.68	0.78
F10		Eq. (3.42)	0.465	-2.532	3.311	0.46	0.74
F11		Eq. (3.44)	0.544	-2.818	3.485	0.49	0.72
F12		Eq. (3.48)	0.960	-4.098	4.202	0.58	0.77
F13		Eq. (3.49)	0.987	-4.867	5.290	0.62	0.76
F14		Eq. (3.53)	0.187	-1.378	2.429	0.34	0.77
F15	Eq. (3.51)	Eq. (3.37)	0.014	-0.102	0.178	0.32	0.73
F16		Eq. (3.41)	0.043	-0.172	0.168	0.58	0.74
F17		Eq. (3.42)	0.021	-0.120	0.171	0.38	0.70
F18		Eq. (3.44)	0.020	-0.114	0.158	0.39	0.67
F19		Eq. (3.48)	0.037	-0.166	0.182	0.52	0.72
F20		Eq. (3.49)	0.006	-0.054	0.102	0.35	0.75
F21		Eq. (3.53)	0.012	-0.095	0.179	0.30	0.72

To confirm the ability of present models, the accuracy of present models (MD1 to MD21) are compared with those of eight existing models shown in Sec. 3.2 (i.e. the models of BJ78, TG83, BS85, SN93, BHV98, RS98, RWS03, and RKS03). Because of the frequent updating of wave field (e.g. every 0.5 hours) to account for the change of beach profile in the beach deformation model, the errors of the predictions from the wave sub-model (or sediment transport sub-model) may accumulate from time to time. Therefore, it is necessary to predict the wave height (or sediment transport rate) with high accuracy (as much as possible).

The measured *rms* wave heights from 13 sources (1723 cases) of collected experimental results (see Table 3.1) are used to examine the models. The collected experiments shown in Table 3.1 are separated into three groups according to the experiment-scales, i.e. small-scale, large-scale, and field experiments. A considerably good model should predict well for the three experiment-scales and all collected data.

The *rms* wave height transformation is computed by numerical integration of the energy flux balance equation [Eq. (3.3)] with the present and existing dissipation models. A backward finite difference scheme is used to solve the energy flux balance equation [Eq. (3.3)]. The errors (ER) of models MD1 to MD21 for three experiment-scales and all collected data are shown in Table 3.9 while the errors (ER) of the existing models are shown in Table 3.10. It can be seen from Table 3.10 that the errors (ER) of the existing models for the three experiment-scales vary between 6.7% to 18.7% and the average of the errors is about 10%. As there is no exact criterion to judge a good model, the average error of the existing models (ER = 10%) is used as a criterion to judge the applicability of the

models. In the present study, a considerably good model should give an error that is less than the average error of the existing models (ER < 10%). The results from Tables 3.9 and 3.10 can be summarized as follows.

(a) The error (ER) for small-scale experiments varies between 7.0% to 29.2%. The accuracy of the top five models for small-scale experiments in descending order are MD3, BS85, MD19, MD15, and MD21 (7.0% ≤ ER ≤ 7.4%).

(b) The error (ER) for large-scale experiments varies between 6.6% to 10.4%. The accuracy of the top five models for large-scale experiments in descending order are MD3, BS85, BHV98, MD19, and MD15 (6.6% ≤ ER ≤ 7.1%).

(c) The error (ER) for field experiments varies between 8.2% to 18.7%. The accuracy of the top five models for field experiments in descending order are MD19, MD16, MD17, MD15, and MD20 (8.2% ≤ ER ≤ 9.3%).

(d) The error (ER) for all collected data, which is used to indicate the overall accuracy, varies between 7.7% to 15.4%. The overall accuracy of the top five models in descending order are MD19, MD16, MD17, MD15, and MD21 (7.7% ≤ ER ≤ 8.5%).

(e) It is expected that a good model should be able to predict well for the three experiment-scales. The models that give good predictions (ER < 10.0) for all experiment-scales are MD3, MD15, MD16, MD17, MD19, MD20, and MD21. These models seem to be able to be used for computing H_{rms} . However, lesser error is better. Unfortunately, there is no model that gives the best prediction for all experiment-scales. The model MD3 gives the best prediction for small-scale and large-scale experiments and good predictions for the field experiments, while the model MD19 gives the best prediction for field experiments, the third-best prediction for small-scale experiments, and the fourth-best prediction for large-scale experiments. The these two models seem to be suitable for computing H_{rms} .

(f) Substituting D_s formula and the constants (K_1 to K_4) of MD3 into Eq. (3.56), the model MD3 is expressed as

$$D_B = \frac{\rho g H_b^2}{4T}\left[0.293 - 1.601\left(\frac{H_{rms}}{H_b}\right) + 2.096\left(\frac{H_{rms}}{H_b}\right)^2\right] \quad for \quad \frac{H_{rms}}{H_b} > 0.46 \qquad (3.57)$$

in which H_b is determined from Eq. (3.42). The model MD3 is similar to that of BS85. The main difference between the models MD3 and BS85 is the formula of Q_b which makes the model MD3 simpler than that of BS85. The model MD3 gives the best prediction for small-scale and large-scale experiments, while the model BS85 gives the second-best prediction. For field experiments, the model MD3 also gives better prediction than that of BS85. Although the model MD3 is simpler than that of BS85, the accuracy is better for all experiment-scales. Moreover, the accuracy of MD3 is better than those of existing models for all experiment-scales and all collected data.

(g) Substituting D_s formula and the constants (K_1 to K_4) of MD19 into Eq. (3.56), the model MD19 is expressed as

$$D_B = \frac{\rho g c_g H_b^2}{8h}\left[0.037 - 0.166\left(\frac{H_{rms}}{H_b}\right) + 0.182\left(\frac{H_{rms}}{H_b}\right)^2\right] \quad for \quad \frac{H_{rms}}{H_b} > 0.52 \qquad (3.58)$$

in which H_b is determined from Eq. (3.48). The model MD19 is similar to that of RKS03. The main difference between the models MD19 and RKS03 is the formula

of Q_b which makes the accuracy of model MD19 better than that of RKS03 for all experiment-scales. However, the model MD19 is more complicate than that of RKS03.

(h) As none of existing models gives good predictions ($ER < 10.0$) for all experiment-scales, it may be concluded that the present models (MD3 and MD19) give overall better predictions than those of existing models. Moreover, the models MD3 and MD19 are simpler than most of the existing models (except the model of RKS03). Considering overall performance, the model MD19 seems to be better than that of MD3. Therefore, the model MD19 is recommended to use in the computation of *rms* wave height transformation.

Table 3.9. Errors (ER) of present D_B models [Eq. (3.56)] with different D_s and H_b formulas for 3 experiment-scales and all collected data (using the calibrated constants from Table 3.8 and measured data from Table 3.1).

Models	D_s Formulas	H_b Formulas	Errors (ER)			
			Small-scale (152 data)	Large-scale (6705 data)	Field (11285 data)	All data (18142 data)
MD1	Eq. (3.35)	Eq. (3.37)	24.06	8.17	11.56	10.41
MD2		Eq. (3.41)	12.61	8.02	11.11	9.98
MD3		Eq. (3.42)	6.96	6.62	9.77	8.58
MD4		Eq. (3.44)	9.24	7.70	10.24	9.29
MD5		Eq. (3.48)	25.91	8.20	10.57	9.82
MD6		Eq. (3.49)	9.93	9.08	10.94	10.24
MD7		Eq. (3.53)	29.22	8.24	11.61	10.51
MD8	Eq. (3.39)	Eq. (3.37)	15.70	8.01	11.37	10.16
MD9		Eq. (3.41)	12.60	8.01	11.12	9.98
MD10		Eq. (3.42)	8.76	7.08	10.56	9.26
MD11		Eq. (3.44)	9.30	7.65	10.90	9.69
MD12		Eq. (3.48)	15.52	8.05	10.73	9.78
MD13		Eq. (3.49)	16.19	10.42	11.88	11.38
MD14		Eq. (3.53)	17.57	8.05	11.48	10.26
MD15	Eq. (3.51)	Eq. (3.37)	7.28	7.11	9.04	8.31
MD16		Eq. (3.41)	7.93	7.14	8.67	8.10
MD17		Eq. (3.42)	8.02	7.15	8.72	8.13
MD18		Eq. (3.44)	15.53	9.28	10.50	10.09
MD19		Eq. (3.48)	7.24	6.96	8.20	7.74
MD20		Eq. (3.49)	9.60	7.53	9.26	8.62
MD21		Eq. (3.53)	7.38	7.17	9.33	8.52

Table 3.10. Errors (ER) of existing D_B models for 3 experiment-scales and all collected data (measured data from Table 3.1).

Models	D_B Formulas	H_b Formulas	Errors (ER)			
			Small-scale (152 data)	Large-scale (6705 data)	Field (11285 data)	All data (18142 data)
BJ78	Eq. (3.34)	Eq. (3.37)	8.80	10.05	18.68	15.41
TG83	Eq. (3.38)	Eq. (3.41)	18.42	7.97	10.60	9.69
BS85	Eq. (3.34)	Eq. (3.42)	6.98	6.68	10.69	9.18
SN93	Eq. (3.43)	Eq. (3.44)	11.61	9.92	15.68	13.52
BHV98	Eq. (3.45)	Eq. (3.44)	9.93	6.72	11.47	9.70
RS98	Eq. (3.47)	Eq. (3.48)	8.71	7.14	10.11	9.00
RWS03	Eq. (3.45)	Eq. (3.49)	11.65	8.06	10.73	9.75
RKS03	Eq. (3.50)	Eq. (3.53)	7.72	8.56	11.58	10.43

3.3. Transformation of Significant Wave Heights

The significant wave height (which is defined as the average of the highest one-third wave heights) is most frequently used in the field of coastal and ocean engineering (Goda, 2000; and Andreas and Wang, 2007), especially in the design of coastal and ocean structures. The wave heights are usually available in deepwater but not available at the required depths in shallow water. The wave heights in shallow water can be determined from wave models. Common approaches to model the significant wave height transformation may be classified into three main approaches, i.e. representative wave approach (commonly referred to as significant wave representation method), wave-by-wave approach, and conversion approach.

For the significant wave representation method, the regular wave models are directly applied to irregular waves by using the significant wave height. The method has been widely used since the introduction of the significant waves. It is easy to understand and also simple to use. However, the characteristics of the irregular waves (e.g. wave height and period) are statistical variability in contrast to regular waves, which has a single height, period, and direction. As the significant wave representation method does not consider such variability, the method may possibly contain a large estimation error (Goda, 2000).

The wave-by-wave approach considers the propagation of individual waves in the irregular wave train. The incident individual waves may be determined from irregular wave records or from probability density function (*pdf*) of wave heights. The propagation of each individual wave is computed by using an appropriate regular wave model. Recombining the individual wave heights at the required depth yields the irregular wave train, which is used to determine the significant wave height or other representative wave heights. Several models have been proposed based on this approach, differing mainly in the regular wave model used to simulate the propagation of the individual waves (e.g. the models of Mizuguchi, 1982; Dally, 1992; Kuriyama, 1996; and Goda, 2004). This approach is particularly useful if a detailed wave height distribution is required. However, it has the disadvantage of being time consuming, which may not be suitable for some practical work.

The conversion approach is used to convert the representative wave heights from one to another through the known relationships. The root mean square wave height (H_{rms}) is usually used as a reference wave height of the conversion because it is the output of many wave models (e.g. the models of Battjes and Janssen, 1978; Thornton and Guza, 1983; Larson, 1995; and Rattanapitikon, 2007). Therefore, the significant wave height (H_s) can be determined from the known relationship between H_{rms} and H_s (e.g. the relationships of Longuet-Higgins, 1952; Battjes and Groenendijk, 2000; and Rattanapitikon and Shibayama, 2007). This approach is simpler than the wave-by-wave approach but slightly more complicated than the significant wave representation method.

The present section focuses on the significant wave representation method, as this appears to be the simplest method. Many researchers pointed out that the significant wave representation method could give inconsistent or erroneous results in the computation of significant wave height transformation (Goda, 2000). It seems that no literature has pointed out that the significant wave representation method is applicable in the surf zone. Consequently, engineers have been reluctant to use the significant wave representation method. However, the significant wave representation method has the merits of easy understanding, simple application and it is not necessary to assume the shape of the *pdf* of wave heights. It will be useful for some practical work if this approach can be used to compute the significant wave heights in shallow water. Moreover, Rattanapitikon et al. (2003) reported that the representative wave approach can be used to compute H_{rms} with

very good accuracy. It may also be used to compute H_s. This study is carried out to investigate the possibility of using the significant wave representation method.

This section is divided into four main parts. The first part describes the collected data. The second part describes some existing regular wave models. The third part describes modeling of irregular waves using significant wave representation method. The fourth part deals with the modification of the selected model.

3.3.1. Collected laboratory data

For the significant wave representation method, the regular wave model is directly applied to irregular waves by using the significant wave height. The present study is, therefore, concerned with both regular and irregular wave models. The experiments performed under regular and irregular wave conditions are used to calibrate and examine the models.

3.3.1.1. Regular wave data

Laboratory data of regular wave heights inside the surf zone from 13 sources (total 492 cases) have been collected for calibration and examination of the regular wave models. The experiments cover a wide range of wave and bottom topography conditions, including small-scale and large-scale experiments. The experiments cover a variety of beach conditions and cover a range of deepwater wave steepness (H_o/L_o, where H_o is the deepwater wave height and L_o is the deepwater wavelength) from 0.003 to 0.112. A summary of the collected laboratory data is given in Table 3.11.

Table 3.11. Summary of collected experimental data used to calibrate and verify the regular wave models.

Sources	Beach Condition	No. of cases	No. of data	H_o/L_o
Cox and Kobayashi (1997)	plane beach	1	5	0.015
Hansen and Svendsen (1984)	plane beach	1	5	0.019
Horikawa and Kuo (1966)	plane and stepped beach	213	2127	0.006-0.100
Hurue (1990)	plane beach	1	4	0.038
Nadaoka et al. (1982)	plane beach	2	11	0.013-0.080
Nagayama (1983)	plane, stepped and barred beach	12	171	0.025-0.055
Okayasu et al. (1988)	plane beach	10	62	0.009-0.054
Sato et al. (1988)	plane beach	3	25	0.031-0.050
Sato et al. (1989)	plane beach	2	11	0.019-0.036
Shibayama and Horikawa (1985)	sandy beach	10	85	0.028-0.036
Smith and Kraus (1990)	plane and barred beach	101	506	0.008-0.096
Kajima et al. (1983)	sandy beach	79	1397	0.003-0.112
Kraus and Smith (1994)	sandy beach	57	429	0.003-0.066
Total		492	4838	0.003-0.112

Most of the experiments were carried out in small-scale wave flumes, except the experiments of Kajima et al. (1983) and Kraus and Smith (1994) which were carried out in large-scale wave flumes. The data sources are the same as those used by Rattanapitikon et al. (2003).

3.3.1.2. Irregular wave data

Laboratory data of significant wave height transformation from 6 sources, totaling 282 cases, were collected for calibration and examination of the irregular wave models. A summary of the collected laboratory data is shown in Table 3.12.

Table 3.12. Summary of collected experimental data used to calibrate and verify the irregular wave models.

Sources	Test Series	Descriptions	No. of cases	No. of data	H_{so}/L_o
Hurue (1990)	Hu1	plane beach	1	7	0.037
Smith and Kraus (1990)	R2000	plane beach	1	8	0.070
	R22xx	barred beach	3	24	0.070
	R6000	plane beach	1	8	0.040
	R62xx	barred beach	3	24	0.040
	R8000	plane beach	1	8	0.030
	R82xx	barred beach	3	24	0.030
Katayama (1991)	Ka1&Ka2	barred beach	2	16	0.041, 0.044
Ting (2001)	Ti1	plane beach	1	7	0.024
Kraus and Smith (1994)	ST10	erosion toward equilibrium	26	416	0.013-0.064
	ST20	acoustic profiler tests	8	128	0.002-0.057
	ST30	accretion toward equilibrium	19	304	0.003-0.007
	ST40	dedicated hydrodynamics	12	192	0.005-0.050
	ST50	dune erosion, test 1	8	128	0.012-0.057
	ST60	dune erosion, test 2	9	144	0.009-0.022
	ST70	seawall, test 1	9	144	0.022-0.032
	ST80	Seawall, test 2	3	48	0.022
	ST90	berm flooding, test 1	3	48	0.050
	STAO	Foredune erosion	1	16	0.050
	STCO	Seawall, test 3	8	127	0.004-0.057
	STDO	berm flooding, test 2	3	48	0.050
	STJO	Narrow-crested mound	10	160	0.005-0.050
	STKO	broad-crested mound	9	144	0.005-0.050
Dette et al. (1998)	A8	1:20 beach slope, normal	7	147	0.010
	A9	1:20 beach slope, storm	15	390	0.018
	B1	1:10 beach slope, normal	8	191	0.010
	B2	1:10 beach slope, storm	15	392	0.018
	C1	1:5 beach slope, normal	4	95	0.010
	C2	1:5 beach slope, storm	17	459	0.018
	H1	1:15 beach slope, normal	2	43	0.010
	H2	1:15 beach slope, storm	15	398	0.018
	D1&D3	D.P.[1], no overtopping, normal	7	158	0.010
	D2	D.P.[1], no overtopping, storm	11	297	0.018
	E	D.P.[1], with overtopping, storm	11	297	0.018
	F	no D.P.[1], storm	12	324	0.018
	G	no D.P.[1], underwater barrier	14	365	0.012-0.018
Total			282	5729	0.002-0.064

[1] D.P. = dune protection.

The collected data are separated into 2 groups based on the experiment-scale, i.e. small-scale and large-scale experiments. The experiments of Hurue (1990), Smith and Kraus (1990), Katayama (1991), and Ting (2001) were performed in small-scale wave flumes under fixed bed conditions, while the experiments of Kraus and Smith (1994) and Dette et al. (1998) were undertaken in large-scale wave flumes under movable bed (sandy bed) conditions. The data cover a range of deepwater wave steepness (H_{so}/L_o, where H_{so} is the deepwater significant wave height) from 0.002 to 0.064. A brief description of the experiments is given below.

The experiment of Hurue (1990) was conducted to study wave and undertow velocity on a plane beach. The experiment was performed in a small-scale wave flume, which was 17 m long and 0.5 m wide. The beach topography was 1/20 uniform slope with the smooth

bottom. The incident significant wave height of 0.09 m and wave period of 1.26s was generated based on the Bretschneider-Mitsuyasu spectrum (Bretschneider, 1968 and Mitsuyasu, 1970). Water surface elevations were measured at seven cross-shore locations using a capacitance-type gage.

The experiment of Smith and Kraus (1990) was conducted to investigate the macro-features of wave breaking over bars and artificial reefs using a small wave flume of 45.70 m long, 0.46 m wide, and 0.91 m deep. Both regular and irregular waves were employed in this experiment. A total of 12 cases were performed for irregular wave tests. Three irregular wave conditions were generated for three bar configurations as well as for a plane beach. A JONSWAP (Hasselmann et al., 1973) computer signal was generated for spectral width parameter of 3.3 and spectral peak periods of 1.07, 1.56, and 1.75 s with significant wave heights of 0.12, 0.15, and 0.14 m respectively. Water surface elevations were measured at eight cross-shore locations using resistance-type gages.

The experiment of Katayama (1991) was conducted to study wave and undertow velocity on a bar-type beach. The experiment was performed in a small-scale wave flume, which was 17 m long and 0.5 m wide. The bar-type beach consisted of the first 5 m of 1/20, the next 1 m of -1/20, and the last 4 m of 1/20 slopes. The incident significant wave heights of 0.06 and 0.08 m and wave periods of 0.95 and 1.14 s were generated based on the Bretschneider-Mitsuyasu spectrum (Bretschneider, 1968 and Mitsuyasu, 1970). Water surface elevations were measured at eight cross-shore locations using a capacitance-type gages.

The experiment of Ting (2001) was conducted to study wave and turbulence velocities in a broad-banded irregular wave surf zone. The experiment was performed in a small-scale wave flume, which was 37 m long, 0.91 m wide and 1.22 m deep. A false bottom with 1/35 slope built of marine plywood was installed in the flume to create a plane beach. The irregular waves were developed from the TMA spectrum (Bouws et al., 1985), with a spectral peak period of 2.0 s, a spectrally based significant wave height of 0.15 m and spectral width parameter of 3.3. Water surface elevations were measured at seven cross-shore locations using a resistance-type gage.

The SUPERTANK laboratory data collection project (Kraus and Smith, 1994) was conducted to investigate cross-shore hydrodynamic and sediment transport processes from August 5 to September 13, 1992 at Oregon State University, Corvallis, Oregon, USA. A 76-m-long sandy beach was constructed in a large wave tank of 104 m long, 3.7 m wide, and 4.6 m deep. Wave conditions included both regular and irregular waves. In all, 20 major tests were performed, and each major test consisted of several cases. Most of the tests (14 major tests) were performed under the irregular wave actions. The wave conditions were designed to balance the need for repetition of wave conditions to move the beach profile toward equilibrium and development of a variety of conditions for hydrodynamic studies. The TMA spectral shape (Bouws et al., 1985) was used to design all irregular wave tests. The collected experiments for irregular waves included 128 cases of wave and beach conditions (a total of 2047 wave records), covering incident significant wave heights from 0.2 m to 1.0 m, spectral peak periods from 3.0 sec to 10.0 sec, and spectral width parameter between 3.3 (broad-banded) and 100 (narrow-banded). Sixteen resistance-type gages were used to measure water surface elevations across shore.

SAFE Project (Dette et al., 1998) was carried out to improve the methods of design and performance assessment of beach nourishment. The SAFE Project consisted of four activities, one of which was to perform experiments in a large-scale wave flume in Hannover, Germany. A 250-m-long sandy beach was constructed in a large wave tank of 300 m long, 5 m wide and 7 m deep. The test program was divided into two major phases. The first phase (cases A, B, C, and H) was aimed to study the beach deformation of

equilibrium profile with different beach slope changes. The equilibrium beach profile was adopted from the Bruun (1954)'s approach ($h = 0.12x^{2/3}$). In the second phase, the sediment transport behaviors of dunes with and without structural aid were investigated (cases D, E, F, and G). The TMA spectral shape (Bouws et al., 1985) was used to design all irregular wave tests. The tests were performed under normal wave conditions (H_{so}/L_o = 0.010, water depth in the horizontal section = 4.0 m) and storm wave conditions (H_{so}/L_o = 0.018, water depth in the horizontal section = 5.0 m). A total of 27 wave gages was installed over a length of 175 m along one wall of the flume. The collected experiments included 138 cases of wave and beach conditions, covering deepwater wave steepness (H_{so}/L_o) from 0.010 to 0.018.

3.3.2. Regular wave model

The regular wave height transformation across-shore can be computed from the energy flux conservation as

$$\frac{\partial(Ec_g)}{\partial x} = -D_B \tag{3.93}$$

where $E = \rho g H^2/8$ is the wave energy density, ρ is the water density, g is the acceleration due to gravity, H is the wave height, c_g is the group velocity, x is the distance in cross shore direction, and D_B is the energy dissipation rate due to wave breaking which is zero outside the surf zone. The energy dissipation rate due to bottom friction is neglected. In the present study, all variables are based on the linear wave theory.

The wave height transformation can be computed from the energy flux conservation (Eq. (3.93)) by substituting the formula of the energy dissipation rate (D_B) and numerically integrating from offshore to shoreline. The difficulty of Eq. (3.93) is how to formulate the energy dissipation rate caused by the breaking waves.

During the past decades, various models have been developed for computing the energy dissipation of regular wave breaking. Widely used concepts for computing energy dissipation rate (D_B) for regular wave breaking are the bore concept and the stable energy concept.

The bore concept is based on the similarity between the breaking wave and the hydraulic jump. Several models have been proposed based on slightly different assumptions on the conversion from energy dissipation of hydraulic jump to energy dissipation of a breaking wave. Some existing D_B models, which were developed based on the bore concept, are listed below.

a) Battjes and Janssen (1978): $$D_B = 0.47\frac{\rho g H^2}{4T} \tag{3.94}$$

b) Thornton and Guza (1983): $$D_B = 0.67\frac{\rho g H^3}{4Th} \tag{3.95}$$

c) Deigaard et al. (1991): $$D_B = 0.48\frac{\rho g h H^3}{T(4h^2 - H^2)} \tag{3.96}$$

where h is the water depth, and T is the wave period. The constants in the above models were calibrated by Rattanapitikon et al. (2003) based on a wide range of experimental conditions as shown in Table 3.11.

The stable energy concept was introduced by Dally et al. (1985) based on an analysis of the measured breaking wave height on horizontal slope of Horikawa and Kuo (1966). When a breaking wave enters an area with horizontal bed, the breaking continues (the

wave height decreases) until some stable wave height is attained. The development of the stable energy concept was based on an observation of stable wave height on horizontal slope. Dally et al. (1985) assumed that the energy dissipation rate was proportional to the difference between the local energy flux per unit depth and the stable energy flux per unit depth. Several models have been proposed on the basis of this concept. The main difference is the formula for computing the stable wave height (for more detail, please see Rattanapitikon et al., 2003). Some existing D_B models, which were developed based on the stable energy concept, are listed as follows.

a) Dally et al. (1985):
$$D_B = 0.15\frac{\rho g c_g}{8h}\left[H^2 - (0.4h)^2\right] \tag{3.97}$$

b) Rattanapitikon and Shibayama (1998):
$$D_B = 0.15\frac{\rho g c}{8h}\left\{H^2 - \left[h\exp\left(-0.36 - \frac{1.25h}{\sqrt{LH}}\right)\right]^2\right\} \tag{3.98}$$

c) Rattanapitikon et al. (2003):
$$D_B = 0.15\frac{\rho g c_g}{8h}\left\{H^2 - \left[0.073L\tanh(kh)\right]^2\right\} \tag{3.99}$$

where c is the local phase velocity, L is the local wavelength, and k is the local wave number. The second terms on the right hand side of Eqs. (3.97) to (3.99) are the terms of stable wave height. The energy dissipation will be zero if the wave height is less than the stable wave height.

The verification results of the six existing models are presented in the paper by Rattanapitikon et al. (2003). The results are also shown in Table 3.16 for comparison with the modified model (described in Sec. 3.3.4).

3.3.3. Irregular wave model

For the representative wave approach, the energy flux of the representative wave represents the average energy flux of an irregular wave train. The governing equation (energy flux conservation) of the representative wave (H_{rms}) can be derived based on the assumptions of linear wave theory and Rayleigh distribution of wave heights (for more detail, please see e.g. Larson, 1995). Although the crude assumptions of the representative wave approach may not be theoretically justified (mainly because of the nonlinearity of each individual wave), the approach is physical validity (the prediction agrees well with actual measurements). There are many wave models that are successful in using the energy flux conservation of the representative wave (H_{rms}) for computing the transformation of H_{rms} across-shore, e.g. the models of Battjess and Janssen (1978), Thornton and Guza (1983), Larson (1995), Baldock et al. (1998), Ruessink et al. (2003), and Rattanapitikon (2007). If the energy flux conservation of H_{rms} is valid, the energy flux conservation of H_s should also be valid; because H_{rms} can be converted to H_s through the known coefficient (i.e. $H_s = 1.42H_{rms}$ for the Rayleigh distribution).

In the present study, for the significant wave representation method, the regular wave model is applied directly to irregular waves by using the significant wave height (H_s) and the spectral peak period (T_p). The spectral peak period is used because it is the most commonly used parameter and typically reported for the irregular wave data.

Since the D_B formulas shown in Sec. 3.3.2 (Eqs. (3.94) to (3.99)) were developed for regular waves, it is not clear which formula is suitable for the significant wave

representation method. Therefore, all of them were used to investigate the possibility of simulating the significant wave height transformation.

Substituting the dissipation formula (Eqs. (3.94) to (3.99) respectively) into Eq. (3.93) and applying for significant wave height (H_s) and spectral peak period (T_p), the irregular wave models can be expressed as

model (1): $$\frac{\rho g}{8}\frac{\partial\left(H_s^2 c_g\right)}{\partial x} = -K_1 \frac{\rho g H_s^2}{4T_p} \tag{3.100}$$

model (2): $$\frac{\rho g}{8}\frac{\partial\left(H_s^2 c_g\right)}{\partial x} = -K_2 \frac{\rho g H_s^3}{4T_p h} \tag{3.101}$$

model (3): $$\frac{\rho g}{8}\frac{\partial\left(H_s^2 c_g\right)}{\partial x} = -K_3 \frac{\rho g h H_s^3}{T_p(4h^2 - H_s^2)} \tag{3.102}$$

model (4): $$\frac{\rho g}{8}\frac{\partial\left(H_s^2 c_g\right)}{\partial x} = -K_4 \frac{\rho g c_g}{8h}\left[H_s^2 - (K_s h)^2\right] \tag{3.103}$$

model (5): $$\frac{\rho g}{8}\frac{\partial\left(H_s^2 c_g\right)}{\partial x} = -K_6 \frac{\rho g c}{8h}\left\{H_s^2 - \left[K_7 h \exp\left(-0.36 - \frac{1.25h}{\sqrt{LH_s}}\right)\right]^2\right\} \tag{3.104}$$

model (6): $$\frac{\rho g}{8}\frac{\partial\left(H_s^2 c_g\right)}{\partial x} = -K_8 \frac{\rho g c_g}{8h}\left\{H_s^2 - \left[K_9 L \tanh(kh)\right]^2\right\} \tag{3.105}$$

where K_1 - K_9 are the coefficients. It can be seen from Eqs. (3.94)-(3.99) that the coefficients K_1 - K_9 for the regular wave models are 0.47, 0.67, 0.48, 0.15, 0.4, 0.15, 1.0, 0.15, and 0.073 respectively. When applying to the irregular wave, K_1 - K_9 are the adjustable coefficients to allow for the effect of the transformation to irregular waves. Hereafter, Eqs. (3.100)-(3.105) are referred to as MD1, MD2, MD3, MD4, MD5, and MD6 respectively. The variables c_g, c, L, and k in the models MD1-MD6 are calculated based on the spectral peak period (T_p).

The breaking criterion of Miche (1944) is applied to determine incipient wave breaking of the significant wave height (H_{sb}) as

$$H_{sb} = K_{10} L \tanh(kh) \tag{3.106}$$

where K_{10} is the coefficient. The published value of K_{10} for regular wave breaking is 0.142. When applying to the irregular waves, K_{10} is the adjustable coefficient to allow for effect of the transformation to irregular waves. The energy dissipation (D_B) terms on the right hand side of models MD1-MD6 occur when $H_s \geq H_{sb}$ and is equal to zero when $H_s < H_{sb}$.

3.3.3.1. Trial simulation

The objective of this section is to test the applicability of models MD1-MD6 by using the coefficients K_1 - K_{10} which were proposed by the previous researchers for regular waves (shown in the second column of Table 3.13). All collected data shown in Table 3.12 are used to examine the models.

The basic parameter for determination of the overall accuracy of the model is the average *rms* relative error (ER_{avg}), which is defined as

$$ER_{avg} = \frac{\sum_{n=1}^{tn} ER_{gn}}{tn} \tag{3.107}$$

where n is the data group number, ER_{gn} is the rms relative error of the group no. n, and tn is the total number of data group. The small value of ER_{avg} indicates good overall accuracy of the wave model.

The rms relative error of each data group (ER_g) is defined as

$$ER_g = 100\sqrt{\frac{\sum_{i=1}^{nc}(H_{ci} - H_{mi})^2}{\sum_{i=1}^{nc} H_{mi}^2}} \tag{3.108}$$

where i is the wave height number, H_{ci} is the computed significant wave height of number i, H_{mi} is the measured significant wave height of number i, and nc is the total number of measured significant wave heights in each data group.

The question of how good a model is usually defined in a qualitative ranking (e.g. excellence, very good, good, fair, and poor). As the error of some existing irregular wave models is in the range of 7 to 21% (please see Rattanapitikon, 2007, Table 5), the qualification of error ranges of an irregular wave model may be classify into five ranges (i.e. excellence ($ER_g < 5.0$), very good ($5.0 \le ER_g < 10.0$), good ($10.0 \le ER_g < 15.0$), fair ($15.0 \le ER_g < 20.0$), and poor ($ER_g \ge 20.0$)) and the acceptable error should be less than 10%.

The transformation of the significant wave height from the models MD1-MD6 is determined by taking numerical integration from offshore to shoreline. The energy dissipation is set to be zero when $H_s < H_{sb}$. The incipient wave breaking (H_{sb}) is computed from Eq. (3.106). The forward finite difference scheme is used to solve the differential equations. The length step (Δx) is set to be equal to the length between the points of measured wave heights, except if $\Delta x > 5$m, Δx is set to be 5 m. The length steps (Δx) used in the present study are 0.2 - 1.5 m for small-scale experiments and 2.1 - 5.0 m for large-scale experiments. Using the coefficients K_1 - K_{10} which were proposed for regular waves, errors of the models MD1-MD6 on predicting H_s for two groups of experiment-scales are shown in Table 3.13. It can be seen from Table 3.13 that all models give unaccepted results in simulating the significant wave height transformation. This is a confirmation of the findings of the previous researchers. The unaccepted results may be due to: 1) the incipient breaking point of regular wave and irregular wave may not be the same point and 2) the amount of energy dissipation of regular wave and irregular wave may not be the same. Therefore, the prediction may be more accurate if the coefficients (K_1 - K_{10}) are re-calibrated by using the significant wave height data.

Table 3.13. The errors (ER_g and ER_{avg}) of the models MD1-MD6 (using the coefficients of regular waves) for 2 groups of experiment-scales (measured data from Table 3.12).

Models	Coefficients	ER_g		ER_{avg}
		small-scale	large-scale	
MD1 (Eq. (3.101))	$K_1 = 0.47,\ K_{10} = 0.142$	25.5	13.1	19.3
MD2 (Eq. (3.102))	$K_2 = 0.67,\ K_{10} = 0.142$	24.0	10.9	17.4
MD3 (Eq. (3.103))	$K_3 = 0.48,\ K_{10} = 0.142$	22.7	11.3	17.0
MD4 (Eq. (3.104))	$K_4 = 0.15,\ K_5 = 0.4,\ K_{10} = 0.142$	27.9	10.7	19.3
MD5 (Eq. (3.105))	$K_6 = 0.15,\ K_7 = 1.0,\ K_{10} = 0.142$	25.4	10.3	17.9
MD6 (Eq. (3.106))	$K_8 = 0.15,\ K_9 = 0.073,\ K_{10} = 0.142$	26.1	10.5	18.3

3.3.3.2. Model calibration and selection

A calibration of each model is conducted by varying the coefficients (K_1 - K_{10}) in the model until the minimum error (ER_{avg}) between measured and computed significant wave heights is obtained. The optimum values of K_1 - K_{10} are shown in the second column of Table 3.14. The errors of models MD1-MD6 on simulating H_s for two groups of experiment-scales are shown in the third to fifth columns of Table 3.14. The examination results from Table 3.14 can be summarized as follows:

(i) The accuracy of all models is improved significantly after calibration.

(j) For small-scale wave flumes, the models MD3, MD5, and MD6 give very good predictions ($5.0 \le ER_g < 10.0$), while the other models (MD1, MD2, and MD4) give good predictions ($10.0 \le ER_g < 15.0$). The accuracy levels of the models in descending order are MD6, MD3, MD5, MD2, MD4, and MD1.

(k) For large-scale wave flumes, all models give very good predictions ($5.0 \le ER_g < 10.0$). The accuracy levels of the models in descending order are MD5, MD6, MD2, MD3, MD4, and MD1.

(l) The overall accuracy levels of the models in descending order are MD5, MD6, MD3, MD2, MD4, and MD1.

(m) The models MD3, MD5, and MD6 give very good predictions ($5.0 \le ER_g < 10.0$) for both small-scale and large-scale experiments. These models can be used for computing the significant wave height transformation. However, lesser error is better. The models MD5 and MD6 give almost the same accuracy and are more accurate than the others.

(n) The average error (ER_{avg}) of the models MD5 and MD6 are 7.5% and 7.6% respectively. These numbers confirm in a quantitative sense the high degree of realism generated by the models. This means that the significant wave representation method is acceptable for computing the significant wave height transformation across-shore.

Table 3.14. The errors (ER_g and ER_{avg}) of the models MD1-MD6 (using the calibrated coefficients) and the modified model (MD7) for 2 groups of experiment-scales (measured data from Table 3.12).

Models	Coefficients	ER_g		ER_{avg}
		small-scale	large-scale	
MD1 (Eq. (3.101))	$K_1 = 0.34,\ K_{10} = 0.098$	13.5	8.4	10.9
MD2 (Eq. (3.102))	$K_2 = 0.53,\ K_{10} = 0.098$	11.9	6.5	9.2
MD3 (Eq. (3.103))	$K_3 = 0.40,\ K_{10} = 0.098$	9.4	6.8	8.1
MD4 (Eq. (3.104))	$K_4 = 0.09,\ K_5 = 0.42,\ K_{10} = 0.076$	12.2	7.1	9.6
MD5 (Eq. (3.105))	$K_6 = 0.09,\ K_7 = 1.07,\ K_{10} = 0.076$	9.5	5.5	7.5
MD6 (Eq. (3.106))	$K_8 = 0.09,\ K_9 = 0.076,\ K_{10} = 0.076$	9.3	5.8	7.6
MD7 (Eq. (3.118))	$K_{11} = 0.095,\ K_{12} = -0.263,\ K_{13} = 0.179$	8.1	5.7	6.9

Overall, the models MD5 and MD6 give nearly the same accuracy. It may be interesting to look at the comparison in more detail. Table 3.15 shows the errors (ER_g) of MD5 and MD6 for 36 groups of test series. It can be seen from Table 3.15 that the models MD5 and MD6 give nearly the same overall accuracy (ER_{avg} of MD5 = 7.7% and ER_{avg} of MD6 = 7.6%). As the average errors (ER_{avg}) of models MD5 and MD6 from Tables 3.14 and 3.15 are almost the same, it is difficult to judge which model is better than the other. Evaluation of these two models may have to be based on their simplicity.

Substituting the calibrated coefficients $K_6 = 0.09,\ K_7 = 1.07,\ K_8 = 0.09,\ K_9 = 0.076$, and $K_{10} = 0.076$ into the corresponding equations (Eqs. (3.104)-(3.106)), the irregular wave models (MD5 and MD6) for computing H_s can be expressed as

$$\text{MD5:}\quad \frac{\rho g}{8}\frac{\partial\left(H_s^2 c_g\right)}{\partial x} = -0.09\frac{\rho g c}{8h}\left[H_s^2 - \left(1.07h\exp\left(-0.36 - \frac{1.25h}{\sqrt{LH_s}}\right)\right)^2\right] \tag{3.109}$$

$$\text{MD6:}\quad \frac{\rho g}{8}\frac{\partial\left(H_s^2 c_g\right)}{\partial x} = -0.09\frac{\rho g c_g}{8h}\left[H_s^2 - \left(0.076L\tanh(kh)\right)^2\right] \tag{3.110}$$

in which the incipient wave breaking or the starting point to include the energy dissipation into the models is determined from the following formula.

$$H_{sb} = 0.076L\tanh(kh) \tag{3.111}$$

The energy dissipation of MD5 and MD6 is zero when the stable wave height (the second term on the right hand side of Eqs. (3.109) and (3.110)) is greater than the significant wave height. It can be seen that the stable wave height of MD6 (second term on the right hand side of Eq. (3.110)) is the same as the formula that used for computing the breaker height (Eq. (3.111)). This means that it is not necessary to check the incipient wave breaking. Equation (3.110) can be used to compute the significant wave heights for the entire zone (from offshore to shoreline). This makes the model MD6 simpler than the model MD5. In terms of accuracy and simplicity, the model MD6 is the best and is recommended for computing the significant wave height transformation across-shore. As the model MD6 (Eq. (3.110)) is very simple, it may also serve as a reference model to test more complicated models against.

Table 3.15. The errors (ER_g and ER_{avg}) of the models MD5-MD6 (using the calibrated coefficients) and the modified model (MD7) for 36 groups of test series.

Sources	Test series	MD5	MD6	MD7
Hurue (1990)	Hu1	7.6	5.9	6.2
Smith and Kraus (1990)	R2000	11.7	7.5	6.6
	R22xx	12.0	11.3	9.9
	R6000	7.3	5.0	5.9
	R62xx	10.3	10.9	9.3
	R8000	3.8	4.6	4.2
	R82xx	10.4	10.8	8.8
Katayama (1991)	Ka1&Ka2	8.0	9.0	9.7
Ting (2001)	Ti1	4.8	3.1	3.1
Kraus and Smith (1994)	ST10	6.8	4.8	4.8
	ST20	5.4	5.2	5.0
	ST30	6.5	6.4	6.4
	ST40	8.3	8.4	8.3
	ST50	7.0	7.2	6.9
	ST60	8.3	8.6	7.9
	ST70	7.2	6.8	6.3
	ST80	9.6	9.4	8.9
	ST90	5.2	5.5	4.5
	STAO	5.7	4.9	4.3
	STCO	13.1	11.4	11.6
	STDO	10.1	10.7	10.4
	STJO	10.6	10.9	9.6
	STKO	21.7	21.4	20.9
Dette et al. (1998)	A8	10.9	13.0	12.3
	A9	2.9	4.9	5.1
	B1	7.6	9.1	8.1
	B2	4.2	4.5	4.2
	C1	9.9	11.5	10.4
	C2	4.0	4.8	4.7
	H1	4.4	5.4	6.1
	H2	4.8	4.3	3.7
	D1&D3	9.0	9.8	9.6
	D2	4.3	5.4	5.7
	E	3.2	4.0	4.4
	F	3.6	3.9	4.0
	G	6.4	5.1	5.8
Average error (ER_{avg})		7.7	7.6	7.3

3.3.4. Model modification

Although, the model MD6 gives very good predictions, it may be modified to achieve even greater accuracy. The energy dissipation term in model MD6 is derived from the regular wave model of Rattanapitikon et al. (2003), which were developed based on the stable energy concept of Dally et al. (1985). The model MD6 (Eq. (3.110)) can be re-written as

$$\frac{\rho g}{8}\frac{\partial\left(H_s^2 c_g\right)}{\partial x} = -\frac{\rho g H_s^2 c_g}{8h}\left[0.09 - 0.09\left(\frac{H_{sb}}{H_s}\right)^2\right] \tag{3.112}$$

in which H_{sb} is calculated from Eq. (3.111). It can be seen that the energy dissipation term on the right hand side of Eq. (3.112) can be written in a general form as a product of energy flux per unit depth and a dimensionless function (f) as

$$\frac{\rho g}{8}\frac{\partial\left(H_s^2 c_g\right)}{\partial x} = -\frac{\rho g H_s^2 c_g}{8h} f\left\{\frac{H_{sb}}{H_s}\right\} \tag{3.113}$$

where f is a function of H_{sb}/H_s. The function f may be considered as a fraction of energy dissipation, while the energy flux per unit depth may be considered as a potential rate of energy dissipation. The function f of the stable energy concept (MD6) can be expressed as

$$f = -0.09\left(\frac{H_{sb}}{H_s}\right)^2 + 0.09 \tag{3.114}$$

It should be noted that Eq. (3.112) (or Eq. (3.114)) is derived based on the assumption that the energy dissipation rate is proportional to the difference between the energy flux per unit depth and the stable energy flux per unit depth. If the assumption is correct, the relationship between f and H_{sb}/H_s should be a concave-down shape (since $d^2 f / d\left(H_{sb}/H_s\right)^2$ is a negative value). It may be worthwhile to check this assumption through the relationship between f and H_{sb}/H_s. The data for plotting the relationship are the measured data of f and H_{sb}/H_s. The measured f can be determined from the measured wave heights as follows.

Using a forward finite difference scheme to describe the wave model (Eq. (3.113)), the formula for determining measured f is expressed as

$$f_j = -\frac{\left(H_{s,j+1}^2 c_{g,j+1} - H_{s,j}^2 c_{g,j}\right)}{\left(x_{j+1} - x_j\right)}\frac{h_j}{H_{s,j}^2 c_{g,j}} \tag{3.115}$$

where j is the grid number. Hereafter, the variable f determined from Eq. (3.115) is referred to as the measured f.

The required data set for plotting the relationship between f and H_{sb}/H_s is the measured data of h, T_p, H_s, and x. The computation of other related variables (e.g. L, k, and c_g) is based on linear wave theory. The breaker height (H_{sb}) is determined from Eq. (3.111). To avoid a large fluctuation in the relationship, the data of wave height variation across shore should have a small fluctuation.

Because of a small fluctuation of wave height variation across shore, the data from Dette et al. (1998) are used for plotting the relationship between measured f and H_{sb}/H_s. The relationship between measured f and H_{sb}/H_s is shown in Fig. 3.2.

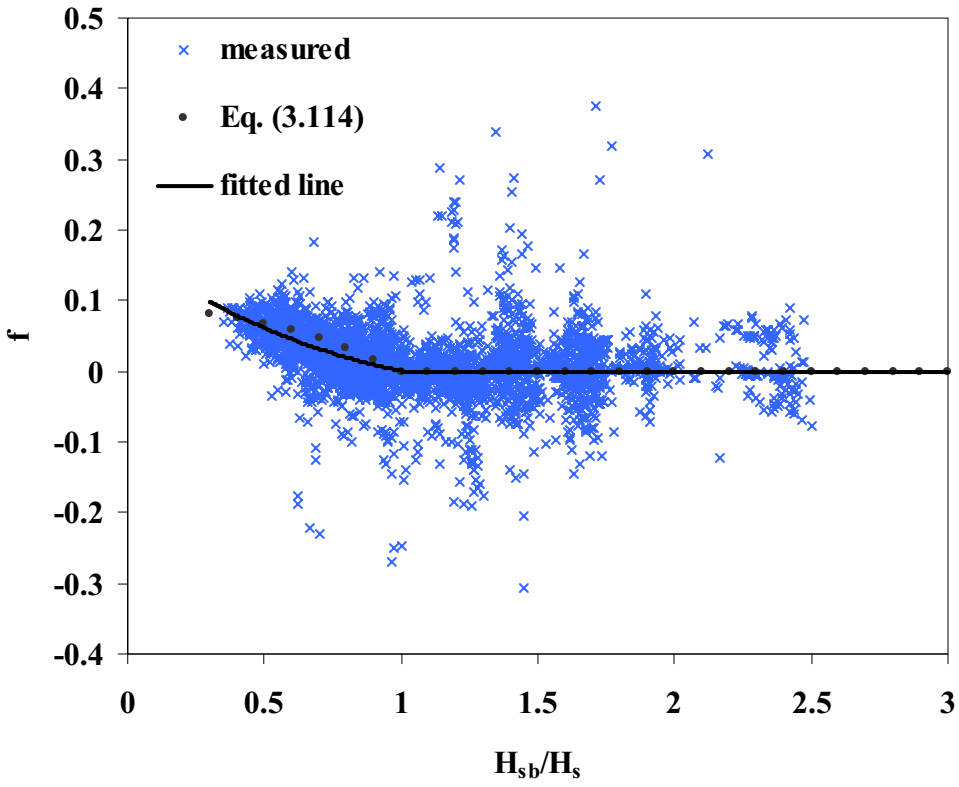

Fig. 3.2. Relationship between f and H_{sb}/H_s (measured data from Dette et al., 1998).

The line of computed f from Eq. (3.114) is shown as the dotted line in Fig. 3.2. It can be seen that Eq. (3.114) is fitted reasonably well to the measured f. However, the shape of measured f trends to be concave-up instead of concave-down as Eq. (3.114). It seems to be better to fit f with a quadratic equation as

$$f = K_{11}\left(\frac{H_{sb}}{H_s}\right)^2 + K_{12}\left(\frac{H_{sb}}{H_s}\right) + K_{13} \tag{3.116}$$

where K_{11} - K_{13} are the coefficients. From the multi-regression analysis (between measured f and H_{sb}/H_s) by using the data that $H_{sb}/H_s \le 1.0$, the values of K_{11} - K_{13} are 0.09, -0.26, and 0.17 respectively. The best-fitted line is shown as the solid line in Fig. 3.2. However, the values of K_{11} - K_{13} are not used in the wave model because the values of K_{11} - K_{13} are optimum only for the data of Dette et al. (1998), and they may change slightly when applying to all collected laboratory data.

Substituting Eq. (3.116) into Eq. (3.113), the general form of the modified model can be expressed as

$$\text{MD7:}\quad \frac{\rho g}{8}\frac{\partial\left(H_s^2 c_g\right)}{\partial x} = -\frac{\rho g H_s^2 c_g}{8h}\left[K_{11}\left(\frac{H_{sb}}{H_s}\right)^2 + K_{12}\left(\frac{H_{sb}}{H_s}\right) + K_{13}\right] \tag{3.117}$$

The collected irregular wave data shown in Table 3.12 are used to calibrate the model MD7 (Eq. (3.117)). The wave height transformation is computed by numerical integration of the model MD7 (Eq. (3.117)). The forward finite difference scheme is used to solve the

models. The calibration of the model is conducted by varying the values of K_{11} - K_{13} until the minimum error (ER_{avg}) of the model is obtained. The optimum values of K_{11} - K_{13} are 0.095, -0.263, and 0.179 respectively. The errors (ER_g and ER_{avg}) of model MD7 are shown in the last row of Table 3.14 and the last column of Table 3.15. It can be seen from Tables 3.14-3.15 that the model MD7 gives the best predictions.

To gain an impression of overall performance of the modified model (MD7) for computing H_s, the results of model MD7 are plotted against the measured data. Comparison between measured and computed significant wave heights from the model MD7 for all cases are shown in Fig. 3.3. Examples of computed significant wave height transformation across-shore are shown in Figs. 3.4 and 3.5. Case numbers in Figs. 3.4 and 3.5 are kept to be the same as the originals. Overall, it can be seen that the model MD7 gives a quite realistic simulation of the significant wave height transformation across-shore. However, the present model has certain limitations, which may restrict its use. The limitations of the model MD7 can be listed as follows.

a) The model gives the worst prediction for the case of broad-crested mound (ER_g = 20.9%, see test no. STKO in Table 3.15). The main error is caused by a sharp drop in measured wave height at a distance of x = 44.2 m on top of the bar (see Fig. 3.5d). This sharp drop occurred in all cases of the test no. STKO (at x = 44.2 m). It is difficult to find out the reason for such a sharp drop in the wave height.

b) The model gives only good predictions ($ER_g \approx 10\%$) for the wave on the barred beach or narrow-crested mound (see test no. R22xx, R62xx, R82xx, Ka1&Ka2, and STJO in Table 3.15; see also Figs. 3.4c-3.6g, and 3.5c). The model could not predict the rapid increase and decrease in wave heights near the bar. The model tends to give over prediction for the wave heights around the trough of narrow-bar (see Fig. 3.4c-3.4e) while it tends to give under prediction around the trough of the broad-bar (see Figs. 3.4f-3.4g).

c) As the model MD7 (Eq. (3.117)) is an empirical model, its validity may be limited according to the range of experimental conditions which were employed in the calibration. The present formula should be applicable for deepwater wave steepness (H_{so}/L_o) ranging between 0.002 and 0.064.

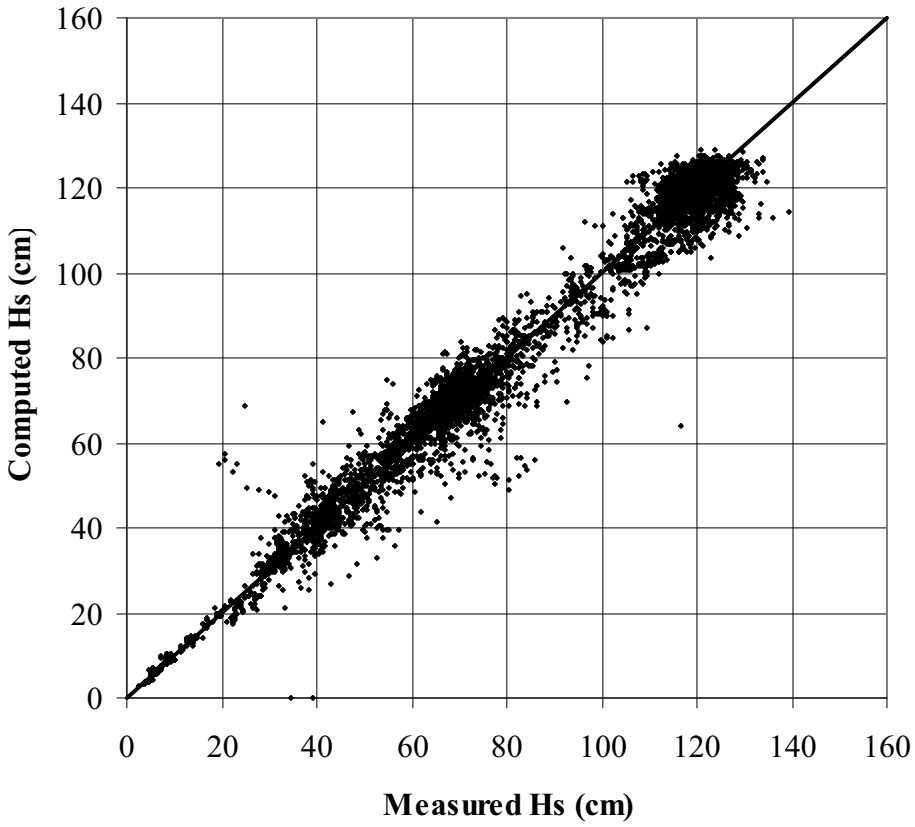

Fig. 3.3. Comparison between measured and computed significant wave height by using the model MD7 (measured data from Table 3.12).

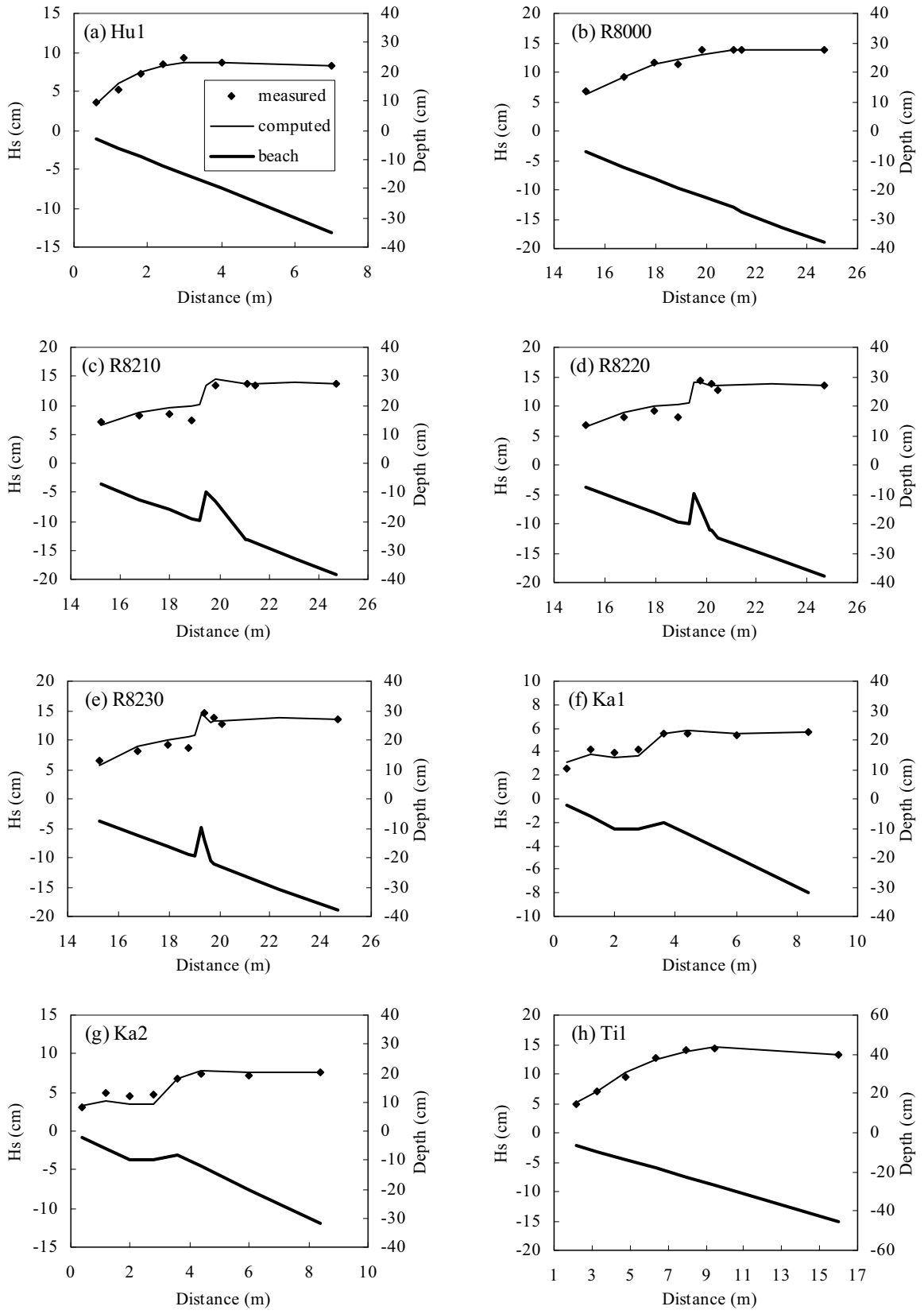

Fig. 3.4. Examples of measured and computed significant wave height transformation by using the model MD7 (measured data from small-scale experiments).

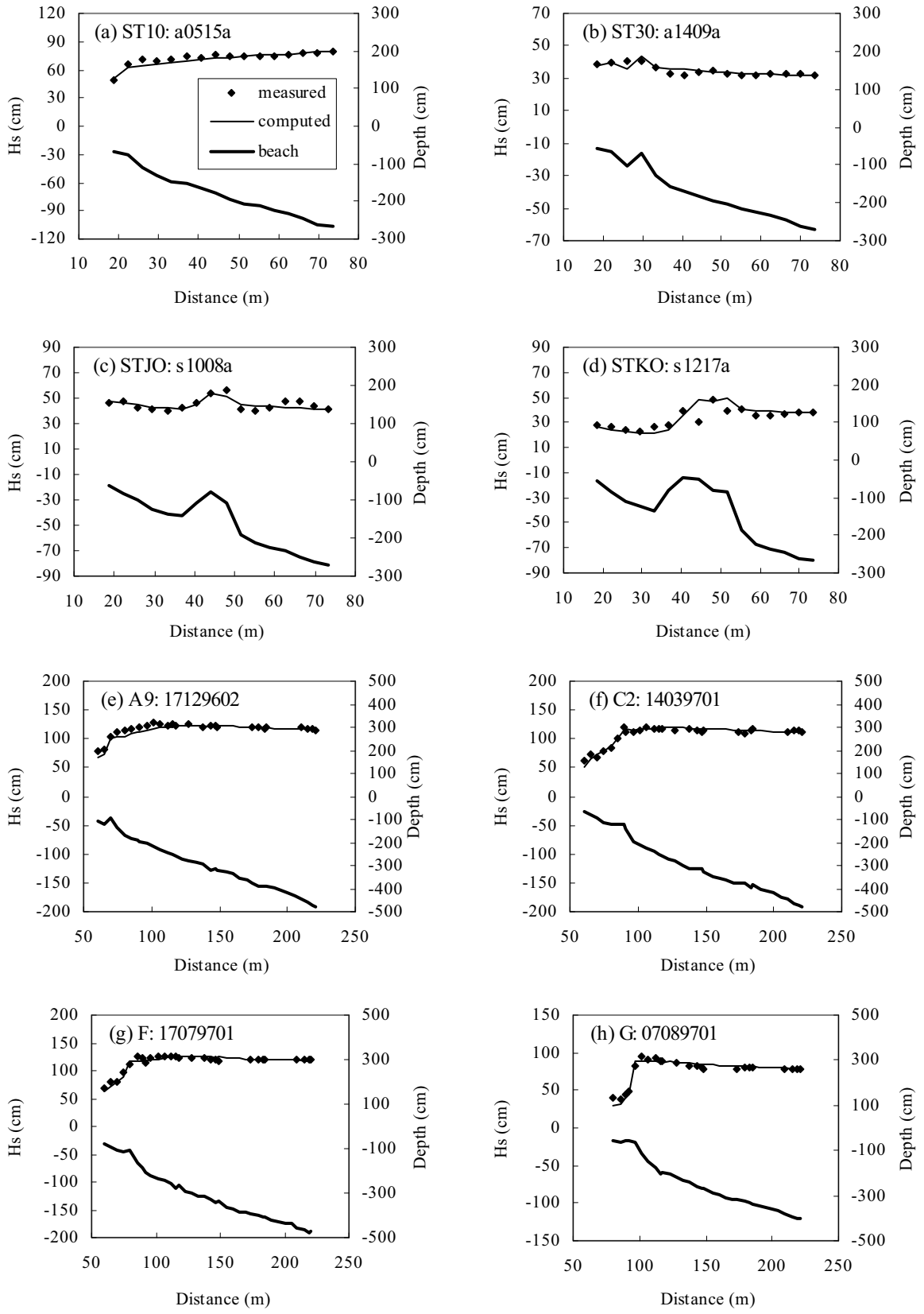

Fig. 3.5. Examples of measured and computed significant wave height transformation by using the model MD7 (measured data from large-scale experiments).

As shown in Sec. 3.3.3 that the regular wave model for computing H can be applied directly for computing H_s, it is expected that the irregular wave model for computing H_s should also be applicable for computing H. The model MD7 (Eq. (3.117)) is applied to regular waves as

$$\text{MD8:} \quad \frac{\rho g}{8}\frac{\partial\left(H^2 c_g\right)}{\partial x} = -\frac{\rho g H^2 c_g}{8h}\left[K_{14}\left(\frac{H_b}{H}\right)^2 + K_{15}\left(\frac{H_b}{H}\right) + K_{16}\right] \tag{3.118}$$

where K_{14} - K_{16} are the coefficients which can be determined from model calibration and H_b is the breaker height of the regular waves which is determined from the breaking criterion of Miche (1944).

The collected regular wave data shown in Table 3.11 are used to calibrate the model MD8 (Eq. (3.118)). The wave height transformation is computed by numerical integration of the model MD8. The forward finite difference scheme is used to solve the models. The calibration of the model is conducted by varying the values of K_{14} - K_{16} until the minimum error (ER_{avg}) of the model is obtained. The optimum values of K_{14} - K_{16} are 0.010, -0.128, and 0.226 respectively. The errors (ER_g and ER_{avg}) of the model MD8 and the existing regular wave models (shown in Sec. 3.3.2) are shown in Table 3.16. It can be seen from Table 3.16 that it is possible to use the model MD8 for computing regular wave heights transformation.

Substituting the calibrated coefficients K_{11} - K_{16} into Eqs. (3.117) and (3.118), the modified models for irregular and regular waves can be expressed as

$$\text{MD7:} \quad \frac{\rho g}{8}\frac{\partial\left(H_s^2 c_g\right)}{\partial x} = -\frac{\rho g H_s^2 c_g}{8h}\left[0.095\left(\frac{H_{sb}}{H_s}\right)^2 - 0.263\left(\frac{H_{sb}}{H_s}\right) + 0.179\right] \tag{3.119}$$

$$\text{MD8:} \quad \frac{\rho g}{8}\frac{\partial\left(H^2 c_g\right)}{\partial x} = -\frac{\rho g H^2 c_g}{8h}\left[0.010\left(\frac{H_b}{H}\right)^2 - 0.128\left(\frac{H_b}{H}\right) + 0.226\right] \tag{3.120}$$

Table 3.16. The errors (ER_g and ER_{avg}) of the six existing regular wave and the modified model (MD8) for 2 groups of experiment-scales (measured data from Table 3.11).

Regular wave models	ER_g		ER_{avg}
	Small-scale	Large-scale	
Battjes and Janssen (1978)	34.4	49.0	41.7
Thornton and Guza (1983)	22.1	26.0	24.0
Deigaard et al. (1991)	23.2	23.1	23.1
Dally et al. (1985)	17.3	20.2	18.8
Rattanapitikon and Shibayama, (1998)	16.3	16.6	16.4
Rattanapitikon et al. (2003)	16.3	17.7	17.0
MD8	15.9	17.5	16.7

3.4. Transformation of Maximum Wave Heights

The maximum wave height is one of the most essential required factors for the design of coastal structures. Wave data are usually available in deepwater but not available in the shallow water at the depths required. The wave heights in shallow water can be determined from wave height transformation model. Common methods to predict the maximum wave height in shallow water region may be classified into three main methods, i.e. highest wave representation method, individual wave method, and conversion method.

For the highest wave representation method, the maximum wave at offshore boundary is treated as a regular wave. The transformation of maximum wave height is calculated by using a regular wave model. The method is mainly used for structural design (Goda, 1985). When waves propagate to the nearshore zone, wave profiles steepen and eventually waves break. The higher waves tend to break at the greater distance from the shore while the lower waves still shoaling. At a certain location in the surf zone, the irregular wave train consists of breaking and shoaling waves and the highest wave at one location may not come from the same wave as the incident maximum wave height. Therefore, this method may be considered as an empirical method. The use of regular wave model directly may give under estimation of the maximum wave height in the surf zone. However, the method has the merit of simple application. It will be useful for practical works, if this method can be use for computing $H_{\max}$.

The individual wave method considers the propagation of individual waves in the time domain. The incident individual waves may be determined from the irregular wave records or from probability density function (*pdf*) of wave height. These individual waves are then propagated shoreward independently using an appropriate regular wave model, assuming no wave-to-wave interaction. A new irregular wave train (or a new *pdf* of wave height) at the required location can be constructed from the simulation results of all individual waves. The maximum wave height can be determined directly from the irregular wave train at the required location. However if the result from the model is the *pdf* of wave height, the maximum wave is set as that of highest one-250th wave ($H_{1/250}$). The result from this method is expected to be the best. However, the method has the demerit of time-consuming and it may not suitable for practical works.

The conversion method determines $H_{\max}$ from a relationship between H_{rms} to be $H_{\max}$. The method comprises of two parts of calculation, i.e. compute the H_{rms} transformation by using a suitable irregular wave model and then use an empirical formula to convert H_{rms} to be $H_{\max}$. Various irregular wave models can be used to compute H_{rms} (e.g. the model of Battjes and Janssen, 1978; Thornton and Guza, 1983; Baldock et al., 1998; and Rattanapitikon, 2007). Most of the existing can be used to compute H_{rms} (Rattanapitikon, 2007). The $H_{\max}$ can be determined from the known relationship between H_{rms} to be $H_{\max}$ (e.g. the relationships of Longuet-Higgins, 1952; and Rattanapitikon and Shibayama, 2007). Based on the experimental data from small-scale, large-scale, and field experiments, Rattanapitikon and Shibayama (2007) showed that the relationship of Longuet-Higgins (1952) gives the average error of about 30% while their relationship gives the average error of about 12%.

The present study focuses on the highest representation wave method as this appears to be the simple method for computing the $H_{\max}$ in shallow water. This paper is divided into two main parts. The first part describes some existing regular wave models. The second part describes modeling of irregular waves using highest wave representation method.

3.4.1. Regular wave model

The regular wave height transformation across-shore can be computed from the energy flux conservation as

$$\frac{\partial\left(Ec_g\right)}{\partial x} = -D_B \tag{3.121}$$

where $E = \rho g H^2 / 8$ is the wave energy density, ρ is the water density, g is the acceleration due to gravity, H is the wave height, c_g is the group velocity, x is the distance in cross shore direction, and D_B is the energy dissipation rate due to wave breaking which is zero outside the surf zone. The energy dissipation rate due to bottom friction is neglected. In the present study, all variables are based on the linear wave theory. Substituting $E = \rho g H^2 / 8$ into Eq. (3.121), the energy flux conservation can be written in terms of wave height as

$$\frac{\rho g}{8}\frac{\partial\left(H^2 c_g\right)}{\partial x} = -D_B \tag{3.122}$$

The wave height transformation can be computed from the energy flux conservation (Eq. (3.122)) by substituting the formula of the energy dissipation rate (D_B) and numerically integrating from offshore to shoreline. The difficulty of Eq. (3.122) is how to formulate the energy dissipation rate caused by the breaking waves.

During the past decades, various models have been developed for computing the energy dissipation of regular wave breaking. A briefly reviews of some existing D_B models are shown in the paper of Rattanapitikon (2008). The models are listed below.

a) Battjes and Janssen (1978): $$D_B = 0.47\frac{\rho g H^2}{4T} \tag{3.123}$$

b) Thornton and Guza (1983): $$D_B = 0.67\frac{\rho g H^3}{4Th} \tag{3.124}$$

c) Deigaard et al. (1991): $$D_B = 0.48\frac{\rho g h H^3}{T(4h^2 - H^2)} \tag{3.125}$$

d) Dally et al. (1985): $$D_B = 0.15\frac{\rho g c_g}{8h}\left[H^2 - (0.4h)^2\right] \tag{3.126}$$

e) Rattanapitikon and Shibayama (1998):

$$D_B = 0.15\frac{\rho g c}{8h}\left\{H^2 - \left[h\exp\left(-0.36 - \frac{1.25h}{\sqrt{LH}}\right)\right]^2\right\} \tag{3.127}$$

f) Rattanapitikon et al. (2003): $$D_B = 0.15\frac{\rho g c_g}{8h}\left[H^2 - (0.52H_b)^2\right] \tag{3.128}$$

g) Rattanapitikon (2008): $$D_B = \frac{\rho g H^2 c_g}{8h}\left[0.010\left(\frac{H_b}{H}\right)^2 - 0.128\left(\frac{H_b}{H}\right) + 0.226\right] \tag{3.129}$$

where h is the water depth, T is the wave period, c is the local phase velocity, L is the local wavelength, k is the local wave number, and H_b is the breaker height which can be calculated from Miche's (1944) formula as

$$H_b = 0.14L\tanh\left(kh\right) \tag{3.130}$$

3.4.2. Highest Wave Representation Model

For the highest wave representation approach, the wave models developed originally for regular waves are applied directly to irregular waves by using the equivalent regular waves based on the maximum wave height. When waves propagate to the nearshore zone, wave profiles steepen and eventually waves break. The higher waves tend to break at the greater distance from the shore while the lower waves still shoaling. At a certain location in the surf zone, the irregular wave train consists of breaking and shoaling waves and the highest wave at one location may not come from the same wave as the incident maximum wave height. Therefore, the use of regular wave model directly may give under estimation of the maximum wave height in the surf zone. Although the maximum wave at one location may not be the same wave as another location, the measured profile of $H_{\max}$ across shore is usually decay smoothly as the profile of regular wave height. It may be possible to apply the energy dissipation model of the regular wave for computing $H_{\max}$.

Since the dissipation formulas in section 2 [Eqs. (3.123) to (3.129)] were developed for regular waves, it is not clear which formula is suitable for the highest wave representation approach. Therefore, all of them are used to investigate the possibility of simulating the irregular wave height transformation by using the highest wave representation approach.

Substituting the dissipation formula [Eqs. (3.123) to (3.129), respectively] into Eq. (3.122) and applying for maximum wave heights, the highest wave representation models can be expressed as

model (1):
$$\frac{\rho g}{8}\frac{\partial\left(H_{\max}^2 c_g\right)}{\partial x} = -K_1 \frac{\rho g H_{\max}^2}{4T_p} \tag{3.131}$$

model (2):
$$\frac{\rho g}{8}\frac{\partial\left(H_{\max}^2 c_g\right)}{\partial x} = -K_2 \frac{\rho g H_{\max}^3}{4T_p h} \tag{3.132}$$

model (3):
$$\frac{\rho g}{8}\frac{\partial\left(H_{\max}^2 c_g\right)}{\partial x} = -K_3 \frac{\rho g h H_{\max}^3}{T_p(4h^2 - H_{\max}^2)} \tag{3.133}$$

model (4):
$$\frac{\rho g}{8}\frac{\partial\left(H_{\max}^2 c_g\right)}{\partial x} = -K_4 \frac{\rho g c_g}{8h}\left[H_{\max}^2 - (K_5 h)^2\right] \tag{3.134}$$

model (5):
$$\frac{\rho g}{8}\frac{\partial\left(H_{\max}^2 c_g\right)}{\partial x} = -K_6 \frac{\rho g c}{8h}\left\{H_{\max}^2 - \left[K_7 h \exp\left(-0.36 - \frac{1.25h}{\sqrt{LH_{\max}}}\right)\right]^2\right\} \tag{3.135}$$

model (6):
$$\frac{\rho g}{8}\frac{\partial\left(H_{\max}^2 c_g\right)}{\partial x} = -K_8 \frac{\rho g c_g}{8h}\left[H_{\max}^2 - (K_9 H_{\max b})^2\right] \tag{3.136}$$

model (7):
$$\frac{\rho g}{8}\frac{\partial\left(H_{\max}^2 c_g\right)}{\partial x} = \frac{\rho g H_{\max}^2 c_g}{8h}\left[K_{10}\left(\frac{H_{\max b}}{H_{\max}}\right)^2 + K_{11}\left(\frac{H_{\max b}}{H_{\max}}\right) + K_{12}\right] \tag{3.137}$$

where K_1 - K_{12} are the coefficients and the breaking criterion of Miche (1944) is applied to determine incipient wave breaking as

$$H_{\max b} = K_{13} L \tanh(kh) \tag{3.138}$$

where K_{13} is the coefficient. Hereafter, Eqs. (3.131)-(3.137) are referred to as MD1, MD2, MD3, MD4, MD5, MD6, and MD7 respectively. The energy dissipation (D_B) terms on the right hand side of models MD1-MD7 occur when $H_{\max} \geq H_{\max b}$ and is equal to zero when $H_{\max} < H_{\max b}$.

It can be seen from Eqs. (3.123)-(3.129) that the coefficients K_1 - K_{13} for the regular wave models are 0.47, 0.67, 0.48, 0.15, 0.4, 0.15, 1.0, 0.15, 0.52, 0.010, -0.128, 0.226, and 0.14 respectively. When applying to the irregular wave, K_1 - K_{13} are the adjustable coefficients to allow for the effect of the transformation to irregular waves. The variables c_g, c, L, and k in the models MD1-MD7 are calculated based on the spectral peak period (T_p).The spectral peak period is used because it is the most commonly used parameter and typically reported for the irregular wave data.

3.4.2.1. Trial simulation

The objective of this section is to test the applicability of models MD1-MD7 by using the coefficients K_1 - K_{13} which were proposed by the previous researchers for regular waves (shown in the second column of Table 3.18). Laboratory data of maximum wave height transformation from 4 sources, totaling 279 cases, were collected for calibration and examination of the irregular wave models. A summary of the collected laboratory data is shown in Table 3.17. The collected data are separated into 2 groups based on the experiment-scale, i.e. small-scale and large-scale experiments. The experiments of Smith and Kraus (1990), and Ting (2001) were performed in small-scale wave flumes under fixed bed conditions, while the experiments of Kraus and Smith (1994) and Dette et al. (1998) were undertaken in large-scale wave flumes under movable bed (sandy bed) conditions. The data cover a range of deepwater wave steepness (H_{so}/L_o, where H_{so} is the deepwater significant wave height) from 0.002 to 0.064.

The basic parameter for determination of the overall accuracy of the model is the average rms relative error (ER_{avg}), which is defined as

$$ER_{avg} = \frac{\sum_{n=1}^{tn} ER_{gn}}{tn} \tag{3.139}$$

where n is the data group number, ER_{gn} is the rms relative error of the group no. n, and tn is the total number of data groups. A small value of ER_{avg} indicates good overall accuracy of the wave model.

The rms relative error of each data group (ER_g) is defined as

$$ER_g = 100\sqrt{\frac{\sum_{i=1}^{nc}(H_{ci} - H_{mi})^2}{\sum_{i=1}^{nc} H_{mi}^2}} \tag{3.140}$$

where i is the wave height number, H_{ci} is the computed maximum wave height of number i, H_{mi} is the measured maximum wave height of number i, and nc is the total number of measured maximum wave heights in each data group.

The question of how good a model is is usually defined in a qualitative ranking (e.g. excellent, very good, good, fair, and poor). As the error of some existing irregular wave models is in the range of 7 to 21% (please see Rattanapitikon, 2007, Table 3.18), the qualification of error ranges of an irregular wave model may be classified into five ranges (i.e. excellent ($ER_g < 5.0$), very good ($5.0 \le ER_g < 10.0$), good ($10.0 \le ER_g < 15.0$), fair ($15.0 \le ER_g < 20.0$), and poor ($ER_g \ge 20.0$)) and the acceptable error should be less than 10%.

Table 3.17. Summary of collected experimental data used to calibrate and verify the irregular wave models.

Sources	Test Series	Descriptions	No. of cases	No. of Data	H_{so}/L_o
Smith and Kraus (1990)	R2000	plane beach	1	8	0.070
	R22xx	barred beach	3	24	0.070
	R6000	plane beach	1	8	0.040
	R62xx	barred beach	3	24	0.040
	R8000	plane beach	1	8	0.030
	R82xx	barred beach	3	24	0.030
Ting (2001)	Ti1	plane beach	1	7	0.024
Kraus and Smith (1994)	ST10	erosion toward equilibrium	26	416	0.013-0.064
	ST20	acoustic profiler tests	8	128	0.002-0.057
	ST30	Accretion toward equilibrium	19	304	0.003-0.007
	ST40	Dedicated hydrodynamics	12	192	0.005-0.050
	ST50	dune erosion, test 1	8	128	0.012-0.057
	ST60	dune erosion, test 2	9	144	0.009-0.022
	ST70	seawall, test 1	9	144	0.022-0.032
	ST80	Seawall, test 2	3	48	0.022
	ST90	berm flooding, test 1	3	48	0.050
	STAO	Foredune erosion	1	16	0.050
	STCO	Seawall, test 3	8	127	0.004-0.057
	STDO	berm flooding, test 2	3	48	0.050
	STJO	Narrow-crested mound	10	160	0.005-0.050
	STKO	broad-crested mound	9	144	0.005-0.050
Dette et al. (1998)	A8	1:20 beach slope, normal	7	147	0.010
	A9	1:20 beach slope, storm	15	390	0.018
	B1	1:10 beach slope, normal	8	191	0.010
	B2	1:10 beach slope, storm	15	392	0.018
	C1	1:5 beach slope, normal	4	95	0.010
	C2	1:5 beach slope, storm	17	459	0.018
	H1	1:15 beach slope, normal	2	43	0.010
	H2	1:15 beach slope, storm	15	398	0.018
	D1&D3	D.P.[1], no overtopping, normal	7	158	0.010
	D2	D.P.[1], no overtopping, storm	11	297	0.018
	E	D.P.[1], with overtopping, storm	11	297	0.018
	F	no D.P.[1], storm	12	324	0.018
	G	no D.P.[1], underwater barrier	14	365	0.012-0.018
Total			279	5706	0.002-0.064

[1] D.P. = dune protection.

The transformation of the maximum wave height from the models MD1-MD7 is determined by taking numerical integration from offshore to shoreline. The energy dissipation is set to be zero when $H_s < H_{\max b}$. The incipient wave breaking ($H_{\max b}$) is computed from Eq. (3.138). The forward finite difference scheme is used to solve the differential equations. The length step (Δx) is set to be equal to the length between the points of measured wave heights, except if $\Delta x > 5$m, Δx is set to be 5 m. The length steps (Δx) used in the present study are 0.2 - 1.5 m for small-scale experiments and 2.1 - 5.0 m for large-scale experiments.

Using the coefficients K_1 - K_{13} which were proposed for regular waves, errors of the models MD1-MD7 on predicting $H_{\max}$ for two groups of experiment-scales are shown in Table 3.18. It can be seen from Table 3.18 that all models give unacceptable results in simulating the maximum wave height transformation. This is a confirmation of the

findings of the previous researchers. The unacceptable results may be due to: 1) the incipient breaking point of regular wave and irregular wave may not be the same point and 2) the amount of energy dissipation of regular waves and irregular waves may not be the same. Therefore, the prediction may be more accurate if the coefficients (K_1 - K_{13}) are re-calibrated by using the maximum wave height data.

Table 3.18. The errors (ER_g and ER_{avg}) of the models MD1-MD7 (using the coefficients of regular waves) for 2 groups of experiment-scales (measured data from Table 3.17).

Models	Coefficients	ER_g		ER_{avg}
		small-scale	large-scale	
MD1 (Eq. (3.131))	$K_1 = 0.47,\ K_{13} = 0.142$	27.2	14.4	20.8
MD2 (Eq. (3.132))	$K_2 = 0.67,\ K_{13} = 0.142$	34.7	15.1	24.9
MD3 (Eq. (3.133))	$K_3 = 0.48,\ K_{13} = 0.142$	34.8	19.1	27.0
MD4 (Eq. (3.134))	$K_4 = 0.15,\ K_5 = 0.4,\ K_{13} = 0.142$	22.0	17.0	19.5
MD5 (Eq. (3.135))	$K_6 = 0.15,\ K_7 = 1.0,\ K_{13} = 0.142$	21.2	16.4	18.8
MD6 (Eq. (3.136))	$K_8 = 0.15,\ K_9 = 0.073,\ K_{13} = 0.142$	20.5	16.7	18.6
MD7 (Eq. (3.137))	$K_{10} = 0.010,\ K_{11} = -0.128,$ $K_{12} = 0.226,\ K_{13} = 0.142$	30.1	25.1	27.6

3.4.2.2. Model calibration and selection

A calibration of each model is conducted by varying the coefficients (K_1 - K_{13}) in the model until the minimum error (ER_{avg}) between measured and computed maximum wave heights is obtained. The optimum values of K_1 - K_{13} are shown in the second column of Table 3.19. The errors of models MD1-MD7 on simulating $H_{\max}$ for two groups of experiment-scales are shown in the third to fifth columns of Table 3.19.

Table 3.19. The errors (ER_g and ER_{avg}) of the models MD1-MD7 (using the calibrated coefficients) for 2 groups of experiment-scales (measured data from Table 3.17).

Models	Coefficients	ER_g		ER_{avg}
		small-scale	large-scale	
MD1 (Eq. (3.131))	$K_1 = 0.32,\ K_{13} = 0.14$	18.0	15.8	16.9
MD2 (Eq. (3.132))	$K_2 = 0.22,\ K_{13} = 0.086$	14.6	10.8	12.7
MD3 (Eq. (3.133))	$K_3 = 0.25,\ K_{13} = 0.086$	16.0	12.9	14.5
MD4 (Eq. (3.134))	$K_4 = 0.08,\ K_5 = 0.49,\ K_{13} = 0.086$	12.0	12.0	12.0
MD5 (Eq. (3.135))	$K_6 = 0.08,\ K_7 = 1.25,\ K_{13} = 0.086$	11.2	10.4	10.8
MD6 (Eq. (3.136))	$K_8 = 0.07,\ K_9 = 0.086,\ K_{13} = 0.086$	10.4	10.4	10.4
MD7 (Eq. (3.137))	$K_{10} = 0.123,\ K_{11} = -0.298,$ $K_{12} = 0.180,\ K_{13} = 0.086$	9.4	10.5	10.0

The examination results from Table 3.19 can be summarized as follows:

(o) The accuracy of all models is improved significantly after calibration.

(p) For small-scale wave flumes, the model MD7 gives very good predictions ($5.0 \le ER_g < 10.0$); the models MD2, MD4, MD5, and MD6 give good predictions ($10.0 \le ER_g < 15.0$); and the other models (MD1 and MD3) give fair predictions ($15.0 \le ER_g < 20.0$). The accuracy levels of the models in descending order are MD7, MD6, MD5, MD4, MD2, MD3, and MD1.

(q) For large-scale wave flumes, most models (MD2 to MD7) give good predictions ($10.0 \le ER_g < 15.0$), while the other (MD1) gives fair predictions ($15.0 \le ER_g < 20.0$). The accuracy levels of the models in descending order are MD6, MD5, MD7, MD2, MD4, MD3, and MD1.

(r) The overall accuracy levels of the models in descending order are MD7, MD6, MD5, MD4, MD2, MD3, and MD1.

(s) The models MD2, MD4, MD5, MD6, and MD7 give good predictions ($10.0 \le ER_g < 15.0$) for both small-scale and large-scale experiments. These models can be used for computing the maximum wave height transformation. However, lesser error is better. The model MD7 gives the best predictions (ER_{avg} = 10.2%).

(t) As the conversion method gives the average error of about 12% (mentioned in Sec. 1), while the average error (ER_{avg}) of the model MD7 is about 10%, the model MD7 seems to be acceptable for computing the maximum wave height transformation across-shore.

Substituting the calibrated coefficients K_{10} = 0.123, K_{11} = -0.298, K_{12} = 0.180, and K_{13} = 0.086 into the corresponding equations (Eqs. (3.137)-(3.138)), the wave model (MD7) for computing $H_{\max}$ can be expressed as

$$\text{MD7:}\quad \frac{\rho g}{8}\frac{\partial\left(H_{\max}^2 c_g\right)}{\partial x} = \frac{\rho g H_{\max}^2 c_g}{8h}\left[0.123\left(\frac{H_{\max b}}{H_{\max}}\right)^2 - 0.298\left(\frac{H_{\max b}}{H_{\max}}\right) + 0.180\right] \tag{3.141}$$

in which the incipient wave breaking is determined from the following formula.

$$H_{\max b} = 0.086L\tanh(kh) \tag{3.142}$$

V. CONCLUSIONS

Based on a large amount of published experimental results covering a wide range of test conditions under regular irregular wave actions, simple models are developed for computing the breaking wave and the transformation of three common representative wave heights (i.e. H_{rms}, $H_{1/3}$, and $H_{\max}$). The study can be divided into 5 parts. The first part describes the breaking wave formulas. The second to the fourth parts describe the development of wave models using representative wave approach. The last part describes the formulas for computing the representative wave heights using the conversion approach. The following is the conclusions of each part.

1. The first part of this study was undertaken to find out the breaking wave formulas, which can be used with the assumption of linear wave shoaling. A total of 695 cases collected from 26 sources of published laboratory data were used to examine the formulas for computing the breaker depth, assumed orbital to phase velocity ratio, and assumed breaker height. With regard to breaker depth formulas, the examination of 4 existing formulas (i.e. the formulas of Ogawa and Shuto, 1984; Dean and Dalrymple, 1984; and Gourlay, 1992; and Rattanapitikon, 2000) indicate that the formula of Rattanapitikon (2000) gives the best prediction with average error (ER_{avg}) of 15% but none of them can be used for a wide range of conditions. The existing formulas give considerable error for the cases of $H_o / L_o > 0.1$. A new formula was developed based on the reanalysis of the existing formulas. The new formula gives good overall prediction for general conditions (ER_{avg} = 12%). With regard to assumed orbital to phase velocity ratio and assumed breaker height, only the formulas of Isobe (1987) are available. The examination of Isobe's (1987) formulas show that the formulas give overall fairly good predictions (ER_{avg} = 19%); the formulas give good predictions for large-scale experiments, but fair predictions for small-scale experiments. The formulas of Isobe (1987) were modified by recalibrating the constants in the formulas. The average error (ER_{avg}) of the modified formula is 16%. The modified formulas are simpler but give better predictions than those of Isobe (1987). The new formulas were developed by reanalysis of the existing formulas. The new formulas give excellent predictions for all conditions (ER_{avg} = 3%).

2. The second part is undertaken to find out the suitable dissipation models, which can be used to compute H_{rms} for a wide range of experimental conditions. A total of 1723 cases from 13 sources of published experimental data are used to verify the models. The transformation of H_{rms} is computed from the energy flux conservation law. Eight existing dissipation models are selected to verify their applicability. The coefficients in all models are recalibrated before comparing the applicability of the models. The comparison shows that all selected models can be used for computing H_{rms}, with ER_{avg} of about 8.2-11.4%. The model of Battjes and Stive (1985) gives the best predictions (with ER_{avg} of 8.2%). The existing models are also modified by changing the breaker height formulas, inside the dissipation models and recalibrations. Substituting the seven formulas of H_b into the six existing dissipation models, 42 possible models are considered in this study. It is found that the accuracy

of most existing models is improved significantly by using the suitable breaker height formula. There are six suitable models (i.e. the model of BS85 and 5 modified models), which can be used for computing H_{rms}. The new model was also developed based of a framework of the dissipation model of Battjes and Janssen (1978). The model of Battjes and Janssen (1978) consists of three main formulas, i.e. the formulas of energy dissipation of a single broken wave, breaker height (H_b), and fraction of breaking waves (Q_b). The present study focuses mainly on the new derivation of Q_b formula. Unlike the common derivation, the formula of Q_b was derived directly from the measured wave heights by inverting the wave model together with dissipation model. The new model is better but simpler that that of BS85.

3. The third part was carried out to investigate the possibility of using the significant wave representation method. The significant wave height transformation across-shore was computed from the energy flux conservation. The selected six regular wave models were directly applied to the irregular waves (by using significant wave height and spectral peak period) to investigate their applicability for simulating significant wave height transformation. The breaking criterion of Miche (1944) was applied to compute the incipient breaker height. Laboratory data from small-scale and large-scale wave flumes were used to calibrate and examine the models. It was found that three regular wave models (with new coefficients) can be used for computing the significant wave heights with very good accuracy. This leads to the conclusion that the concept of significant wave representation method can be used for computing the significant wave height transformation across-shore. The best existing model can be re-written as a product of energy flux per unit depth and dimensionless function ($f\{H_{sb}/H_s\}$). The modification is performed by deriving the new formula of function f. The general form of f is derived from plotting the relationship between measured f and H_{sb}/H_s. Compared with the existing models, the modified model gives the best prediction. The modified model (with different coefficients) can also be applied to predict the regular wave height transformation.

4. The fourth part was carried out to investigate the possibility of using the highest wave representation method. The maximum wave height transformation across-shore was computed from the energy flux conservation. The selected six regular wave models were directly applied to the irregular waves (by using maximum wave height and spectral peak period) to investigate their applicability for simulating maximum wave height transformation. The breaking criterion of Miche (1944) was applied to compute the incipient breaker height. Laboratory data from small-scale and large-scale wave flumes were used to calibrate and examine the models. It was found that three regular wave models (with new coefficients) can be used for computing the maximum wave heights with good accuracy. This leads to the conclusion that the concept of highest wave representation method can be used for computing the maximum wave height transformation across-shore.

5. The last part concentrates on the relationships for conversion from H_{rms} to be $\overline{H}$, $H_{1/3}$, $H_{1/10}$, and $H_{\max}$ for shallow water region. Widely accepted relationships are derived based on the assumption of the Rayleigh distribution. The first objective of this study is to investigate the errors of estimating representative wave heights by using the relationships derived from the Rayleigh distribution in shallow water. Experimental data from small-scale, large-scale, and field experiments were used to examine the accuracy of the relationships. The examination showed that the assumption of Rayleigh distribution is not violated largely in shallow water,

especially for large-scale and field experiments. The relationships derived from Rayleigh distribution give very good estimations on $\overline{H}$ and $H_{1/3}$, good estimation on $H_{1/10}$ but fair estimations on $H_{\max}$. The proportional coefficients (β) in the relationships were plotted with three dimensionless parameters (H_{rms}/h, H_{rms}/H_{tr}, and H_{rms}/H_b). It was found that the coefficients β are governed mainly by the fraction of breaking waves (or H_{rms}/H_b) and the new coefficients β have been proposed as a function of H_{rms}/H_b. Comparing with the coefficients β derived from the Rayleigh distribution, the new coefficients β give slightly better accuracy on estimating $\overline{H}$ and $H_{1/3}$, and give better accuracy on estimating $H_{1/10}$ and $H_{\max}$. The new coefficients reveal that the Rayleigh distribution is valid in the offshore zone but gives overestimation of the number of large waves and underestimation of the number of small waves in the surf zone. The wave height distribution is gradually deviated from the Rayleigh distribution in the outer surf zone and the deviation becomes maximum at the inner surf zone.

REFERENCES

Andreas, E. L. and Wang, S. (2007). Predicting significant wave height off the northeast coast of the United States, Ocean Engineering 34 (8-9), 1328-1335.

Baldock, T. E., Holmes, P., Bunker, S. and Van Weert, P. (1998). Cross-shore hydrodynamics within an unsaturated surf zone, Coastal Engineering 34 (3-4), 173-196.

Battjes, J. A. and Groenendijk, H. W. (2000). Wave height distributions on shallow foreshores, Coastal Engineering 40 (3), 161-182.

Battjes, J. A. and Janssen, J. P. F. M. (1978). Energy loss and set-up due to breaking of random waves, Proc. 16th Coastal Eng. Conf., ASCE, 569-589.

Battjes, J. A. and Stive, M. J. F. (1985). Calibration and verification of a dissipation model for random breaking waves, J. Geophysical Research 90 (C5), 9159-9167.

Birkemeier, W. A., Donoghue, C., Long, C. E., Hathaway, K. K. and Baron C. F. (1997). The DELILAH Nearshore Experiment: Summary Data Report. US Army Corps of Engineers, Waterways Experiment Station, Vicksburg, MS.

Bouws, E., Gunther, H., Rosenthal, W. and Vincent, C. L. (1985). Similarity of the wind wave spectrum in finite depth water, J. Geophysical Research 90 (C1), 975-986.

Bowen, A. J., Inman, D. L. and Simmons, V. P. (1968). Wave set-down and set-up, J. Geophysical Research 73 (8), 2569-2577.

Bretschneider, C. L. (1968). Significant waves and wave spectrum, Ocean Industry, February, 40-46.

Bruun, P. (1954). Coastal Erosion and Development of Beach Profiles, US Army Beach Erosion Board, Tech. Memorandum No. 44, US Army Corps of Engineers.

Collins, J. I. and Weir, W. (1969). Probabilities of wave characteristics in the surf zone, Tetra Tech. Report, TC-149, Pasadena, California, USA, 122 p.

Cox, D. T., Kobayashi, N. and Okayasu, A. (1994). Vertical variations of fluid velocities and shear stress in surf zones, Proc. 24th Coastal Eng. Conf., ASCE, 98-112.

Cox, T. and Kobayashi, N. (1997). Kinematic undertow model with logarithmic boundary layer, J. Waterway, Port, Coastal and Ocean Engineering, ASCE 123 (6), 354-360.

Dally, W. R. (1990). Random breaking waves: a close-form solution for planar beaches, Coastal Engineering 14 (3), 233-263.

Dally, W. R. (1992). Random breaking waves: field verification of a wave-by-wave algorithm for engineering application, Coastal Engineering 16 (4), 369-397.

Dally, W. R., Dean, R. G. and Dalrymple, R. A. (1985). Wave height variation across beaches of arbitrary profile, J. Geophysical Research 90 (C6), 11917-11927.

Dean, R. G. (1965). Stream function representation of nonlinear ocean waves, J. Geophysical Research 70 (18), 4561-4572.

Dean, R. G. and Dalrymple, R. A. (1984). Water Wave Mechanics for Engineers and Scientists, Prentice-Hall, Inc., 115 p.

Dean, R. G. and Dalrymple, R. A. (1994). Water Wave Mechanics for Engineers and Scientists, World Scientific Publishing Co. Pte. Ltd., 193 p.
Deigaard, R., Justesen, P. and Fredsoe, J. (1991). Modelling of undertow by a one-equation turbulence model, Coastal Engineering 15 (5-6), 431-458.
Demerbilek, Z. and Vincent, L. (2006). Water wave mechanics (Part 2 – Chapter 1), Coastal Engineering Manual, EM1110-2-1100, Coastal and Hydraulics Laboratory – Engineering Research and Development Center, WES, U.S. Army Corps of Engineers, pp. II-1-75.
Dette, H. H, Peters, K. and Newe, J. (1998). MAST III – SAFE Project: Data Documentation, Large Wave Flume Experiments '96/97. Report No. 825 and 830, Leichtweiss-Institute, Technical University Braunschweig.
Elfrink, B., Hanes, D. M. and Ruessink, B. G. (2006). Parameterization and simulation of near bed orbital velocities under irregular waves in shallow water, Coastal Engineering 53, 915-927.
Galvin, C.J. (1969). Breaker travel and choice of design wave height, J. Waterways and Harbors Division, ASCE 95 (WW2), 175-200.
Goda, Y. (1964). Wave forces on a vertical circular cylinder: experiments and a proposed method of wave force computation, Rept. Port and Harbor Research Institute, Ministry of Transport, No. 8.
Goda, Y. (1970). A synthesis of breaker indices, Trans. Japan Society of Civil Engineers 2, 227-230.
Goda, Y. (1974). Estimation of wave statistics from spectral information, in Proc. Ocean Waves Measurement and Analysis Conference, ASCE, 320-337.
Goda, Y. (1977). Numerical experiments on the statistical variability of ocean waves, Rep. Port and Habour Research Institute 16, 3-26.
Goda, Y. (1979). A review on statistical interpretation of wave data, Report of Port and Harbour Research Institute 18, 5-32.
Goda, Y. (2000). Random Seas and the Design of Maritime Structures, World Scientific Publishing Co. Pte. Ltd.
Goda Y. (2004). A 2-D random wave transformation model with gradational breaker index, Coastal Engineering Journal, JSCE 46 (1), 1-38.
Goodknight, R. C. and Russel, T. L. (1963). Investigation of the statistics of wave heights, J. Waterways and Harbors Division, ASCE 89 (WW2), 29-55.
Gourlay, M. R. (1978). Wave Generated Currents, Ph.D. Thesis, Dept. of Civil Eng., University of Queensland.
Gourlay, M. R. (1992). Wave set-up, wave run-up and beach water table: Interaction between surf zone hydraulics and groundwater hydraulics, Coastal Engineering 17 (1-2), 93-144.
Grasmeijer, B. T. and van Rijn, L. C. (1999). Transport of fine sands by currents and waves, III: breaking waves over barred profile with ripples. J. of Waterway, Port, Coastal, and Ocean Eng. 125 (2), 71-79.
Hamilton, D. G. and Ebersole, B. A. (2001). Establishing uniform longshore currents in a large-scale sediment transport facility, Coastal Engineering 42 (3), 199-218.
Hamm, L., Madsen, P. A. and Peregrine, D. H. (1993). Wave transformation in the nearshore zone: a review, Coastal Engineering, 21 (1-3), 5-39.
Hansen, J. B. and Svendsen, I. A. (1979). Regular waves in shoaling water experimental data, Series paper No. 21, Institute of Hydrodynamics and Hydraulic Eng., Technical University of Denmark, Denmark, 243 p.
Hansen, J. B. and Svendsen, I. A. (1984). A theoretical and experiment study of undertow, Proc. 19th Coastal Engineering Conf., ASCE, 2246-2262.

Hansen, J. B. (1990). Periodic waves in the surf zone: Analysis of experimental data, Coastal Eng. 14 (1), 19-41.

Hasselmann, K., Barnett, T. P., Bouws, E., Carlson, H., Cartwright, D. E., Enke, K., Ewing, J. A., Gienapp, H., Hasselmann, D. E., Kruseman, P., Meerburg, A., Müller, P., Olbers, D. J., Richter, K., Sell, W. and Walden, H. (1973). Measurements of wind-wave growth and swell decay during the Joint North Sea Wave Project (JONSWAP), Deutsche Hydrographische Zeitschrift A8 (12), 1–95.

Hattori, M. and Aono, T. (1985). Experimental study on turbulence structures under breaking waves, Coastal Engineering in Japan, 28, 97-116.

Herbers, T. H. C., Elgar, S., Guza, R. T. and O'Reilly, W. C. (2006). Surface gravity waves and nearshore circulation, DUCK94 Experiment Data Server: SPUV Pressure Sensor Wave Height Data. Available online at: http://dksrv.usace.army.mi/jg/dk94dir.

Horikawa, K. and Kuo, C. T. (1966). A study of wave transformation inside the surf zone, Proc. 10th Coastal Eng. Conf., ASCE, 217-233.

Hughes, S. A. and Borgman, L. E. (1987). Beta-Rayleigh distribution for shallow water wave heights, in Proc. of the American Society of Civil Engineers Specialty Conference on Coastal Hydrodynamics, ASCE, 17-31.

Hurue, M. (1990). Two-Dimensional Distribution of Undertow due to Irregular Waves, B.Eng. Thesis, Dept. of Civil Eng., Yokohama National University, Japan. (in Japanese)

Hwung, H. H., Chyan, J. M. and Chung, Y. C. (1992). Energy dissipation and air bubbles mixing inside surf zone, Proc. 23rd Coastal Eng. Conf., ASCE, 308-321.

Isobe, M. (1985). Calculation and application of first-order cnoidal wave theory, Coastal Engineering 9 (4), 309-325.

Isobe, M. (1987). A parabolic equation model for transformation of irregular waves due to refraction, diffraction and breaking, Coastal Engineering in Japan, JSCE 30, 33-47.

Iversen, H. W. (1952). Laboratory study of breakers, Gravity Waves, Circular 52, US Bureau of Standards, 9-32.

Iwagaki, Y., Sakai, T., Tsukioka, K. and Sawai, N. (1974). Relationship between vertical distribution of water particle velocity and type of breakers on beaches, Coastal Engineering in Japan, JSCE 17, 51-58.

Kajima, R., Shimizu, T., Maruyama, K. and Saito, S. (1982). Experiments of beach profile change with a large wave flume, Proc. 18th Coastal Engineering Conf., ASCE, 1385-1404.

Kajima, R., Shimizu, T., Maruyama, K. and Saito, S. (1983). On-offshore Sediment Transport Experiment by Using Large Scale Wave Flume, Collected Data No. 1-8, Central Research Institute of Electric Power Industry, Japan (in Japanese).

Kamphuis, J. W. (1991). Incipient wave breaking, Coastal Eng. 15 (3), 185-203.

Katayama, H. (1991). Cross-shore Velocity Distribution due to Breaking of Irregular Waves on a Bar-Type Beach, B.Eng. Thesis, Department of Civil Engineering, Yokohama National University, Japan (in Japanese).

Komar, P. D. and Gaughan, M. K. (1972). Airy wave theory and breaker height prediction, Proc. 13rd Coastal Eng. Conf., ASCE, 405-418.

Kraus, N. C., Gingerich, K. J. and Rosati, J. D. (1989). DUCK85 Surf Zone Sand Transport Experiment, Technical Report CERC-89-5, U.S. Army Corps of Engineers, Waterways Experiment Station.

Kraus, N.C. and Smith, J.M. (1994). SUPERTANK Laboratory Data Collection Project, Tech. Report CERC-94-3, Waterways Experiment Station, US Army Corps of Engineers, Vols. 1-2, 515 p.
Kuriyama, Y. (1996). Model of wave height and fraction of breaking waves on a barred beach, Proc. 25th Coastal Engineering Conf., ASCE, 247-259.
Larson, M. and Kraus, N. C. (1989). SBEACH: Numerical model for simulating storm-induced beach change, Report 1, Tech. Report CERC-89-9, Waterways Experiment Station, US Army Corps of Engineers, 267 p.
Larson, M. (1995). Model for decay of random waves in surf zone J. Waterway, Port, Coastal, and Ocean Engineering, ASCE 121 (1), 1-12.
Le Mehaute, B. and Koh, R. C. Y. (1967). On the breaking of waves arriving at an angle to the shore, J. Hydraulic Research 5 (1), 67-88.
Longuet-Higgins, M. S. (1952). On the statistical distribution of the heights of sea waves, J. Marine Research 11 (3), 246-266.
Madsen, O. S. (1976). Wave climate of the continental margin: Elements of its mathematical description, D. J. Stanley and D. J. P. Swift (Editors), Marine Sediment Transport in Environmental Management, Wiley, New York, 65-87.
McCowan, J. (1894). On the highest waves of a permanent type, Philosophical Magazine, Edinburgh 38 (5), 351-358.
Mendez, F. J., Losada, I. J. and Medina, R. (2004). Transformation model of wave height distribution on planar beaches, Coastal Engineering 50 (3), 97-115.
Miche, R. (1944). Mouvements ondulatoires des mers en profondeur constante on decroissante, Ann. des Ponts et Chaussees, Ch.114, 131-164, 270-292, and 369-406.
Mitsuyasu, H. (1962). Experimental study on wave force against a wall, Rept. Transportation Technical Res. Inst., No. 47 (in Japanese).
Mitsuyasu, H. (1970). On the growth of spectrum of wind-generated waves (2) - spectral shape of wind waves at finite fetch, Proc. 17th Japanese Conf. Coastal Engineering, 1-7 (in Japanese).
Mizuguchi, M. (1980). An heuristic model of wave height distribution in surf zone, Proc. 17th Coastal Engineering Conf., ASCE, 278-289.
Mizuguchi, M. (1982). Individual wave analysis of irregular wave deformation in the nearshore zone, Proc. 18th Coastal Engineering Conf., ASCE, 485-504.
Nadaoka, K., Kondoh, T. and Tanaka. N. (1982). The structure of velocity field within the surf zone revealed by means of laser-doppler anemometry, Port and Harbor Research Institute 21 (2), 50-102 (in Japanese).
Nagayama, S. (1983). Study on the Change of Wave Height and Energy in the Surf Zone, Bach. Thesis, Civil Eng., Yokohama National University, Japan, 24-35 (in Japanese).
Nairn, R. B. (1990). Prediction of Cross-shore Sediment Transport and Beach Profile Evolution, Ph.D. thesis, Dept. of Civil Eng., Imperial College, London.
Ogawa, Y. and Shuto, N. (1984). Run-up of periodic waves on beaches of non-uniform slope, Proc. 19th Coastal Eng. Conf., ASCE, 328-344.
Okayasu, A., Shibayama, T. and Mimura, N. (1986). Velocity field under plunging waves, Proc. 20th Coastal Eng. Conf., ASCE, 660-674.
Okayasu, A., Shibayama, T. and Horikawa, K. (1988). Verification of undertow in the surf zone, Proc. 21st Coastal Eng. Conf., ASCE, 478-491.
Oliveira, F. S. B. F. (2007). Numerical modelling of deformation of multi-directional random waves over a varying topography, Ocean Engineering 34 (2), 337-342.

Ostendorf, D. W. and Madsen, O. S. (1979). An analysis of longshore current and associated sediment transport in the surf zone, Report No. 241, Dept. of Civil Eng., MIT, 169 p.
Ozaki, A., Sasaki, M. and Usui, Y. (1977). Study on rip currents: experimental observation of nearshore circulation on a sloping bottom, Coastal Eng. in Japan, JSCE 20, 147-158.
Rattanapitikon, W. (1995). Cross-Shore Sediment Transport and Beach Deformation Model, Dissertation, Dept. Civil Engineering, Yokohama National University, Yokohama, Japan, 90 p.
Rattanapitikon, W. and Shibayama T. (1998). Energy dissipation model for regular and irregular breaking waves, Coastal Engineering Journal 40 (4), 327-346.
Rattanapitikon, W. and Shibayama, T. (2000). Verification and modification of breaker height formulas, Coastal Eng. Journal, JSCE 42 (4), 389-406.
Rattanapitikon, W., Vivattanasirisak, T. and Shibayama, T. (2003). A proposal of new breaker height formula, Coastal Engineering Journal, JSCE 45 (1), 29-48.
Rattanapitikon, W., Karunchintadit, R. and Shibayama, T. (2003). Irregular wave height transformation using representative wave approach, Coastal Engineering Journal 45 (3), 489-510.
Rattanapitikon, W. and Shibayama T. (2007). Estimation of shallow water representative wave heights, Coastal Engineering Journal, JSCE 49 (3), 291-310.
Rattanapitikon, W. (2007). Calibration and modification of energy dissipation models for irregular waves breaking, Ocean Engineering 34 (11-12), 1592-1601.
Roelvink, J. A. and Reniers A. J. H. M. (1995). LIP 11D Delta Flume Experiments: A Data Set for Profile Model Validation, Report No. H 2130, Delft Hydraulics.
Ruessink, B. G., Walstra, D. J. R. and Southgate, H. N. (2003). Calibration and verification of a parametric wave model on barred beaches, Coastal Engineering 48 (3), 139-149.
Saeki, H. and Sasaki, M. (1973). A study of the deformation of waves after breaking, Proc. 20th Japanese Conf. on Coastal Engineering, JSCE, 559-564 (in Japanese).
Sato, S., Fukuhama, M. and Horikawa, K. (1988). Measurements of near-bottom velocities in random waves on a constant slope, Coastal Eng. in Japan, JSCE 31 (2), 219-229.
Sato, S., Isayama, T. and Shibayama, T. (1989). Long-wave component in near bottom velocity under random waves on a gentle slope, Coastal Eng. in Japan, JSCE 32 (2), 149-159.
Sato, S., Homma, K. and Shibayama, T. (1990). Laboratory study on sand suspension due to breaking waves, Coastal Eng. in Japan, JSCE 33 (2), 219-231.
Seyama, A. and Kimura, A. (1988). The measured properties of irregular wave breaking and wave height change after breaking on slope, Proc. 21st Coastal Eng. Conf., ASCE, 419-432.
Shibayama, T. and Horikawa, K. (1985). Numerical model for two-dimensional beach transformation, Proc. of Japan Society of Civil Engineers, No. 357/II-3 (Hydraulic and Sanitary), 167-176.
Shuto, N. (1974). Non-linear long waves in channel of variable section, Coastal Engineering in Japan, JSCE 17, 1-12.
Singamsetti, S. R. and Wind, H. G. (1980). Characteristics of breaking and shoaling periodic waves normally incident on to plane beaches of constant slope, Report M 1371, Delft Hydraulic Lab., Delft, The Netherlands.
Smith, D. A. (1974). Radiation stress effects on wave set-up in the surf zone, M.Sc. Thesis, Dept. of Civil Eng., University of London, Imperial College.

Smith, J. M. and Kraus, N. C. (1990). Laboratory study on macro-features of wave breaking over bars and artificial reefs, Technical Report CERC-90-12, WES, U.S. Army Corps of Engineers, 232 p.

Southgate, H. N. and Nairn, R. B. (1993). Deterministic profile modelling of nearshore processes, Part 1. Waves and currents. Coastal Engineering, 19 (1-2), 27-56.

Stive, M. J. F. (1984). Energy dissipation in wave breaking on gentle slopes, Coastal Engineering 8 (2), 99-127.

Stokes, G. G. (1847). On the theory of oscillatory waves, Trans. Camb. Phil. Soc. 8, 411-455.

Sultan, N. (1995). Irregular wave kinematics in the surf zone, Ph.D. Dissertation, Texas A&M University, College Station, Texas, USA.

Sunamura, T. and Horikawa, K. (1974). Two-dimensional beach transformation due to waves, Proc. 14th Coastal Eng. Conf., ASCE, 920-938.

Sunamura, T. (1980). A laboratory study of offshore transport of sediment and a model for eroding beaches, Proc. 17th Coastal Eng. Conf., ASCE, 1051-1070.

Thornton, E. B. and Guza, R. T. (1983). Transformation of wave height distribution, J. Geophysical Research 88 (C10), 5925-5938.

Thornton, E. B. and Guza, R. T. (1986). Surf zone longshore currents and random waves: field data and model, J. Physical Oceanography 16 (7), 1165-1178.

Ting, C. K. and Kirby, J. T. (1994). Observation of undertow and turbulence in a laboratory surf zone, Coastal Eng. 24 (1-2), 51-80.

Ting, F. C. K. (2001). Laboratory study of wave and turbulence velocity in broad-banded irregular wave surf zone, Coastal Engineering 43 (3-4), 183-208.

Ting, F. C. K. (2002). Laboratory study of wave and turbulence characteristics in narrow-banded irregular breaking waves, Coastal Engineering 46 (4), 291-313.

Van Dorn, W. G. (1978). Breaking invariants in shoaling waves, J. Geophysical Research 83 (C6), 2981-2988.

Visser, P. J. (1977). Wave Set-up: Experimental Investigation on Normally Incident Waves, Report No. 77-1, Laboratory of Fluid Mech., Dept. of Civil Eng., Delft University of Tech., Delft, The Netherlands.

Visser, P. J. (1982). The Proper Longshore Current in a Wave Basin, Report No. 82-1, Laboratory of Fluid Mech., Dept. of Civil Eng., Delft University of Tech., Delft, The Netherlands, 86 p.

Walker, J. R. (1974). Wave transformations over a sloping bottom and over a three-dimensional shoal, Miscellaneous Report No. 11, University of Hawaii, Look Lab-75-11, Honlulu, Hawaii, USA.

Watanabe, A., Hara, T. and Horikawa, K. (1984). Study on breaking condition for compound wave trains, Coastal Engineering in Japan, JSCE 27, 71-82.

Weggel, J. R. (1972). Maximum breaker height, J. Waterways, Harbors Eng. Div. 98 (WW4), 529-548.

OUTPUTS

International Journals:

1) Rattanapitikon, W. and Shibayama, T. (2006). Breaking wave formulas for breaking depth and orbital to phase velocity ratio, Coastal Engineering Journal (JSCE), Vol. 48, No. 4, 395-416.
2) Rattanapitikon, W. (2007). Calibration and modification of energy dissipation models for irregular waves breaking, Ocean Engineering, Vol. 34, 1592-1601.
3) Rattanapitikon, W. and Shibayama, T. (2007). Estimation of shallow water representative wave heights, Coastal Engineering Journal (JSCE), Vol. 49, No. 3, 291-310.
4) Rattanapitikon, W. (2008). Transformation of significant wave height using representative wave approach, Ocean Engineering, Vol. 35, 1259-1270.
5) Rattanapitikon, W. and Sawanggun, S. (2008). Energy dissipation model for a parametric wave approach based on laboratory and field experiments, Songklanakarin J. of Science and Technology (accepted).

International Conferences:

1) Rattanapitikon, W. and Sawanggun, S. (2007). Modification of a parametric model, The 4th International Conference on Asian and Pacific Coasts [CD-ROM], September 21-24, Nanjing, China, pp. 346-357.

APPENDIX: PAPER REPRINTS

A.1 Breaking wave formulas for breaking depth and orbital to phase velocity ratio

Reprinted from:

Rattanapitikon, W. and Shibayama, T. (2006). Breaking wave formulas for breaking depth and orbital to phase velocity ratio, Coastal Engineering Journal (JSCE), Vol. 48, No. 4, 395-416.

World Scientific
www.worldscientific.com

JAPAN SOCIETY OF CIVIL ENGINEERS
COASTAL ENGINEERING COMMITTEE

Coastal Engineering Journal, Vol. 48, No. 4 (2006) 395–416

BREAKING WAVE FORMULAS FOR BREAKING DEPTH AND ORBITAL TO PHASE VELOCITY RATIO

WINYU RATTANAPITIKON

Civil Engineering Program,
Sirindhorn International Institute of Technology,
Thammasat University, Pathum Thani 12121, Thailand
winyu@siit.tu.ac.th

TOMOYA SHIBAYAMA

Department of Civil Engineering,
Yokohama National University, 79-5 Tokiwadai,
Hodogaya-ku, Yokohama, 240-8501, Japan
tomo@ynu.ac.jp

Received 23 March 2006
Revised 31 August 2006

This study was undertaken to find out the suitable breaking wave formulas for computing breaker depth, and corresponding orbital to phase velocity ratio and breaker height converted with linear wave theory. A large amount and wide range of published laboratory data (695 cases collected from 26 sources of published laboratory data) were used to examine and develop the breaker formulas. Examination of some existing formulas indicates that none of them can be used for a wide range of experimental conditions. New breaker formulas were developed based on the re-analysis of the existing formulas. Overall, the new formulas give good predictions over a wide range of experimental conditions.

Keywords: Breaking point; breaker depth; orbital to phase velocity ratio; incipient wave breaking.

1. Introduction

When waves propagate from offshore to the near shore zone, wave profiles become steep. The increase in wave steepness continues until the wave breaks. To analyze the coastal processes, breaking point is one of the most essentially required factors. In the wave model (or beach deformation model), it is necessary to determine the breaking point accurately because the breaking point is the point at which to start

including the energy dissipation rate or surface roller into the wave model. Unless the breaking point is accurately predicted (no matter how exact the equations governing wave deformation in and outside the surf zone will be), an accurate computation of the wave field or other wave-induced phenomena cannot be expected.

In the wave model, the breaker height is commonly used to indicate the location of wave breaking. Many breaker height formulas have been proposed over the past century [see Rattanapitikon *et al.*, 2003]. These formulas can be used to determine the breaking point if wave shoaling is computed accurately. However, it is well known that the linear wave theory gives underestimation of wave height just before the breaking point. Therefore, if the breaker height formula is used together with the linear wave shoaling, the predicted breaking point will shift on shoreward of the real one [Isobe, 1987]. This will cause certain error in the computation of wave height transformation and other wave-induced phenomena, e.g. undertow, suspended sediment concentration, sediment transport, and beach deformation.

There are two methods for dealing with the problem of underestimating the linear wave shoaling. The first method uses nonlinear wave theories for computing wave shoaling [e.g. Stokes, 1847; Dean, 1965; Shuto, 1974; and Isobe, 1985]. The second one uses linear wave theory to compute wave shoaling and uses other variables, instead of breaker height, to compute the breaking point [e.g. Watanabe *et al.*, 1984; Isobe, 1987; and Rattanapitikon, 1995]. Since the linear wave theory is most widely used in practice, the present study concentrates on the second method of using other variables to determine the breaking point. The variables that may be used to determine the breaking point are breaker depth, orbital to phase velocity ratio at the breaking point based on linear wave shoaling (hereafter referred to as assumed orbital to phase velocity ratio), and breaker height based on linear wave shoaling (hereafter referred to as assumed breaker height). Various formulas have been proposed to compute these three variables [e.g. Ogawa and Shuto, 1984; Dean and Dalrymple, 1984; Isobe, 1987; and Rattanapitikon, 1995]. The objective of this study is to find out the reliable formulas for computing these three variables.

All of the existing breaking wave formulas are empirically determined from the laboratory data. It is known that the validity of empirical formula may be limited according to the range of wave and bottom slope conditions that were employed in calibration or verification. To make an empirical formula reliable, it is necessary to calibrate or verify the formula with a large amount and wide range of laboratory data.

As it is difficult to measure the breaking point of each individual wave in the field, small-scale and large-scale laboratory experiments are the sources of quantitative information for examination of the breaking point formulas. Laboratory data of the breaking point from 26 sources, covering 695 cases, have been collected for the examination of the breaking wave formulas. The data set used in this study is the same as that used in the analysis of breaker height formula of Rattanapitikon *et al.* [2003]. These data are used for analysis because no data source differs significantly

from other data sources (see Figs. 5 and 6 in the paper of Rattanapitikon *et al.*, 2003). The data cover a wide range of wave and bottom slope conditions: the deepwater wave steepness (H_o/L_o) ranging between 0.001 and 0.112, and the bottom slope (m) ranging between 0 and 0.38. The data include four types of beach conditions, i.e. plane beach, barred beach, stepped beach and movable (sandy) beach. All experiments were performed for regular waves in both small-scale and large-scale wave flumes. The experiments of Kajima *et al.* [1982] and Kraus and Smith [1994] were performed in large-scale wave flumes and other experiments were performed in small-scale wave flumes. The small-scale experiments were conducted under fixed beach conditions whereas the large-scale experiments were carried out under movable beach conditions. A summary of the collected laboratory data is given in Table 1.

This paper is divided into two main sections. The first section describes the breaker depth formulas while the second section describes the formulas for computing assumed orbital to phase velocity ratio and assumed breaker height.

2. Breaker Depth Formulas

It is known that the limitation of empirical formulas depends on the range of laboratory data. As the previous formulas were developed based on a limited range of laboratory data, it is expected that errors of the existing formulas are large when compared with a wide range of laboratory data. However, some existing formulas may give good predictions for a wide range of laboratory data. Therefore, it is necessary to examine the accuracy of existing formulas before developing new formulas.

2.1. *Examination of existing formulas*

Brief reviews of selected breaker depth formulas are described below.

(a) Goda [1970] analyzed several sets of laboratory data of breaking waves on slopes obtained by several researchers [Iversen, 1952; Mitsuyasu, 1962; and Goda, 1964]. The experiments cover a range of $0.01 < m < 0.1$ and $0.003 < H_o/L_o < 0.07$. He proposed a diagram presenting criteria for predicting breaker depth. The diagram is expressed in terms of the ratio of breaker depth to deepwater wave height (h_b/H_o) as a function of deepwater wave steepness (H_o/L_o) and bottom slope (m). As it is not convenient to use this diagram in the wave model, it is not considered in the present study.

(b) Ogawa and Shuto [1984] reanalyzed the same data set as used by Goda [1970] and obtained the following formula:

$$h_b = 0.46 H_o m^{-0.12} \left(\frac{H_o}{L_o}\right)^{-0.2} \tag{1}$$

where h_b is the breaker depth, m is the bottom slope, H_o is the deepwater wave height, and L_o is the deepwater wavelength. This formula is referred to as OS84 hereafter.

Table 1. Summary of collected experimental data.

No	Sources	No. of cases	Beach conditions	m^{**}	H_o/L_o
1	Cox *et al.* [1994]	1	plane beach	0.03	0.016
2	Galvin [1969]*	19	plane beach	0.05–0.20	0.001–0.051
3	Hansen and Svendsen [1979]	17	plane beach	0.03	0.002–0.069
4	Hattori and Aono [1985]	3	stepped beach	0.00	0.006–0.021
5	Horikawa and Kuo [1966]	98	plane beach	0.01–0.05	0.006–0.073
		60	stepped beach	0.00	0.007–0.100
6	Hwung *et al.* [1992]	2	plane beach	0.07	0.026–0.048
7	Iversen [1952]*	63	plane beach	0.02–0.10	0.003–0.080
8	Iwagaki *et al.* [1974]	39	plane beach	0.03–0.10	0.005–0.074
9	Kajima *et al.* [1982]***	98	movable beach	0.00–0.29	0.003–0.112
10	Kraus and Smith [1994]***	23	movable beach	0.01–0.13	0.003–0.066
11	Mizuguchi [1980]*	1	plane beach	0.10	0.045
12	Nadaoka *et al.* [1982]	12	plane beach	0.05	0.013–0.080
13	Nagayama [1983]	1	plane beach	0.05	0.027
		5	barred beach	0.05	0.025–0.051
		6	stepped beach	0.00–0.05	0.025–0.055
14	Okayasu *et al.* [1986]	2	plane beach	0.05	0.023–0.025
15	Okayasu *et al.* [1988]	10	plane beach	0.03–0.05	0.009–0.054
16	Ozaki *et al.* [1977]	20	plane beach	0.10	0.005–0.060
17	Saeki and Sasaki [1973]*	2	plane beach	0.02	0.005–0.039
18	Sato *et al.* [1988]	3	plane beach	0.05	0.031–0.050
19	Sato *et al.* [1989]	2	plane beach	0.03	0.019–0.036
20	Sato *et al.* [1990]	7	plane beach	0.05	0.003–0.073
21	Singamsetti and Wind [1980]*	95	plane beach	0.03–0.20	0.018–0.079
22	Smith and Kraus [1990]*	5	plane beach	0.03	0.009–0.092
		75	barred beach	0.03–0.38	0.008–0.096
23	Stive [1984]	2	plane beach	0.03	0.010–0.032
24	Ting and Kirby [1994]	2	plane beach	0.03	0.002–0.020
25	Visser [1982]*	7	plane beach	0.05–0.10	0.014–0.079
26	Walker [1974]*	15	plane beach	0.03	0.001–0.037
	Total	695		0.00–0.38	0.001–0.112

*data from Smith and Kraus [1990]
**measured seaward of the breaking point
***large-scale laboratory

(c) Dean and Dalrymple [1984] used linear wave theory to derive a breaker depth formula from energy flux conservation together with the breaker height formula of McCowan [1894].

$$h_b = \frac{1}{g^{1/5}\kappa^{4/5}} \left(\frac{H_o^2 c_o}{2} \right)^{2/5} \tag{2}$$

where $\kappa = 0.78$ is a constant in the formula of McCowan [1984], g is the gravity acceleration, and c_o is the deepwater phase velocity. Using linear wave theory, Eq. (2) is re-written in the similar form as Eq. (1) as

$$h_b = 0.64 H_o \left(\frac{H_o}{L_o} \right)^{-0.2} \tag{3}$$

This formula is referred to as DD84 hereafter. It should be noted that Eq. (2) [or Eq. (3)] was not calibrated with any laboratory data.

(d) Gourlay [1992] proposed an empirical formula based on seven sources of laboratory data [Bowen *et al.*, 1968; Smith, 1974; Visser, 1977; Gourlay, 1978; Van Dorn, 1978; Stive, 1984; and Hansen and Svendsen, 1979]. The experiments cover a range of $0.022 < m < 0.1$ and $0.001 < H_o/L_o < 0.066$. The data were used to plot the relationship between h_b/H_o and $m^2 H_o/L_o$. The curve fitting yields

$$h_b = 0.259 H_o m^{-0.34} \left(\frac{H_o}{L_o} \right)^{-0.17} \tag{4}$$

This formula is referred to as GL92 hereafter.

(e) The breaker depth formula can also be derived from the existing breaker height formulas. In the present study, the breaker depth formula is derived from the breaker height formulas of Rattanapitikon and Shibayama [2000], which were modified from the breaker height formulas of Komar and Gaughan [1972] and Goda [1970]. The breaker height formulas are expressed as follows:

$$H_b = (10.02m^3 - 7.46m^2 + 1.32m + 0.55) H_o \left(\frac{H_o}{L_o} \right)^{-0.2} \tag{5}$$

$$H_b = 0.17 L_o \left[1 - \exp\left(\frac{\pi h_b}{L_o} (16.21m^2 - 7.07m - 1.55) \right) \right] \tag{6}$$

where H_b is the breaker height.

Substituting H_b from Eq. (5) into Eq. (6), yields

$$h_b = \frac{L_o}{\pi(16.21m^2 - 7.07m - 1.55)} \ln \Bigg[1 - (58.94m^3 - 43.88m^2 + 7.76m + 3.24) \left(\frac{H_o}{L_o} \right)^{0.8} \Bigg] \tag{7}$$

This formula is referred to as RS00 hereafter.

A straightforward way to examine the accuracy of a formula is to compare the computed breaker depth data with the laboratory data. The basic parameter for determination of the overall accuracy of the formula is the average root mean square relative error (ER_{avg}), which is defined as

$$ER_{avg} = \frac{\sum_{j=1}^{\text{in}} ER_{gj}}{tn} \tag{8}$$

where ER_{gj} is the root mean square relative error of the data group j (the group number), and tn is the total number of groups. The small value of ER_{avg} indicates good overall accuracy of the formula.

The group rms relative error (ER_g) is defined as

$$ER_g = 100\sqrt{\frac{\sum_{i=1}^{ng}(h_{ci} - h_{mi})^2}{\sum_{i=1}^{ng} h_{mi}^2}} \tag{9}$$

where i is the breaker depth number, h_{ci} is the computed breaker depth of number i, h_{mi} is the measured breaker depth of number i, and ng is the total number of measured breaker depths in each data group.

The laboratory data from 26 sources are used to examine the validity of each formula. The laboratory data cover a wide range of wave and bottom conditions ($0.001 \leq H_o/L_o \leq 0.112$, and $0 \leq m \leq 0.38$). In order to see the performance of each formula clearly, the experimental conditions are divided into various groups of deepwater wave steepness (H_o/L_o), bottom slope (m) and experiment scale.

As the breaker depth diagram of Goda [1970] shows that h_b/H_o increases rapidly when $H_o/L_o > 0.1$, the laboratory data are divided into two groups of deepwater wave steepness, i.e. $H_o/L_o \leq 0.1$, and $H_o/L_o > 0.1$. Following the classification of Rattanapitikon and Shibayama [2000], the bottom slope of the collected data is divided into four groups, i.e. horizontal ($m = 0$), gentle ($0 < m \leq 0.07$), intermediate ($0.07 < m \leq 0.10$), and steep ($0.1 < m \leq 0.38$). The experiment scale is separated into 2 groups, i.e. small-scale and large-scale experiments. The collected data shown in Table 1 are separated into 11 groups of deepwater wave steepness, bottom slope and experiment scale (see Table 2). The total number of cases for each group is shown in the fourth column of Table 2.

The computations of the breaker depth formulas are carried out with 26 sources of collected data (see Table 1). The variables required for the examinations are h_b, H_o, L_o, and m. The bottom slope (m) used in the computation is the local bottom slope seaward of the breaking point and the negative slope is set to be zero. The errors (ER_g) of OS84, DD84, GL92 and RS00 for each group are shown in the fifth to eighth columns of Table 2. The examination results from Table 2 are summarized as follows:

Table 2. The root mean square relative error (ER_g) of the formulas for computing the breaker depth (laboratory data from 26 sources shown in Table 1).

Experiment	H_o/L_o	Bottom Slope	No. of Cases	OS84	DD84	GL92	RS00	Eq. (14)
Small scale	≤ 0.1	$m = 0$	64	N.A.*	17.7	N.A.*	19.2	17.1
		$0 < m \leq 0.07$	338	13.7	16.0	26.1	11.6	12.7
		$0.07 < m \leq 0.10$	102	14.8	15.0	21.4	13.5	12.8
		$0.1 < m \leq 0.38$	70	13.8	19.2	33.2	16.0	12.5
		ER_{avg} (for 4 groups)		14.1	17.0	26.9	15.0	13.8
Large scale	≤ 0.1	$m = 0$	3	N.A.*	26.1	N.A.*	11.1	11.1
		$0 < m \leq 0.07$	33	13.9	20.1	43.3	14.6	13.7
		$0.07 < m \leq 0.10$	21	11.9	12.2	18.9	10.5	10.3
		$0.1 < m \leq 0.38$	46	18.3	27.5	21.2	17.4	18.1
		ER_{avg} (for 4 groups)		14.7	21.5	27.8	13.4	13.3
Large scale	> 0.1	$m = 0$	0	—	—	—	—	—
		$0 < m \leq 0.07$	8	40.2	43.4	36.5	19.0	6.0
		$0.07 < m \leq 0.10$	3	39.9	37.5	46.1	16.0	5.9
		$0.1 < m \leq 0.38$	7	37.2	28.2	52.5	20.6	10.4
		ER_{avg} (for 3 groups)		39.1	36.4	45.0	18.5	7.5
		ER_{avg} (for 11 groups)		22.6	23.9	33.2	15.4	11.9

*N.A. = Not Applicable

(a) The overall accuracy of each existing formula for small-scale and large-scale experiments is nearly the same.
(b) The formulas of OS84 and RS00 give good prediction for cases of $H_o/L_o \leq 0.1$ but fair prediction for cases of $H_o/L_o > 0.1$, while the formulas of DD84 and GL92 give fair prediction for most conditions.
(c) The formula of OS84 is better than that of DD84 because of the term of bottom-slope-effect.
(d) The formula of OS84 gives good prediction for cases of $H_o/L_o \leq 0.1$ but it is not valid for the breaking wave on the horizontal bed ($m = 0$) and should not be used for cases of $H_o/L_o > 0.1$.
(e) For cases of $H_o/L_o > 0.1$, only the formula of RS00 predicts increase of h_b/H_o at $H_o/L_o > 0.1$, while other existing formulas do not have this property.
(f) Considering the simplicity and accuracy of the formula, the formula of OS84 is more attractive than that of RS00 for cases of $H_o/L_o \leq 0.1$.
(g) The formula of RS00 seems to be the best but it is the longest one. Moreover, it should be used with care for cases of $H_o/L_o > 0.1$.
(h) Overall, the predictions of all existing formulas are unsatisfactory for cases of $H_o/L_o > 0.1$.

2.2. *Formula development*

From the existing breaker depth formulas, the breaker depth may depend on the deepwater wave height (H_o), the deepwater wavelength (L_o), and the bottom slope at the breaking location (m). Therefore, the possible breaker depth formula can be expressed as the following functions.

$$\frac{h_b}{H_o} = f_1\left\{m, \frac{H_o}{L_o}\right\} \tag{10}$$

$$\frac{h_b}{L_o} = f_2\left\{m, \frac{H_o}{L_o}\right\} \tag{11}$$

where f_1 and f_2 are functions proposed for each formula.

The laboratory data from 26 sources (shown in Table 1) are used to develop a new breaker depth formula. The required data for the development are h_b, H_o, m, and L_o. The data of h_b, m, and T were measured directly from the experiments, while the data of H_o and L_o are computed by using linear wave theory. The development of a new formula is separated into two stages. The first stage is determination of the general relationship between h_b/H_o versus H_o/L_o (or h_b/L_o versus H_o/L_o). After that, the bottom-slope-effect is included explicitly into the general formula obtained from the first stage.

2.2.1. *Relationship between h_b/H_o and H_o/L_o*

The relationship between h_b/H_o and H_o/L_o is plotted to determine the possible form of the fitting equation (see Fig. 1). The relationship in Fig. 1 can be fitted with a power function. However, the parameter h_b/H_o tends to increase rapidly when $H_o/L_o > 0.1$. It is better to separate the formula into two parts, i.e. for

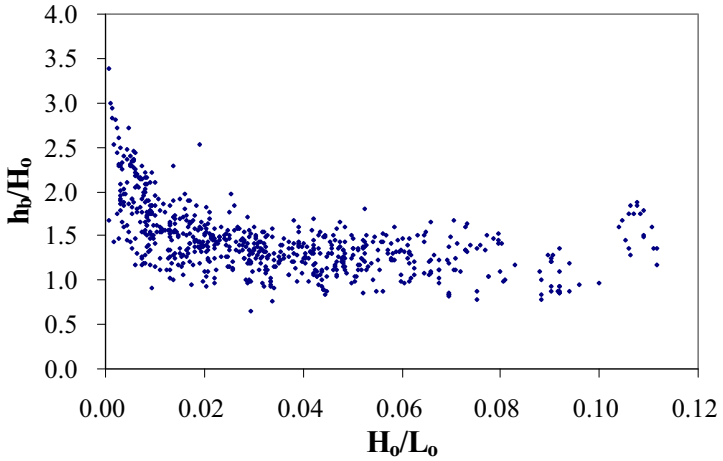

Fig. 1. Relationship between h_b/H_o and H_o/L_o (laboratory data from 26 sources shown in Table 1).

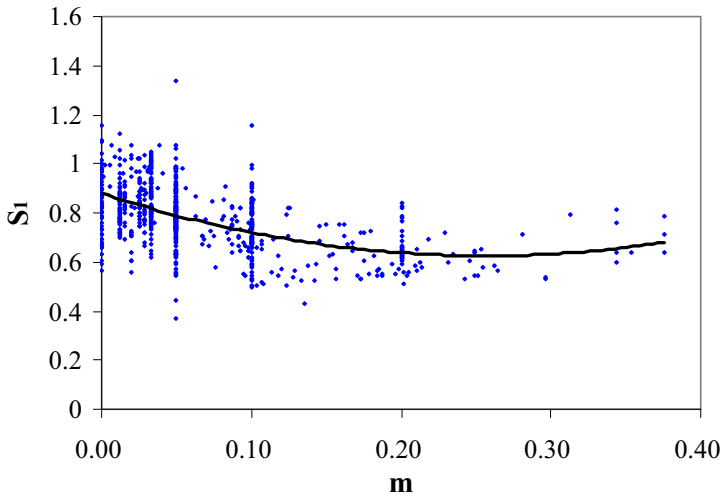

Fig. 2. Relationship between slope effect coefficient S_1 and bottom slope m when $K_1 = -0.16$ (laboratory data from 26 sources shown in Table 1 excluding the data that $H_o/L_o > 0.1$). Solid line is the computed S_1 from Eq. (13).

$H_o/L_o \leq 0.1$ and for $H_o/L_o > 0.1$. The general formula can be expressed in form of step function as

$$\frac{h_b}{H_o} = S_1 \left(\frac{H_o}{L_o}\right)^{K_1} \quad \text{for} \quad \frac{H_o}{L_o} \leq 0.1 \tag{12a}$$

$$\frac{h_b}{H_o} = S_1 \left(\frac{H_o}{L_o}\right)^{K_2} \quad \text{for} \quad \frac{H_o}{L_o} > 0.1 \tag{12b}$$

where S_1 is the slope effect coefficient, and K_1 and K_2 are constants.

Using the laboratory data of h_b, H_o, and L_o for cases that $H_o/L_o \leq 0.1$, the data of S_1 can be determined from Eq. (12a), if constant K_1 is given. For a given constant K_1, the relationship between S_1 versus m is plotted to determine the correlation. Then the constant K_1 is gradually adjusted until it gives the best correlation. The relationship shows the best correlation when $K_1 = -0.16$ (see Fig. 2). The scatter in Fig. 2 is caused by Eq. (12). The scatter shows a weak correlation between S_1 and m. However, it still has some correlation. The relationship in Fig. 2 can be fitted with a parabolic function. The coefficients in the parabolic function are determined from multi-regression analysis. After the analysis, it is found that the best-fit formula for S_1 can be expressed as

$$S_1 = 3.86m^2 - 1.98m + 0.88 \tag{13}$$

Using the laboratory data for the cases that $H_o/L_o > 0.1$, the constant K_2 can be determined from regression analysis. The regression analysis between $\ln(h_b/(S_1 H_o))$ and $\ln(H_o/L_o)$ yields $K_2 = -0.34$.

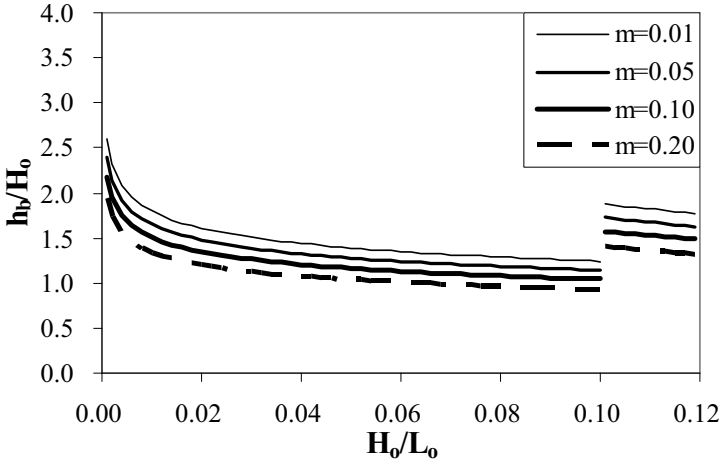

Fig. 3. The plots of Eq. (14) for 4 bottom slopes ($m = 0.01$, $m = 0.05$, $m = 0.10$, and $m = 0.20$).

Substituting Eq. (13) and $K_1 = -0.16$, $K_2 = -0.34$ into Eq. (12), yields

$$h_b = (3.86m^2 - 1.98m + 0.88)H_o \left(\frac{H_o}{L_o}\right)^{-0.16} \quad \text{for} \quad \frac{H_o}{L_o} \leq 0.1 \tag{14a}$$

$$h_b = (3.86m^2 - 1.98m + 0.88)H_o \left(\frac{H_o}{L_o}\right)^{-0.34} \quad \text{for} \quad \frac{H_o}{L_o} > 0.1 \tag{14b}$$

The plots of Eq. (14) for 4 bottom slopes ($m = 0.01$, $m = 0.05$, $m = 0.10$, and $m = 0.20$) are shown as the lines in Fig. 3. The computations of the breaker depth from Eq. (14) are carried out with 26 sources of collected data (see Table 1). The verification results are shown in the last column of Table 2. The verification results are summarized as follows:

(a) Equation (14) gives better predictions than the existing formulas (except RS00) for all conditions while gives better predictions than the formula of RS00 for most conditions.
(b) Although Eq. (14) is more complicated than the formula of RS00 (which is the longest and the best existing formula), the accuracy of Eq. (14) for the cases of $H_o/L_o > 0.1$ is significantly better than that of RS00 (ER_{avg} of RS00 is 18.5% while ER_{avg} of Eq. (14) is 7.5%).
(c) In comparison with the existing formulas, overall accuracy of Eq. (14) is slightly better for the cases of $H_o/L_o \leq 0.1$, but much better for the cases of $H_o/L_o > 0.1$.
(d) The overall accuracy of Eq. (14) is significantly better than that of existing formulas, and its use is recommended for computing the breaker depth. However, since the formula is based on deepwater wave height, it is not possible to model the multiple breaking and reformation in a wave model.

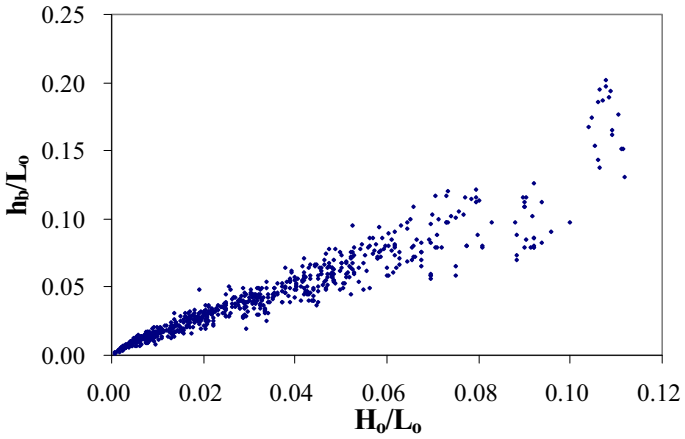

Fig. 4. Relationship between h_b and H_o/L_o (laboratory data from 26 sources shown in Table 1).

The validity of empirical formulas may be limited according to the range of experimental conditions used in the calibrations or verifications. Therefore, the use of Eq. (14) becomes questionable for the beaches having slope greater than 0.38 and for the deepwater wave steepness (H_o/L_o) greater than 0.112. Moreover, since the experimental data is not available for the range of $0.100 < H_o/L_o < 0.104$ (see Fig. 1), caution should be taken when using Eq. (14b) for this narrow range. The step function in Eq. (14) can be avoided by adding the equation for the transition zone ($0.100 < H_o/L_o < 0.104$) but Eq. (14) will become quite complicated. Because of the complexity of equation, unavailability of experimental data, and the narrow range of transition zone, the transition zone is not considered in this study.

2.2.2. *Relationship between h_b/L_o and H_o/L_o*

The relationships between h_b/L_o and H_o/L_o is plotted to determine the possible form of fitting equation (see Fig. 4). Figure 4 shows that the relationship can also be fitted with a power function as in Fig. 1. Therefore, the general formula can be expressed in the same form as in Eq. (12). Following the same procedure as in Sec. 2.2.1, the final formula is the same as shown in Eq. (14).

3. Assumed Orbital to Phase Velocity Ratio and Assumed Breaker Height

The objective of this section is to find out the reliable formulas for computing the assumed orbital to phase velocity ratio at the breaking ($\hat{u}_b/c_b$) and assumed breaker height (H_b'). These two variables are considered at the same time because one variable can be converted into the other by using linear wave theory. Similar to the previous section, examination of existing formulas is performed before developing new formulas.

3.1. *Examination of existing formulas*

Only two formulas have been proposed to compute — $\hat{u}_b/c_b$ and H'_b. A brief review of the formulas is described below.

Watanabe *et al.* [1984] pointed out that the assumed orbital to phase velocity ratio is more suitable for the computation of composite waves breaking. They employed the linear wave theory to determine the assumed breaker height (H'_b) from the known deepwater wave height (H_o), water depth at breaking (h_b) and wave period (T).

$$H'_b = H_o \sqrt{\frac{c_o}{2c_{gb}}} \tag{15}$$

where c_{gb} is the group velocity at the breaking point.

Then the assumed orbital velocity ($\hat{u}_b$) at the mean water level is computed from H'_b, h_b, and T by using linear wave theory as

$$\hat{u}_b = \frac{H'_b c_b k_b}{2\tanh(k_b h_b)} = \frac{\pi c_b H'_b}{L_o \tanh^2(k_b h_b)} \tag{16}$$

where c_b is the phase velocity at the breaking point, and k_b is the wave number at the breaking point.

By reanalyzing the same data set as used by Goda [1970], the breaker depth diagram of Goda [1970] was converted into a diagram, which shows the relationship between assumed orbital to phase velocity ratio ($\hat{u}_b/c_b$) versus relative water depth (h_b/L_o), and bottom slope (m). For convenience in numerical calculation, the diagram of Watanabe *et al.* [1984] was approximated by Isobe [1987] as

$$\hat{u}_b = c_b \left\{ 0.53 - 0.3\exp\left[-3\sqrt{\frac{h_b}{L_o}}\right] + 5m_b^{3/2}\exp\left[-45\left(\sqrt{\frac{h_b}{L_o}} - 0.1\right)^2\right]\right\} \tag{17}$$

This formula is referred to as WI87a hereafter.

Since wave height is the convenient variable for many wave models, Rattanapitikon [1995] converted Eq. (17) to be expressed in terms of assumed breaker height (H'_b) by using linear wave theory.

$$H'_b = \frac{L_o \tanh^2(k_b h_b)}{\pi}\left\{0.53 - 0.3\exp\left[-3\sqrt{\frac{h_b}{L_o}}\right] + 5m_b^{3/2}\exp\left[-45\left(\sqrt{\frac{h_b}{L_o}} - 0.1\right)^2\right]\right\} \tag{18}$$

This formula is referred to as WI87b hereafter. It should be noted that Eqs. (17) and (18) are identical in terms of linear wave theory.

Table 3. The root mean square relative error (ER_g) of the formulas for computing $\hat{u}_b$ and H'_b (laboratory data from 26 sources shown in Table 1).

Experiment	Bottom Slope	No. of Cases	Formulas for computing $\hat{u}_b$			Formulas for computing H'_b		
			WI87a	Eq. (20)	Eq. (31)	WI87b	Eq. (21)	Eq. (30)
Small scale	$m = 0$	64	21.9	20.2	4.1	21.0	19.3	4.0
	$0 < m \leq 0.07$	338	16.7	15.0	2.7	15.4	13.6	2.4
	$0.07 < m \leq 0.10$	102	17.6	15.8	3.7	16.2	14.4	3.4
	$0.1 < m \leq 0.38$	70	37.4	19.4	2.6	41.7	20.9	2.7
	ER_{avg} (for 4 groups)		23.4	17.6	3.3	23.5	17.1	3.1
Large scale	$m = 0$	3	12.8	11.5	1.5	13.2	11.8	1.5
	$0 < m \leq 0.07$	41	11.8	15.6	4.2	11.7	15.5	4.4
	$0.07 < m \leq 0.10$	24	14.1	12.5	3.1	13.0	12.0	3.1
	$0.1 < m \leq 0.38$	53	19.9	17.4	3.3	19.3	16.4	3.0
	ER_{avg} (for 4 groups)		14.6	14.3	3.0	14.3	13.9	3.0
	ER_{avg} (for 8 groups)		19.0	15.9	3.2	18.9	15.5	3.1

The collected data shown in Table 1 are used to examine the formulas of WI87a and WI87b. The required data in the examination are $\hat{u}_b$, H'_b, h_b, L_o, c_b, m, and k_b. The water depth (h_b) and the bottom slope (m) were measured directly from the experiments. The data of H'_b and $\hat{u}_b$ are determined by using Eqs. (15) and (16) respectively. Other variables are computed based on the linear wave theory from the known h_b and T.

As the variation of $\hat{u}_b/c_b$ for the cases of $H_o/L_o > 0.1$ shows the same trend as that of $H_o/L_o \leq 0.1$ [see Fig. 4 in the paper of Watanabe *et al.*, 1984], the collected laboratory data are divided on the basis of bottom slope and experiment scale. The computations of $\hat{u}_b$ and H'_b from Eqs. (17) and (18) are carried out with 26 sources of collected data (see Table 1). The errors ER_g of WI87a and WI87b for 8 groups of bottom slope and experiment scale are shown in the fourth and seventh columns of Table 3. The examination results from Table 3 are summarized as follows:

(a) As formulas of WI87a and WI87b are identical in terms of linear wave theory, it is not surprising to see that the accuracy of both formulas is nearly the same.
(b) Although the development of formulas WI87a and WI87b were based on small-scale experiments, they surprisingly give good prediction for the large-scale experiments but fair prediction for the small-scale experiments. However, what is considered a good formula should give good predictions for both small-scale and large-scale experimental conditions. The formulas of WI87a and WI87b should be modified for better predictions.
(c) The errors of WI87a and WI87b tend to vary with the bottom slope. The error is pronounced for the breaking wave on the steep slope.

3.2. *Formula modification*

Since WI87a and WI87b give fair predictions for the small-scale experiments and the error of predictions tend to vary with the bottom slope, it is expected that reformulating the term of bottom-slope-effect and changing the constants in the formula can improve the accuracy. Equation (17) can be written in a general form as

$$\frac{\hat{u}_b}{c_b} = K_3 + K_4 \exp\left[-K_5\sqrt{\frac{h_b}{L_o}}\right] + K_6(m_b^{K_7} + K_8)\exp\left[-K_9\left(\sqrt{\frac{h_b}{L_o}} - K_{10}\right)^2\right] \quad (19)$$

where K_3 to K_{10} are constants. The constants K_3, K_4 and K_6 can be determined from multi-regression analysis, if the constants K_5, K_7, K_8, K_9, and K_{10} are given. The constants K_5, K_7, K_8, K_9, and K_{10} are gradually adjusted until they give the minimum error. The best fitted K_3 to K_{10} are 0.46, 0.0, 3.0, 1.0, 0.95, -0.1, 13.0, and 0.1 respectively. As K_4 is equal to zero, the second term on the right-hand side of Eq. (19) is not significant. Substituting all the constants into Eq. (19), yields

$$\hat{u}_b = c_b\left\{0.46 + (m_b^{0.95} - 0.1)\exp\left[-13\left(\sqrt{\frac{h_b}{L_o}} - 0.1\right)^2\right]\right\} \quad (20)$$

Various functions of bottom-slope-effect have been tried to replace the term "$m_b^{0.95} - 0.1$" in Eq. (20), i.e. power, linear, quadratic, and cubic models. It is found that the accuracy of those functions is not better than that of "$m_b^{0.95} - 0.1$".

Similar to Rattanapitikon [1995], Eq. (20) is converted to express in terms of the assumed breaker height (H_b') by using linear wave theory.

$$H_b' = \frac{L_o \tanh^2(k_b h_b)}{\pi}\left\{0.46 + (m_b^{0.95} - 0.1)\exp\left[-13\left(\sqrt{\frac{h_b}{L_o}} - 0.1\right)^2\right]\right\} \quad (21)$$

The errors (ER_g) of Eqs. (20) and (21) for 8 groups of bottom slope and experiment scale are shown in the fifth and eighth columns of Table 3. It can be seen that although Eqs. (20) and (21) are slightly simpler than those of WI87a and WI87b, they seem to give better predictions for a wide range of experimental conditions. The overall accuracy of Eqs. (20) and (21) for large-scale experiments is nearly the same as that of WI87a and WI87b. For small-scale experiments, the accuracy of Eqs. (20) and (21) is significantly better than that of WI87a and WI87b.

3.3. *Formula development*

Although Eqs. (20) and (21) give good predictions, it may be possible to develop new formulas which give better predictions than Eqs. (20) and (21). As the formulas for computing $\hat{u}_b/c_b$ and H_b' are considered to be identical, it is better to analyze them at the same time. The assumed breaker height (H_b') and assumed orbital

to phase velocity ratio ($\hat{u}_b/c_b$) may depend on the variables at the deepwater or breaking conditions, i.e. deepwater wavelength (L_o), deepwater wave height (H_o), still water depth at the breaking location (h_b), wavelength at the breaking location (L_b), and bottom slope at the breaking location (m). The possible breaker index can be expressed as the following functions.

$$\frac{\hat{u}_b}{c_b} = f_3\left\{m, \frac{h_b}{L_b}, \frac{h_b}{L_o}, \frac{H_o}{L_o}\right\} \tag{22}$$

$$\frac{H'_b}{h_b} = f_4\left\{m, \frac{h_b}{L_b}, \frac{h_b}{L_o}, \frac{H_o}{L_o}\right\} \tag{23}$$

$$\frac{H'_b}{L_b} = f_5\left\{m, \frac{h_b}{L_b}, \frac{h_b}{L_o}, \frac{H_o}{L_o}\right\} \tag{24}$$

$$\frac{H'_b}{H_o} = f_6\left\{m, \frac{h_b}{L_b}, \frac{h_b}{L_o}, \frac{H_o}{L_o}\right\} \tag{25}$$

$$\frac{H'_b}{L_o} = f_7\left\{m, \frac{h_b}{L_b}, \frac{h_b}{L_o}, \frac{H_o}{L_o}\right\} \tag{26}$$

where f_3 to f_7 are functions proposed in each formula.

The laboratory data from 26 sources (shown in Table 1) are used to develop the new formulas for computing H'_b and $\hat{u}_b/c_b$. The required data for the development are h_b, H_o, m, L_o, c_b, L_b, H'_b, and $\hat{u}_b$. The data of h_b, m, and T were measured directly from the experiments. The data of H_o, L_o, c_b, and L_b are computed by using linear wave theory. The data of H'_b and $\hat{u}_b$ are computed from Eqs. (15) and (16) respectively.

Each breaker index may be a function of four dimensionless parameters as shown in Eqs. (22) to (26). However, not all of the dimensionless parameters are contained in each existing breaker index and it is difficult to consider all these dimensionless parameters simultaneously. A common way to do is to select only one dimensionless parameter as a dominant parameter governing each breaker index. The selection of dominant parameter is performed by plotting the relationship between each breaker index and each dimensionless parameter. A much simpler relationship is expected for the breaking wave on step beach ($m = 0$) because the parameter m can be excluded from the formula. Therefore, the development of a new formula is separated into two stages. For the first stage, the breaking waves on step beach ($m = 0$) are analyzed to identify a "basic form" of breaker index. After that, the bottom-slope-effect is included explicitly into the basic formula obtained from the first stage.

The laboratory data of the breaking waves on step beach [i.e. the experiments from Hattori and Aono, 1985; Horikawa and Kuo, 1966; and Nagayama, 1983] are used to determine a basic form of breaker index. An attempt is made to correlate the breaking indices ($\hat{u}_b/c_b$, H'_b/h_b, H'_b/L_b, H'_b/H_o, and H'_b/L_o) with the possible

dimensionless parameters (h_b/L_b, h_b/L_o, and H_o/L_o). A total of fifteen possible relations is plotted to identify the best correlation. It is found that the relationship between H'_b/L_o and H_o/L_o shows the best correlation and it is selected as a basic form of breaking index. Examples of relationships between $\hat{u}_b/c_b$ and H'_b/L_o versus h_b/L_b, h_b/L_o, and H_o/L_o are shown in Figs. 5 and 6.

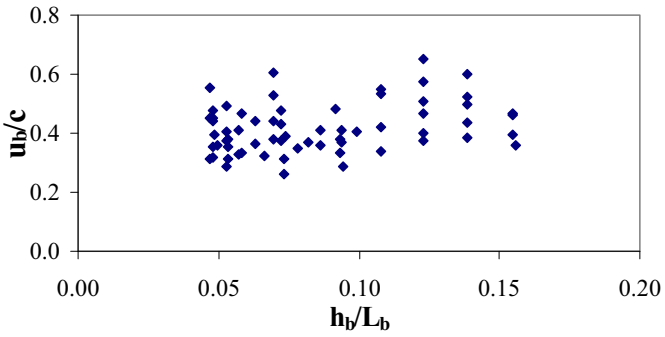

(a)

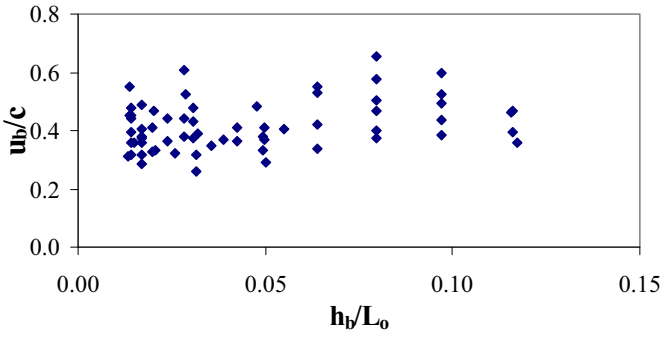

(b)

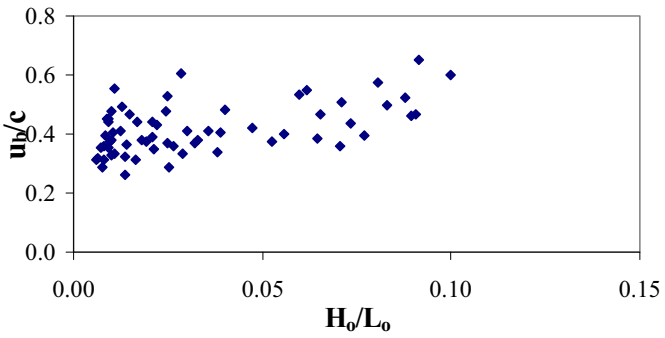

(c)

Fig. 5. Relationships between $\hat{u}_n/c_b$ and (a) h_b/L_b, (b) h_b/L_o, (c) H_o/L_o for the case of breaking wave on step beach [laboratory data from Hattori and Aono, 1985; Horikawa and Kuo, 1966; and Nagayama, 1983].

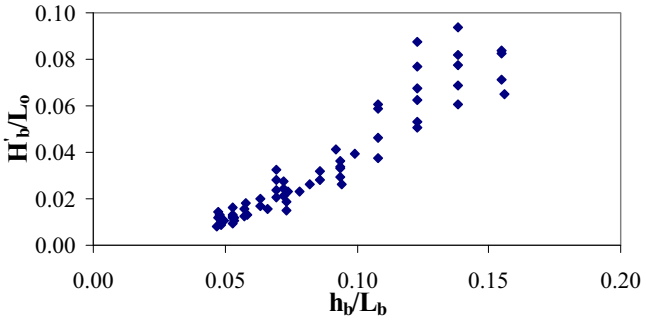

(a)

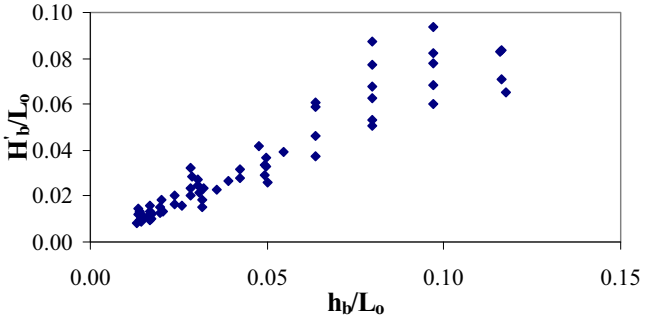

(b)

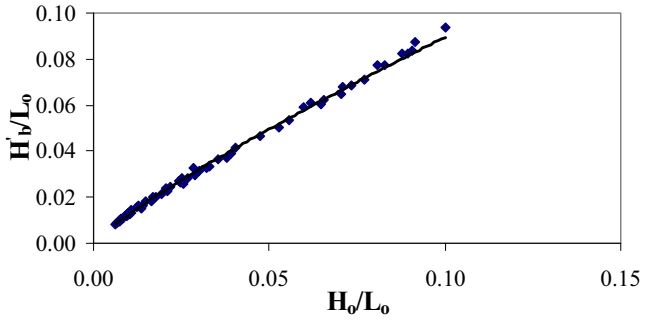

(c)

Fig. 6. Relationships between H'_b/L_o and (a) h_b/L_b, (b) h_b/L_o, (c) H_o/L_o for the case of breaking wave on step beach [laboratory data from Hattori and Aono, 1985; Horikawa and Kuo, 1966; and Nagayama, 1983]. Solid line in figure (c) is the fitted line.

The relationship between H'_b/L_o and H_o/L_o (in Fig. 6(c)) can be fitted with a power function as

$$\frac{H'_b}{L_o} = K_{11}\left(\frac{H_o}{L_o}\right)^{K_{12}} \tag{27}$$

where K_{11} and K_{12} are constants. From the regression analysis between $\log(H'_b/L_o)$ and $\log(H_o/L_o)$, the values of K_{11}, K_{12}, and the correlation coefficient (R^2) are 0.64,

0.85, and 0.99 respectively. The best-fitted line is shown as the solid line in Fig. 6(c). However, the values of K_{11} and K_{12} are not used in the next analysis because they may change slightly when the bottom-slope-effect and all collected laboratory data are included in the analysis.

The analysis is extended by incorporating the laboratory data of the breaking waves on various bottom slopes. All the laboratory data shown in Table 1 are used in the analysis. This revised analysis is based entirely on the basic formula obtained from the first stage of development [Eq. (27)]. The slope effect coefficient is included in Eq. (27) by replacing the constant K_{11} as

$$\frac{H_b'}{L_o} = S_2 \left(\frac{H_o}{L_o}\right)^{K_{12}} \tag{28}$$

where S_2 is the bottom-slope-effect coefficient.

Using the data of H_o, L_o, and H_b', the data of S_2 can be determined from Eq. (28), if the constant K_{12} is given. For a given constant K_{12}, the relationship between S_2 and m is plotted to determine the correlation. Then the constant K_{12} is gradually adjusted until it gives the best correlation. The relationship between S_2 and m shows the best correlation when $K_{12} = 0.83$ (see Fig. 7). Using regression analysis, the best-fit formula for S_2 can be expressed as

$$S_2 = -0.57m^2 + 0.31m + 0.58 \tag{29}$$

Substituting Eq. (29) and $K_{12} = 0.83$ into Eq. (28), yields

$$H_b' = (-0.57m^2 + 0.31m + 0.58)L_o \left(\frac{H_o}{L_o}\right)^{0.83} \tag{30}$$

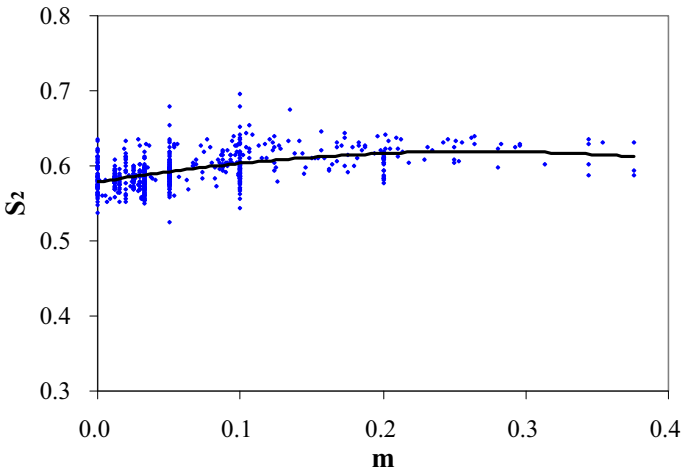

Fig. 7. Relationship between slope effect coefficient S_2 and bottom slope m when $K_{12} = 0.83$ (laboratory data from 26 sources shown in Table 1). Solid line is the computed S_2 from Eq. (29).

It can be seen from Fig. 7 that S_2 (y-axis) varies between 0.55 and 0.65. This narrow band of variation indicates that the effect of bottom slope (m) on Eq. (30) is limited.

Equation (30) can be converted to express in terms of the assumed orbital velocity ($\hat{u}_b$), by using linear wave theory, as

$$\hat{u}_b = \frac{(-0.57m^2 + 0.31m + 0.58)\pi c_b}{\tanh^2(k_b h_b)} \left(\frac{H_o}{L_o}\right)^{0.83} \tag{31}$$

The errors (ER_g) of Eqs. (30) and (31) for 8 groups of bottom slope and experiment scale are shown in the last and the sixth columns of Table 3. Table 3 shows that Eqs. (30) and (31) give surprisingly excellent predictions for both small-scale and large-scale experiments. The formulas give the best prediction for all conditions. However, they cannot be used in modeling the multiple breaking and reformation in a wave model because the formulas depend on deepwater wave height.

As the proposed formulas are empirical formulas, they are applicable in the limited range of experimental conditions that are used in the calibrations or verifications. Therefore, the use of Eqs. (30) and (31) becomes questionable for the beaches having slope greater than 0.38 and for the deepwater wave steepness greater than 0.112.

4. Conclusions

This study was undertaken to find out the breaking wave formulas, which can be used with the assumption of linear wave shoaling. A total of 695 cases collected from 26 sources of published laboratory data were used to examine the formulas for computing the breaker depth, assumed orbital to phase velocity ratio, and assumed breaker height. The data cover a wide range of wave and bottom slope conditions ($0.001 \leq H_o/L_o \leq 0.112$, and $0 \leq H_o/L_o \leq 0.38$).

With regard to breaker depth formulas, the examination of 4 existing formulas [i.e. the formulas of Ogawa and Shuto, 1984; Dean and Dalrymple, 1984; and Gourlay, 1992] indicate that the formula of Rattanapitikon [2000] give the best prediction with average error (ER_{avg}) of 15% but none of them can be used for a wide range of conditions. The existing formulas give considerable error for the cases of $H_o/L_o > 0.1$. A new formula was developed based on the reanalysis of the existing formulas. The new formula gives good overall prediction for general conditions ($ER_{avg} = 12\%$). The overall accuracy of the new formula for the cases of $H_o/L_o \leq 0.1$ is slightly better than those of existing formulas but the accuracy is significant better for cases of $H_o/L_o > 0.1$.

With regard to assumed orbital to phase velocity ratio and assumed breaker height, only the formulas of Isobe [1987] are available. The examination of Isobe's [1987] formulas show that the formulas give overall fairly good predictions ($ER_{avg} = 19\%$); the formulas give good predictions for large-scale experiments, but fair

predictions for small-scale experiments. The formulas of Isobe [1987] were modified by recalibrating the constants in the formulas. The average error (ER_{avg}) of the modified formula is 16%. The modified formulas are simpler but give better predictions than those of Isobe [1987]. The new formulas were developed by reanalysis of the existing formulas. The new formulas give excellent predictions for all conditions ($ER_{avg} = 3\%$).

Acknowledgments

This research was sponsored by the Thailand Research Fund.

References

Cox, D. T., Kobayashi, N. & Okayasu, A. [1994] "Vertical variations of fluid velocities and shear stress in surf zones, in *Proc. 24th Coastal Engineering Conf., ASCE*, pp. 98–112.

Bowen, A. J., Inman, D. L. & Simmons, V. P. [1968] "Wave set-down and set-up," *J. Geophysical Research* **73**, 2569–2577.

Dean, R. G. [1965] "Stream function representation of nonlinear ocean waves," *J. Geophysical Research* **70**, 4561–4572.

Dean, R. G. & Dalrymple, R. A. [1984] *Water Wave Mechanics for Engineers and Scientists* (Prentice-Hall, Inc.), pp. 115.

Galvin, C. J. [1969] "Breaker travel and choice of design wave height," *J. Waterways and Harbors Division, ASCE* **95**, 175–200.

Goda, Y. [1964] Wave forces on a vertical circular cylinder: Experiments and a proposed method of wave force computation, Rept. Port and Harbor Research Institute, Ministry of Transport, No. 8.

Goda, Y. [1970] "A synthesis of breaker indices," *Transactions of Japan Society of Civil Engineers* **2**, pp. 227–230.

Gourlay, M. R. [1978] *Wave Generated Currents*, PhD Thesis, Department of Civil Engineering, University of Queensland.

Gourlay, M. R. [1992] "Wave set-up, wave run-up and beach water table: Interaction between surf zone hydraulics and groundwater hydraulics," *Coastal Engineering* **17**, 93–144.

Hansen, J. B. & Svendsen, I. A. [1979] Regular waves in shoaling water experimental data, Series paper No. 21, Institute of Hydrodynamics and Hydraulic Eng., Technical University of Denmark, Denmark.

Hattori, M. & Aono, T. [1985] "Experimental study on turbulence structures under breaking waves," *Coastal Engineering in Japan, JSCE* **28**, 97–116.

Horikawa, K. & Kuo, C. T. [1966] "A study of wave transformation inside the surf zone," in *Proc. 10th Coastal Engineering Conf., ASCE*, pp. 217–233.

Hwung, H. H., Chyan, J. M. & Chung, Y. C. [1992] "Energy dissipation and air bubbles mixing inside surf zone," in *Proc. 23rd Coastal Engineering Conf., ASCE*, pp. 308–321.

Isobe, M. [1985] "Calculation and application of first-order cnoidal wave theory," *Coastal Engineering* **9**, 309–325.

Isobe, M. [1987] "A parabolic equation model for transformation of irregular waves due to refraction, diffraction and breaking," *Coastal Engineering in Japan, JSCE* **30**, 33–47.

Iversen, H. W. [1952] "Laboratory study of breakers," Gravity Waves, Circular 52, US Bureau of Standards, pp. 9–32.

Iwagaki, Y., Sakai, T., Tsukioka, K. & Sawai, N. [1974] "Relationship between vertical distribution of water particle velocity and type of breakers on beaches," *Coastal Engineering in Japan, JSCE* **17**, 51–58.

Kajima, R., Shimizu, T., Maruyama, K. & Saito, S. [1982] "Experiments of beach profile change with a large wave flume," in *Proc. 18th Coastal Engineering Conf., ASCE*, pp. 1385–1404.

Komar, P. D. & Gaughan, M. K. [1972] "Airy wave theory and breaker height prediction," in *Proc. 13rd Coastal Engineering Conf., ASCE*, pp. 405–418.

Kraus, N. C. & Smith, J. M. [1994] SUPERTANK Laboratory Data Collection Project, Tech. Report CERC-94-3, Waterways Experiment Station, US Army Corps of Engineers, Vol. 1–2.

McCowan, J. [1894] "On the highest waves of a permanent type," *Philosophical Magazine, Edinburgh* **38**(5), 351–358.

Mizuguchi, M. [1980] "An heuristic model of wave height distribution in surf zone," in *Proc. 17th Coastal Engineering Conf., ASCE*, pp. 278–289.

Mitsuyasu, H. [1962] "Experimental study on wave force against a wall," Rept. Transportation Technical Res. Inst., No. 47 (in Japanese).

Nadaoka, K., Kondoh, T. & Tanaka, N. [1982] "The structure of velocity field within the surf zone revealed by means of laser-doppler anemometry," *Port and Harbor Research Institute* **21**(2), pp. 50–102 (in Japanese).

Nagayama, S. [1983] *Study on the Change of Wave Height and Energy in the Surf Zone*, Bach. Thesis, Civil Eng., Yokohama National University, Japan, pp. 24–35 (in Japanese).

Ogawa, Y. & Shuto, N. [1984] "Run-up of periodic waves on beaches of non-uniform slope," in *Proc. 19th Coastal Engineering Conf., ASCE*, pp. 328–344.

Okayasu, A., Shibayama, T. & Mimura, N., [1986] "Velocity field under plunging waves," in *Proc. 20th Coastal Engineering Conf., ASCE*, pp. 660–674.

Okayasu, A., Shibayama, T. & Horikawa, K. [1988] "Verification of undertow in the surf zone," in *Proc. 21st Coastal Engineering Conf., ASCE*, pp. 478–491.

Ozaki, A., Sasaki, M. & Usui, Y. [1977] "Study on rip currents: Experimental observation of nearshore circulation on a sloping bottom," *Coastal Engineering in Japan, JSCE* **20**, 147–158.

Rattanapitikon, W. [1995] *Cross-Shore Sediment Transport and Beach Deformation Model*, Dissertation, Dept. Civil Engineering, Yokohama National University, Yokohama, Japan, pp. 90.

Rattanapitikon, W. & Shibayama, T. [2000] "Verification and modification of breaker height formulas," *Coastal Engineering Journal, JSCE* **42**, 389–406.

Rattanapitikon, W., Vivattanasirisak, T. & Shibayama, T. [2003] "A proposal of new breaker height formula," *Coastal Engineering Journal, JSCE* **45**, 29–48.

Saeki, H. & Sasaki, M. [1973] "A study of the deformation of waves after breaking," in *Proc. 20th Japanese Conf. on Coastal Engineering, JSCE*, pp. 559–564 (in Japanese).

Sato, S., Fukuhama, M. & Horikawa, K. [1988] "Measurements of near-bottom velocities in random waves on a constant slope," *Coastal Engineering in Japan, JSCE* **31**, 219–229.

Sato, S., Isayama, T. & Shibayama, T. [1989] "Long-wave component in near bottom velocity under random waves on a gentle slope," *Coastal Engineering in Japan, JSCE* **32**, 149–159.

Sato, S., Homma, K. & Shibayama, T. [1990] "Laboratory study on sand suspension due to breaking waves," *Coastal Engineering in Japan, JSCE* **33**, 219–231.

Shuto, N. [1974] "Non-linear long waves in channel of variable section," *Coastal Engineering in Japan, JSCE* **17**, 1–12.

Singamsetti, S. R. and Wind, H. G. [1980] Characteristics of breaking and shoaling periodic waves normally incident on to plane beaches of constant slope, Report M 1371, Delft Hydraulic Lab., Delft, The Netherlands.

Smith, D. A. [1974] *Radiation Stress Effects on Wave Set-up in the Surf Zone*, M.Sc. Thesis, Department of Civil Engineering, University of London, Imperial College.

Smith, J. M. & Kraus, N. C. [1990] Laboratory study on macro-features of wave breaking over bars and artificial reefs, Technical Report CERC-90-12, WES, U.S. Army Corps of Engineers.

Stive, M. J. F. [1984] "Energy dissipation in wave breaking on gentle slopes," *Coastal Engineering* **8**, 99–127.

Stokes, G. G. [1847] "On the theory of oscillatory waves," *Trans. Camb. Phil. Soc.* **8**, 411–455.

Ting, C. K. & Kirby, J. T. [1994] "Observation of undertow and turbulence in a laboratory surf zone," *Coastal Engineering* **24**, 51–80.

Van Dorn, W. G. [1978] "Breaking invariants in shoaling waves," *J. Geophysical Research* **83**, 2981–2988.

Visser, P. J. [1977] Wave set-up: Experimental investigation on normally incident waves, Report No. 77-1, Laboratory of Fluid Mech., Dept. of Civil Eng., Delft University of Tech., Delft, The Netherlands.

Visser, P. J. [1982] The proper longshore current in a wave basin, Report No. 82-1, Laboratory of Fluid Mech., Dept. of Civil Eng., Delft University of Tech., Delft, The Netherlands.

Walker, J. R. [1974] Wave transformations over a sloping bottom and over a three-dimensional shoal, Miscellaneous Report No. 11, University of Hawaii, Look Lab-75-11, Honolulu, Hawaii, USA.

Watanabe, A., Hara, T. & Horikawa, K. [1984] "Study on breaking condition for compound wave trains," *Coastal Engineering in Japan, JSCE* **27**, 71–82.

Available online at www.sciencedirect.com
ScienceDirect
Ocean Engineering 34 (2007) 1592–1601
OCEAN ENGINEERING
www.elsevier.com/locate/oceaneng

Calibration and modification of energy dissipation models for irregular wave breaking

Winyu Rattanapitikon*

Civil Engineering Program, Sirindhorn International Institute of Technology, Thammasat University, P.O. Box 22 Thammasat Rangsit Post Office, Pathum Thani 12121, Thailand

Received 22 June 2006; accepted 15 November 2006
Available online 11 February 2007

Abstract

This study is undertaken to recalibrate eight existing energy dissipation models and find out the suitable models, which can be used to compute H_{rms} for a wide range of experimental conditions. The examination shows that the coefficients in the existing models are not the optimal values for a wide range of experimental conditions. Using the new calibrated coefficients, all existing models can be used for computing H_{rms} and the model of Battjes, J.A., Stive, M.J.F. [1985. Calibration and verification of a dissipation model for random breaking waves. Journal of Geophysical Research 90 (C5), 9159–9167] gives the best predictions. The existing models are also modified by changing the breaker height formulas in the dissipation models. The accuracy of most existing models is improved significantly by using the suitable breaker height formula.

Keywords: Energy dissipation; Wave height transformation; Wave model; Parametric approach; Representative wave approach; Root mean square wave height; Surf zone

1. Introduction

The transformation of root mean square (rms) wave heights has been a subject of study for decades because of its importance in studying beach deformations and the design of coastal structures. When waves propagate to the nearshore zone, wave profiles steepen and eventually waves break. The higher waves tend to break at the greater distance from the shore. Closer to the shore, more and more waves are breaking, until in the inner surf zone almost all the waves are breaking. Once the waves start to break, a part of the wave energy is transformed into turbulence and heat, and wave height decreases towards the shore.

Common methods to model irregular wave height transformation can be classified into four main approaches, i.e. representative wave approach, spectral approach, probabilistic approach, and parametric approach. A brief review of these approaches is presented in the paper of Rattanapitikon et al. (2003). For computing beach deformation, the wave model should be kept as simple as possible because of the frequent updating of wave field to account for the change of bottom profiles. The parametric and representative wave approaches seem to be suitable for the beach deformation models. Because of the simplicity of the representative wave approach, the model of this approach is expected to give lesser accuracy than that of the parametric approach. However, it is not clear whether this lesser accuracy is significant or not. The parametric and representative wave approaches are both considered in this study. These two approaches rely on the macroscopic features of breaking waves and predict only the transformation of rms wave height. The rms wave height transformation is computed from the energy flux conservation law as

$$\frac{\partial(Ec_g \cos\theta)}{\partial x} = -D_B, \tag{1}$$

where E is the wave energy density, c_g the group velocity, θ the mean wave angle, x the distance in cross shore direction, and D_B the energy dissipation rate due to wave

*Tel.: +66 2564 3221; fax: +66 2986 9112.
E-mail address: winyu@siit.tu.ac.th.

0029-8018/$ - see front matter © 2007 Elsevier Ltd. All rights reserved.
doi:10.1016/j.oceaneng.2006.11.005

breaking which is zero outside the surf zone. The energy dissipation rate due to bottom friction is neglected. In the present study, all variables are based on the linear wave theory.

Snell's law is employed to describe wave refraction:

$$\frac{\sin\theta}{c} = \text{constant}, \tag{2}$$

where c is the phase velocity.

From the linear wave theory, the wave energy density (E) is equal to $\rho g H_{\text{rms}}^2/8$. Therefore, Eq. (1) can be written in terms of rms wave height as

$$\frac{\rho g}{8}\frac{\partial(H_{\text{rms}}^2 c_{\text{g}}\cos\theta)}{\partial x} = -D_{\text{B}}, \tag{3}$$

where H_{rms} is the rms wave height.

The rms wave height transformation can be computed from the energy flux balance equation (Eq. (3)) by substituting the model of energy dissipation rate (D_{B}) and numerically integrating from offshore to shoreline. In the offshore zone, the energy dissipation rate is set to zero. The main difficulty of Eq. (3) is how to formulate the energy dissipation rate caused by the breaking waves.

During the past decades, various energy dissipation models have been proposed for computing H_{rms} in the surf zone. Because of the complexity of the wave breaking mechanism, most of the energy dissipation models were developed based on the empirical or semi-empirical approach. To make an empirical formula reliable, it has to be calibrated or verified with a wide range of experimental conditions. However, most of the previous models were developed with limited experimental conditions. Therefore, their validity may be limited according to the range of experimental conditions that were employed in calibration or verification. Moreover, since the models are different, the computed results from various models should differ from each other and from the measured data. No direct study has been made to describe clearly the accuracy of each model on the estimation of H_{rms} for a wide range of experimental conditions. It is not clear which model is suitable for computing the transformation of H_{rms}. The main objective of this study is to find out the suitable models that predict well for a wide range of experimental conditions.

This paper is divided into five main parts. The first part describes the collected data. The second part briefly reviews the existing dissipation models. The third part is examination of existing models. The fourth part is recalibration and comparison of the existing models for identifying the suitable models. The last part describes the modification of the existing models.

2. Collected experimental data

The experimental data of rms wave height transformation from 13 sources, covering 1723 cases of wave and bottom conditions, have been collected for examination of the dissipation models. The experiments cover a wide range of wave and bottom topography conditions, including small-scale, large-scale and field experiments. The experiments cover a variety of beach conditions and cover a range of deepwater wave steepness ($H_{\text{rmso}}/L_{\text{o}}$) from 0.0007 to 0.0588. A summary of the collected laboratory data is given in Table 1. Most of the data sources are the same as that used by Rattanapitikon et al. (2003). The additional data are from the DELILAH project (Birkemeier et al., 1997) and DUCK94 project (Herbers et al., 2006). A brief summary of the DELILAH and DUCK94 projects are summarized below.

Duck Experiment on Low-frequency and Incident-band Longshore and Across-shore Hydrodynamics (DELILAH) project was conducted on the barred beach in Duck, North Carolina, USA in October 1990. The objective of the project is to improve fundamental understanding and modeling of surf zone physics. The experiment emphasized

Table 1
Summary of collected experimental data

Sources	No. of cases	No. of points	Beach conditions	$H_{\text{rmso}}/L_{\text{o}}$	Apparatus
Hurue (1990)	1	7	Plane beach	0.0259	Small-scale
Smith and Kraus (1990)	12	96	Plane and barred beach	0.0214–0.0588	Small-scale
Sultan (1995)	1	12	Plane beach	0.0042	Small-scale
Grasmeijer and van Rijn (1999)	2	20	Sandy beach	0.0142–0.0168	Small-scale
Hamilton and Ebersole (2001)	1	10	Plane beach	0.0165	Small-scale
Ting (2001)	1	7	Plane beach	0.0161	Small-scale
Kraus and Smith (1994): SUPERTANK project	128	2223	Sandy beach	0.0011–0.0452	Large-scale
Roelvink and Reniers (1995): LIP 11D project	95	923	Sandy beach	0.0039–0.0279	Large-scale
Dette et al. (1998): MAST III—SAFE project	138	3559	Sandy beach	0.0061–0.0147	Large-scale
Thornton and Guza (1986)	4	60	Sandy beach	0.0012–0.0013	Field
Kraus et al. (1989): DUCK85 project	8	90	Sandy beach	0.0007–0.0018	Field
Birkemeier et al. (1997): DELILAH project	745	5049	Sandy beach	0.0007–0.0254	Field
Herbers et al. (2006): DUCK94 project	587	6104	Sandy beach	0.0009–0.0290	Field
Total	1723	18,160		0.0007–0.0588	

surf zone hydrodynamics in the presence of a changing barred bathymetry. Nine pressure gauges were installed to measure the nearshore wave heights across-shore and one of them was in the swash zone. Tidal elevations were measured at the FRF pier. The measured wave heights are available at http://dksrv.usace.army.mi/jg/del90dir. The data of wave heights and water depths measured during October 2–21, 1990 are available. The wave heights and water depths data are available at approximately every 34 min. A total of 776 sets of measured wave heights and water depths are available on the data server. A data set that has only a few points of measurements is not suitable to use for verifying the models. A total of 745 data sets are considered in this study.

DUCK94 project was conducted on the barred beach in Duck, North Carolina, USA during August–October 1994. The project objective is the same as that of DELILAH. The experiment emphasized surf zone hydrodynamics, sediment transport and morphological evolution. Thirteen experiments were carried out by 19 organizations. The experiment of wave height transformation was performed by Herbers, T. H. C., Elgar, S., Guza, R. T., and O'Reilly, W. C. Thirteen pressure gauges were installed to measure the nearshore wave heights across-shore and one of them was in the swash zone. Tidal elevations were measured at the FRF pier. The measured wave heights, and water depths are available at http://dksrv.usace.army.mi/jg/dk94dir. The wave heights data are available at approximately every 17 min while the water depths data are available at every 3 h. The wave heights and water depths at every 3 h that were measured during August 15–October 31, 1994 are used in the present study. Excluding the data sets that have only a few points of measurements, a total of 587 data sets are considered in the present study.

3. Existing energy dissipation models

During the past decades, various energy dissipation models have been developed based on the parametric approach and the representative wave approach. Brief reviews of some existing dissipation models are described below.

(a) Battjes and Janssen (1978), hereafter referred to as BJ78, proposed to compute D_B by multiplying the fraction of irregular breaking waves (Q_b) by the energy dissipation of a single broken wave. The energy dissipation of a broken wave is described by the bore analogy and assuming that all broken waves have a height equal to breaking wave height (H_b) as

$$D_B = K_1 Q_b \frac{\rho g H_b^2}{4T_p}, \tag{4}$$

where T_p is the spectral peak period, and K_1 the coefficient introduced to account for the difference between breaking wave and hydraulic jump. The published value of K_1 is 1.0. The fraction of breaking waves (Q_b) was derived based on the assumption that the probability density function (pdf) of wave height could be modeled with a Rayleigh distribution truncated at the breaking wave height (H_b) and all broken waves have a height equal to the breaking wave height. The result is

$$\frac{1-Q_b}{-\ln Q_b} = \left(\frac{H_{rms}}{H_b}\right)^2 \tag{5}$$

in which the breaking wave height (H_b) is determined from the formula of Miche (1944) with additional constant (K_3):

$$H_b = K_2 L \tanh(K_3 kh), \tag{6}$$

where L is the wavelength related to T_p, k the wave number, h the water depth, and K_2 and K_3 the coefficients. Based on their laboratory data, the coefficients K_2 and K_3 are determined at 0.14 and 0.91, respectively. This model is widely used for computing D_B. However, the additional constant K_3 may be changed slightly for the best fit with other experimental data, e.g. it is determined at 0.89 for Oliveira (2007).

Since Eq. (5) is an implicit equation, an iteration process is necessary to compute the fraction of breaking waves (Q_b). It will be more convenient if we can compute Q_b from the explicit form of Eq. (5). Rattanapitikon and Shibayama (1998) proposed the explicit form of Q_b based on multiple regression analysis (with correlation coefficient $R^2 = 0.999$) as

$$Q_b = \begin{cases} 0 & \text{for } \frac{H_{rms}}{H_b} \leqslant 0.43 \quad \text{(a)} \\ 1.785\left(\frac{H_{rms}}{H_b}\right)^3 - 0.280\left(\frac{H_{rms}}{H_b}\right)^2 - 0.738\left(\frac{H_{rms}}{H_b}\right) + 0.235 & \text{for } 0.43 < \frac{H_{rms}}{H_b} < 1.0 \quad \text{(b)} \\ 1 & \text{for } \frac{H_{rms}}{H_b} \geqslant 1.0 \quad \text{(c)} \end{cases} \tag{7}$$

As Eqs. (5) and (7) give almost identical results ($R^2 = 0.999$), for convenience, Eq. (7) is used in this study.

(b) Thornton and Guza (1983), hereafter referred to as TG83, proposed to compute D_B by integrating from 0 to ∞ the product of the dissipation for a single broken wave and the pdf of the breaking wave height. The energy dissipation of a single broken wave is described by the bore model, which is slightly different from the bore model of BJ78. The pdf of breaking wave height is expressed as a weighting of the Rayleigh distribution. By introducing the formula of the weighting, a model of D_B

was proposed:

$$D_B = K_4 \frac{3\sqrt{\pi}}{4}\left(\frac{H_{rms}}{H_b}\right)^2\left\{1-\frac{1}{[1+(H_{rms}/H_b)^2]^{2.5}}\right\}\frac{\rho g H_{rms}^3}{4T_p h}, \quad (8)$$

where K_4 is the coefficient introduced to account for the difference between breaking wave and hydraulic jump. The published value of K_4 is 0.51 for laboratory data. The breaker height (H_b) is determined from the following formula:

$$H_b = K_5 h, \quad (9)$$

where K_5 is the coefficient of depth limit breaker height. The published value of K_5 is 0.42.

(c) Battjes and Stive (1985), hereafter referred to as BS85, used the same energy dissipation model as that of BJ78:

$$D_B = K_6 Q_b \frac{\rho g H_b^2}{4T_p}, \quad (10)$$

where K_6 is the coefficient. The published value of K_6 is 1.0, and Q_b is computed from Eq. (7). They modified the model of BJ78 by recalibrating the coefficient K_3 in the breaker height formula (Eq. (6)). The coefficient K_3 was related to the deepwater wave steepness (H_{rmso}/L_o). After calibration, the breaking wave height was modified to be

$$H_b = K_7 L \tanh\left\{\left[K_8 + K_9 \tanh\left(K_{10}\frac{H_{rmso}}{L_o}\right)\right]kh\right\}, \quad (11)$$

where H_{rmso} is the deepwater rms wave height, L_o the deepwater wavelength and K_7–K_{10} are the coefficients. The published values of K_7–K_{10} are 0.140, 0.57, 0.45, and 33, respectively. Hence, the model of BS85 is similar to that of BJ78 except for the formula of H_b.

(d) Southgate and Nairn (1993), hereafter referred to as SN93, modified the model of BJ78 by changing the expression of energy dissipation of a single broken wave from the bore model of BJ78 to be the bore model of TG83 as

$$D_B = K_{11} Q_b \frac{\rho g H_b^3}{4T_p h}, \quad (12)$$

where K_{11} is the coefficient. The published value of K_{11} is 1.0 and Q_b is computed from Eq. (7). The breaker height (H_b) is determined from the formula of Nairn (1990) as

$$H_b = h\left[K_{12} + K_{13}\tanh\left(K_{14}\frac{H_{rmso}}{L_o}\right)\right], \quad (13)$$

where K_{12}–K_{14} are the coefficients. The published values of K_{12}–K_{14} are 0.39, 0.56, and 33, respectively.

(e) Baldock et al. (1998), hereafter referred to as BHV98, proposed to compute D_B by integrating from H_b to ∞ the product of the dissipation for a single broken wave and the pdf of the wave height. The energy dissipation of a single broken wave is described by the bore analogy of BJ78. The pdf of wave height inside the surf zone was assumed to be the Rayleigh distribution:

$$D_B = K_{15}\exp\left[-\left(\frac{H_b}{H_{rms}}\right)^2\right]\frac{\rho g(H_b^2+H_{rms}^2)}{4T_p} \quad \text{for } H_{rms} < H_b, \quad (14a)$$

$$D_B = K_{15}\exp[-1]\frac{\rho g 2H_b^2}{4T_p} \quad \text{for } H_{rms} \geqslant H_b. \quad (14b)$$

The published coefficient K_{15} is 1.0. The breaker height (H_b) is determined from the formula of Nairn (1990) as

$$H_b = h\left[K_{16} + K_{17}\tanh\left(K_{18}\frac{H_{rmso}}{L_o}\right)\right], \quad (15)$$

where K_{16}–K_{18} are the coefficients. The published values of K_{16}–K_{18} are 0.39, 0.56, and 33, respectively.

(f) Rattanapitikon and Shibayama (1998), hereafter referred to as RS98, modified the model of BJ78 by changing the expression of energy dissipation of a single broken wave from the bore concept to the stable energy concept

$$D_B = K_{19} Q_b \frac{c_g \rho g}{8h}\left[H_{rms}^2 - \left(h\exp(-K_{20} - K_{21}\frac{h}{\sqrt{LH_{rms}}})\right)^2\right], \quad (16)$$

where K_{19}–K_{21} are the coefficients. The published values of K_{19}–K_{21} are 0.10, 0.58, and 2.0, respectively. The fraction of breaking wave (Q_b) is computed from Eq. (7). The breaking wave height (H_b) is computed by using the breaking criteria of Goda (1970) as

$$H_b = K_{22} L_o\left\{1-\exp\left[-1.5\frac{\pi h}{L_o}(1+15m^{4/3})\right]\right\}, \quad (17)$$

where m is the average bottom slope and K_{22} is the coefficient. The published value of K_{22} is 0.10.

(g) Ruessink et al. (2003) hereafter referred to as RWS03, used the same energy dissipation model as that of BHV98:

$$D_B = K_{23}\exp\left[-\left(\frac{H_b}{H_{rms}}\right)^2\right]\frac{\rho g(H_b^2+H_{rms}^2)}{4T_p} \quad \text{for } H_{rms} < H_b, \quad (18a)$$

$$D_B = K_{23}\exp[-1]\frac{\rho g 2H_b^2}{4T_p} \quad \text{for } H_{rms} \geqslant H_b, \quad (18b)$$

where K_{23} is the coefficient and the published value of K_{23} is 1.0. The breaker height formula of BJ78 (Eq. (6)) is used to determine H_b. The coefficient K_3 in Eq. (6) was related to the product of wave number and water depth (kh). After calibration, the breaker height formula was modified to be

$$H_b = K_{24} L \tanh[(K_{25}kh + K_{26})kh], \quad (19)$$

where K_{24}–K_{26} are the coefficients. The published values of K_{24}–K_{26} are 0.14, 0.86, and 0.33, respectively. Hence, the model of RWS03 is similar to that of BHV98 except for the formula of H_b.

Table 2
The errors ER_g and ER_{avg} of the existing models for three groups of experiment scale (using the default coefficients)

Apparatus	Models							
	BJ78 (Eq. (4))	TG83 (Eq. (8))	BS85 (Eq. (10))	SN93 (Eq. (12))	BHV98 (Eq. (14))	RS98 (Eq. (16))	RWS03 (Eq. (18))	RKS03 (Eq. (20))
Small-scale	9.1	21.2	7.4	11.9	10.6	9.4	11.7	8.0
Large-scale	11.0	8.8	7.3	10.1	6.8	7.3	8.2	8.9
Field	18.0	11.3	10.4	14.7	13.5	10.1	10.1	12.9
ER_{avg}	12.7	13.8	8.3	12.3	10.3	8.9	10.0	9.9

(h) Rattanapitikon et al. (2003) hereafter referred to as RKS03, applied the dissipation model for regular wave for computing the dissipation for irregular waves:

$$D_B = K_{27}\frac{\rho g c_g}{8h}[H_{rms}^2 - (K_{28}H_b)^2], \tag{20}$$

where K_{27} and K_{28} are the coefficients. The published values of K_{27} and K_{28} are 0.12 and 0.42. The breaker height (H_b) is computed by using the breaking criteria of Miche (1944) as

$$H_b = K_{29}L\tanh(kh), \tag{21}$$

where K_{29} is the coefficient. The published value of K_{29} is 0.14. The greatest asset of RKS03's model is its simplicity and ease of application. The model was developed based on the representative wave approach while other models were developed based on the parametric approach.

4. Examination of existing models

The objective of this section is to examine the applicability of the eight existing dissipation models on simulating H_{rms}. The measured rms wave heights from 13 sources (total 1723 cases) of published experimental results (shown in Table 1) are used to examine the existing models.

The rms wave height transformation is computed by numerical integration of the energy flux balance equation (Eq. (3)) with the energy dissipation rate of the existing models (Eqs. (4), (8), (10), (12), (14), (16), (18), and (20)). A backward finite difference scheme is used to solve the energy flux balance equation (Eq. (3)).

The basic parameter for determination of the overall accuracy of a model is the average rms relative error (ER_{avg}), which is defined as

$$ER_{avg} = \frac{\sum_{j=1}^{tn} ER_{gj}}{tn}, \tag{22}$$

where ER_{gj} is the rms relative error of the data group j (the group number), and tn is the total number of groups. The small value of ER_{avg} indicates good overall accuracy of the model.

The group rms relative error (ER_g) is defined as

$$ER_g = 100\sqrt{\frac{\sum_{j=1}^{ng}(H_{ci} - H_{mi})^2}{\sum_{i=1}^{ng} H_{mi}^2}}, \tag{23}$$

where i is the wave height number, H_{ci} the computed wave height of number i, H_{mi} the measured wave height of number i, and ng the total number of measured wave heights in each data group.

The collected experiments are separated into three groups according to the experiment scale, i.e. small-scale, large-scale, and field experiments. It is expected that a good model should be able to predict well for the three groups of experiment scale. Therefore, the average error (ER_{avg}) from the three groups of experiment scale are used as a main criteria to verify the models.

Using the default coefficients (K_1–K_{29}) in the computations, the errors (ER_g and ER_{avg}) of each dissipation model for three groups of experiment scale have been computed and shown in Table 2. It can be seen from Table 2 that the model of BS85 is the best. The overall accuracy of models in descending order are the models of BS85, RS98, RKS03, RWS03, BHV98, SN93, BJ78, and TG83. Because most models were developed based on the limited experimental conditions, the coefficients in the models may not be the optimal values. Therefore, the errors in Table 2 should not be used to judge the applicability of the selected models. The coefficients in all models should be recalibrated before comparing the applicability of the models.

5. Model calibration and comparison

The measured data shown in Table 1 are used to calibrate the coefficients (K_1–K_{29}) in the dissipation models. The calibrations are conducted by gradually adjusting the coefficients K_1–K_{29} until the minimum error (ER_{avg}) of each model is obtained. The optimum values of K_1–K_{29} are shown in the third column of Table 3.

Using the calibrated coefficients in the computations, the errors (ER_g and ER_{avg}) of each dissipation model for three groups of experiment scale have been computed and shown in Table 4. The results can be summarized as follows:

(a) After calibrations, the accuracy of most models (except BS85) are improved significantly, while the accuracy of BS85 is slightly improved. This shows that the coefficients in the existing models are not the optimal values.
(b) The errors of the existing models for three groups of experiment scale are not much different. It means that those models may not have scale effect.

Table 3
Default and calibrated coefficients of the existing models

Models	Default coefficients	Calibrated coefficients
BJ78 (Eq. (4))	$K_1 = 1.0$, $K_2 = 0.14$, $K_3 = 0.91$	$K_1 = 0.92$, $K_2 = 0.14$, $K_3 = 0.76$
TG83 (Eq. (8))	$K_4 = 1.0$, $K_5 = 0.42$	$K_4 = 0.10$, $K_5 = 0.168$
BS85 (Eq. (10))	$K_6 = 1.0$, $K_7 = 0.14$, $K_8 = 0.57$, $K_9 = 0.45$, $K_{10} = 33$	$K_6 = 1.0$, $K_7 = 0.14$, $K_8 = 0.57$, $K_9 = 0.51$, $K_{10} = 28$
SN93 (Eq. (12))	$K_{11} = 1.0$, $K_{12} = 0.39$, $K_{13} = 0.56$, $K_{14} = 33$	$K_{11} = 1.40$, $K_{12} = 0.46$, $K_{13} = 0.55$, $K_{14} = 21$
BHV98 (Eq. (14))	$K_{15} = 1.0$, $K_{16} = 0.39$, $K_{17} = 0.56$, $K_{18} = 33$	$K_{15} = 1.06$, $K_{16} = 0.50$, $K_{17} = 0.28$, $K_{18} = 43$
RS98 (Eq. (16))	$K_{19} = 0.10$, $K_{20} = 0.58$, $K_{21} = 2.0$, $K_{22} = 0.10$	$K_{19} = 0.08$, $K_{20} = 0$, $K_{21} = 7.3$, $K_{22} = 0.105$
RWS03 (Eq. (18))	$K_{23} = 1.0$, $K_{24} = 0.14$, $K_{25} = 0.86$, $K_{26} = 0.33$	$K_{23} = 1.05$, $K_{24} = 0.14$, $K_{25} = 0.70$, $K_{26} = 0.45$
RKS03 (Eq. (20))	$K_{27} = 0.12$, $K_{28}{*}K_{29} = 0.0588$	$K_{27} = 0.07$, $K_{28}{*}K_{29} = 0.047$

Table 4
The errors ER_g and ER_{avg} of the existing models for three groups of experiment scale (using the calibrated coefficients)

Apparatus	Models							
	BJ78 (Eq. (4))	TG83 (Eq. (8))	BS85 (Eq. (10))	SN93 (Eq. (12))	BHV98 (Eq. (14))	RS98 (Eq. (16))	RWS03 (Eq. (18))	RKS03 (Eq. (20))
Small-scale	11.3	13.0	7.1	9.7	9.3	8.7	10.6	8.7
Large-scale	8.1	8.0	7.2	7.9	6.6	7.2	7.8	7.4
Field	12.4	13.2	10.4	10.9	10.3	9.3	9.7	9.7
ER_{avg}	10.6	11.4	8.2	9.5	8.7	8.4	9.4	8.6

(c) The overall accuracy of models in descending order are the models of BS85, RS98, RKS03, BHV98, RWS03, SN93, BJ78, and TG83.
(d) Considering the overall accuracy of all models in Table 4, it can be concluded that all selected models can be used for practical work ($8.2 \leqslant ER_{avg} \leqslant 11.4$). However, lesser error is better. The model that gives very good prediction (with ER_{avg} of 8.2%) is the model of BS85. The model gives very good predictions on the laboratory experiments and good predictions on the field experiments.

6. Model modification

Although the existing models give overall good predictions, they may be modified for better predictions. Following the works of BS85 and RWS03, the modification is carry out by changing the breaker height (H_b) formula in each dissipation model. All of the H_b and D_B formulas shown in Section 3 will be used in this section. It can be seen from Section 3 that there are seven formulas for H_b (Eqs. (6), (9), (11), (13), (17), (19), and (21)) and six formulas for D_B (Eqs. (4), (8), (12), (14), (16), and (20)). Eqs. (10), (15), and (18) have been left out of the lists because they are the same as Eqs. (4), (13), and (14), respectively.

Substituting the seven formulas of H_b into the six existing dissipation models, 42 possible models are considered in this section. Table 5 shows the combination of H_b and D_B formulas for the 42 possible dissipation models and 8 of which are the existing models (M1, M3, M9, M18, M25, M27, M33, and M42). The calibration of possible dissipation models are performed by using the measured data shown in Table 1. The calibrations are conducted by gradually adjusting the coefficients until the minimum error (ER_{avg}) of each model is obtained. The calibrated coefficients and average errors (ER_{avg}) from three groups of experiment scale are shown in the fourth and fifth columns of Table 5. The results can be summarized as follows:

The accuracy of most existing models (except BS85) can be improved by changing the breaker height (H_b) formula. The model of BS85 (M3) already has a suitable combination of the formulas for H_b and D_B.

The H_b formula of BS85 (Eq. (11)) is suitable for all D_B formulas while the H_b formulas of BJ78 (Eq. (6)) and BHV98 (Eq. (19)) are suitable for the D_B formula of RKS03 (Eq. (20)).

There are six models (M3, M24, M31, M36, M38, and M41) that give very good accuracy (with ER_{avg} of about 8.1–8.2%) and three of them are from the D_B formula of the representative wave approach (Eq. (20)).

Substituting the calibrated coefficients into the formulas of D_B and H_b, the top six models that give very good prediction (with ER_{avg} of about 8.1–8.2%) can be written as

$$\text{M3 (BS85)}: \quad D_B = Q_b \frac{\rho g H_b^2}{4T_p} \tag{24}$$

in which the fraction of breaking wave (Q_b) is computed from Eq. (7). The breaker height (H_b) is computed by using

Table 5
Calibrated coefficients and average errors ER_{avg} of all 42 possible dissipation models

Model no.	D_B formulas	H_b formulas	Calibrated coefficients	ER_{avg}
M1	Eq. (4)	Eq. (6)	$K_1 = 0.92$, $K_2 = 0.14$, $K_3 = 0.76$	10.6
M2		Eq. (9)	$K_1 = 0.94$, $K_5 = 0.63$	10.6
M3		Eq. (11)	$K_1 = 1.0$, $K_7 = 0.14$, $K_8 = 0.57$, $K_9 = 0.51$, $K_{10} = 28$	8.2
M4		Eq. (13)	$K_1 = 1.0$, $K_{12} = 0.48$, $K_{13} = 0.33$, $K_{14} = 36$	9.0
M5		Eq. (17)	$K_1 = 0.92$, $K_{22} = 0.14$	10.6
M6		Eq. (19)	$K_1 = 1.0$, $K_{24} = 0.14$, $K_{25} = 0.78$, $K_{26} = 0.40$	9.7
M7		Eq. (21)	$K_1 = 1.0$, $K_{29} = 0.12$	11.7
M8	Eq. (8)	Eq. (6)	$K_4 = 0.24$, $K_2 = 0.049$, $K_3 = 0.86$	11.5
M9		Eq. (9)	$K_4 = 0.1$, $K_5 = 0.168$	11.4
M10		Eq. (11)	$K_4 = 0.38$, $K_7 = 0.065$, $K_8 = 0.45$, $K_9 = 1.10$, $K_{10} = 20$	8.4
M11		Eq. (13)	$K_4 = 0.21$, $K_{12} = 0.14$, $K_{13} = 0.31$, $K_{14} = 19$	8.7
M12		Eq. (17)	$K_4 = 0.43$, $K_{22} = 0.069$	11.2
M13		Eq. (19)	$K_4 = 0.22$, $K_{24} = 0.04$, $K_{25} = 0.80$, $K_{26} = 0.70$	11.2
M14		Eq. (21)	$K_4 = 0.25$, $K_{29} = 0.044$	11.7
M15	Eq. (12)	Eq. (6)	$K_{11} = 1.40$, $K_2 = 0.13$, $K_3 = 0.82$	10.5
M16		Eq. (9)	$K_{11} = 1.31$, $K_5 = 0.62$	10.1
M17		Eq. (11)	$K_{11} = 1.43$, $K_7 = 0.14$, $K_8 = 0.55$, $K_9 = 0.47$, $K_{10} = 32$	8.7
M18		Eq. (13)	$K_{11} = 1.40$, $K_{12} = 0.46$, $K_{13} = 0.55$, $K_{14} = 21$	9.5
M19		Eq. (17)	$K_{11} = 1.36$, $K_{22} = 0.137$	10.3
M20		Eq. (19)	$K_{11} = 1.52$, $K_{24} = 0.14$, $K_{25} = 0.84$, $K_{26} = 0.36$	10.0
M21		Eq. (21)	$K_{11} = 1.48$, $K_{29} = 0.11$	10.8
M22	Eq. (14)	Eq. (6)	$K_{15} = 1.15$, $K_2 = 0.15$, $K_3 = 0.76$	10.5
M23		Eq. (9)	$K_{15} = 1.05$, $K_5 = 0.66$	10.0
M24		Eq. (11)	$K_{15} = 1.24$, $K_7 = 0.15$, $K_8 = 0.59$, $K_9 = 0.51$, $K_{10} = 25$	8.1
M25		Eq. (13)	$K_{15} = 1.06$, $K_{12} = 0.50$, $K_{13} = 0.28$, $K_{14} = 43$	8.7
M26		Eq. (17)	$K_{15} = 1.22$, $K_{22} = 0.15$	10.6
M27		Eq. (19)	$K_{15} = 1.05$, $K_{24} = 0.14$, $K_{25} = 0.70$, $K_{26} = 0.45$	9.4
M28		Eq. (21)	$K_{15} = 1.43$, $K_{29} = 0.13$	11.7
M29	Eq. (16)	Eq. (6)	$K_{19} = 0.07$, $K_{20} = 1.0$, $K_{21} = 3.6$, $K_2 = 0.09$, $K_3 = 0.88$	8.8
M30		Eq. (9)	$K_{19} = 0.08$, $K_{20} = 0.36$, $K_{21} = 3.9$, $K_5 = 0.47$	8.9
M31		Eq. (11)	$K_{19} = 0.10$, $K_{20} = 0.55$, $K_{21} = 2.1$, $K_7 = 0.10$, $K_8 = 0.56$, $K_9 = 0.45$, $K_{10} = 33$	8.2
M32		Eq. (13)	$K_{19} = 0.10$, $K_{20} = 0.37$, $K_{21} = 2.3$, $K_{12} = 0.25$, $K_{13} = 0.24$, $K_{14} = 80$	8.8
M33		Eq. (17)	$K_{19} = 0.08$, $K_{20} = 0$, $K_{21} = 7.3$, $K_{22} = 0.105$	8.4
M34		Eq. (19)	$K_{19} = 0.07$, $K_{20} = 0.66$, $K_{21} = 1.9$, $K_{24} = 0.09$, $K_{25} = 0.65$, $K_{26} = 0.44$	8.4
M35		Eq. (21)	$K_{19} = 0.06$, $K_{20} = 2.6$, $K_{21} = 2.2$, $K_{29} = 0.079$	8.8
M36	Eq. (20)	Eq. (6)	$K_{27} = 0.07$, $K_{28}{}^*K_2 = 0.066$, $K_3 = 0.68$	8.2
M37		Eq. (9)	$K_{27} = 0.07$, $K_{28}{}^*K_5 = 0.266$	8.4
M38		Eq. (11)	$K_{27} = 0.07$, $K_{28}{}^*K_7 = 0.061$, $K_8 = 0.63$, $K_9 = 0.21$, $K_{10} = 39$	8.2
M39		Eq. (13)	$K_{27} = 0.07$, $K_{28}{}^*K_{12} = 0.266$, $K_{13} = 0$, $K_{14} = 33$	8.4
M40		Eq. (17)	$K_{27} = 0.08$, $K_{28}{}^*K_{22} = 0.061$	8.4
M41		Eq. (19)	$K_{27} = 0.07$, $K_{28}{}^*K_{24} = 0.047$, $K_{25} = 0.44$, $K_{26} = 0.78$	8.2
M42		Eq. (21)	$K_{27} = 0.07$, $K_{28}{}^*K_{29} = 0.047$	8.6

the breaker height formula of BS85 as

$$H_b = 0.14L \tanh\left\{\left[0.57 + 0.51 \tanh\left(28\,\frac{H_{rmso}}{L_o}\right)\right]kh\right\}, \tag{25}$$

$$\text{M24}: D_B = 1.24 \exp\left[-\left(\frac{H_b}{H_{rms}}\right)^2\right]\frac{\rho g(H_b^2 + H_{rms}^2)}{4T_p} \quad \text{for } H_{rms} < H_b, \tag{26a}$$

$$D_B = 1.24 \exp[-1]\frac{\rho g 2H_b^2}{4T_p} \quad \text{for } H_{rms} \geqslant H_b \tag{26b}$$

in which the breaker height (H_b) is determined from the breaker height formula of BS85 as

$$H_b = 0.15L \tanh\left\{\left[0.59 + 0.51 \tanh\left(25\frac{H_{rmso}}{L_o}\right)\right]kh\right\}, \tag{27}$$

$$\text{M31}: D_B = 0.1Q_b\frac{c_g\rho g}{8h}\left[H_{rms}^2 - \left(h \exp(-0.55 - 2.1\frac{h}{\sqrt{LH_{rms}}})\right)^2\right] \tag{28}$$

in which the fraction of breaking wave (Q_b) is computed from Eq. (7). The breaker height (H_b) is computed by using

the breaker height formula of BS85 as

$$H_b = 0.1L \tanh\left\{\left[0.56 + 0.45 \tanh\left(33\frac{H_{rmso}}{L_o}\right)\right]kh\right\}, \quad (29)$$

$$M36: D_B = 0.07\frac{\rho g c_g}{8h}[H_{rms}^2 - (0.066L \tanh(0.68kh))^2], \quad (30)$$

$$M38: D_B = 0.07\frac{\rho g c_g}{8h}\left[H_{rms}^2 - \left(0.061L \tanh\left(0.63kh + 0.21kh \tanh\left(39\frac{H_{rmso}}{L_o}\right)\right)\right)^2\right], \quad (31)$$

$$M41: D_B = 0.07\frac{\rho g c_g}{8h}[H_{rms}^2 - (0.047L \tanh(0.44(kh)^2 + 0.78kh))^2], \quad (32)$$

Overall, the six models (M3, M24, M31, M36, M38, and M41) give nearly the same accuracy. It may be interesting to see the comparison in more detail. Table 6 shows the errors of the six models for three groups of experiment scale while Table 7 shows the errors for 13 groups of data sources. The results can be summarized as follows:

(a) It can be seen from Tables 6 and 7 that no model gives significantly better results than the others. However, considering the consistency of the models through the variance of errors in Table 7, the model M36 seem to be slightly better than the others.
(b) Although overall errors (ER_{avg}) of all models are very good, the models do not predict very well for all sources of data.
(c) Because of the simplicity of the representative wave approach, it is expected that this approach will give lesser accuracy than that of the parametric approach. However, the results show that the accuracy of the models of the representative approach (M36, M38, and M41) are almost the same as those of the parametric wave approach (M3, M24, and M31). This may lead to the conclusion that the concept of representative wave approach can be used for computing the irregular wave height transformation.
(d) The greatest asset of the representative approach is its simplicity and ease of application, i.e. the rms wave height transformation in the nearshore zone can be

Table 6
The errors ER_{avg} and ER_{avg} of the six suitable models for three groups of experiment scale

Apparatus	Models					
	M3 Eq. (24)	M24 Eq. (26)	M31 Eq. (28)	M36 Eq. (30)	M38 Eq. (31)	M41 Eq. (32)
Small-scale	7.1	7.1	8.8	8.0	8.1	8.0
Large-scale	7.2	6.6	6.1	7.3	6.9	7.3
Field	10.4	10.4	9.7	9.4	9.7	9.2
ER_{avg}	8.2	8.1	8.2	8.2	8.2	8.2

Table 7
The errors ER_g of the six suitable models for each source of data

Sources	Models					
	M3 Eq. (24)	M24 Eq. (26)	M31 Eq. (28)	M36 Eq. (30)	M38 Eq. (31)	M41 Eq. (32)
Hurue (1990)	4.6	4.3	5.4	9.7	10.7	9.9
Smith and Kraus (1990)	8.1	8.3	10.4	9.8	9.7	9.7
Sultan (1995)	13.9	12.8	14.9	11.4	14.4	13.0
Grasmeijer and van Rijn (1999)	3.9	3.9	3.7	3.8	3.7	3.6
Hamilton and Ebersole (2001)	2.1	2.1	5.3	3.5	3.9	3.5
Ting (2001)	8.6	8.7	10.1	5.5	5.3	5.4
SUPERTANK project	13.6	11.3	9.7	10.5	11.0	10.7
LIP11D project	6.1	5.6	6.9	9.5	7.7	8.9
SAFE project	5.5	5.6	5.0	6.1	5.7	6.1
Thornton and Guza (1986)	14.7	16.0	9.6	9.2	9.1	8.7
DUCK85 project	12.6	11.6	12.0	13.4	18.2	17.1
DELILAH project	9.1	9.0	8.8	8.7	9.5	8.7
DUCK94 project	11.4	11.5	10.3	9.9	9.7	9.7
Variance of ER_g	16.3	15.4	9.4	8.1	15.6	12.8

computed by using only one equation (e.g. Eq. (30)). Therefore, the dissipation models from the representative wave approach (M36, M38, and M41) are suitable to use in the computation of irregular wave height transformation.

(e) Considering accuracy, variance of errors, and simplicity of the possible models, the model M36 (Eq. (30)) seems to be the most attractive model.

7. Conclusions

This study is undertaken to find out the suitable dissipation models, which can be used to compute H_{rms} for a wide range of experimental conditions. A total of 1723 cases from 13 sources of published experimental data are used to verify the models. The experiments cover small-scale, large-scale, and field experimental conditions. The transformation of H_{rms} is computed from the energy flux conservation law. Eight existing dissipation models, which were developed based on parametric and representative wave approaches, are selected to verify their applicability. The verification results are presented in terms of average rms relative error of three experiment scales (ER_{avg}). Because most of the existing models were developed based on the limited experimental conditions, the coefficients in the models may not be the optimal values. Therefore, coefficients in all models are recalibrated before comparing the applicability of the models. The comparison shows that all selected models can be used for computing H_{rms}, with ER_{avg} of about 8.2–11.4%. The model of Battjes and Stive (1985) gives the best predictions (with ER_{avg} of 8.2%).

The existing models are also modified by changing the breaker height formulas, inside the dissipation models and recalibrations. Substituting the seven formulas of H_b into the six existing dissipation models, 42 possible models are considered in this study. It is found that the accuracy of most existing models is improved significantly by using the suitable breaker height formula. There are six suitable models (i.e. the model of BS85 and 5 modified models), which can be used for computing H_{rms}. The verification also shows that the models of parametric and representative wave approaches give almost the same accuracy. Considering accuracy, variance of errors, and simplicity of the possible models, the model M36 is recommended.

Acknowledgments

This research was sponsored by the Thailand Research Fund. The data collection of the DELILAH and DUCK94 projects were funded by the US Office of Naval Research and the US National Science Foundation. Thanks and sincere appreciation are expressed to the researchers names listed in Table 1 for publishing the valuable data.

References

Baldock, T.E., Holmes, P., Bunker, S., Van Weert, P., 1998. Cross-shore hydrodynamics within an unsaturated surf zone. Coastal Engineering 34 (3–4), 173–196.

Battjes, J.A., Stive, M.J.F., 1985. Calibration and verification of a dissipation model for random breaking waves. Journal of Geophysical Research 90 (C5), 9159–9167.

Battjes, J.A., Janssen, J.P.F.M., 1978. Energy loss and set-up due to breaking of random waves. In: Proceedings of the 16th Conference on Coastal Engineering, ASCE, pp. 569–587.

Birkemeier, W.A., Donoghue, C., Long, C.E., Hathaway, K.K., Baron, C.F., 1997. The DELILAH Nearshore Experiment: Summary Data Report. US Army Corps of Engineers, Waterways Experiment Station, Vicksburg, MS.

Dette, H.H., Peters, K., Newe, J., 1998. MAST III—SAFE Project: Data Documentation, Large Wave Flume Experiments '96/97, Report No. 825 and 830. Leichtweiss-Institute, Technical University Braunschweig.

Goda, Y., 1970. A synthesis of breaking indices. Transactions of the Japan Society of Civil Engineers 2 (Part 2), 227–230.

Grasmeijer, B.T., van Rijn, L.C., 1999. Transport of fine sands by currents and waves, III: breaking waves over barred profile with ripples. Journal of Waterway, Port, Coastal, and Ocean Engineering 125 (2), 71–79.

Hamilton, D.G., Ebersole, B.A., 2001. Establishing uniform longshore currents in a large-scale sediment transport facility. Coastal Engineering 42 (3), 199–218.

Herbers, T.H.C., Elgar, S., Guza, R.T., O'Reilly, W.C., 2006. Surface gravity waves and nearshore circulation. DUCK94 Experiment Data Server: SPUV Pressure Sensor Wave Height Data. Available online at: 〈http://dksrv.usace.army.mi/jg/dk94dir〉.

Hurue, M., 1990. Two-dimensional distribution of undertow due to irregular waves. B.Eng. Thesis, Department of Civil Enginering, Yokohama National University, Japan (in Japanese).

Kraus, N.C., Smith, J.M., 1994. SUPERTANK Laboratory Data Collection Project, vols. 1–2, Technical Report CERC-94-3, US Army Corps of Engineers, Waterways Experiment Station.

Kraus, N.C., Gingerich, K.J., Rosati, J.D., 1989. DUCK85 Surf Zone Sand Transport Experiment, Technical Report CERC-89-5, US Army Corps of Engineers, Waterways Experiment Station.

Miche, R., 1944. Mouvements ondulatoires des mers en profondeur constante on decroissante. Ann. des Ponts et Chaussees, pp. 131–164, 270–292, 369–406 (Chapter 114).

Nairn, R.B., 1990. Prediction of cross-shore sediment transport and beach profile evolution. Ph.D. Thesis, Department of Civil Engineering, Imperial College, London.

Oliveira, F.S.B.F., 2007. Numerical modelling of deformation of multi-directional random waves over a varying topography. Ocean Engineering 34(2), 337–342.

Rattanapitikon, W., Shibayama, T., 1998. Energy dissipation model for regular and irregular breaking waves. Coastal Engineering Journal 40 (4), 327–346.

Rattanapitikon, W., Karunchintadit, R., Shibayama, T., 2003. Irregular wave height transformation using representative wave approach. Coastal Engineering Journal 45 (3), 489–510.

Roelvink, J.A., Reniers, A.J.H.M., 1995. LIP 11D Delta Flume Experiments: A Data Set for Profile Model Validation. Report No. H 2130, Delft Hydraulics.

Ruessink, B.G., Walstra, D.J.R., Southgate, H.N., 2003. Calibration and verification of a parametric wave model on barred beaches. Coastal Engineering 48 (3), 139–149.

Sultan, N., 1995. Irregular wave kinematics in the surf zone. Ph.D. Dissertation, Texas A&M University, College Station, TX, USA.

Southgate, H.N., Nairn, R.B., 1993. Deterministic profile modelling of nearshore processes. Part 1. Waves and currents. Coastal Engineering 19 (1–2), 27–56.

Smith, J.M., Kraus, N.C., 1990. Laboratory study on macro-features of wave breaking over bars and artificial reefs. Technical Report CERC-90-12, US Army Corps of Engineers, Waterways Experiment Station.

Thornton, E.B., Guza, R.T., 1983. Transformation of wave height distribution. Journal of Geophysical Research 88 (C10), 5925–5938.

Thornton, E.B., Guza, R.T., 1986. Surf zone longshore currents and random waves: field data and model. Journal of Physical Oceanography 16, 1165–1178.

Ting, F.C.K., 2001. Laboratory study of wave and turbulence velocity in broad-banded irregular wave surf zone. Coastal Engineering 43 (3–4), 183–208.

World Scientific
www.worldscientific.com

JAPAN SOCIETY OF CIVIL ENGINEERS
COASTAL ENGINEERING COMMITTEE

Coastal Engineering Journal, Vol. 49, No. 3 (2007) 291–310

ESTIMATION OF SHALLOW WATER REPRESENTATIVE WAVE HEIGHTS

WINYU RATTANAPITIKON
Civil Engineering Program,
Sirindhorn International Institute of Technology,
Thammasat University, Pathum Thani 12121, Thailand
winyu@siit.tu.ac.th

TOMOYA SHIBAYAMA
Department of Civil Engineering,
Yokohama National University, 79-5 Tokiwadai,
Hodogaya-ku, Yokohama 240-8501, Japan
tomo@ynu.ac.jp

Received 10 November 2006
Revised 6 March 2007

If the Rayleigh distribution of wave heights is valid, the representative wave heights can all be converted one to another through the known relationships. In shallow water, it has been pointed out by many researchers that the wave height distribution deviates from the Rayleigh distribution. However, it is not clear whether this deviation can lead to significant errors on the estimation of representative wave heights or not. Experimental data from small-scale, large-scale, and field experiments were used to examine the errors of the relationships derived from the Rayleigh distribution on estimating representative wave heights. The examination indicates that if H_{rms} is given, the relationships give overall very good estimations on $\bar{H}$ and $H_{1/3}$, good estimation on $H_{1/10}$ but fair estimation on $H_{\max}$. The effect of wave breaking was empirically incorporated into the relationships. The new relationships give better estimation than the relationships derived from the Rayleigh distribution.

Keywords: Representative wave heights; Rayleigh distribution; mean wave height; significant wave height; highest one-tenth wave height; maximum wave height.

1. Introduction

To analyze coastal processes and design of coastal structures, wave height is one of the most essentially required factors. The wave heights are usually available in

deepwater but not available at the depths required in shallow water. The wave heights in shallow water can be determined from wave models. The output of many wave models [e.g. Battjes and Janssen, 1978; Thornton and Guza, 1983; Larson, 1995; and Rattanapitikon *et al.*, 2003] is the root mean square wave height (H_{rms}). Nevertheless, other representative wave heights [e.g. mean wave height ($\bar{H}$), significant wave height ($H_{1/3}$), average of the highest one-tenth wave height ($H_{1/10}$), and maximum wave height ($H_{\max}$)] are also required for studying coastal processes and design of coastal structures. Thus, it is necessary to know the relationships between the representative wave heights. This study concentrates on the relationships for conversion from to be H_{rms} to be $\bar{H}$, $H_{1/3}$, $H_{1/10}$, and $H_{\max}$.

In deepwater, the probability density function (*pdf*) of measured wave heights from different oceans have been found to closely obey the Rayleigh distribution [Demerbilek and Vincent, 2006]. Widely accepted relationships between the representative wave heights are derived based on the assumption of the Rayleigh distribution of wave heights. The representative wave heights can all be converted one to another through the known proportional coefficients (β).

When waves propagate to shallow water, wave profiles steepen and eventually waves break. The higher waves tend to break at a greater distance from the shore. Closer to the shore, more and more waves are breaking, until in the inner surf zone, almost all the waves break. Investigations of shallow-water wave records from many studies indicate that the wave heights deviate considerably from the Rayleigh distribution [e.g. Dally, 1990; Battjes and Groenendijk, 2000; and Mendez *et al.*, 2004]; consequently, the relationships derived from the Rayleigh distribution may not be valid in shallow water. However, some researchers have pointed out that the wave heights distribution deviates slightly from the Rayleigh distribution and the relationships derived from the Rayleigh distribution are acceptable [e.g. Goodknight and Russell, 1963; Goda, 1974; and Thornton and Guza, 1983]. It can be seen that the validity of the relationships derived from the Rayleigh distribution is doubtful for shallow water. This make engineers hesitate to use the relationships in shallow water. The first objective of this study is to examine the errors of estimating the representative wave heights by using the relationships derived from the Rayleigh distribution.

It is expected that the deviation of wave height from the Rayleigh distribution is mainly caused by wave breaking. To improve the accuracy of the prediction, the effect of wave breaking should be empirically incorporated into the formulas. Several researchers have developed empirical *pdf* of wave heights taking into account depth-limited wave breaking [e.g. Hughes and Borgman, 1987; Battjes and Groenendijk, 2000; and Elfrink *et al.*, 2006]. For design purposes, it may not be necessary to know the *pdf* of wave heights; only a representative wave height is required. Although the representative wave heights can be determined from the *pdf*, it may not be convenient to do so. It is more reasonable to determine the representative wave height directly from a simple formula. It seems that no literature has proposed

empirical formulas taking into account the effect of wave breaking which can be used to compute the representative wave heights directly. Therefore, the second objective of this study is to develop empirical formulas to compute the representative wave heights.

Experimental data from 5 sources, including 146 cases and 2,238 wave records, are collected to verify the relationships. The experiments cover small-scale, large-scale and field experiments. The laboratory data cover a range of deepwater wave steepness (H_{rmso}/L_o) from 0.001 to 0.059 while the field experiments were measured during hurricanes and tropical storms. A summary of the collected experimental data is shown in Table 1. A brief summary of the collected experiments are summarized below.

The experiment of Smith and Kraus [1990] was conducted to investigate the macro-features of wave breaking over bars and artificial reefs using a small wave tank of 45.70 m long, 0.46 m wide, and 0.91 m deep. Both regular and irregular waves were employed in this experiment. A total of 12 cases were performed for irregular wave tests. Three irregular wave conditions were generated for three bar configurations as well as for a plane beach. A JONSWAP computer signal was

Table 1. Summary of collected experimental data used to verify the formulas.

Sources	Major Test No.	Description	H_{rmso}/L_o *	Apparatus
Smith and Kraus [1990]	SKR2	Plane and barred beach	0.057–0.059	Small-scale
	SKR6	Plane and barred beach	0.033–0.034	
	SKR8	Plane and barred beach	0.021–0.022	
Ting [2001]	Ting1	Plane beach	0.016	Small-scale
Ting [2002]	Ting2	Plane beach	0.015	Small-scale
Kraus and Smith [1994]: SUPERTANK project	ST10	Erosion toward equilibrium	0.007–0.046	Large-scale
	ST20	Acoustic profiler tests	0.001–0.045	
	ST30	Accretion toward equilibrium	0.001–0.004	
	ST40	Dedicated hydrodynamics	0.002–0.035	
	ST50	Dune erosion, Test 1 of 2	0.004–0.042	
	ST60	Dune erosion, Test 2 of 2	0.005–0.039	
	ST70	Seawall, Test 1 of 3	0.012–0.021	
	ST80	Seawall, Test 2 of 3	0.016–0.018	
	ST90	Berm flooding, Test 1 of 2	0.039–0.046	
	STAO	Foredune erosion	0.036–0.036	
	STCO	Seawall, Test 3 of 3	0.002–0.042	
	STDO	Berm flooding, Test 2 of 2	0.028–0.040	
	STJO	Narrow-crested offshore mound	0.002–0.040	
	STKO	Broad-crested offshore mound	0.002–0.038	
Goodknight and Russell [1963]	Audrey	Hurricane: Jun 25–28, 1957	0.011–0.021	Field
	Bertha	Tropical storm: Aug 8–9, 1957	0.015–0.024	
	Ella	Hurricane: Sep 4–6, 1958	0.012–0.025	
	Esther	Tropical storm: Sep 18–19, 1957	0.012–0.025	

*using linear wave theory

generated for spectral width parameter of 3.3 and spectral peak periods of 1.0, 1.5, and 1.75 s with significant wave heights of 12.1, 15.5, and 14.5 cm respectively.

The experiments of Ting [2001] and Ting [2002] were conducted to study wave and turbulence velocities in a broad-banded [Ting, 2001] and narrow-band [Ting, 2002] irregular wave surf zone. The experiments were performed in a two-dimensional wave tank that is 37 m long, 0.91 m wide and 1.22 m deep. A false bottom with 1 on 35 slope built of marine plywood was installed in this tank to create a plane beach. The irregular waves were developed from the TMA spectrum, with a spectral peak period of 2.0 s, a spectrally based significant wave height of 15.2 cm for the broad-banded spectrum and 12.3 cm for the narrow-banded spectrum, and spectral width parameter of 3.3 for the broad-banded spectrum and 100 for the narrow-banded spectrum. Water surface elevations were measured at seven cross-shore locations using a resistance-type gage.

The SUPERTANK laboratory data collection project [Kraus and Smith, 1994] was conducted to investigate cross-shore hydrodynamic and sediment transport processes, during the period August 5 to September 13, 1992, at Oregon State University, Corvallis, Oregon, USA. A 76-m-long sandy beach was constructed in a large wave tank of 104 m long, 3.7 m wide, and 4.6 m deep. Wave conditions involved regular and irregular waves. The 20 major tests were performed and each major test consisted of several cases. Most of the major tests were performed under the irregular wave actions. However, 6 major tests were performed under regular wave actions, i.e. test no. STBO, STEO, STFO, STGO, STHO, and STIO. Only the tests of irregular waves are considered in this study (see Table 1). The wave conditions were designed to balance the need for repetition of wave conditions to move the beach profile toward equilibrium and development of a variety of conditions for hydrodynamic studies. The TMB spectral shape was used to design all irregular wave tests. The collected experiments for irregular waves include 128 cases of wave and beach conditions (total 2048 wave records), covering incident significant wave heights from 0.2 m to 1.0 m, spectral peak periods from 3.0 sec to 10.0 sec and spectral width parameter between 3.3 (broad-banded) and 100 (narrow-banded).

The experiment of Goodknight and Russell [1963] was constructed to measure wave height statistics in the Gulf of Mexico during two hurricanes (Audrey in 1957 and Ella in 1958) and two tropical storms (Bertha and Esther in 1957). The wave-gage platform was located at a site approximately 2.4 km from shore, due south of New Orleans, La., in a water depth of approximately 10 m. The Calresearch step-resistance-type gage was used to measure water surface elevations. The wave gage recorded water-surface elevations as a function of time during 15-min recording periods at 2-hr intervals.

2. Representative Wave Heights Derived from the Rayleigh Distribution

The representative wave heights, which are usually defined and considered in this study, are mean wave ($\bar{H}$), root mean square wave (H_{rms}), significant wave height ($H_{1/3}$), average of the highest one-tenth wave ($H_{1/10}$), and maximum wave ($H_{\max}$). The relationships between the representative wave heights can be derived if a probability function of wave height distribution is given. The widely accepted distribution function is the Rayleigh distribution.

The Rayleigh distribution was proposed to describe the distribution of the intensity of sounds, which is the superposition of sound waves from an infinite number of sources. The distribution is applicable for waves having a spectrum confined in a narrow frequency band (narrow-band condition). Longuet-Higgins [1952] demonstrated that the Rayleigh distribution is also applicable to the wave heights in the sea. The validity of the distribution for deepwater waves has been confirmed by many researchers, even though the bandwidth may not always be narrow-banded [Demerbilek and Vincent, 2006]. The probability density function (*pdf*) is written as:

$$f(H) = \frac{2H}{H_{rms}^2} \exp\left[-\left(\frac{H}{H_{rms}}\right)^2\right] \tag{1}$$

where $f(H)$ is the probability density function of wave height (H), and H_{rms} is the root mean square (rms) wave height, which is defined as:

$$H_{rms} = \sqrt{\frac{\sum H^2}{M}} \tag{2}$$

where M is the total number of individual waves identified by the zero-crossing method.

If the distribution of wave heights is the Rayleigh distribution, the representative wave heights can be obtained by manipulating the probability function [see also Dean and Dalrymple, 1994; or Goda, 2000]. The $\bar{H}$, $H_{1/3}$, and $H_{1/10}$ are expressed in terms of H_{rms} as:

$$\bar{H} = 0.89 H_{rms} \tag{3}$$

$$H_{1/3} = 1.42 H_{rms} \tag{4}$$

$$H_{1/10} = 1.80 H_{rms} \tag{5}$$

Since the Rayleigh distribution of wave heights does not have an upper bound, the maximum wave height ($H_{\max}$) cannot be determined from the distribution. The maximum wave height varies with the total number of waves (M) in a record and has its own probability density function. Based on the Rayleigh distribution of

maximum wave height, Longuet-Higgins [1952] derived an approximate formula for the expected value of the maximum wave height in M waves as:

$$H_{\max} = \left(\sqrt{\ln M} + \frac{0.2886}{\sqrt{\ln M}} \right) H_{rms} \tag{6}$$

Once the H_{rms} is computed from the wave model, other representative wave heights ($\bar{H}$, $H_{1/3}$, $H_{1/10}$, and $H_{\max}$) can be determined from Eqs. (3) to (6). The reliability of Eqs. (3) to (6) depends on the validity of the Rayleigh distribution. In shallow water, some researchers demonstrated that the wave heights distribution deviates slightly from the Rayleigh distribution but some researchers pointed out that the wave heights distribution deviates considerably from the Rayleigh distribution. It is not clear whether the use of Eqs. (3) to (6) is acceptable or not. Therefore, the objective of this section is to examine the accuracy of Eqs. (3) to (6) for estimating $\bar{H}$, $H_{1/3}$, $H_{1/10}$, and $H_{\max}$ in shallow water.

The parameter, which is usually used to examine the accuracy of the predictions, is the relative root-mean-square error [e.g. Battjes and Groenendijk, 2000]. However, the deviation of wave height from the Rayleigh distribution generally decreases as the length of a wave record increases [Goda, 1977]. To reduce the effect of the record length (or total number of waves in a record) on the deviation, the relative root-weighted-mean-square error (ER_g) is used to examine the accuracy of the predictions in which the total number of waves in a record is used as a weight. The relative root-weighted-mean-square error is defined as:

$$ER_g = \sqrt{\frac{\sum_{i=1}^{ng} n_i \left(\frac{H_{mi} - H_{ci}}{H_{mi}}\right)^2}{\sum_{i=1}^{ng} n_i}} \tag{7}$$

where i is the number of a wave record, n_i is the total number of waves in the wave record no. i, H_{ci} is the computed representative wave height of the wave record no. i, H_{mi} is the measured representative wave height of the wave record number i, and ng is the total number of wave records.

The collected experiments shown in Table 1 are separated into three groups according to the experiment scale, i.e. small-scale, large-scale, and field experiments. It is expected that a good formula should be able to predict well for the three groups of experiment scale. Therefore, the average error (ER_{avg}) is used as a basic parameter to determine the overall accuracy of the formula. The average error is defined as:

$$ER_{avg} = \sqrt{\frac{\sum_{j=1}^{t_n} ER_{gj}^2}{t_n}} \tag{8}$$

where j is the number of data group, ER_{gj} is the relative root-weighted-mean-square error of the group numbered j, and t_n is the total number of data group. The small value of ER_{avg} indicates good overall accuracy of the formula.

Table 2. The errors (ER_g and ER_{avg}) of Rayleigh distribution [Eqs. (3) to (6)] on the estimation of $\bar{H}$, $H_{1/3}$, $H_{1/10}$, and $H_{\max}$ for three groups of experiment scale.

Experiments	Total No. of Cases	Total No. of Wave Records	$\bar{H}$	$H_{1/3}$	$H_{1/10}$	$H_{\max}$
Small-scale	14	110	4.9	9.6	16.3	47.5
Large-scale	128	2048	2.5	2.6	6.6	17.4
Field	4	80	4.2	3.1	4.9	10.5
ER_{avg}			4.0	6.0	10.6	29.8

The examinations of Eqs. (3) to (6) are carried out by using the measured representative wave heights (i.e. H_{rms}, $\bar{H}$, $H_{1/3}$, $H_{1/10}$, and $H_{\max}$) from Table 1. From the measured H_{rms}, the other representative wave heights ($\bar{H}$, $H_{1/3}$, $H_{1/10}$, and $H_{\max}$) are computed by using Eqs. (3) to (6), then the average errors (ER_{avg}) of each representative wave heights have been computed. Table 2 shows the errors (ER_g and ER_{avg}) for three groups of experiment scale while Table 3 shows the errors (ER_g) for all groups of major test. The results from Tables 2 and 3 are summarized as follows:

(a) The errors for large-scale and field experiment are nearly the same (except for $H_{\max}$) whereas the errors for small-scale experiments are considerably larger than those for large-scale and field experiments.
(b) Overall, Eqs. (3) and (4) give very good estimations on $\bar{H}$ and $H_{1/3}$ while Eq. (5) gives good estimation on $H_{1/10}$ but Eq. (6) gives fair estimation on $H_{\max}$. The overall average errors of the formulas for computing $\bar{H}$, $H_{1/3}$, $H_{1/10}$, and $H_{\max}$ are 4.0%, 6.0%, 10.6%, and 29.8% respectively. The errors tend to be larger for the larger representative wave heights.
(c) As Eqs. (3) to (5) give good estimation on the representative wave heights, it may be concluded that the assumption of Rayleigh distribution is not violated largely in shallow water. However, Eq. (6) should be used with care because it gives a considerable error, especially for small-scale experiments.
(d) As the Rayleigh distribution is derived based on the assumption of narrow-band spectrum, it is expected that the error of broadband condition should be greater than that of narrow-band condition. Surprisingly, the error of test no. Ting1 (broadband condition) is not greater than that of Ting2 (narrow-band condition). This shows that the effect of bandwidth on wave height distribution may not be significant in shallow water if the spectral width parameter is in the range of 3.3 to 100.

Although the relationships derived from the Rayleigh distribution give good estimations on $\bar{H}$, $H_{1/3}$, $H_{1/10}$ (except for $H_{\max}$), it may be possible to improve their accuracy, especially for estimating $H_{\max}$. The objective of the next section is to improve the accuracy on the estimation of the representative wave heights.

Table 3. The errors (ER_g) of Rayleigh distribution [Eqs. (3) to (6)] on the estimation of $\bar{H}$, $H_{1/3}$, $H_{1/10}$, and $H_{\max}$ for all groups of major test.

Sources	Major Test No.	Total No. of Cases	Total No. of Wave Records	Total No. of Waves in a Records	$\bar{H}$	$H_{1/3}$	$H_{1/10}$	$H_{\max}$
Smith and Kraus [1990]	SKR2	4	32	500	4.6	10.4	N.A.*	51.0
	SKR6	4	32	500	5.4	10.9	N.A.*	50.8
	SKR8	4	32	500	4.8	8.0	N.A.*	41.3
Ting [2001]	Ting1	1	7	186–207	3.4	6.6	14.1	32.5
Ting [2002]	Ting2	1	7	154–162	5.2	8.9	18.8	38.3
Kraus and Smith [1994]:	ST10	26	416	274–1636	2.0	2.5	7.1	22.2
	ST20	8	128	461–900	1.8	2.2	5.2	14.8
	ST30	19	304	197–1100	3.4	2.7	5.1	11.2
	ST40	12	192	388–1385	3.1	1.9	7.0	12.0
	ST50	8	128	190–603	1.8	2.1	5.2	15.2
	ST60	9	144	267–416	1.9	2.0	5.7	13.6
	ST70	9	144	152–660	2.0	1.9	5.5	15.7
	ST80	3	48	160–1477	1.8	1.5	3.5	13.5
	ST90	3	48	193–418	2.4	2.5	6.5	18.9
	STAO	1	16	193–221	4.9	3.9	5.4	15.1
	STCO	8	128	202–953	2.5	2.1	5.6	14.7
	STDO	3	48	363–416	3.5	3.8	9.0	24.7
	STJO	10	160	205–1692	2.8	3.5	8.9	20.3
	STKO	9	144	227–2046	2.3	3.0	6.9	17.1
Goodknight and Russell [1963]	Audrey	1	14	95–319	4.0	2.6	4.1	12.0
	Bertha	1	20	126–228	2.9	2.5	4.5	9.1
	Ella	1	25	116–182	4.5	4.2	5.0	8.9
	Esther	1	21	113–222	5.2	2.4	5.7	12.2
Total		146	2238					

*N.A. = Not Available

3. Formula Development

For developing the empirical formulas, equations (3) to (6) are written in general forms as:

$$\bar{H} = \beta_m H_{rms} \tag{9}$$

$$H_{1/3} = \beta_{1/3} H_{rms} \tag{10}$$

$$H_{1/10} = \beta_{1/10} H_{rms} \tag{11}$$

$$H_{\max} = \beta_{\max} \left(\sqrt{\ln M} + \frac{0.2886}{\sqrt{\ln M}} \right) H_{rms} \tag{12}$$

where β is the proportional coefficient, β_m, $\beta_{1/3}$, $\beta_{1/10}$, and $\beta_{\max}$ are the proportional coefficients of $\bar{H}$, $H_{1/3}$, $H_{1/10}$, and $H_{\max}$ respectively. The coefficients β_m, $\beta_{1/3}$, $\beta_{1/10}$, and $\beta_{\max}$ that derived from the Rayleigh distribution are 0.89, 1.42, 1.80, and

1.00 respectively [see Eqs. (3) to (6)]. The errors from Tables 2 and 3 show that the wave height distribution deviates slightly from the Rayleigh distribution. It is expected that the wave breaking is the primary cause of the deviation. Therefore, the coefficients β_m, $\beta_{1/3}$, $\beta_{1/10}$, and $\beta_{\max}$ (hereafter referred to as β) should not be constants and they may be a function of wave breaking.

3.1. *Formula derivation*

Various dimensionless parameters may influence the coefficients β. The variables, which may influence the coefficients β, are selected based on the previous researchers' experiences. It is expected that the variable that affect the wave height distribution may also affect the variation of coefficients β. The variables, which may affect the distribution of wave heights, are described below.

(a) Hughes and Borgman [1987] recommended the Beta-Rayleigh distribution for describing irregular wave height in shallow water. They introduced the term of rms wave height to breaker height ratio (H_{rms}/H_b) to account the effect of wave breaking into the distribution. The breaker height (H_b) was suggested to be proportional to the water depth (h). Therefore, the influence variable is H_{rms}/h.

(b) Battjes and Groenendijk [2000] proposed to account the influence of transitional wave height to wave height ratio (H_{tr}/H_{rms}) into the Rayleigh distribution. The transitional wave height (H_{tr}) is defined as a limiting wave height for non-breaking waves. The empirical formula of transitional wave height (H_{tr}) is expressed as:

$$H_{tr} = (0.35 + 5.8S)h \tag{13}$$

where S is the bottom slope, and h is the water depth.

(c) Elfrink *et al.* [2006] modified the Rayleigh distribution by taking the influence of rms wave height to water depth ratio (H_{rms}/h) into account. Although the influence variable of Elfrink *et al.* [2006] is the same as that of Hughes and Borgman [1987], the distribution function is different.

(d) As wave breaking may cause the wave height distribution deviates from the Rayleigh distribution, the variable that may affect the coefficients β is the fraction of wave breaking (Q_b). Battjes and Janssen [1978] derived the formula of Q_b based on the assumption of truncated Rayleigh distribution at the breaker height (H_b) and proposed to compute Q_b as:

$$\frac{1 - Q_b}{-\ln Q_n} = \left(\frac{H_{rms}}{H_b}\right)^2 \tag{14}$$

Since Eq. (14) is an implicit equation, an iteration process is necessary to compute the fraction of breaking waves (Q_b). Rattanapitikon and Shibayama [1998]

proposed the explicit form of Eq. (14) based on multiple regression analysis (with correlation coefficient $R^2 = 0.999$) as:

$$Q_b = \begin{cases} 0 & \text{for } \dfrac{H_{rms}}{H_b} \le 0.43 \\ 1.785\left(\dfrac{H_{rms}}{H_b}\right)^3 - 0.280\left(\dfrac{H_{rms}}{H_b}\right)^2 - 0.738\left(\dfrac{H_{rms}}{H_b}\right) + 0.235 & \text{for } 0.43 < \dfrac{H_{rms}}{H_b} < 1.0 \\ 1 & \text{for } \dfrac{H_{rms}}{H_b} \ge 1.0 \end{cases} \tag{15}$$

The breaker height (H_b) can be determined from the breaking criteria of Goda [1970] as:

$$H_b = 0.1 L_o \left\{ 1 - \exp\left[-1.5 \frac{\pi h}{L_o} (1 + 15 S^{4/3}) \right] \right\} \tag{16}$$

where L_o is the deepwater wavelength related to the spectral peak period (T_p). The coefficient 0.1 is used according to Rattanapitikon and Shibayama [1998]. It can be seen from Eq. (14) or Eq. (15) that the fraction of wave breaking (Q_b) is governed by H_{rms}/H_b. Including the affect of the fraction of breaking wave, the general function of the coefficients β may be expressed as a function of H_{rms}/H_b.

From the above considerations, there are three dimensionless parameters (H_{rms}/h, H_{rms}/H_{tr}, and H_{rms}/H_b) that may affect the variation of the coefficients β. The possible formulas of coefficients β can be expressed as the following function:

$$\beta = f_1 \left\{ \frac{H_{rms}}{h}, \frac{H_{rms}}{H_{tr}}, \frac{H_{rms}}{H_b} \right\} \tag{17}$$

where f_1 is a function.

As the deviation of the Rayleigh distribution is expected to be caused by waves breaking, comparing among the dimensionless parameters (H_{rms}/h, H_{rms}/H_{tr}, and H_{rms}/H_b), the parameter H_{rms}/H_b seems to have more physical meaning than the others because it represents the fraction of breaking waves.

The measured representative wave heights from the collected experiments (shown in Table 1) are used to determine the relationships. The required data for deriving the formula of the coefficients β are $\bar{H}$, H_{rms}, $H_{1/3}$, $H_{1/10}$, $H_{\max}$, M, T_p, h, and S. The coefficients β_m, $\beta_{1/3}$, $\beta_{1/10}$, and $\beta_{\max}$ are determined from Eqs. (9) and (12). The data of L_o is computed by using linear wave theory. The data of H_{tr} is determined from Eq. (13) while H_b is determined from Eq. (16).

An attempt is made to correlate the coefficients β_m, $\beta_{1/3}$, $\beta_{1/10}$, and $\beta_{\max}$ with the possible dimensionless parameters (H_{rms}/h, H_{rms}/H_{tr}, and H_{rms}/H_b). A total of 12 possible relations (3 relations for each coefficient β) are plotted to see the correlations (see Figs. 1 to 3). Figures 1 to 3 show that the coefficients β vary systematically across shore and the variations of coefficients β are in similar fashion. Comparing the

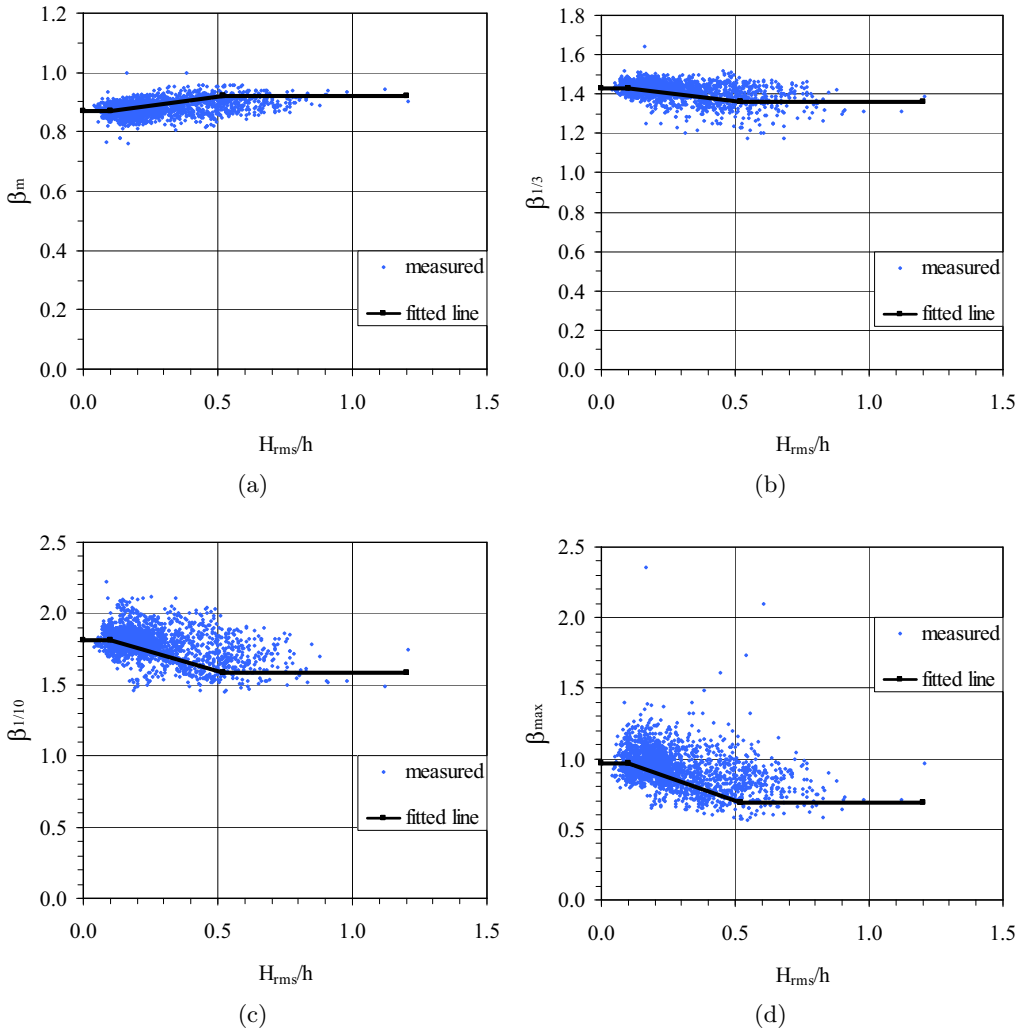

Fig. 1. Relationships between H_{rms}/h versus (a) β_m, (b) $\beta_{1/3}$, (c) $\beta_{1/10}$, and (d) $\beta_{\max}$.

relationships in Figs. 1 to 3, it is not clear which dimensionless parameter gives the best correlation. Therefore, all of them are considered to determine the coefficients β.

It can be seen from Figs. 1 to 3 that the relationships can be separated into 3 zones. The coefficients β are constant for the first zone then gradually changed in the second zone and finally become constant again in the third zone. These 3 zones seem to correspond with the zone in coastal region, especially for Fig. 3. The zone in coastal region may be separated into 3 zones based on the fraction of breaking waves (Q_b) as offshore zone ($Q_b = 0$), outer surf zone ($0 < Q_b < 1.0$), and inner surf zone ($Q_b = 1$). According to Eq. (15), $Q_b = 0$ when $H_{rms}/H_b \leq 0.43$ and $Q_b = 1$ when $H_{rms}/H_b \geq 1.0$. These criteria seem to correspond well with the zones in Fig. 3.

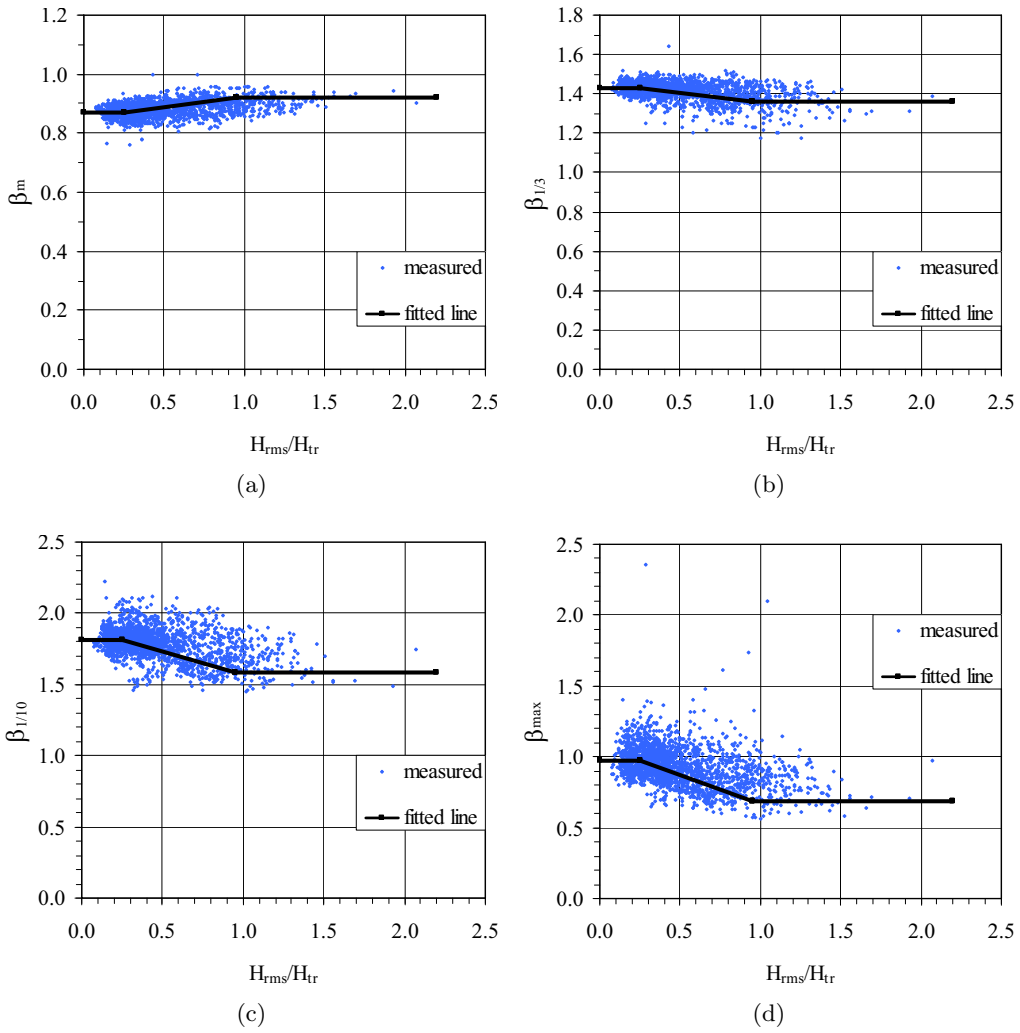

Fig. 2. Relationships between H_{rms}/H_{tr} versus (a) β_m, (b) $\beta_{1/3}$, (c) $\beta_{1/10}$, and (d) $\beta_{\max}$.

Thus, the 3 zones of coefficients β in Figs. 1 to 3 may be considered as offshore zone, outer surf zone, and inner surf zone. The coefficients β are constants for the offshore zone then gradually changed in the outer surf zone and finally become constants again in the inner zone. Therefore, the general form of β, which can be applied to β_m, $\beta_{1/3}$, $\beta_{1/10}$, and $\beta_{\max}$, is expressed as:

$$\beta = K_1 \qquad \text{for } X \le x_1 \tag{18a}$$

$$\beta = K_1 + \frac{(K_2 - K_1)}{(x_2 - x_1)}(X - x_1) \quad \text{for } x_1 < X < x_2 \tag{18b}$$

$$\beta = K_2 \qquad \text{for } X \ge x_2 \tag{18c}$$

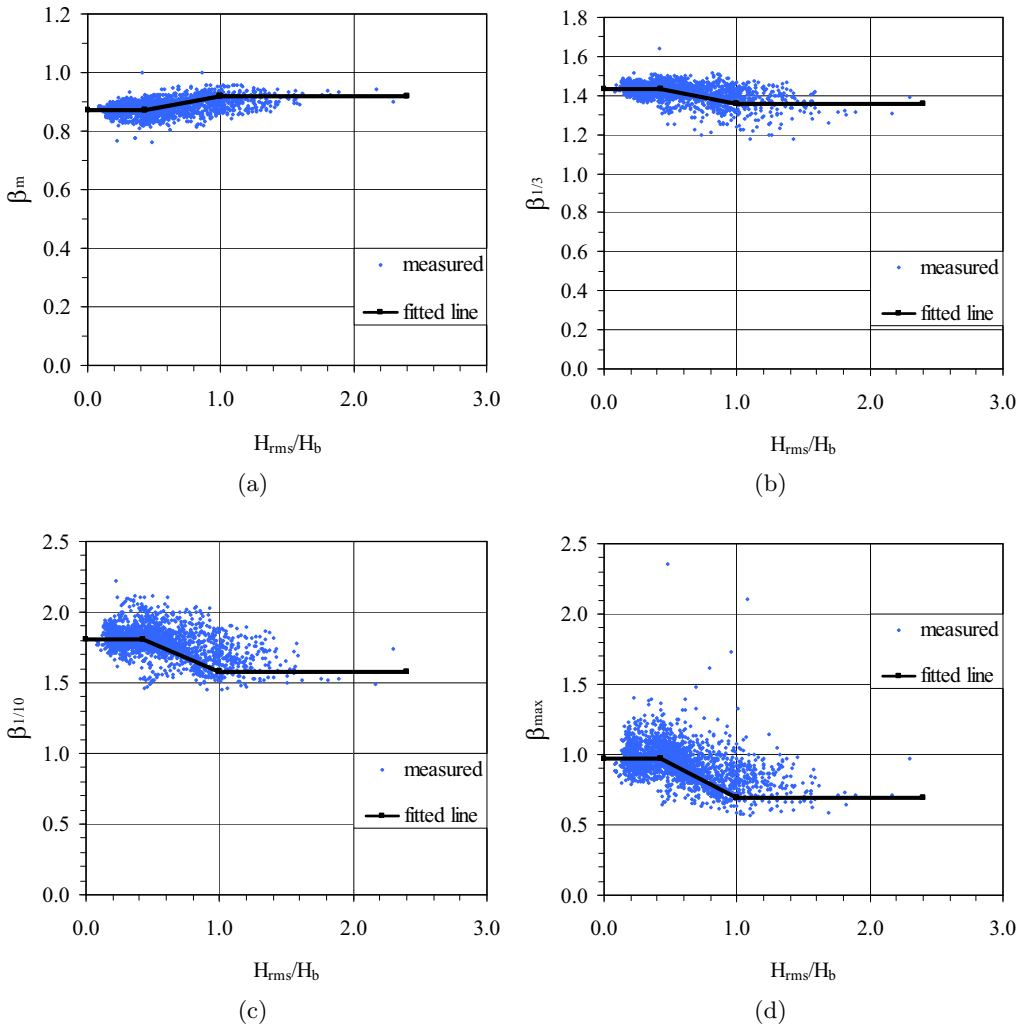

Fig. 3. Relationships between H_{rms}/H_b versus (a) β_m, (b) $\beta_{1/3}$, (c) $\beta_{1/10}$, and (d) $\beta_{\max}$.

where X is the dimensionless parameter (H_{rms}/h or H_{rms}/H_{tr} or H_{rms}/H_b), and K_1, K_2, x_1, and x_2 are constants which can be determined from formula calibration.

3.2. *Formula calibration*

The approximated values of the constants K_1, K_2, x_1, and x_2 for β_m, $\beta_{1/3}$, $\beta_{1/10}$ and $\beta_{\max}$ are determined from visual fit of Figs. 1 to 3. These approximated values are use as the initial values in the calibration. Using the coefficients β from Eq. (18) with the given constants (K_1, K_2, x_1, and x_2), the corresponding representative wave heights ($\bar{H}$, $H_{1/3}$, $H_{1/10}$, and $H_{\max}$) are computed from Eqs. (9) to (12), respectively. Then the errors (ER_g and ER_{avg}) for each representative wave height have been computed from Eqs. (7) and (8). The calibration of each formula is performed by

gradually adjusting the constants K_1, K_2, x_1, and x_2 until the error (ER_{avg}) becomes minimum. The general formulas of β (β_m, $\beta_{1/3}$, $\beta_{1/10}$ and $\beta_{\max}$) in terms of H_{rms}/h, H_{rms}/H_{tr}, and H_{rms}/H_b are expressed as follows:

(a) Formula of coefficients β in terms of H_{rms}/h:

$$\beta = K_1 \qquad \text{for } \frac{H_{rms}}{h} \leq 0.10 \tag{19a}$$

$$\beta = K_1 + \frac{(K_2 - K_1)}{(0.52 - 0.10)}\left(\frac{H_{rms}}{h} - 0.10\right) \quad \text{for } 0.10 < \frac{H_{rms}}{h} < 0.52 \tag{19b}$$

$$\beta = K_2 \qquad \text{for } \frac{H_{rms}}{h} \geq 0.52 \tag{19c}$$

(b) Formula of coefficients β in terms of H_{rms}/H_{tr}:

$$\beta = K_1 \qquad \text{for } \frac{H_{rms}}{H_{tr}} \leq 0.25 \tag{20a}$$

$$\beta = K_1 + \frac{(K_2 - K_1)}{(0.95 - 0.25)}\left(\frac{H_{rms}}{H_{tr}} - 0.25\right) \quad \text{for } 0.25 < \frac{H_{rms}}{H_{tr}} < 0.95 \tag{20b}$$

$$\beta = K_2 \qquad \text{for } \frac{H_{rms}}{H_{tr}} \geq 0.95 \tag{20c}$$

(c) Formula of coefficients β in terms of H_{rms}/H_b:

$$\beta = K_1 \qquad \text{for } \frac{H_{rms}}{H_b} \leq 0.43 \tag{21a}$$

$$\beta = K_1 + \frac{(K_2 - K_1)}{(1.0 - 0.43)}\left(\frac{H_{rms}}{H_b} - 0.43\right) \quad \text{for } 0.43 < \frac{H_{rms}}{H_b} < 1.0 \tag{21b}$$

$$\beta = K_2 \qquad \text{for } \frac{H_{rms}}{H_b} \geq 1.0 \tag{21c}$$

in which the best fitted constants (K_1 and K_2) for coefficients β_m, $\beta_{1/3}$, $\beta_{1/10}$, and $\beta_{\max}$ are shown in Table 4. The fitted lines from Eqs. (19) to (21) are shown as the solid lines in Figs. 1 to 3.

Table 4. Best fitted constants K_1 and K_2 for the coefficients β_m, $\beta_{1/3}$, $\beta_{1/10}$ and $\beta_{\max}$.

Constants	Coefficients β			
	β_m	$\beta_{1/3}$	$\beta_{1/10}$	$\beta_{\max}$
K_1	0.87	1.43	1.81	0.97
K_2	0.92	1.36	1.58	0.69

The examinations of Eqs. (19) to (21) are carried out by using the measured representative wave heights (i.e. H_{rms}, $\bar{H}$, $H_{1/3}$, $H_{1/10}$, and $H_{\max}$) from Table 1. The representative wave heights are computed by substituting the corresponding equation of coefficients β [from Eqs. (19) to (20)] into Eqs. (9) to (12). Table 5 shows the errors (ER_g and ER_{avg}) of Eqs. (19) to (21) on computing $\bar{H}$, $H_{1/3}$, $H_{1/10}$, and $H_{\max}$ for three groups of experiment scale while Table 6 shows the errors (ER_g) for all groups of major test. The results from Tables 5 and 6 are summarized as follows:

(a) Comparison among the overall errors (ER_{avg}) of Eqs. (19) to (21), Eq. (21) seems to be the best. This means that the variation of coefficients β is mainly governed by the fraction of breaking waves (or H_{rms}/H_b).
(b) Comparing with the relationships derived from Rayleigh distribution [Eqs. (3) to (5)], Eq. (21) gives slightly better estimation on $\bar{H}$, $H_{1/3}$, $H_{1/10}$ for large-scale and field experiments and give considerably better for small-scale experiments. For estimating $H_{\max}$, the accuracy of Eq. (21) is significantly better than that derived from Rayleigh distribution [Eq. (6)] for the three experiment-scales.
(c) The overall average errors (ER_{avg}) of Eq. (21) for computing $\bar{H}$, $H_{1/3}$, $H_{1/10}$, and $H_{\max}$ are 3.1%, 4.5%, 6.0%, and 12.2% respectively. In comparison with ER_{avg} of Eqs. (3) to (6) that shown in Table 2, Eq. (21) gives slightly better accuracy on the estimation of $\bar{H}$ and $H_{1/3}$, gives better accuracy on the estimation of $H_{1/10}$, and gives significantly better accuracy on the estimation of $H_{\max}$.

As Eq. (21) is better than the relationships derived from the Rayleigh distribution [Eqs. (3) to (6)], it may be used to indicate the limitation of Rayleigh distribution in shallow water. Equation (21) reveals some limitations of the Rayleigh distribution as follows:

(a) In the offshore zone ($H_{rms}/H_b \leq 0.43$), the coefficients β_m, $\beta_{1/3}$, $\beta_{1/10}$, and $\beta_{\max}$ are equal to 0.87, 1.43, 1.81, and 0.97 respectively. These values are nearly the same as those derived from the Rayleigh distribution. This shows that the Rayleigh distribution may be valid not only in the deepwater but also in the offshore zone or non-breaking wave zone. This also reveals the limitation of the present formulas. The formulas are limited to be used for the cases that the wave height distribution in the deepwater (or in the offshore zone) is close to the Rayleigh distribution. In the field, it has been shown by many researchers that the deepwater wave height distribution obeys the Rayleigh distribution. However, for cases of laboratory experiments, irregular wave behavior is dependent on the given wave history to wave generator. The present formula should be used only for cases that the incident wave height distribution is close to the Rayleigh distribution (e.g. JONSWAP and TMA spectrums).
(b) In the surf zones ($H_{rms}/H_b > 0.43$), the coefficients $\beta_{1/3}$, $\beta_{1/10}$, and $\beta_{\max}$ are smaller than those derived from the Rayleigh distribution. This shows that

Table 5. The errors (ER_g and ER_{avg}) of present formulas [Eqs. (19) to (21)] on the estimation of $\bar{H}$, $H_{1/3}$, $H_{1/10}$, and $H_{\max}$ for three groups of experiment scale.

Experiments	Eq. (19)				Eq. (20)				Eq. (21)			
	$\bar{H}$	$H_{1/3}$	$H_{1/10}$	$H_{\max}$	$\bar{H}$	$H_{1/3}$	$H_{1/10}$	$H_{\max}$	$\bar{H}$	$H_{1/3}$	$H_{1/10}$	$H_{\max}$
Small-scale	3.2	6.9	6.3	15.6	3.3	7.0	6.4	16.5	3.2	6.9	7.0	14.6
Large-scale	2.6	2.6	6.4	13.8	2.6	2.6	6.1	13.2	2.5	2.5	5.9	12.7
Field	3.9	3.1	5.2	9.1	4.3	3.5	6.2	11.4	3.7	2.8	4.9	8.5
ER_{avg}	3.3	4.6	6.0	13.1	3.5	4.8	6.2	13.9	3.1	4.5	6.0	12.2

Table 6. The errors (ER_g) of present formulas [Eq. (19) to (21)] on the estimation of $\bar{H}$, $H_{1/3}$, $H_{1/10}$, and $H_{\max}$ for all groups of major test.

Major test No.	Eq. (19)				Eq. (20)				Eq. (21)			
	$\bar{H}$	$H_{1/3}$	$H_{1/10}$	$H_{\max}$	$\bar{H}$	$H_{1/3}$	$H_{1/10}$	$H_{\max}$	$\bar{H}$	$H_{1/3}$	$H_{1/10}$	$H_{\max}$
SKR2	3.2	8.0	N.A.*	20.6	3.3	8.1	N.A.*	22.0	2.9	7.9	N.A.*	17.4
SKR6	3.4	7.8	N.A.*	14.8	3.5	7.9	N.A.*	15.5	3.4	7.7	N.A.*	14.4
SKR8	3.2	5.2	N.A.*	10.1	3.3	5.3	N.A.*	10.7	3.5	5.4	N.A.*	11.5
Ting1	1.6	3.4	5.2	12.2	1.6	3.4	5.4	12.3	1.9	3.5	5.9	12.9
Ting2	2.9	5.8	7.4	12.9	3.0	5.8	7.5	13.4	3.2	5.9	8.2	15.6
ST10	1.5	1.7	3.9	10.2	1.6	1.6	3.5	10.2	1.4	1.6	3.4	8.7
ST20	2.3	2.1	4.9	11.8	2.3	2.2	4.7	11.3	2.2	2.0	4.3	10.8
ST30	3.9	3.5	8.5	18.8	3.7	3.3	8.0	17.8	3.4	3.1	7.5	16.8
ST40	3.4	2.7	9.0	17.6	3.2	2.5	8.4	16.1	3.1	2.5	8.2	15.7
ST50	2.0	2.1	5.0	12.5	2.0	2.1	4.5	11.4	2.0	2.0	4.2	11.1
ST60	1.9	2.0	6.2	14.0	1.8	1.8	5.5	12.4	1.6	1.7	5.2	11.8
ST70	2.1	2.0	4.7	11.5	2.0	1.9	4.1	10.4	2.0	1.8	3.9	10.4
ST80	2.5	2.7	7.1	13.2	2.2	2.5	6.3	12.1	2.2	2.4	5.9	11.9
ST90	1.8	2.2	4.7	8.3	1.6	2.0	4.0	7.5	1.9	2.3	4.8	8.5
STAO	4.6	4.2	4.9	5.4	4.0	3.8	3.9	4.8	4.4	4.1	4.6	5.4
STCO	2.6	2.2	6.2	14.6	2.6	2.1	5.7	13.5	2.5	2.1	5.8	13.8
STDO	2.9	3.0	4.4	11.8	3.1	3.2	5.0	12.6	2.9	3.0	4.3	11.5
STJO	2.9	3.5	8.1	14.9	3.0	3.6	8.2	15.2	2.8	3.5	8.0	15.1
STKO	2.7	2.9	5.8	11.2	2.9	3.1	6.1	11.4	2.9	3.1	6.2	11.8
Audrey	3.6	2.5	4.0	8.2	4.0	2.9	5.2	10.5	3.4	2.3	3.6	7.4
Bertha	2.3	2.4	4.8	8.6	2.8	2.8	5.6	10.9	2.1	2.2	4.4	8.1
Ella	4.5	4.3	6.1	9.4	5.0	4.9	7.4	12.7	4.3	4.0	5.5	8.0
Esther	4.6	2.4	5.5	9.7	4.9	2.8	5.9	11.1	4.4	2.2	5.4	10.1

*N.A. = Not Available

the Rayleigh distribution tends to give an overestimation of the larger wave heights. Oppositely, the coefficient β_m is slightly larger than that derived from the Rayleigh distribution. This shows that the Rayleigh distribution tends to give an underestimation of the smaller wave heights. The overestimation of large wave heights and underestimation of small wave heights of the Rayleigh distribution in the surf zone was also reported by Battjes and Groenendijk [2000].

(c) The gradual change of coefficients β in the outer surf zone ($0.43 < H_{rms}/H_b < 1.0$) indicates that the wave height distribution is gradually deviated from the Rayleigh distribution and the deviation becomes maximum at the inner surf zone ($H_{rms}/H_b \geq 1.0$). As the coefficients β are governed by H_{rms}/H_b and the fraction of breaking waves (total number of braking waves per total number waves, Q_b) is also governed by H_{rms}/H_b, it may be concluded that the coefficients β are governed by Q_b. The deviation of coefficients β from those of Rayleigh distribution in the surf zone ($H_{rms}/H_b > 0.43$) reveals that the wave breaking (or Q_b) is the main factor to cause the wave height distribution (or β) deviate from that of Rayleigh. Seaward of the incipient wave breaking ($H_{rms}/H_b < 0.43$), the wave height distribution is close to the Rayleigh distribution as no wave is breaking ($Q_b = 0$). When the waves propagate onshore in the outer surf zone, the fraction of breaking waves (Q_b) increases as more and more waves are breaking. At each spatial point in the outer surf zone, there are both broken and unbroken waves. The broken wave heights decrease due to energy dissipation while the non-broken wave heights still increase due to wave shoaling. This causes the wave height distribution to deviate from the Rayleigh distribution. The deviation is gradually increased (as more and more waves are breaking) until almost all waves are breaking in the inner surf zone.

It should be noted that Eq. (21) is an empirical formula. Its validity may be limited according to the range of experimental conditions that are employed in the calibration. The present formula should be applicable for deepwater wave steepness (H_{rmso}/L_o) ranging between 0.001 and 0.059 and it is limited to be used for cases that the wave height distribution in the deepwater (or in the offshore zone) is close to the Rayleigh distribution.

4. Conclusions

This study concentrates on the relationships for conversion from H_{rms} to be $\bar{H}$, $H_{1/3}$, $H_{1/10}$, and $H_{\max}$ for shallow water region. Widely accepted relationships are derived based on the assumption of the Rayleigh distribution. It is well known that the wave height distribution in shallow water deviates from the Rayleigh distribution. However, it is not clear whether this deviation can lead to significant errors on the estimation of representative wave heights or not. The first objective of this study is to investigate the errors of estimating representative wave heights by using the relationships derived from the Rayleigh distribution in shallow water.

Experimental data from small-scale, large-scale, and field experiments were used to examine the accuracy of the relationships. The examination showed that the assumption of Rayleigh distribution is not violated largely in shallow water, especially for large-scale and field experiments. The relationships derived from Rayleigh distribution give very good estimations on $\bar{H}$ and $H_{1/3}$, good estimation on $H_{1/10}$ but fair estimations on $H_{\max}$. The errors of small-scale experiments are considerably larger than those of large-scale and field experiments.

An attempt was made to improve the accuracy of the estimations. The proportional coefficients (β) in the relationships were plotted with three dimensionless parameters (H_{rms}/h, H_{rms}/H_{tr}, and H_{rms}/H_b). It was found that the coefficients β are governed mainly by the fraction of breaking waves (or H_{rms}/H_b) and the new coefficients β have been proposed as a function of H_{rms}/H_b. Comparing with the coefficients β derived from the Rayleigh distribution, the new coefficients β give slightly better accuracy on estimating $\bar{H}$ and $H_{1/3}$, and give better accuracy on estimating $H_{1/10}$ and $H_{\max}$. The new coefficients reveal that the Rayleigh distribution is valid in the offshore zone but gives overestimation of the number of large waves and underestimation of the number of small waves in the surf zone. The wave height distribution is gradually deviated from the Rayleigh distribution in the outer surf zone and the deviation becomes maximum at the inner surf zone.

Acknowledgments

This research was sponsored by the Thailand Research Fund.

References

Battjes, J. A. & Groenendijk, H. W. [2000] "Wave height distributions on shallow foreshores," *Coastal Engineering* **40**, 161–182.

Battjes, J. A. & Janssen, J. P. F. M. [1978] "Energy loss and set-up due to breaking of random waves," in *Proc. 16th Coastal Engineering Conf. ASCE*, pp. 569–589.

Dally, W. R. [1990] "Random breaking waves: A closed-form solution for planar beaches," *Coastal Engineering* **14**, 233–263.

Dean, R. G. & Dalrymple, R. A. [1994] *Water Wave Mechanics for Engineers and Scientists* (World Scientific Publishing Co. Pte. Ltd.), p. 193.

Demerbilek, Z. & Vincent, L. [2006] "Water wave mechanics (Part 2 — Chapter 1)," Coastal Engineering Manual, EM1110-2-1100, Coastal and Hydraulics Laboratory — Engineering Research and Development Center, WES, U.S. Army Corps of Engineers, pp. II-1-75.

Elfrink, B., Hanes, D. M. & Ruessink, B. G. [2006] "Parameterization and simulation of near bed orbital velocities under irregular waves in shallow water," *Coastal Engineering* **53**, 915–927.

Goda, Y. [1970] "A synthesis of breaking indices," *Transaction Japan Society of Civil Engineers* **2**, 227–230.

Goda, Y. [1974] "Estimation of wave statistics from spectral information," in *Proc. Ocean Waves Measurement and Analysis Conference, ASCE*, pp. 320–337.

Goda, Y. [1977] "Numerical experiments on the statistical variability of ocean waves," *Rep. Port and Habour Research Institute* **16**, 3–26.

Goda, Y. [2000] *Random Seas and the Design of Maritime Structures* (World Scientific Publishing Co. Pte. Ltd.), p. 263.

Goodknight, R. C. & Russel, T. L. [1963] "Investigation of the statistics of wave heights," *J. Waterways and Harbors Division, ASCE* **89**(WW2), 29–55.

Hughes, S. A. & Borgman, L. E. [1987] "Beta-Rayleigh distribution for shallow water wave heights," in *Proc. of the American Society of Civil Engineers Specialty Conference on Coastal Hydrodynamics*, ASCE, pp. 17–31.

Kraus, N. C. & Smith, J. M. [1994] SUPERTANK Laboratory Data Collection Project, Technical Report CERC-94-3, WES, U.S. Army Corps of Engineers, pp. 55–73.

Larson, M. [1995] "Model for decay of random waves in surf zone," *J. Waterway, Port, Coastal, and Ocean Engineering, ASCE* **121**(1), 1–12.

Longuet-Higgins, M. S. [1952] "On the statistical distribution of the heights of sea waves," *J. Marine Research* **11**(3), 245–266.

Mendez, F. J., Losada, I. J. & Medina, R. [2004] "Transformation model of wave height distribution on planar beaches," *Coastal Engineering* **50**, 97–115.

Rattanapitikon, W. & Shibayama, T. [1998] "Energy dissipation model for regular and irregular breaking waves," *Coastal Engineering Journal, JSCE* **40**(4), 327–346.

Rattanapitikon, W., Karunchintadit, R. & Shibayama, T. [2003] "Irregular wave height transformation using representative wave approach," *Coastal Engineering Journal, JSCE* **45**(3), 489–510.

Smith, J. M. & Kraus, N. C. [1990] Laboratory Study on Macro-Features of Wave Breaking over Bars and Artificial Reefs, Technical Report CERC-90-12, WES, U.S. Army Corps of Engineers, pp. 59–74 and C36-C39.

Thornton, E. B. & Guza, R. T. [1983] "Transformation of wave height distribution," *J. Geophysical Research* **88**(C10), 5925–5938.

Ting, F. C. K. [2001] "Laboratory study of wave and turbulence velocity in broad-banded irregular wave surf zone," *Coastal Engineering* **43**, 183–208.

Ting, F. C. K. [2002] "Laboratory study of wave and turbulence characteristics in narrow-banded irregular breaking waves," *Coastal Engineering* **46**, 291–313.

Ocean Engineering 35 (2008) 1259–1270

Contents lists available at ScienceDirect

Ocean Engineering

journal homepage: www.elsevier.com/locate/oceaneng

Verification of significant wave representation method

Winyu Rattanapitikon *

Civil Engineering Program, Sirindhorn International Institute of Technology, Thammasat University, Pathum Thani 12121, Thailand

ARTICLE INFO

Article history:
Received 14 August 2007
Accepted 18 March 2008
Available online 26 March 2008

Keywords:
Irregular wave model
Significant wave height
Representative wave approach
Significant wave representation method
Energy dissipation

ABSTRACT

The significant wave representation method is the simplest method for computing the transformation of significant wave height across-shore. However, many engineers are reluctant to use this method because many researchers have pointed out that the method possibly contains a large estimation error. Nevertheless, Rattanapitikon et al. [Rattanapitikon, W., Karunchintadit, R., Shibayama, T., 2003. Irregular wave height transformation using representative wave approach. Coastal Engineering Journal, JSCE 45(3), 489–510.] showed that the wave representation method could be used to compute the transformation of root mean square wave heights. It may also be possible to use it for computing the significant wave height transformation. Therefore, this study was carried out to examine the possibility of simulating significant wave height transformation across-shore by using the significant wave representation method. Laboratory data from small- and large-scale wave flumes were used to calibrate and examine the models. Six regular wave models were applied directly to irregular waves by using the significant wave height and spectral peak period. The examination showed that three regular wave models (with new coefficients) could be used to compute the significant wave height transformation with very good accuracy. On the strength of both accuracy and simplicity of the three models, a suitable model is recommended for computing the significant wave height transformation. The suitable model was also modified for better predictions. The modified model (with different coefficients) can be used to compute either regular wave height or significant wave height transformation across-shore.

1. Introduction

The significant wave height (which is defined as the average of the highest one-third wave heights) is most frequently used in the field of coastal and ocean engineering (Goda, 2000; Andreas and Wang, 2007), especially in the design of coastal and ocean structures. The wave heights are usually available in deepwater but not available at the required depths in shallow water. The wave heights in shallow water can be determined from wave models. Common approaches to model the significant wave height transformation may be classified into three main approaches, i.e., representative wave approach (commonly referred to as significant wave representation method), wave-by-wave approach, and conversion approach.

For the significant wave representation method, the regular wave models are directly applied to irregular waves by using the significant wave height. The method has been widely used since the introduction of the significant waves. It is easy to understand and also simple to use. However, the characteristics of the irregular waves (e.g., wave height and period) are statistically variable in contrast to regular waves, which have a single height, period, and direction. As the significant wave representation method does not consider such variability, the method may possibly contain a large estimation error (Goda, 2000).

The wave-by-wave approach considers the propagation of individual waves in the irregular wave train. The incident individual waves may be determined from irregular wave records or from probability density function (pdf) of wave heights. The propagation of each individual wave is computed by using an appropriate regular wave model. Recombining the individual wave heights at the required depth yields the irregular wave train, which is used to determine the significant wave height or other representative wave heights. Several models have been proposed based on this approach, differing mainly in the regular wave model used to simulate the propagation of the individual waves (e.g., the models of Mizuguchi, 1982; Dally, 1992; Kuriyama, 1996; Goda, 2004). This approach is particularly useful if a detailed wave height distribution is required. However, it has the disadvantage of being time consuming, which may not be suitable for some practical work.

The conversion approach is used to convert the representative wave heights from one to another through the known relationships. The root mean square wave height (H_{rms}) is usually used as a reference wave height of the conversion because it is the output

* Tel.: +66 2564 3221; fax: +66 2986 9112.
E-mail address: winyu@siit.tu.ac.th

0029-8018/$ - see front matter © 2008 Elsevier Ltd. All rights reserved.
doi:10.1016/j.oceaneng.2008.03.008

of many wave models (e.g., the models of Battjes and Janssen, 1978; Thornton and Guza, 1983; Larson, 1995; Rattanapitikon, 2007). Therefore, the significant wave height (H_s) can be determined from the known relationship between H_{rms} and H_s (e.g., the relationships of Longuet-Higgins, 1952; Battjes and Groenendijk, 2000; Rattanapitikon and Shibayama, 2007). This approach is simpler than the wave-by-wave approach but slightly more complicated than the significant wave representation method.

The present study focuses on the significant wave representation method, as this appears to be the simplest method. Many researchers pointed out that the significant wave representation method could give inconsistent or erroneous results in the computation of significant wave height transformation (Goda, 2000). It seems that no literature has pointed out that the significant wave representation method is applicable in the surf zone. Consequently, engineers have been reluctant to use the significant wave representation method. However, the significant wave representation method has the merits of easy understanding, simple application and it is not necessary to assume the shape of the pdf of wave heights. It will be useful for some practical work if this approach can be used to compute the significant wave heights in shallow water. Moreover, Rattanapitikon et al. (2003) reported that the representative wave approach can be used to compute H_{rms} with very good accuracy. It may also be used to compute H_s. This study is carried out to investigate the possibility of using the significant wave representation method.

This paper is divided into four main parts. The first part describes the collected data. The second part describes some existing regular wave models. The third part describes modeling of irregular waves using significant wave representation method. The fourth part deals with the modification of the selected model.

2. Collected laboratory data

For the significant wave representation method, the regular wave model is directly applied to irregular waves by using the significant wave height. The present study is, therefore, concerned with both regular and irregular wave models. The experiments performed under regular and irregular wave conditions are used to calibrate and examine the models.

2.1. Regular wave data

Laboratory data of regular wave heights inside the surf zone from 13 sources (total 492 cases) have been collected for calibration and examination of the regular wave models. The experiments cover a wide range of wave and bottom topography conditions, including small- and large-scale experiments. The experiments cover a variety of beach conditions and cover a range of deepwater wave steepness (H_o/L_o, where H_o is the deepwater wave height and L_o is the deepwater wavelength) from 0.003 to 0.112. A summary of the collected laboratory data is given in Table 1. Most of the experiments were carried out in small-scale wave flumes, except the experiments of Kajima et al. (1983) and Kraus and Smith (1994) which were carried out in large-scale wave flumes. The data sources are the same as those used by Rattanapitikon et al. (2003).

2.2. Irregular wave data

Laboratory data of significant wave height transformation from six sources, totaling 282 cases, were collected for calibration and examination of the irregular wave models. A summary of the collected laboratory data is shown in Table 2. The collected data are separated into two groups based on the experiment-scale, i.e., small- and large-scale experiments. The experiments of Hurue (1990), Smith and Kraus (1990), Katayama (1991), and Ting (2001) were performed in small-scale wave flumes under fixed bed conditions, while the experiments of Kraus and Smith (1994) and Dette et al. (1998) were undertaken in large-scale wave flumes under movable bed (sandy bed) conditions. The data cover a range of deepwater wave steepness (H_{so}/L_o, where H_{so} is the deepwater significant wave height) from 0.002 to 0.064. A brief description of the experiments is given below.

The experiment of Hurue (1990) was conducted to study wave and undertow velocity on a plane beach. The experiment was performed in a small-scale wave flume, which was 17 m long and 0.5 m wide. The beach topography was 1/20 uniform slope with the smooth bottom. The incident significant wave height of 0.09 m and wave period of 1.26 s was generated based on the Bretschneider–Mitsuyasu spectrum (Bretschneider, 1968; Mitsuyasu, 1970). Water surface elevations were measured at seven cross-shore locations using a capacitance-type gage.

The experiment of Smith and Kraus (1990) was conducted to investigate the macro-features of wave breaking over bars and artificial reefs using a small wave flume of 45.70 m long, 0.46 m wide, and 0.91 m deep. Both regular and irregular waves were employed in this experiment. A total of 12 cases were performed for irregular wave tests. Three irregular wave conditions were generated for three bar configurations as well as for a plane beach. A JONSWAP (Hasselmann et al., 1973) computer signal was generated for spectral width parameter of 3.3 and spectral peak periods of 1.07, 1.56, and 1.75 s with significant wave heights of

Table 1
Summary of collected experimental data used to calibrate and verify the regular wave models

Sources	Beach condition	No. of cases	No. of data	H_o/L_o
Cox and Kobayashi (1997)	Plane beach	1	5	0.015
Hansen and Svendsen (1984)	Plane beach	1	5	0.019
Horikawa and Kuo (1966)	Plane and stepped beach	213	2127	0.006–0.100
Hurue (1990)	Plane beach	1	4	0.038
Nadaoka et al. (1982)	Plane beach	2	11	0.013–0.080
Nagayama (1983)	Plane, stepped, and barred beach	12	171	0.025–0.055
Okayasu et al. (1988)	Plane beach	10	62	0.009–0.054
Sato et al. (1988)	Plane beach	3	25	0.031–0.050
Sato et al. (1989)	Plane beach	2	11	0.019–0.036
Shibayama and Horikawa (1985)	Sandy beach	10	85	0.028–0.036
Smith and Kraus (1990)	Plane and barred beach	101	506	0.008–0.096
Kajima et al. (1983)	Sandy beach	79	1397	0.003–0.112
Kraus and Smith (1994)	Sandy beach	57	429	0.003–0.066
Total		492	4838	0.003–0.112

Table 2
Summary of collected experimental data used to calibrate and verify the irregular wave models

Sources	Test series	Descriptions	No. of cases	No. of data	H_{so}/L_o
Hurue (1990)	Hu1	Plane beach	1	7	0.037
Smith and Kraus (1990)	R2000	Plane beach	1	8	0.070
	R22xx	Barred beach	3	24	0.070
	R6000	Plane beach	1	8	0.040
	R62xx	Barred beach	3	24	0.040
	R8000	Plane beach	1	8	0.030
	R82xx	Barred beach	3	24	0.030
Katayama (1991)	Ka1&Ka2	Barred beach	2	16	0.041, 0.044
Ting (2001)	Ti1	Plane beach	1	7	0.024
Kraus and Smith (1994)	ST10	Erosion toward equilibrium	26	416	0.013–0.064
	ST20	Acoustic profiler tests	8	128	0.002–0.057
	ST30	Accretion toward equilibrium	19	304	0.003–0.007
	ST40	Dedicated hydrodynamics	12	192	0.005–0.050
	ST50	Dune erosion, test 1	8	128	0.012–0.057
	ST60	Dune erosion, test 2	9	144	0.009–0.022
	ST70	Seawall, test 1	9	144	0.022–0.032
	ST80	Seawall, test 2	3	48	0.022
	ST90	Berm flooding, test 1	3	48	0.050
	STAO	Foredune erosion	1	16	0.050
	STCO	Seawall, test 3	8	127	0.004–0.057
	STDO	Berm flooding, test 2	3	48	0.050
	STJO	Narrow-crested mound	10	160	0.005–0.050
	STKO	Broad-crested mound	9	144	0.005–0.050
Dette et al. (1998)	A8	1:20 beach slope, normal	7	147	0.010
	A9	1:20 beach slope, storm	15	390	0.018
	B1	1:10 beach slope, normal	8	191	0.010
	B2	1:10 beach slope, storm	15	392	0.018
	C1	1:5 beach slope, normal	4	95	0.010
	C2	1:5 beach slope, storm	17	459	0.018
	H1	1:15 beach slope, normal	2	43	0.010
	H2	1:15 beach slope, storm	15	398	0.018
	D1&D3	D.P.[a], no overtopping, normal	7	158	0.010
	D2	D.P.[a], no overtopping, storm	11	297	0.018
	E	D.P.[a], with overtopping, storm	11	297	0.018
	F	No D.P.[a], storm	12	324	0.018
	G	No D.P.[a], underwater barrier	14	365	0.012–0.018
Total			282	5729	0.002–0.064

[a] D.P., dune protection.

0.12, 0.15, and 0.14 m, respectively. Water surface elevations were measured at eight cross-shore locations using resistance-type gages.

The experiment of Katayama (1991) was conducted to study wave and undertow velocity on a bar-type beach. The experiment was performed in a small-scale wave flume, which was 17 m long and 0.5 m wide. The bar-type beach consisted of the first 5 m of 1/20, the next 1 m of −1/20, and the last 4 m of 1/20 slopes. The incident significant wave heights of 0.06 and 0.08 m and wave periods of 0.95 and 1.14 s were generated based on the Bretschneider–Mitsuyasu spectrum (Bretschneider, 1968; Mitsuyasu, 1970). Water surface elevations were measured at eight cross-shore locations using a capacitance-type gages.

The experiment of Ting (2001) was conducted to study wave and turbulence velocities in a broad-banded irregular wave surf zone. The experiment was performed in a small-scale wave flume, which was 37 m long, 0.91 m wide, and 1.22 m deep. A false bottom with 1/35 slope built of marine plywood was installed in the flume to create a plane beach. The irregular waves were developed from the TMA spectrum (Bouws et al., 1985), with a spectral peak period of 2.0 s, a spectrally based significant wave height of 0.15 m and spectral width parameter of 3.3. Water surface elevations were measured at seven cross-shore locations using a resistance-type gage.

The SUPERTANK laboratory data collection project (Kraus and Smith, 1994) was conducted to investigate cross-shore hydrodynamic and sediment transport processes from August 5 to September 13, 1992 at Oregon State University, Corvallis, OR, USA. A 76-m-long sandy beach was constructed in a large wave tank of 104 m long, 3.7 m wide, and 4.6 m deep. Wave conditions included both regular and irregular waves. In all, 20 major tests were performed, and each major test consisted of several cases. Most of the tests (14 major tests) were performed under the irregular wave actions. The wave conditions were designed to balance the need for repetition of wave conditions to move the beach profile toward equilibrium and development of a variety of conditions for hydrodynamic studies. The TMA spectral shape (Bouws et al., 1985) was used to design all irregular wave tests. The collected experiments for irregular waves included 128 cases of wave and beach conditions (a total of 2047 wave records), covering incident significant wave heights from 0.2 to 1.0 m, spectral peak periods from 3.0 to 10.0 s, and spectral width parameter between 3.3 (broad-banded) and 100 (narrow-banded). Sixteen resistance-type gages were used to measure water surface elevations across-shore.

SAFE Project (Dette et al., 1998) was carried out to improve the methods of design and performance assessment of beach nourishment. The SAFE Project consisted of four activities, one of

which was to perform experiments in a large-scale wave flume in Hannover, Germany. A 250-m-long sandy beach was constructed in a large wave tank of 300 m long, 5 m wide, and 7 m deep. The test program was divided into two major phases. The first phase (cases A, B, C, and H) was aimed to study the beach deformation of equilibrium profile with different beach slope changes. The equilibrium beach profile was adopted from Bruun's (1954) approach ($h = 0.12x^{2/3}$). In the second phase, the sediment transport behaviors of dunes with and without structural aid were investigated (cases D, E, F, and G). The TMA spectral shape (Bouws et al., 1985) was used to design all irregular wave tests. The tests were performed under normal wave conditions ($H_{so}/L_o = 0.010$, water depth in the horizontal section = 4.0 m) and storm wave conditions ($H_{so}/L_o = 0.018$, water depth in the horizontal section = 5.0 m). A total of 27 wave gages was installed over a length of 175 m along one wall of the flume. The collected experiments included 138 cases of wave and beach conditions, covering deepwater wave steepness (H_{so}/L_o) from 0.010 to 0.018.

3. Regular wave model

The regular wave height transformation across-shore can be computed from the energy flux conservation as

$$\frac{\partial(Ec_g)}{\partial x} = -D_B, \tag{1}$$

where $E = \rho g H^2/8$ is the wave energy density, ρ is the water density, g is the acceleration due to gravity, H is the wave height, c_g is the group velocity, x is the distance in cross-shore direction, and D_B is the energy dissipation rate due to wave breaking which is zero outside the surf zone. The energy dissipation rate due to bottom friction is neglected. In the present study, all variables are based on the linear wave theory.

The wave height transformation can be computed from the energy flux conservation (Eq. (1)) by substituting the formula of the energy dissipation rate (D_B) and numerically integrating from offshore to shoreline. The difficulty of Eq. (1) is how to formulate the energy dissipation rate caused by the breaking waves.

During the past decades, various models have been developed for computing the energy dissipation of regular wave breaking. Widely used concepts for computing energy dissipation rate (D_B) for regular wave breaking are the bore concept and the stable energy concept.

The bore concept is based on the similarity between the breaking wave and the hydraulic jump. Several models have been proposed based on slightly different assumptions on the conversion from energy dissipation of hydraulic jump to energy dissipation of a breaking wave. Some existing D_B models, which were developed based on the bore concept, are listed as follows:

(a) Battjes and Janssen (1978):

$$D_B = 0.47\frac{\rho g H^2}{4T}, \tag{2}$$

(b) Thornton and Guza (1983):

$$D_B = 0.67\frac{\rho g H^3}{4Th}, \tag{3}$$

(c) Deigaard et al. (1991):

$$D_B = 0.48\frac{\rho g h H^3}{T(4h^2 - H^2)}, \tag{4}$$

where h is the water depth and T is the wave period. The constants in the above models were calibrated by Rattanapitikon et al. (2003) based on a wide range of experimental conditions as shown in Table 1.

The stable energy concept was introduced by Dally et al. (1985) based on an analysis of the measured breaking wave height on horizontal slope of Horikawa and Kuo (1966). When a breaking wave enters an area with horizontal bed, the breaking continues (the wave height decreases) until some stable wave height is attained. The development of the stable energy concept was based on an observation of stable wave height on horizontal slope. Dally et al. (1985) assumed that the energy dissipation rate was proportional to the difference between the local energy flux per unit depth and the stable energy flux per unit depth. Several models have been proposed on the basis of this concept. The main difference is the formula for computing the stable wave height (for more detail, please see Rattanapitikon et al., 2003). Some existing D_B models, which were developed based on the stable energy concept, are listed as follows:

(a) Dally et al. (1985):

$$D_B = 0.15\frac{\rho g c_g}{8h}[H^2 - (0.4h)^2], \tag{5}$$

(b) Rattanapitikon and Shibayama (1998):

$$D_B = 0.15\frac{\rho g c}{8h}\left\{H^2 - \left[h\exp\left(-0.36 - \frac{1.25h}{\sqrt{LH}}\right)\right]^2\right\}, \tag{6}$$

(c) Rattanapitikon et al. (2003):

$$D_B = 0.15\frac{\rho g c_g}{8h}\{H^2 - [0.073L\tanh(kh)]^2\}, \tag{7}$$

where c is the local phase velocity, L is the local wavelength, and k is the local wave number. The second terms on the right-hand side of Eqs. (5)–(7) are the terms of stable wave height. The energy dissipation will be zero if the wave height is less than the stable wave height.

The verification results of the six existing models are presented in the paper by Rattanapitikon et al. (2003). The results are also shown in Table 6 for comparison with the modified model (described in Section 5).

4. Irregular wave model

For the representative wave approach, the energy flux of the representative wave represents the average energy flux of an irregular wave train. The governing equation (energy flux conservation) of the representative wave (H_{rms}) can be derived based on the assumptions of linear wave theory and Rayleigh distribution of wave heights. Although the crude assumptions of the representative wave approach may not be theoretically justified (mainly because of the non-linearity of each individual wave), the approach is physically valid (the prediction agrees well with actual measurements). There are many wave models that are successful in using the energy flux conservation of the representative wave (H_{rms}) for computing the transformation of H_{rms} across-shore, e.g., the models of Battjes and Janssen (1978), Thornton and Guza (1983), Larson (1995), Baldock et al. (1998), Ruessink et al. (2003), and Rattanapitikon (2007). If the energy flux conservation of H_{rms} is valid, the energy flux conservation of H_s should also be valid because H_{rms} can be converted to H_s through the known coefficient (i.e., $H_s = 1.42H_{rms}$ for the Rayleigh

distribution). The derivation of the governing equation of the significant wave representation method is shown in the Appendix.

In the present study, for the significant wave representation method, the regular wave model is applied directly to irregular waves by using the significant wave height (H_s) and the spectral peak period (T_p). The spectral peak period is used because it is the most commonly used parameter and typically reported for the irregular wave data.

Since the D_B formulas shown in Section 3 (Eqs. (2)–(7)) were developed for regular waves, it is not clear which formula is suitable for the significant wave representation method. Therefore, all of them were used to investigate the possibility of simulating the significant wave height transformation.

Substituting the dissipation formula (Eqs. (2)–(7), respectively) into Eq. (1) and applying for significant wave height (H_s) and spectral peak period (T_p), the irregular wave models can be expressed as

$$\text{model (1)}: \quad \frac{\rho g}{8}\frac{\partial(H_s^2 c_g)}{\partial x} = -K_1 \frac{\rho g H_s^2}{4T_p}, \tag{8}$$

$$\text{model (2)}: \quad \frac{\rho g}{8}\frac{\partial(H_s^2 c_g)}{\partial x} = -K_2 \frac{\rho g H_s^3}{4T_p h}, \tag{9}$$

$$\text{model (3)}: \quad \frac{\rho g}{8}\frac{\partial(H_s^2 c_g)}{\partial x} = -K_3 \frac{\rho g h H_s^3}{T_p(4h^2 - H_s^2)}, \tag{10}$$

$$\text{model (4)}: \quad \frac{\rho g}{8}\frac{\partial(H_s^2 c_g)}{\partial x} = -K_4 \frac{\rho g c_g}{8h}[H_s^2 - (K_5 h)^2], \tag{11}$$

$$\text{model (5)}: \quad \frac{\rho g}{8}\frac{\partial(H_s^2 c_g)}{\partial x} = -K_6 \frac{\rho g c}{8h} \times \left\{H_s^2 - \left[K_7 h \exp\left(-0.36 - \frac{1.25h}{\sqrt{LH_s}}\right)\right]^2\right\}, \tag{12}$$

$$\text{model (6)}: \quad \frac{\rho g}{8}\frac{\partial(H_s^2 c_g)}{\partial x} = -K_8 \frac{\rho g c_g}{8h}\{H_s^2 - [K_9 L \tanh(kh)]^2\}, \tag{13}$$

where K_1–K_9 are the coefficients. It can be seen from Eqs. (2)–(7) that the coefficients K_1–K_9 for the regular wave models are 0.47, 0.67, 0.48, 0.15, 0.4, 0.15, 1.0, 0.15, and 0.073, respectively. When applying to the irregular wave, K_1–K_9 are the adjustable coefficients to allow for the effect of the transformation to irregular waves. Hereafter, Eqs. (8)–(13) are referred to as MD1, MD2, MD3, MD4, MD5, and MD6, respectively. The variables c_g, c, L, and k in the models MD1–MD6 are calculated based on the spectral peak period (T_p).

The breaking criterion of Miche (1944) (see also Tucker and Pitt, 2001, p. 307) is applied to determine incipient wave breaking of the significant wave height (H_{sb}) as

$$H_{sb} = K_{10} L \tanh(kh), \tag{14}$$

where K_{10} is the coefficient. The published value of K_{10} for regular wave breaking is 0.142. When applying to the irregular waves, K_{10} is the adjustable coefficient to allow for effect of the transformation to irregular waves. The energy dissipation (D_B) terms on the right-hand side of models MD1–MD6 occur when $H_s \geqslant H_{sb}$ and is equal to zero when $H_s < H_{sb}$.

4.1. Trial simulation

The objective of this section is to test the applicability of models MD1–MD6 by using the coefficients K_1–K_{10} which were proposed by the previous researchers for regular waves (shown in the second column of Table 3). All collected data shown in Table 2 are used to examine the models.

Table 3
The errors (ER_g and ER_{avg}) of the models MD1– MD6 (using the coefficients of regular waves) for two groups of experiment-scales (measured data from Table 2)

Models	Coefficients	ER_g		ER_{avg}
		Small-scale	Large-scale	
MD1 (Eq. (9))	$K_1 = 0.47$, $K_{10} = 0.142$	25.5	13.1	19.3
MD2 (Eq. (10))	$K_2 = 0.67$, $K_{10} = 0.142$	24.0	10.9	17.4
MD3 (Eq. (11))	$K_3 = 0.48$, $K_{10} = 0.142$	22.7	11.3	17.0
MD4 (Eq. (12))	$K_4 = 0.15$, $K_5 = 0.4$, $K_{10} = 0.142$	27.9	10.7	19.3
MD5 (Eq. (13))	$K_6 = 0.15$, $K_7 = 1.0$, $K_{10} = 0.142$	25.4	10.3	17.9
MD6 (Eq. (14))	$K_8 = 0.15$, $K_9 = 0.073$, $K_{10} = 0.142$	26.1	10.5	18.3

The basic parameter for determination of the overall accuracy of the model is the average rms relative error (ER_{avg}), which is defined as

$$ER_{avg} = \frac{\sum_{n=1}^{tn} ER_{gn}}{tn}, \tag{15}$$

where n is the data group number, ER_{gn} is the rms relative error of the group no. n, and tn is the total number of data groups. A small value of ER_{avg} indicates good overall accuracy of the wave model.

The rms relative error of each data group (ER_g) is defined as

$$ER_g = 100 \times \sqrt{\frac{\sum_{i=1}^{nc}(H_{ci} - H_{mi})^2}{\sum_{i=1}^{nc} H_{mi}^2}}, \tag{16}$$

where i is the wave height number, H_{ci} is the computed significant wave height of number i, H_{mi} is the measured significant wave height of number i, and nc is the total number of measured significant wave heights in each data group.

The question of how good a model is usually defined in a qualitative ranking (e.g., excellent, very good, good, fair, and poor). As the error of some existing irregular wave models is in the range of 7–21% (please see Rattanapitikon, 2007, Table 2), the qualification of error ranges of an irregular wave model may be classified into five ranges (i.e., excellent ($ER_g < 5.0$), very good ($5.0 \leqslant ER_g < 10.0$), good ($10.0 \leqslant ER_g < 5.0$), fair ($15.0 \leqslant ER_g < 20.0$), and poor ($ER_g \geqslant 20.0$)) and the acceptable error should be less than 10%.

The transformation of the significant wave height from the models MD1–MD6 is determined by taking numerical integration from offshore to shoreline. The energy dissipation is set to be zero when $H_s < H_{sb}$. The incipient wave breaking (H_{sb}) is computed from Eq. (14). The forward finite difference scheme is used to solve the differential equations. The length step (Δx) is set to be equal to the length between the points of measured wave heights, except if $\Delta x > 5$ m, Δx is set to be 5 m. The length steps (Δx) used in the present study are 0.2–1.5 m for small-scale experiments and 2.1–5.0 m for large-scale experiments.

Using the coefficients K_1–K_{10} which were proposed for regular waves, errors of the models MD1–MD6 on predicting H_s for two groups of experiment-scales are shown in Table 3. It can be seen from Table 3 that all models give unacceptable results in simulating the significant wave height transformation. This is a confirmation of the findings of the previous researchers. The unacceptable results may be due to: (1) the incipient breaking point of regular wave and irregular wave may not be the same point and (2) the amount of energy dissipation of regular waves and irregular waves may not be the same. Therefore, the prediction may be more accurate if the coefficients (K_1–K_{10}) are re-calibrated by using the significant wave height data.

4.2. Model calibration and selection

A calibration of each model is conducted by varying the coefficients (K_1–K_{10}) in the model until the minimum error (ER_{avg}) between measured and computed significant wave heights is obtained. The optimum values of K_1–K_{10} are shown in the second column of Table 4. The errors of models MD1–MD6 on simulating H_s for two groups of experiment-scales are shown in the third–fifth columns of Table 4. The examination results from Table 4 can be summarized as follows:

(a) The accuracy of all models is improved significantly after calibration.
(b) For small-scale wave flumes, the models MD3, MD5, and MD6 give very good predictions ($5.0 \leqslant ER_g < 10.0$), while the other models (MD1, MD2, and MD4) give good predictions ($10.0 \leqslant ER_g < 15.0$). The accuracy levels of the models in descending order are MD6, MD3, MD5, MD2, MD4, and MD1.
(c) For large-scale wave flumes, all models give very good predictions ($5.0 \leqslant ER_g < 10.0$). The accuracy levels of the models in descending order are MD5, MD6, MD2, MD3, MD4, and MD1.
(d) The overall accuracy levels of the models in descending order are MD5, MD6, MD3, MD2, MD4, and MD1.
(e) The models MD3, MD5, and MD6 give very good predictions ($5.0 \leqslant ER_g < 10.0$) for both small- and large-scale experiments. These models can be used for computing the significant wave height transformation. However, lesser error is better. The models MD5 and MD6 give almost the same accuracy and are more accurate than the others.
(f) The average error (ER_{avg}) of the models MD5 and MD6 are 7.5% and 7.6%, respectively. These numbers confirm in a quantitative sense the high degree of realism generated by the models. This means that the significant wave representation method is acceptable for computing the significant wave height transformation across-shore.

Overall, the models MD5 and MD6 give nearly the same accuracy. It may be interesting to look at the comparison in more detail. Table 5 shows the errors (ER_g) of MD5 and MD6 for 36 groups of test series. It can be seen from Table 5 that the models MD5 and MD6 give nearly the same overall accuracy (ER_{avg} of MD5 = 7.7% and ER_{avg} of MD6 = 7.6%). As the average errors (ER_{avg}) of models MD5 and MD6 from Tables 4 and 5 are almost the same, it is difficult to judge which model is better than the other. Evaluation of these two models may have to be based on their simplicity.

Substituting the calibrated coefficients $K_6 = 0.09$, $K_7 = 1.07$, $K_8 = 0.09$, $K_9 = 0.076$, and $K_{10} = 0.076$ into the corresponding equations (Eqs. (12)–(14)), the irregular wave models (MD5 and MD6) for computing H_s can be expressed as

$$\text{MD5}: \quad \frac{\rho g}{8}\frac{\partial(H_s^2 c_g)}{\partial x} = -0.09\frac{\rho g c}{8h} \times \left[H_s^2 - \left(1.07h\exp\left(-0.36 - \frac{1.25h}{\sqrt{LH_s}}\right)\right)^2\right], \tag{17}$$

$$\text{MD6}: \quad \frac{\rho g}{8}\frac{\partial(H_s^2 c_g)}{\partial x} = -0.09\frac{\rho g c_g}{8h}[H_s^2 - (0.076L\tanh(kh))^2], \tag{18}$$

Table 5
The errors (ER_g and ER_{avg}) of the models MD5– MD6 (using the calibrated coefficients) and the modified model (MD7) for 36 groups of test series

Sources	Test series	MD5	MD6	MD7
Hurue (1990)	Hu1	7.6	5.9	6.2
Smith and Kraus (1990)	R2000	11.7	7.5	6.6
	R22xx	12.0	11.3	9.9
	R6000	7.3	5.0	5.9
	R62xx	10.3	10.9	9.3
	R8000	3.8	4.6	4.2
	R82xx	10.4	10.8	8.8
Katayama (1991)	Ka1&Ka2	8.0	9.0	9.7
Ting (2001)	Ti1	4.8	3.1	3.1
Kraus and Smith (1994)	ST10	6.8	4.8	4.8
	ST20	5.4	5.2	5.0
	ST30	6.5	6.4	6.4
	ST40	8.3	8.4	8.3
	ST50	7.0	7.2	6.9
	ST60	8.3	8.6	7.9
	ST70	7.2	6.8	6.3
	ST80	9.6	9.4	8.9
	ST90	5.2	5.5	4.5
	STAO	5.7	4.9	4.3
	STCO	13.1	11.4	11.6
	STDO	10.1	10.7	10.4
	STJO	10.6	10.9	9.6
	STKO	21.7	21.4	20.9
Dette et al. (1998)	A8	10.9	13.0	12.3
	A9	2.9	4.9	5.1
	B1	7.6	9.1	8.1
	B2	4.2	4.5	4.2
	C1	9.9	11.5	10.4
	C2	4.0	4.8	4.7
	H1	4.4	5.4	6.1
	H2	4.8	4.3	3.7
	D1&D3	9.0	9.8	9.6
	D2	4.3	5.4	5.7
	E	3.2	4.0	4.4
	F	3.6	3.9	4.0
	G	6.4	5.1	5.8
Average error (ER_{avg})		7.7	7.6	7.3

Table 4
The errors (ER_g and ER_{avg}) of the models MD1– MD6 (using the calibrated coefficients) and the modified model (MD7) for two groups of experiment-scales (measured data from Table 2)

Models	Coefficients	ER_g		ER_{avg}
		Small-scale	Large-scale	
MD1 (Eq. (9))	$K_1 = 0.34$, $K_{10} = 0.098$	13.5	8.4	10.9
MD2 (Eq. (10))	$K_2 = 0.53$, $K_{10} = 0.098$	11.9	6.5	9.2
MD3 (Eq. (11))	$K_3 = 0.40$, $K_{10} = 0.098$	9.4	6.8	8.1
MD4 (Eq. (12))	$K_4 = 0.09$, $K_5 = 0.42$, $K_{10} = 0.076$	12.2	7.1	9.6
MD5 (Eq. (13))	$K_6 = 0.09$, $K_7 = 1.07$, $K_{10} = 0.076$	9.5	5.5	7.5
MD6 (Eq. (14))	$K_8 = 0.09$, $K_9 = 0.076$, $K_{10} = 0.076$	9.3	5.8	7.6
MD7 (Eq. (26))	$K_{11} = 0.095$, $K_{12} = -0.263$, $K_{13} = 0.179$	8.1	5.7	6.9

in which the incipient wave breaking or the starting point to include the energy dissipation into the models is determined from the following formula:

$$H_{sb} = 0.076L \tanh(kh). \tag{19}$$

The energy dissipation of MD5 and MD6 is zero when the stable wave height (the second term on the right-hand side of Eqs. (17) and (18)) is greater than the significant wave height. It can be seen that the stable wave height of MD6 (second term on the right-hand side of Eq. (18)) is the same as the formula that is used for computing the breaker height (Eq. (19)). This means that it is not necessary to check the incipient wave breaking. Eq. (18) can be used to compute the significant wave heights for the entire zone (from offshore to shoreline). This makes the model MD6 simpler than the model MD5. In terms of accuracy and simplicity, the model MD6 is the best and is recommended for computing the significant wave height transformation across-shore. As the model MD6 (Eq. (18)) is very simple, it may also serve as a reference model to test more complicated models against.

5. Model modification

Although, the model MD6 gives very good predictions, it may be modified to achieve even greater accuracy. The energy dissipation term in model MD6 is derived from the regular wave model of Rattanapitikon et al. (2003), which was developed based on the stable energy concept of Dally et al. (1985). The model MD6 (Eq. (18)) can be re-written as

$$\frac{\rho g}{8}\frac{\partial(H_s^2 c_g)}{\partial x} = -\frac{\rho g H_s^2 c_g}{8h}\left[0.09 - 0.09\left(\frac{H_{sb}}{H_s}\right)^2\right], \tag{20}$$

in which H_{sb} is calculated from Eq. (19). It can be seen that the energy dissipation term on the right-hand side of Eq. (20) can be written in a general form as a product of energy flux per unit depth and a dimensionless function (f) as

$$\frac{\rho g}{8}\frac{\partial(H_s^2 c_g)}{\partial x} = -\frac{\rho g H_s^2 c_g}{8h} f\left\{\frac{H_{sb}}{H_s}\right\}, \tag{21}$$

where f is a function of H_{sb}/H_s. The function f may be considered as a fraction of energy dissipation, while the energy flux per unit depth may be considered as a potential rate of energy dissipation. The function f of the stable energy concept (MD6) can be expressed as

$$f = -0.09\left(\frac{H_{sb}}{H_s}\right)^2 + 0.09 \quad \text{for } \frac{H_{sb}}{H_s} \leqslant 1.0, \tag{22a}$$

$$f = 0 \quad \text{for } \frac{H_{sb}}{H_s} > 1.0. \tag{22b}$$

It should be noted that Eq. (20) (or Eqs. (22a) and (22b)) is derived based on the assumption that the energy dissipation rate is proportional to the difference between the energy flux per unit depth and the stable energy flux per unit depth. If the assumption is correct, the relationship between f and H_{sb}/H_s should be a concave-down shape (since $d^2f/d(H_{sb}/H_s)^2$ is a negative value). It may be worthwhile to check this assumption through the relationship between f and H_{sb}/H_s. The data for plotting the relationship are the measured data of f and H_{sb}/H_s. The measured

Using a forward finite difference scheme to describe the wave model (Eq. (21)), the formula for determining measured f is expressed as

$$f_j = -\frac{(H_{s,j+1}^2 c_{g,j+1} - H_{s,j}^2 c_{g,j})}{(x_{j+1} - x_j)}\frac{h_j}{H_{s,j}^2 c_{g,j}}, \tag{23}$$

where j is the grid number. Hereafter, the variable f determined from Eq. (23) is referred to as the measured f.

The required data set for plotting the relationship between f and H_{sb}/H_s is the measured data of h, T_p, H_s, and x. The computation of other related variables (e.g., L, k, and c_g) is based on linear wave theory. The breaker height (H_{sb}) is determined from Eq. (19). To avoid a large fluctuation in the relationship, the data of wave height variation across-shore should have a small fluctuation.

Because of a small fluctuation of wave height variation across-shore, the data from Dette et al. (1998) are used for plotting the relationship between measured f and H_{sb}/H_s. The relationship between measured f and H_{sb}/H_s is shown in Fig. 1. The line of computed f from Eqs. (22a) and (22b) is shown as the dotted line in Fig. 1. It can be seen that Eqs. (22a) and (22b) are fitted reasonably well to the measured f. However, the shape of measured f tends to be concave-up instead of concave-down as Eqs. (22a) and (22b) suggests it should. It seems to be better to fit f with a quadratic equation as

$$f = K_{11}\left(\frac{H_{sb}}{H_s}\right)^2 + K_{12}\left(\frac{H_{sb}}{H_s}\right) + K_{13}, \tag{24}$$

where K_{11}–K_{13} are the coefficients. From the multi-regression analysis (between measured f and H_{sb}/H_s) by using the data that $H_{sb}/H_s \leqslant 1.0$, the values of K_{11}–K_{13} are 0.09, −0.26, and 0.17, respectively. The best-fitted line is shown as the solid line in Fig. 1. However, the values of K_{11}–K_{13} are not used in the wave model because the values of K_{11}–K_{13} are optimum only for the data of Dette et al. (1998), and they may change slightly when applying to all collected laboratory data.

Substituting Eq. (24) into Eq. (21), the general form of the modified model can be expressed as

$$\text{MD7}: \quad \frac{\rho g}{8}\frac{\partial(H_s^2 c_g)}{\partial x} = -\frac{\rho g H_s^2 c_g}{8h}\left[K_{11}\left(\frac{H_{sb}}{H_s}\right)^2 + K_{12}\left(\frac{H_{sb}}{H_s}\right) + K_{13}\right]. \tag{25}$$

The collected irregular wave data shown in Table 2 are used to calibrate the model MD7 (Eq. (25)). The wave height transformation is computed by numerical integration of the model MD7 (Eq. (25)). The forward finite difference scheme is used to solve the model. The calibration of the model is conducted by varying

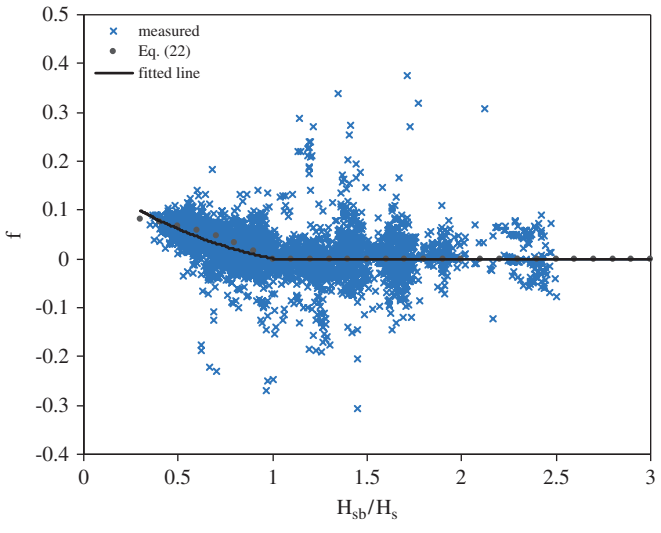

Fig. 1. Relationship between f and H_{sb}/H_s (measured data from Dette et al., 1998).

the values of K_{11}–K_{13} until the minimum error (ER_{avg}) of the model is obtained. The optimum values of K_{11}–K_{13} are 0.095, −0.263, and 0.179, respectively. The errors (ER_g and ER_{avg}) of model MD7 are shown in the last row of Table 4 and the last column of Table 5. It can be seen from Tables 4 and 5 that the model MD7 gives the best predictions.

To gain an impression of overall performance of the modified model (MD7) for computing H_s, the results of model MD7 are plotted against the measured data. Comparison between measured and computed significant wave heights from the model MD7 for all cases are shown in Fig. 2. Examples of computed significant wave height transformation across-shore are shown in Figs. 3 and 4. Case numbers in Figs. 3 and 4 are kept to be the same as the originals. Overall, it can be seen that the model MD7 gives a quite realistic simulation of the significant wave height transformation across-shore. However, the present model has certain limitations, which may restrict its use. The limitations of the model MD7 can be listed as follows:

(a) The model gives the worst prediction for the case of broad-crested mound ($ER_g = 20.9\%$, see test no. STKO in Table 5). The main error is caused by a sharp drop in measured wave height at a distance of $x = 44.2$ m on top of the bar (see Fig. 4d). This sharp drop occurred in all cases of the test no. STKO (at $x = 44.2$ m). It is difficult to find out the reason for such a sharp drop in the wave height.

(b) The model gives only good predictions ($ER_g \approx 10\%$) for the wave on the barred beach or narrow-crested mound (see test no. R22xx, R62xx, R82xx, Ka1&Ka2, and STJO in Table 5; see also Figs. 3c–g and 4c). The model could not predict the rapid increase and decrease in wave heights near the bar. The model tends to give over prediction for the wave heights around the trough of narrow-bar (see Fig. 3c–e) while it tends to give under prediction around the trough of the broad-bar (see Fig. 3f and g).

(c) As the model MD7 (Eq. (25)) is an empirical model, its validity may be limited according to the range of experimental conditions which were employed in the calibration. The present formula should be applicable for deepwater wave steepness (H_{so}/L_o) ranging between 0.002 and 0.064.

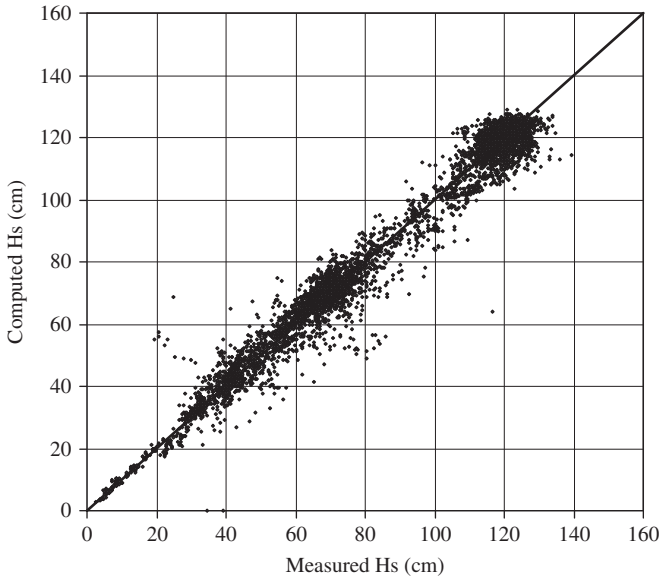

Fig. 2. Comparison between measured and computed significant wave height by using the model MD7 (measured data from Table 2).

(d) It is not clear, whether the model can be applied to the ocean or not because the model is not verified by the field data. However, it has a high possibility to apply the model to the coasts or oceans because the large-scale experiments have a scale approximately the same as the conditions in the oceans. Moreover, it was shown by some researchers (e.g., Wise et al., 1996; Rattanapitikon and Shibayama, 1998) that the models, which were developed based on large-scale experiments, could be applied directly to the real ocean waves.

As shown in Section 4 that the regular wave model for computing H can be applied directly for computing H_s, it is expected that the irregular wave model for computing H_s should also be applicable for computing H. The model MD7 (Eq. (25)) is applied to regular waves as

$$\text{MD8}: \quad \frac{\rho g}{8}\frac{\partial(H^2 c_g)}{\partial x} = -\frac{\rho g H^2 c_g}{8h}\left[K_{14}\left(\frac{H_b}{H}\right)^2 + K_{15}\left(\frac{H_b}{H}\right) + K_{16}\right], \tag{26}$$

where K_{14}–K_{16} are the coefficients which can be determined from model calibration and H_b is the breaker height of the regular waves which is determined from the breaking criterion of Miche (1944).

The collected regular wave data shown in Table 1 are used to calibrate the model MD8 (Eq. (26)). The wave height transformation is computed by numerical integration of the model MD8. The forward finite difference scheme is used to solve the model. The calibration of the model is conducted by varying the values of K_{14}–K_{16} until the minimum error (ER_{avg}) of the model is obtained. The optimum values of K_{14}–K_{16} are 0.010, −0.128, and 0.226, respectively. The errors (ER_g and ER_{avg}) of the model MD8 and the existing regular wave models (shown in Section 3) are shown in Table 6. It can be seen from Table 6 that it is possible to use the model MD8 for computing regular wave heights transformation.

Substituting the calibrated coefficients K_{11}–K_{16} into Eqs. (25) and (26), the modified models for irregular and regular waves can be expressed as

$$\text{MD7}: \quad \frac{\rho g}{8}\frac{\partial(H_s^2 c_g)}{\partial x} = -\frac{\rho g H_s^2 c_g}{8h} \times \left[0.095\left(\frac{H_{sb}}{H_s}\right)^2 - 0.263\left(\frac{H_{sb}}{H_s}\right) + 0.179\right], \tag{27}$$

$$\text{MD8}: \quad \frac{\rho g}{8}\frac{\partial(H^2 c_g)}{\partial x} = -\frac{\rho g H^2 c_g}{8h} \times \left[0.010\left(\frac{H_b}{H}\right)^2 - 0.128\left(\frac{H_b}{H}\right) + 0.226\right]. \tag{28}$$

6. Conclusions

This study was carried out to investigate the possibility of using the significant wave representation method. The significant wave height transformation across-shore was computed from the energy flux conservation. The selected six regular wave models were directly applied to the irregular waves (by using significant wave height and spectral peak period) to investigate their applicability for simulating significant wave height transformation. The breaking criterion of Miche (1944) was applied to compute the incipient breaker height. Laboratory data from small- and large-scale wave flumes were used to calibrate and examine the models. It was found that three regular wave models (with new coefficients) can be used for computing the significant wave heights with very good accuracy (i.e., the models MD3, MD5, and

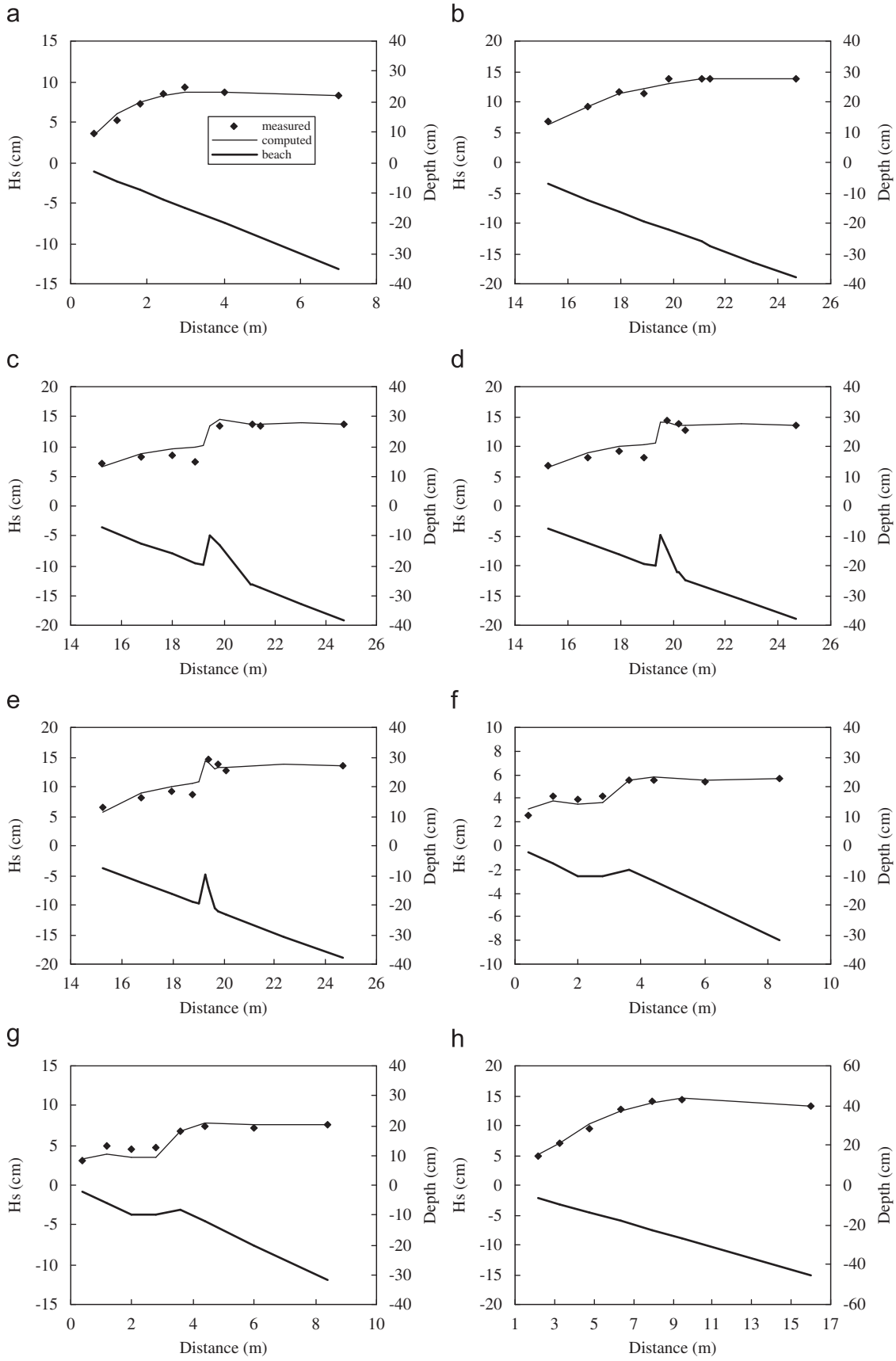

Fig. 3. Examples of measured and computed significant wave height transformation by using the model MD7 (measured data from small-scale experiments). (a) Hu1, (b) R8000, (c) R8210, (d) R8220, (e) R8230, (f) Ka1, (g) Ka2 and (h) Ti1.

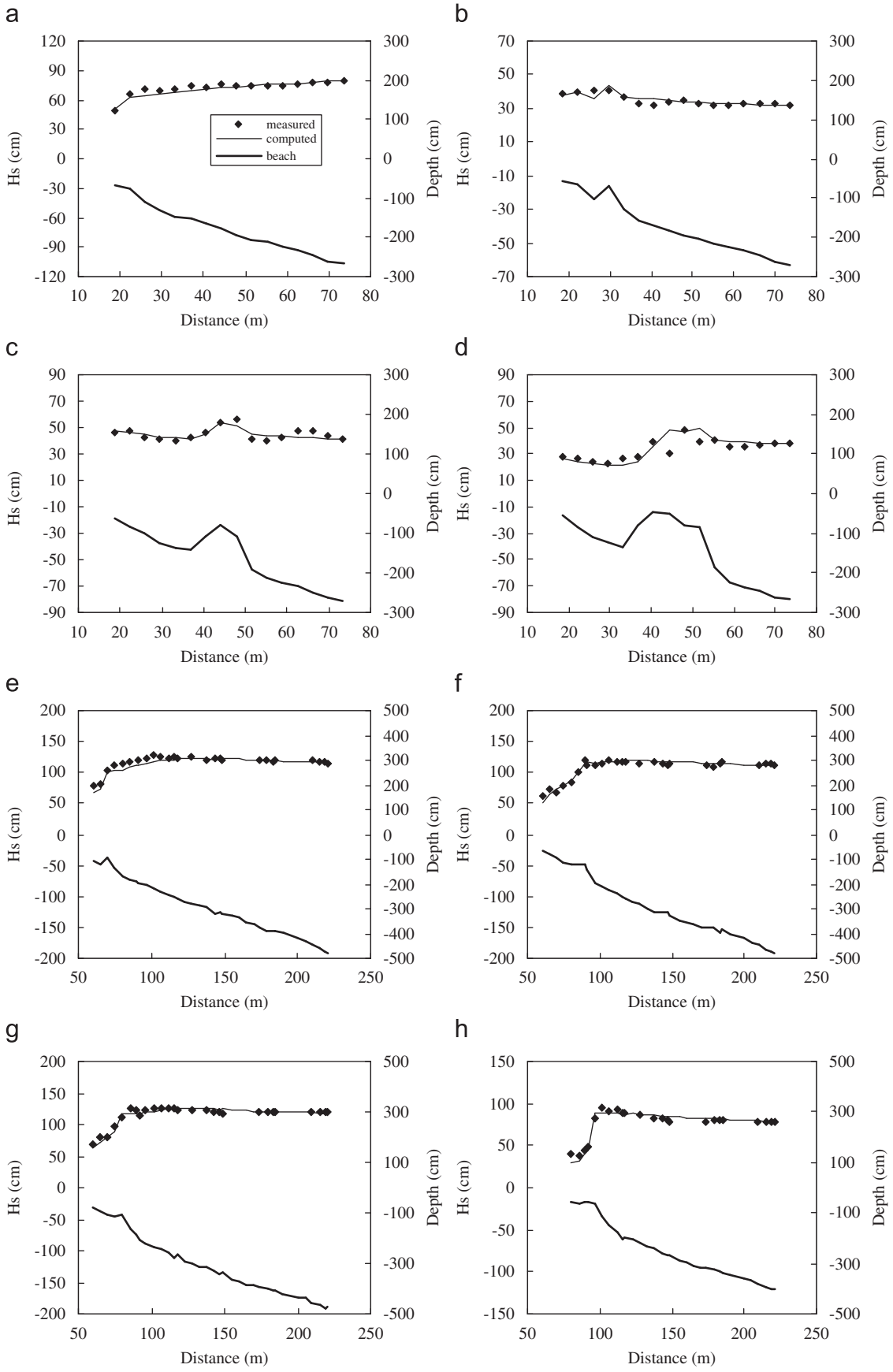

Fig. 4. Examples of measured and computed significant wave height transformation by using the model MD7 (measured data from large-scale experiments) (a) ST10:a0515a, (b) ST30:a1409a, (c) STJO:S1008a, (d) STKO:S1217a, (e) A9:17129602, (f) C2:14039701, (g) F:17079701 and (h) G: 07089701.

Table 6
The errors (ER_g and ER_{avg}) of the six existing regular wave and the modified model (MD8) for two groups of experiment-scales (measured data from Table 1)

Regular wave models	ER_g		ER_{avg}
	Small-scale	Large-scale	
Battjes and Janssen (1978)	34.4	49.0	41.7
Thornton and Guza (1983)	22.1	26.0	24.0
Deigaard et al. (1991)	23.2	23.1	23.1
Dally et al. (1985)	17.3	20.2	18.8
Rattanapitikon and Shibayama (1998)	16.3	16.6	16.4
Rattanapitikon et al. (2003)	16.3	17.7	17.0
MD8	15.9	17.5	16.7

MD6). This leads to the conclusion that the concept of significant wave representation method can be used for computing the significant wave height transformation across-shore. On the strength of both accuracy and simplicity of the three possible models, the model MD6 is recommended for use as the best method for computing the significant wave height transformation across-shore.

Although, the model MD6 gives very good predictions, it can be modified to achieve better predictions. The model MD6 can be rewritten as a product of energy flux per unit depth and dimensionless function ($f\{H_{sb}/H_s\}$). The modification is performed by deriving the new formula of function f. The general form of f is derived from plotting the relationship between measured f and H_{sb}/H_s. The shape of measured f trends to be concave-up and can be fitted with a quadratic equation. All collected data were used in the study to calibrate and examine the modified model. Compared with the three possible models (MD3, MD5, and MD6), the modified model gives the best prediction. The modified model (with different coefficients) can also be applied to predict the regular wave height transformation. As the modified model is an empirical model, its validity may be limited depending on the range of experimental conditions that are employed in the calibration. The model should be applicable for deepwater wave steepness (H_{so}/L_o) ranging between 0.002 and 0.064.

Acknowledgment

This research was sponsored by the Thailand Research Fund and the Commission on Higher Education, Ministry of Education.

Appendix. Governing equation of the significant wave representation method

Considering average energy flux of an irregular wave train (based on linear wave theory),

$$\overline{Ec_g} = \frac{\sum_{i=1}^{N}(E_i c_{gi})}{N} = \frac{1}{8}\rho g \frac{\sum_{i=1}^{N} H_i^2 c_{gi}}{N}, \tag{A.1}$$

where $\overline{Ec_g}$ is the average energy flux of an irregular wave train, E_i is the energy density for the ith individual wave, c_{gi} is the group velocity for the ith individual wave, H_i is the wave height for the ith individual wave, and N is the total number of waves in the irregular wave train.

The Rayleigh distribution serves as a good engineering formula for the distribution of zero-crossing wave heights as demonstrated by many researchers (e.g., Goodknight and Russel, 1963; Goda, 1974; Thornton and Guza, 1983; and Rattanapitikon and Shibayama, 2007). To simplify the analysis, the wave heights are assumed to follow the Rayleigh distribution (narrow-banded in frequency) so that the individual waves have almost the same period and consequently almost the same group velocity (c_g). Therefore, Eq. (A.1) can be simplified to be

$$\overline{Ec_g} = \frac{1}{8}\rho g c_g \frac{\sum_{i=1}^{N} H_i^2}{N}. \tag{A.2}$$

The spectral peak period (T_p) is usually used to compute the group velocity because it is typically reported for the irregular wave data.

Since $\sqrt{\sum_{i=1}^{N} H_i^2/N}$ is equal to the root mean square wave height (H_{rms}), Eq. (A.2) can be written in terms of H_{rms} as

$$\overline{Ec_g} = \frac{1}{8}\rho g H_{rms}^2 c_g. \tag{A.3}$$

The average energy flux conservation of the irregular wave train can be written as

$$\frac{\partial(\overline{Ec_g})}{\partial x} = -\overline{D_B}, \tag{A.4}$$

where $\overline{D_B}$ is the average energy dissipation.

Substituting Eq. (A.3) into Eq. (A.4), the energy flux conservation of the representative wave approach can be expressed as

$$\frac{1}{8}\rho g \frac{\partial(H_{rms}^2 c_g)}{\partial x} = -\overline{D_B}. \tag{A.5}$$

It should be noted that Eq. (A.5) is developed based on linear wave theory and Rayleigh distribution. This crude assumption of the representative wave approach may not be theoretically justified. However, there are many wave models that are successful in using the energy flux conservation (Eq. (A.5)) for computing H_{rms}, e.g., the models of Battjes and Janssen (1978), Thornton and Guza (1983), Larson (1995), Baldock et al. (1998), Ruessink et al. (2003), and Rattanapitikon (2007). Therefore, Eq. (A.5) seems be acceptable for computing H_{rms}.

If the energy flux conservation of the representative wave (Eq. (A.5)) can be used for computing H_{rms}, it may be possible to be used for computing H_s because H_{rms} can be converted to H_s through the known coefficient (i.e., $H_s = \beta H_{rms}$, in which $\beta = 1.42$ for the Rayleigh distribution).

Substituting $H_s = \beta H_{rms}$ into Eq. (A.5), the governing equation of the significant wave representation method can be written as

$$\frac{1}{8}\rho g \frac{\partial(H_s^2 c_g)}{\partial x} = -\overline{D_{Bs}}, \tag{A.6}$$

where $\overline{D_{Bs}} = \beta^2 \overline{D_B}$.

References

Andreas, E.L., Wang, S., 2007. Predicting significant wave height off the northeast coast of the United States. Ocean Engineering 34 (8–9), 1328–1335.
Baldock, T.E., Holmes, P., Bunker, S., Van Weert, P., 1998. Cross-shore hydrodynamics within an unsaturated surf zone. Coastal Engineering 34, 173–196.
Battjes, J.A., Groenendijk, H.W., 2000. Wave height distributions on shallow foreshores. Coastal Engineering 40, 161–182.
Battjes, J.A., Janssen, J.P.F.M., 1978. Energy loss and set-up due to breaking of random waves. In: Proceedings of the 16th Coastal Engineering Conference, ASCE, pp. 569–589.
Bouws, E., Gunther, H., Rosenthal, W., Vincent, C.L., 1985. Similarity of the wind wave spectrum in finite depth water. Journal of Geophysical Research 90 (C1), 975–986.
Bretschneider, C.L., 1968. Significant waves and wave spectrum. Ocean Industry (February), 40–46.
Bruun, P., 1954. Coastal erosion and development of beach profiles. Technical Memorandum No. 44, US Army Beach Erosion Board, US Army Corps of Engineers.
Cox, T., Kobayashi, N., 1997. Kinematic undertow model with logarithmic boundary layer. Journal of Waterway, Port, Coastal and Ocean Engineering, ASCE 123 (6), 354–360.
Dally, W.R., 1992. Random breaking waves: field verification of a wave-by-wave algorithm for engineering application. Coastal Engineering 16, 369–397.

Dally, W.R., Dean, R.G., Dalrymple, R.A., 1985. Wave height variation across beaches of arbitrary profile. Journal of Geophysical Research 90 (C6), 11917–11927.
Deigaard, R., Justesen, P., Fredsoe, J., 1991. Modelling of undertow by a one-equation turbulence model. Coastal Engineering 15, 431–458.
Dette, H.H., Peters, K., Newe, J., 1998. MAST III—SAFE Project: Data Documentation, Large Wave Flume Experiments '96/97. Report No. 825 and 830, Leichtweiss Institute, Technical University Braunschweig, Germany.
Goda, Y., 1974. Estimation of wave statistics from spectral information. In: Proceedings of the Ocean Waves Measurement and Analysis Conference, ASCE, pp. 320–337.
Goda, Y., 2000. Random Seas and the Design of Maritime Structures. World Scientific Publishing Co. Pte. Ltd., Singapore.
Goda, Y., 2004. A 2-D random wave transformation model with gradational breaker index. Coastal Engineering Journal, JSCE 46 (1), 1–38.
Goodknight, R.C., Russel, T.L., 1963. Investigation of the statistics of wave heights. Journal of Waterways and Harbors Division, ASCE 89 (WW2), 29–55.
Hansen, J.B., Svendsen, I.A., 1984. A theoretical and experiment study of undertow. In: Proceedings of the 19th Coastal Engineering Conference, ASCE, pp. 2246–2262.
Hasselmann, K., Barnett, T.P., Bouws, E., Carlson, H., Cartwright, D.E., Enke, K., Ewing, J.A., Gienapp, H., Hasselmann, D.E., Kruseman, P., Meerburg, A., Müller, P., Olbers, D.J., Richter, K., Sell, W., Walden, H., 1973. Measurements of wind–wave growth and swell decay during the Joint North Sea Wave Project (JONSWAP). Deutsche Hydrographische Zeitschrift A 8 (12), 1–95.
Horikawa, K., Kuo, C.T., 1966. A study of wave transformation inside the surf zone. In: Proceedings of the 10th Coastal Engineering Conference, ASCE, pp. 217–233.
Hurue, M., 1990. Two-dimensional distribution of undertow due to irregular waves. B.Eng. Thesis, Department of Civil Engineering, Yokohama National University, Japan (in Japanese).
Kajima, R., Shimizu, T., Maruyama, K., Saito, S., 1983. On-offshore sediment transport experiment by using large scale wave flume. Collected Data No. 1–8, Central Research Institute of Electric Power Industry, Japan (in Japanese).
Katayama, H., 1991. Cross-shore velocity distribution due to breaking of irregular waves on a bar-type beach. B.Eng. Thesis, Department of Civil Engineering, Yokohama National University, Japan (in Japanese).
Kraus, N.C., Smith, J.M., 1994. SUPERTANK Laboratory Data Collection Project, vols. 1–2. Technical Report CERC-94-3, WES, US Army Corps of Engineers.
Kuriyama, Y., 1996. Model of wave height and fraction of breaking waves on a barred beach. In: Proceedings of the 25th Coastal Engineering Conference, ASCE, pp. 247–259.
Larson, M., 1995. Model for decay of random waves in surf zone. Journal of Waterway, Port, Coastal, and Ocean Engineering, ASCE 121 (1), 1–12.
Longuet-Higgins, M.S., 1952. On the statistical distribution of the heights of sea waves. Journal of Marine Research 11 (3), 246–266.
Miche, R., 1944. Mouvements ondulatoires des mers en profondeur constante on decroissante. Ann. des Ponts et Chaussees, Chapter 114, pp. 131–164, 270–292, and 369–406.
Mitsuyasu, H., 1970. On the growth of spectrum of wind-generated waves (2)—spectral shape of wind waves at finite fetch. In: Proceedings of the 17th Japanese Conference on Coastal Engineering, pp. 1–7 (in Japanese).
Mizuguchi, M., 1982. Individual wave analysis of irregular wave deformation in the nearshore zone. In: Proceedings of the 18th Coastal Engineering Conference, ASCE, pp. 485–504.
Nadaoka, K., Kondoh, T., Tanaka, N., 1982. The structure of velocity field within the surf zone revealed by means of laser-doppler anemometry. Report of the Port and Harbor Research Institute 21 (2), pp. 50–102 (in Japanese).
Nagayama, S., 1983. Study on the change of wave height and energy in the surf zone. B.Eng. Thesis, Department of Civil Engineering, Yokohama National University, Japan (in Japanese).
Okayasu, A., Shibayama, T., Horikawa, K., 1988. Vertical variation of undertow in the surf zone. In: Proceedings of the 21st Coastal Engineering Conference, ASCE, pp. 478–491.
Rattanapitikon, W., 2007. Calibration and modification of energy dissipation models for irregular waves breaking. Ocean Engineering 34 (11–12), 1592–1601.
Rattanapitikon, W., Shibayama, T., 1998. Energy dissipation model for regular and irregular breaking waves. Coastal Engineering Journal, JSCE 40 (4), 327–346.
Rattanapitikon, W., Shibayama, T., 2007. Estimation of shallow water representative wave heights. Coastal Engineering Journal, JSCE 49 (3), 291–310.
Rattanapitikon, W., Karunchintadit, R., Shibayama, T., 2003. Irregular wave height transformation using representative wave approach. Coastal Engineering Journal, JSCE 45 (3), 489–510.
Ruessink, B.G., Walstra, D.J.R., Southgate, H.N., 2003. Calibration and verification of a parametric wave model on barred beaches. Coastal Engineering 48, 139–149.
Sato, S., Fukuhama, M., Horikawa, K., 1988. Measurement of near-bottom velocities in random waves on a constant slope. Coastal Engineering in Japan, JSCE 31 (2), 219–229.
Sato, S., Isayama, T., Shibayama, T., 1989. Long-wave component in near-bottom velocity under random waves on a gentle slope. Coastal Engineering in Japan, JSCE 32 (2), 149–159.
Shibayama, T., Horikawa, K., 1985. Numerical model for two-dimensional beach transformation. In: Proceedings of the Japan Society of Civil Engineers, No. 357/II-3 (Hydraulic and Sanitary), pp. 167–176.
Smith, J.M., Kraus, N.C., 1990. Laboratory study on macro-features of wave breaking over bars and artificial reefs. Technical Report CERC-90-12, WES, US Army Corps of Engineers.
Thornton, E.B., Guza, R.T., 1983. Transformation of wave height distribution. Journal of Geophysical Research 88 (C10), 5925–5938.
Ting, F.C.K., 2001. Laboratory study of wave and turbulence velocity in broad-banded irregular wave surf zone. Coastal Engineering 43, 183–208.
Tucker, M.J., Pitt, E.G., 2001. Waves in Ocean Engineering. Elsevier Ocean Engineering Book Series, vol. 5. Elsevier, Amsterdam.
Wise, R.A., Smith, S.J., Larson, M., 1996. SBEACH: Numerical model for simulating storm-induced beach change. Report 4: Cross-Shore Transport Under Random Waves and Model Validation with SUPERTANK and Field Data, Technical Report CERC-89-9, WES, US Army Corps of Engineers.

Songklanakarin J. Sci. Technol.
30 (3), ..., May - Jun. 2008

Songklanakarin Journal of Science and Technology
http://www.sjst.psu.ac.th

Original Article

Energy dissipation model for a parametric wave approach based on laboratory and field experiments

Winyu Rattanapitikon* and Sangapol Sawanggun

Civil Engineering Program, Sirindhorn International Institute of Technology, Thammasat University, Pathum Thani 12121, Thailand

Received .....; Accepted .....

Abstract

This study was undertaken to develop a simple energy dissipation model for computing the root mean square wave height transformation. The parametric wave approach of Battjes and Janssen (1978) was used as a framework for developing the energy dissipation model. In contrast to the common derivation, the fraction of breaking waves was not derived from the assumed probability density function of wave heights, but derived directly from the measured wave heights. The present model was verified extensively for a variety of wave and beach conditions (including small-scale, large-scale, and field experiments), and compared with four existing dissipation models. The present model gives very good accuracy for a wide range of wave and beach conditions and gives better predictions than those of existing models.

Keywords: irregular wave model, energy dissipation, parametric wave, surf zone

1. Introduction

Wave height is one of the most essential required factors for many coastal engineering applications such as the design of coastal structures and the study of beach morphodynamics. When waves propagate in shallow water, their profiles become steeper and they eventually break. Once the waves start to break, a part of the wave energy is transformed into turbulence and heat, and the wave height decreases towards the shore. The rate of energy dissipation of breaking waves is an essential requirement for computing wave height transformation in the surf zone. Several models have been proposed for computing the energy dissipation due to wave breaking, differing mainly in their formulation of the energy dissipation, and whether they were developed for regular (a single broken wave) or irregular waves.

Widely used models for computing the energy dissipation of a regular wave (a single broken wave) seem to be the bore model of Le Mehaute (1962) and the stable energy model of Dally *et al.* (1985). Brief reviews of these two models are described in the paper of Rattanapitikon and Leangruxa (2001). Aside from these two models, a number of alternative models for computing the energy dissipation have been presented. Horikawa and Kuo (1966) estimated the internal energy dissipation from the turbulent velocity fluctuations, which are assumed to decay exponentially with distance from the incipient wave breaking. Sawaragi and Iwata (1974) refined this approach by introducing the Prandt mixing length model to describe the turbulent velocity fluctuations. Mizuguchi (1980) applied an analytical solution for internal energy dissipation due to the viscosity, where the eddy viscosity replaces the molecular kinematic viscosity.

Irregular wave breaking is more complex than regular wave breaking. In contrast to regular waves, there is no well-defined breakpoint for irregular waves. The higher waves tend to break at a greater distance from the shore. Closer to the shore, more and more waves break, until almost all the waves break in the inner surf zone. The energy dissipation model developed for regular waves and extended to irregular waves introduces complexities, primarily with respect to the representation of the probability density function of wave

*Corresponding author.
Email address: winyu@siit.tu.ac.th

heights. Common methods to model irregular wave height transformations can be classified into four main approaches, i.e. representative wave approach, spectral approach, probabilistic approach, and parametric wave approach. For computing beach morphodynamics, the wave model should be kept as simple as possible because of the frequent updating of wave fields to account for the change of the bottom morphology. The parametric and representative wave approaches appear to be simple methods and seem to be suitable for being incorporated in the beach morphodynamic model.

For the representative wave approach, the regular wave model has been directly applied to irregular waves by using representative (or equivalent) waves, while the parametric approach considers the random nature of the waves but describes the energy dissipation rate in terms of time-averaged parameters. The parametric wave models were developed based on the assumed probability density function (*pdf*) of wave heights inside the surf zone. The average rate of energy dissipation is described by integrating the product of energy dissipation of a broken wave and the probability of occurrence of breaking waves. The parametric wave approach is expected to be better than the representative wave approach because it includes the random nature of the waves into the model while the other does not. Therefore, the present study focuses on the parametric wave approach.

The parametric wave models are generally based on the work of Battjes and Janssen (1978). The model relies on the macroscopic features of breaking waves and predicts only the transformation of root-mean-square (*rms*) wave height. The wave height transformation is computed from the energy flux conservation law. It is:

$$\frac{\partial\left(Ec_g\cos\theta\right)}{\partial x} = -D_B \tag{1}$$

where E is the wave energy density, c_g is the group velocity, θ is the mean wave angle, D_B is the distance in the cross shore direction, and is the energy dissipation rate due to wave breaking. The energy dissipation rate due to bottom friction is neglected. All variables are based on linear wave theory and Snell's law is employed to describe wave refraction.

From linear wave theory, the wave energy density (E) is equal to $\rho g H_{rms}^2/8$. Therefore, Equation 1 can be written in terms of wave height as:

$$\frac{\rho g}{8}\frac{\partial\left(H_{rms}^2 c_g\cos\theta\right)}{\partial x} = -D_B \tag{2}$$

where ρ is the density of water, g is the gravitational acceleration, H_{rms} and is the *rms* wave height.

The *rms* wave height transformation can be computed from the energy flux balance equation (Equation 2) by substituting the model of energy dissipation rate (D_B) and numerically integrating from offshore to the shoreline. In the offshore zone, the energy dissipation rate is set to zero. The main difficulty of Equation 2 is how to formulate the energy dissipation rate caused by the breaking waves.

During the past decades, various energy dissipation models for the parametric wave approach have been proposed for computing H_{rms} in the surf zone. Because of the complexity of the wave breaking mechanisms, most of the energy dissipation models were developed based on an empirical or semi-empirical approach. It is well known that the validity of an empirical formula may be limited according to the range of experimental conditions that were employed in the calibrations and verifications. To make an empirical formula reliable, it is necessary to calibrate and verify the formula with a large amount of data and a wide range of experimental conditions. Since many energy dissipation models were developed based on data with limited experimental conditions, there is still a need for more data to confirm the underlying assumptions in order to make the model more reliable. It is the purpose of this study to develop a simple energy dissipation model for the parametric wave approach based on a wide range of experimental conditions.

Experimental data of *rms* wave height transformation from 13 sources, covering 1723 cases of wave and beach conditions, have been collected for verifying the dissipation models. The experiments cover a wide range of wave and bottom topography conditions, including small-scale, large-scale, and field experiments. The experiments cover a variety of beach conditions (i.e. plane, barred, and sandy beaches) and a range of deepwater wave steepnesses (H_{rmso}/L_o) from 0.0007 to 0.0588. A summary of the collected experimental data is given in Table 1. Excluding the introduction and the conclusions, this paper is divided into three main parts. The first part briefly reviews some existing dissipation models for the parametric wave approach. The second part describes the development of the present model. The last part is the verification of the present model in comparison with the existing models.

2. Existing Energy Dissipation Models

During the past decades, various energy dissipation models have been developed based on a framework of the parametric wave approach of Battjes and Janssen (1978). Brief reviews of some existing dissipation models are described below.

a) Battjes and Janssen (1978), hereafter referred to as BJ78, proposed to compute D_B by multiplying the fraction of breaking waves (Q_B) by the energy dissipation of a single broken wave. The energy dissipation of a broken wave (D_{BS}) is determined from a simplified bore-type dissipation model and assumes that all broken waves have a height equal to the breaker height (H_b) as:

$$D_B = Q_{b1}\frac{\rho g H_b^2}{4T_p} \tag{3}$$

where Q_{b1} is the fraction of breaking waves of BJ78, and T_p is the spectral peak period. The fraction of breaking waves (Q_{b1}) was derived based on the assumption that the prob-

Table 1. Summary of collected experimental data.

Sources	Total no. of cases	Total no. of data	Beach conditions	H_{rmso}/L_o	Apparatus
Hurue (1990)	1	7	plane beach	0.0259	small-scale
Smith and Kraus (1990)	12	96	plane and barred beach	0.0214-0.0588	small-scale
Sultan (1995)	1	12	plane beach	0.0042	small-scale
Grasmeijer and Rijn (1999)	2	20	sandy beach	0.0142-0.0168	small-scale
Hamilton and Ebersole (2001)	1	10	plane beach	0.0165	small-scale
Ting (2001)	1	7	plane beach	0.0161	small-scale
Kraus and Smith (1994): SUPERTANK project	128	2,223	sandy beach	0.0011-0.0452	large-scale
Roelvink and Reniers (1995): LIP 11D project	95	923	sandy beach	0.0039-0.0279	large-scale
Dette *et al.* (1998): MAST III – SAFE project	138	3,559	sandy beach	0.0061-0.0147	large-scale
Thornton and Guza (1986)	4	60	sandy beach	0.0012-0.0013	field
Kraus *et al.* (1989): DUCK85 project	8	90	sandy beach	0.0007-0.0018	field
Birkemeier *et al.* (1997): DELILAH project	745	5,033	sandy beach	0.0007-0.0254	field
Herbers *et al.* (2006): DUCK94 project	587	6,102	sandy beach	0.0009-0.0290	field
Total	1,723	18,142		0.0007-0.0588	

ability density function of wave heights could be modeled with a Rayleigh distribution truncated at the breaker height (H_b) and all broken waves have a height equal to the breaker height. The result is:

$$\frac{1-Q_{b1}}{-\ln Q_{b1}} = \left(\frac{H_{rms}}{H_b}\right)^2 \tag{4}$$

in which the breaker height (H_b) is determined from the formula of Miche (1951) with the additional coefficient (γ) in the tan-hyperbolic function as:

$$H_b = 0.14L\tanh(\gamma kh) \tag{5}$$

where L is the wavelength related to T_p, k is the wave number, and h is the water depth. Based on their small-scale laboratory data, the coefficient γ is determined at 0.91. As Equation 4 is an implicit equation, it has to be solved for Q_{b1} either by an iterative technique (e.g. Newton-Raphson technique), or by a 1-D look-up table (Southgate and Nairn, 1993), or by fitting Q_{b1} with a polynomial function as:

$$Q_{b1} = \sum_{n=0}^{7} a_n \left(\frac{H_{rms}}{H_b}\right)^n \tag{6}$$

where a_n is the constant of n^{th} term. A multiple regression analysis is used to determine the constants a_0 to a_7. The correlation coefficient (R^2) of Equation 6 is 0.99999999. The values of the constants a_0 to a_7 are shown in Table 2. Equation 6 is applicable for $0.3 < H_{rms}/H_b < 1.0$. For $H_{rms}/H_b \leq 0.3$, the value of Q_{b1} is very small (less than 10^{-4}) and thus is set as zero. The value of Q_{b1} is set to be 1.0 when $H_{rms}/H_b \geq 1.0$. It should be noted that the two main assumptions for deriving the model (i.e. the assumptions of the simplified bore-type dissipation model and the truncated-Rayleigh distribution of wave heights) are not supported by the experimental data. However, the model has been used successfully in many applications for computing H_{rms} transformation (e.g. Johnson, 2006; and Oliveira, 2007).

Table 2. Values of constants a_0 to a_7 for computing Q_{b1}.

Constants	Values
a_0	0.231707207858562
a_1	-3.609582722187040
a_2	22.594833612442000
a_3	-72.536799430847200
a_4	126.870449066162000
a_5	-120.567666053772000
a_6	60.741998672485400
a_7	-12.725062847137500

b) Battjes and Stive (1985), hereafter referred to as BS85, used the same energy dissipation model as BJ78 (Equation 3). They modified the model of BJ78 by recalibrating the coefficient γ in the breaker height formula (Equation 5). The coefficient γ was related to the deepwater wave steepness (H_{rmso}/L_o) . After calibration with small-scale and

field experiments, the breaker height formula was modified to be:

$$H_b = 0.14L\tanh\left\{\left[0.57+0.45\tanh\left(33\frac{H_{rmso}}{L_o}\right)\right]kh\right\} \quad (7)$$

where H_{rmso} is the deepwater *rms* wave height, and L_o is the deepwater wavelength. Hence, the main difference between the models of BJ78 and BS85 is only the formula for computing H_b.

c) Baldock *et al.* (1998), hereafter referred to as BHV98, proposed to compute D_B by integrating from H_b to ∞ the product of the dissipation for a single broken wave and the *pdf* of the wave heights. The energy dissipation of a single broken wave is described by the bore model of BJ78. The *pdf* of wave heights inside the surf zone was assumed to be a Rayleigh distribution. The result is:

$$D_B = \begin{cases} \exp\left[-\left(\frac{H_b}{H_{rms}}\right)^2\right]\frac{\rho g\left(H_b^2+H_{rms}^2\right)}{4T_p} & for \quad H_{rms} < H_b \\ \exp[-1]\frac{2\rho g H_b^2}{4T_p} & for \quad H_{rms} \geq H_b \end{cases} \quad (8)$$

in which the breaker height (H_b) is determined from the formula of Nairn (1990) as:

$$H_b = h\left[0.39+0.56\tanh\left(33\frac{H_{rmso}}{L_o}\right)\right] \quad (9)$$

Although the model of BHV98 (Equation 8) seems to be quite different from the D_B model of BJ78, it can be rewritten in the similar form as that of BJ78 as:

$$D_B = Q_{b2}\frac{\rho g H_b^2}{4T_p} \quad (10)$$

in which Q_{b2} is a function of H_{rms}/H_b as:

$$Q_{b2} = \begin{cases} \left[1+\left(\frac{H_{rms}}{H_b}\right)^2\right]\exp\left[-\left(\frac{H_{rms}}{H_b}\right)^{-2}\right] & for \quad \frac{H_{rms}}{H_b} < 1 \\ 2\exp[-1] & for \quad \frac{H_{rms}}{H_b} \geq 1 \end{cases} \quad (11)$$

Comparing with the model of BJ78, the parameter Q_{b2} may be also considered as the fraction of breaking waves. The main difference between the models of BJ78 and BHV98 are the formulas for computing H_b and Q_b.

d) Ruessink *et al.* (2003), hereafter referred to as RWS03, used the same energy dissipation model as BHV98 (Equation 8), but a different breaker height formula. The breaker height formula of BJ78 (Equation 5) is modified by adding the term kh into the formula. After calibration with field experiments, the breaker height formula was modified to be:

$$H_b = 0.14L\tanh[(0.86kh+0.33)kh] \quad (12)$$

3. Model Development

In this study, the energy dissipation model of BJ78 is used as a framework for developing the present energy dissipation model. Similar to the model of BJ78, the present model is expressed as:

$$D_B = Q_{b3}\frac{\rho g H_b^2}{4T_p} \quad (13)$$

where Q_{b3} is the fraction of breaking waves of the present study, which is a function of H_{rms}/H_b.

It can be seen from Section 2 that the main difference among the existing models are the formulas for computing Q_b and H_b. It is not clear, which formulas of H_b and Q_b are suitable for modeling D_B (or computing H_{rms}). The objective of this section is to determine suitable formulas of H_b and Q_b for computing the *rms* wave height transformation.

The model of BJ78 was derived based on two main assumptions, the assumptions of truncated-Rayleigh distribution of wave heights and a simplified bore-type dissipation model. It should be noted that the assumption of a truncated-Rayleigh distribution, which is used to derive the formula of Q_b, is not supported by laboratory and field data (Dally, 1990). Some researchers (e.g. Southgate and Nairn, 1993; and Baldock *et al.*, 1998) demonstrated that Equation 4 gives a large error in predicting the fraction of breaking waves (Q_b). Moreover, the simplified bore-type dissipation model for estimating energy dissipation of a single breaking wave ($D_{BS} = \rho g H^2/4T$) is also not supported by laboratory data (Rattanapitikon *et al.*, 2003). Surprisingly, the D_B model of BJ78 seems to give good results in predicting H_{rms} and has proven to be a popular framework for estimating H_{rms} (Ruessink *et al.*, 2003). Because the assumptions for deriving the model are not valid, but the model gives good results in predicting H_{rms}, the D_B model of BJ78 may be considered as an empirical model for computing only H_{rms} (not for computing Q_b and a single breaking wave). As the model is an empirical model, it may not be necessary to derive the formula of Q_b by assuming the *pdf* of wave heights inside the surf zone (as done by BJ78 and BHV98). Moreover, the acceptable *pdf* of wave heights inside the surf zone is not available (Demerbilek and Vincent, 2006). It may not be suitable to derive formulas of Q_b from the assumed *pdf* of wave heights. Alternatively, the formula of Q_b can be derived directly from the measured wave heights by inverting the energy dissipation model (Equation 13) and the wave model (Equation 2). Therefore, in the present study, the formula of Q_b will be newly derived from the measured wave heights.

As Q_b is the function of H_{rms}/H_b, the formula of Q_b can be determined by plotting a relationship between measured Q_b versus H_{rms}/H_b. The required data for determining the formula are the measured data of Q_b and H_{rms}/H_b. The measured Q_b can be determined from the measured wave heights as the following.

Substituting Equation 2 into Equation 13 and using

a backward finite difference scheme to describe the differential equation, the variable Q_{b3} is expressed as:

$$Q_{b3i} = \frac{T_p}{2H_b^2} \frac{\left(H_{rmsi-1}^2 c_{gi-1} \cos\theta_{i-1} - H_{rmsi}^2 c_{gi} \cos\theta_i\right)}{x_i - x_{i-1}} \quad (14)$$

where i is the grid number and the originate of i is at the offshore boundary. Hereafter, the variable Q_{b3} determined from Equation 14 is referred to as measured Q_{b3}.

For determining Q_{b3} from Equation 14, a formula of H_b must be given. As there are four existing breaker height formulas (Equations. 5, 7, 9, and 12), four Q_{b3} can be determined and consequently four relationships between measured Q_{b3} and H_{rms}/H_b are considered in this study. The required data set for determining the measured Q_{b3} are the measured values of h, T_p, H_{rms}, θ, and x. Other related variables (e.g. H_{rmso}, L_o, L, k, and c_g) are computed based on linear wave theory. To avoid a large fluctuation in the relationships, the wave heights variation across the shore should have a small fluctuation.

Because of a variety of wave conditions and a small fluctuation of wave heights variation across the shore, the data from Dette *et al.* (1998) are used for deriving the formulas of Q_{b3} for H_b the four formulas. An example of measured wave height transformation across-shore is shown in Figure 1. However, all collected data shown in Table 1 are used for verification of the models.

The four relationships between measured Q_{b3} versus H_{rms}/H_b (using Equations 5, 7, 9, and 12 for computing H_b) have been plotted to determine a suitable formula of Q_{b3} (see Figures 2 to 5). It can be seen from Figures 2 to 5 that all relationships are fitted well with a quadratic equation as:

$$Q_{b3} = C_1 + C_2\left(\frac{H_{rms}}{H_b}\right) + C_3\left(\frac{H_{rms}}{H_b}\right)^2 \text{ for } \frac{H_{rms}}{H_b} > C_4 \quad (15)$$

where C_1 to C_4 are constants. The fraction of breaking waves

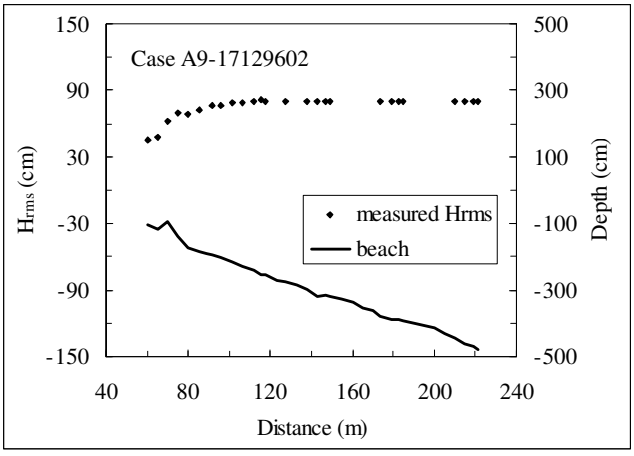

Figure 1. Example of measured wave height transformation across-shore (measured data from Dette *et al.'*, 1998, case A9-17129602).

(Q_{b3}) is set to be zero when $H_{rms}/H_b \le C_4$ (in the offshore zone). The constants C_1 to C_3 can be determined by fitting the curves in Figures 2 to 5. As the constant C_4 is the point where Q_{b3}= 0 (x-intercept), it can be determined from the known constants C_1 to C_3 by solving the quadratic equation. The constants C_1 to C_4 and correlation coefficients (R^2) of

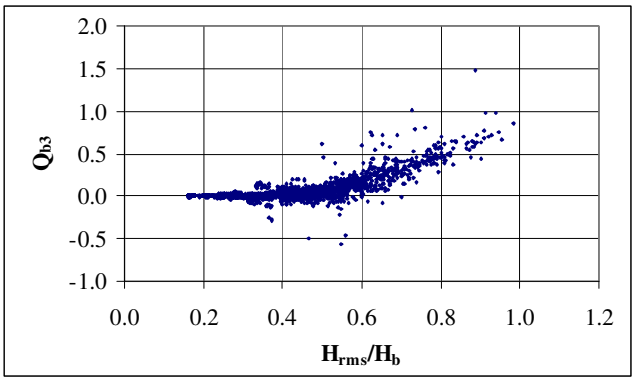

Figure 2. Relationship between measured Q_{b3} versus H_{rms}/H_b in which Equation 5 is used for computing H_b (measured data from Dette *et al.*, 1998).

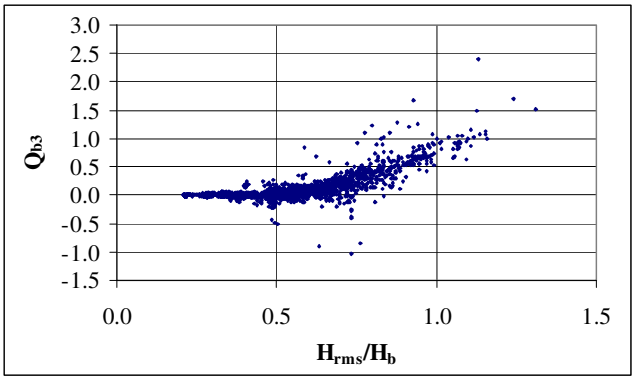

Figure 3. Relationship between measured Q_{b3} versus H_{rms}/H_b in which Equation 7 is used for computing H_b (measured data from Dette *et al.*, 1998).

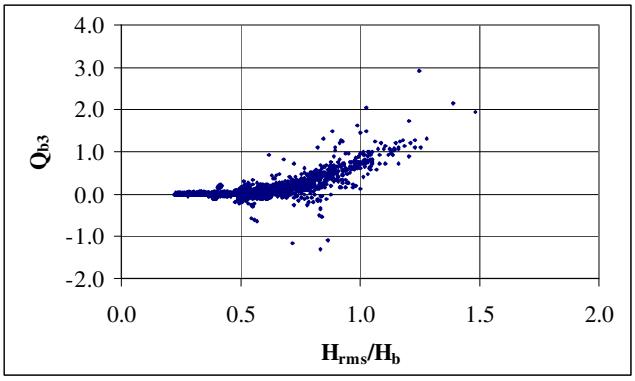

Figure 4. Relationship between measured Q_{b3} versus H_{rms}/H_b in which Equation 9 is used for computing H_b (measured data from Dette *et al.*, 1998).

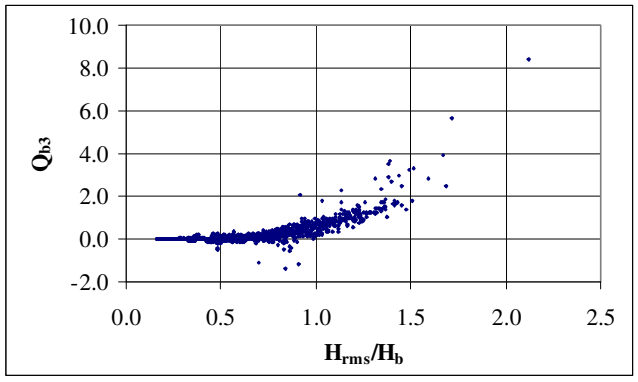

Figure 5. Relationship between measured Q_{b3} versus H_{rms}/H_b in which Equation 12 is used for computing H_b (measured data from Dette *et al.*, 1998).

Equation 15 for four H_b formulas are shown in Table 3. The correlation coefficients (R^2) of the fitting vary between 0.73 to 0.83, which indicates a reasonably good fit.

It should be noted that an attempt is also made to fit the measured Q_{b3} with a cubic equation. However, it is found that the correlation coefficients (R^2) of all models did not significantly improve. Therefore, the quadratic equation is used in this study.

Substituting the formula of for each H_b formula Q_{b3} into Equation 13, the present D_B models (MD1-MD4) can be expressed as:

MD1:

$$D_B = \frac{\rho g H_b^2}{4T}\left[0.189 - 1.282\left(\frac{H_{rms}}{H_b}\right) + 2.073\left(\frac{H_{rms}}{H_b}\right)^2\right]$$

$$\text{for } \frac{H_{rms}}{H_b} > 0.37 \qquad (16)$$

in which H_b is determined from the breaker height formula of BJ78 (Equation 5).

MD2:

$$D_B = \frac{\rho g H_b^2}{4T}\left[0.293 - 1.601\left(\frac{H_{rms}}{H_b}\right) + 2.096\left(\frac{H_{rms}}{H_b}\right)^2\right]$$

$$\text{for } \frac{H_{rms}}{H_b} > 0.46 \qquad (17)$$

in which H_b is determined from the breaker height formula of BS85 (Equation 7).

MD3:

$$D_B = \frac{\rho g H_b^2}{4T}\left[0.309 - 1.614\left(\frac{H_{rms}}{H_b}\right) + 2.013\left(\frac{H_{rms}}{H_b}\right)^2\right]$$

$$\text{for } \frac{H_{rms}}{H_b} > 0.49 \qquad (18)$$

in which H_b is determined from the breaker height formula of Nairn (1990) (Equation 9).

MD4:

$$D_B = \frac{\rho g H_b^2}{4T}\left[0.342 - 1.776\left(\frac{H_{rms}}{H_b}\right) + 2.087\left(\frac{H_{rms}}{H_b}\right)^2\right]$$

$$\text{for } \frac{H_{rms}}{H_b} > 0.56 \qquad (19)$$

in which H_b is determined from the breaker height formula of RWS03 (Equation 12).

4. Model Examination

In the beach morphodynamics model, the wave model has to be run several times to account for the change of beach morphology. It is necessary to estimate the wave height with a high accuracy, because the error of the estimation may be accumulate over time. The objective of this section is to examine the applicability of the present dissipation models on simulating *rms* wave heights (H_{rms}) and to select the best one. To confirm the ability of the present models, the accuracy of the present models was also compared with that of four existing models (shown in Section 2). The measured *rms* wave heights from 13 sources (1723 cases) of collected experimental results (shown in Table 1) are used to examine the models. The collected data are separated into three groups according to the experiment scales, i.e. small-scale, large-scale, and field experiments. It is expected that a good model should be able to predict well for the three groups of experimental scales and well for all collected data.

The basic parameter for determination of the accuracy of a model is the average relative error (*ER*), which is defined as:

Table 3. Calibrated constants (C_1 to C_4) and correlation coefficients (R^2) of Q_{b3} formula (Equation 15) for the four H_b formulas.

No.	Q_{b3} Formulas	H_b Formulas	Calibrated constants				R^2
			C_1	C_2	C_3	C_4	
1	Eq. (15)	Eq. (5)	0.189	-1.282	2.073	0.37	0.77
2	Eq. (15)	Eq. (7)	0.293	-1.601	2.096	0.46	0.75
3	Eq. (15)	Eq. (9)	0.309	-1.614	2.013	0.49	0.73
4	Eq. (15)	Eq. (12)	0.342	-1.776	2.087	0.56	0.83

Table 4. The average relative errors (*ER*) of the existing and the present models for 3 experiment scales and all collected data (measured data from Table 1).

Models	D_B Formulas	h_b Formulas	*ER*			
			Small-scale (152 data)	Large-scale (6705 data)	Field (11285 data)	All data (18142 data)
BJ78	Eq. (3)	Eq. (5)	8.80	10.05	18.68	15.41
BS85	Eq. (3)	Eq. (7)	6.98	6.68	10.69	9.18
BHV98	Eq. (8)	Eq. (9)	9.93	6.72	11.47	9.70
RWS03	Eq. (8)	Eq. (12)	11.65	8.06	10.73	9.75
MD1	Eq. (16)	Eq. (5)	24.06	8.17	11.56	10.41
MD2	Eq. (17)	Eq. (7)	6.96	6.62	9.77	8.58
MD3	Eq. (18)	Eq. (9)	9.24	7.70	10.24	9.29
MD4	Eq. (19)	Eq. (12)	9.93	9.08	10.94	10.24

$$ER = \frac{100}{N}\sum_{j=1}^{N}\left(\frac{\left|H_{mj} - H_{cj}\right|}{H_{mj}}\right) \qquad (20)$$

where j is the wave height number, H_{cj} is the computed wave height of number j, H_{mj} is the measured wave height of number j, and N is the total number of data of measured wave heights. A small value of *ER* indicates a high level of accuracy of the model.

The *rms* wave height transformation is computed by numerical integration of the energy flux balance equation (Equation 2) with the energy dissipation rate of the existing and the present models (i.e. the models of BJ78, BS85, BHV98, RWS03, and MD1 to MD4). A backward finite difference scheme is used to solve the energy flux balance equation (Equation 2). The *ER* of each dissipation model for three experimental scales and all collected data have been computed and shown in Table 4. The results can be summarized as follows:

a) The *ER* of the models for small-scale experiments varies between 7.0% and 24.1%. The accuracy of the models for small-scale experiments in descending order are MD2, BS85, BJ78, MD3, BHV98, MD4, RWS03, and MD1.

b) The *ER* of the models for large-scale experiments varies between 6.6% and 10.1%. The accuracy of the models for large-scale experiments in descending order are MD2, BS85, BHV98, MD3, RWS03, MD1, MD4, and BJ78.

c) The *ER* of the models for field experiments varies between 9.8% and 18.7%. The accuracy of the models for field experiments in descending order are MD2, MD3, BS85, RWS03, MD4, BHV98, MD1, and BJ78.

d) The of the models for all collected data, which is used to indicate the overall accuracy, varies between 8.6% and 15.4%. The overall accuracy of the models for all collected data in descending order are MD2, BS85, MD3, BHV98, RWS03, MD4, MD1, and BJ78.

e) Comparing the overall accuracy of the existing models (BJ78, BS85, BHV98, and RWS03), the model of BS85 gives the best prediction.

f) Comparing the overall accuracy of the present models (MD1-MD4), the model of MD2 gives the best prediction.

g) Considering the overall performance of all models, the model MD2 seems to be the best one. Therefore, MD2 is recommended to use for computing the transformation of H_{rms}.

It can be seen that the model MD2 is similar to the model of BS85. The main difference between the models MD2 and BS85 is the formula of Q_b which makes the model MD2 simpler than the model BS85. Although the model MD2 is simpler than BS85, the accuracy is better.

5. Conclusions

A simple energy dissipation model for computing the *rms* wave height transformation was developed. The *rms* wave height transformation is computed from the energy flux conservation law. The dissipation model of Battjes and Janssen (1978) was used as a framework for developing the present model. The model of Battjes and Janssen (1978) consists of three main formulas, (a) the formulas of energy dissipation of a single broken wave, (b) the breaker height (H_b), and (c) the fraction of breaking waves (Q_b). The present study focuses mainly on the new derivation of the Q_b formula. Unlike the common derivation, the formula of Q_b was derived directly from the measured wave heights by inverting the wave model together with the dissipation model. Based on the four existing breaker height formulas, four Q_b formulas were developed and consequently yielded four dissipation models.

A wide range and large amount of collected experimental data (1723 cases collected from 13 sources) were used to examine the applicability of the present dissipation models on simulating H_{rms} and to select the best one. To confirm the ability of the proposed models, their accuracy was also compared with that of four existing dissipation models. The examination results were presented in terms of average relative error. The examination shows that the model

MD2 gives very good accuracy for a wide range of wave and beach conditions (with *ER* for all collected data of 8.6%) and gives better predictions than that of existing models.

Acknowledgements

This research was sponsored by the Thailand Research Fund and the Commission on Higher Education, Ministry of Education, Thailand. The data collection of the DELILAH and DUCK94 Projects were funded by the US Office of Naval Research and the US National Science Foundation, U.S.A.

References

Baldock, T.E., Holmes, P., Bunker, S. and Van Weert, P. 1998. Cross-shore hydrodynamics within an unsaturated surf zone. Coastal Engineering. 34, 173-196.

Battjes, J.A. and Janssen, J.P.F.M. 1978. Energy loss and set-up due to breaking of random waves. Proceedings of the 16th Coastal Engineering Conference, American Society of Civil Engineers, 569-587.

Battjes, J.A. and Stive, M.J.F. 1985. Calibration and verification of a dissipation model for random breaking waves. Journal of Geophysical Research. 90, 9159-9167.

Birkemeier, W.A., Donoghue, C., Long, C.E., Hathaway, K.K. and Baron, C.F. 1997. The DELILAH Nearshore Experiment: Summary Data Report. US Army Corps of Engineers, Waterways Experiment Station, Vicksburg, MS.

Dally, W. R., Dean, R. G. and Dalrymple, R. A. 1985. Wave height variation across beach. Journal of Geophysical Research. 90(C6), 11917-11927.

Dally, W.R. 1990. Random breaking waves: A closed-form solution for planar beaches. Coastal Engineering. 14, 233-263.

Demerbilek, Z. and Vincent, L. 2006. Water wave mechanics (Part 2 - Chapter 1). Coastal Engineering Manual, EM1110-2-1100, Coastal and Hydraulics Laboratory - Engineering Research and Development Center, Waterways Experiment Station, US Army Corps of Engineers, pp. II-1-75.

Dette, H.H, Peters, K. and Newe, J. 1998. MAST III - SAFE Project: Data Documentation, Large Wave Flume Experiments '96/97. Report No. 825 and 830. Leichtweiss-Institute, Technical University Braunschweig.

Grasmeijer, B.T. and van Rijn, L.C. 1999. Transport of fine sands by currents and waves, III: breaking waves over barred profile with ripples. Journal of Waterways, Port, Coastal, and Ocean Engineering, American Society of Civil Engineers. 125, 71-79.

Hamilton, D.G. and Ebersole, B.A. 2001. Establishing uniform longshore currents in a large-scale sediment transport facility. Coastal Engineering. 42, 199-218.

Herbers, T.H.C., Elgar, S., Guza, R.T. and O'Reilly, W.C. 2006. Surface gravity waves and nearshore circulation. DUCK94 Experiment Data Server: SPUV Pressure Sensor Wave Height Data. Available online at: http://dksrv.usace.army.mi/jg/dk94dir [April 7, 2006].

Horikawa, K. and Kuo, C. T. 1966. A study of wave transformation inside the surf zone. Proceedings of the 10th Coastal Engineering Conference, American Society of Civil Engineers, 217-233.

Hurue, M. 1990. Two-Dimensional Distribution of Undertow due to Irregular Waves. B.Eng. Thesis. Department of Civil Engineering, Yokohama National University, Japan (in Japanese).

Johnson, H.K. 2006. Wave modelling in the vicinity of submerged breakwaters. Coastal Engineering. 53, 39-48.

Kraus, N.C., Gingerich, K.J. and Rosati, J.D. 1989. DUCK85 Surf Zone Sand Transport Experiment. Technical Report CERC-89-5. US Army Corps of Engineers, Waterways Experiment Station, Vicksburg, MS.

Kraus, N.C. and Smith, J.M. 1994. SUPERTANK Laboratory Data Collection Project. Technical Report CERC-94-3. US Army Corps of Engineers, Waterways Experiment Station, Vicksburg, MS.

Le Mehaute, B. 1962. On non-saturated breakers and the wave run-up. Proceedings of the 8th Coastal Engineering Conference, American Society of Civil Engineers, 77-92.

Mizuguchi, M. 1981. An heuristic model of wave height distribution in surf zone. Proceedings of the 17th Coastal Engineering Conference, American Society of Civil Engineers, 278-289.

Miche, R. 1951. Le pouvoir reflechissant des ouvrages maritime exposes a l'action de la houle. Annales Ponts et Chaussees, 121 Annee, pp. 285-319.

Nairn, R.B. 1990. Prediction of Cross-Shore Sediment Transport and Beach Profile Evolution. Ph.D. thesis, Department of Civil Engineering, Imperial College, London.

Oliveira, F.S.B.F. 2007. Numerical modeling of deformation of multi-directional random wave over a varying topography. Ocean Engineering. 34, 337-342.

Rattanapitikon, W. and Shibayama T. 1998. Energy dissipation model for regular and irregular breaking waves. Coastal Engineering Journal, Japan Society of Civil Engineers. 40, 327-346.

Rattanapitikon, W. and Leangruxa, P. 2001. Comparison of dissipation models for regular breaking waves. Songklanakarin Journal of Science and Technology. 23, 63-72.

Rattanapitikon, W., Karunchintadit, R. and Shibayama, T. 2003. Irregular wave height transformation using representative wave approach. Coastal Engineering Journal, Japan Society of Civil Engineers. 45, 489-510.

Roelvink, J.A. and Reniers A.J.H.M. 1995. LIP 11D Delta Flume Experiments: A Data Set for Profile Model Validation. Report No. H 2130. Delft Hydraulics.

Ruessink, B.G., Walstra, D.J.R. and Southgate, H.N. 2003. Calibration and verification of a parametric wave

model on barred beaches. Coastal Engineering. 48, 139-149.

Sawaragi, T. and Iwata, K. 1974. Turbulence effect on wave deformation after breaking. Coastal Engineering in Japan, Japan Society of Civil Engineers. 17, 39-49.

Smith, J.M. and Kraus, N.C. 1990. Laboratory Study on Macro-Features of Wave Breaking Over Bars and Artificial Reefs. Technical Report CERC-90-12. US Army Corps of Engineers, Waterways Experiment Station, Vicksburg, MS.

Southgate, H.N. and Nairn, R.B. 1993. Deterministic profile modelling of nearshore processes, Part 1: Waves and currents. Coastal Engineering. 19, 27-56.

Sultan, N. 1995. Irregular Wave Kinematics in the Surf Zone. Ph.D. Dissertation. Texas A&M University, College Station, Texas, USA.

Thornton, E.B. and Guza, R.T. 1986. Surf zone longshore currents and random waves: field data and model. Journal of Physical Oceanography. 16, 1165-1178.

Ting, F.C.K. 2001. Laboratory study of wave and turbulence velocity in broad-banded irregular wave surf zone. Coastal Engineering. 43, 183-208.

A.6 Modification of a parametric model

Reprinted from:

Rattanapitikon, W. and Sawanggun, S. (2007). Modification of a parametric model, The 4th International Conference on Asian and Pacific Coasts [CD-ROM], September 21-24, Nanjing, China, pp. 346-357.

Asian and Pacific Coasts 2007
September 21-24, 2007, Nanjing, China

MODIFICATION OF A PARAMETRIC WAVE MODEL

Winyu Rattanapitikon[1] and Sangapol Sawanggun[2]

ABSTRACT: This study was undertaken to develop a simple wave model for computing the transformation of root mean square wave height. The parametric wave approach of Battjes and Janssen (1978) was used as a framework for developing the models. The energy dissipation in the wave model is expressed as the product of fraction of breaking waves and energy dissipation of a single broken wave. The fraction of breaking waves was modified in this study. The fraction of breaking waves was not derived from the assumed probability of wave breaking (as did in the common derivation), but derived directly from the measured wave heights by inverting the wave model. Experimental data of root mean square wave height transformation from 13 sources, covering 1,723 cases of wave and beach conditions, have been collected for verifying the models. The experiments cover a wide range of wave and beach conditions, including small-scale, large-scale and field experiments. The modified model was also compared with three existing models, which were developed based on the parametric wave approach. The modified model gives very good accuracy for a wide range of wave and beach conditions and better than those of existing models.

1. Introduction

Wave height is one of the most essential required factors for many coastal engineering applications such as the design of coastal structures and the study of beach deformations. When waves propagate in shallow water, their profiles steepen and they eventually break. The higher waves tend to break at a greater distance from the shore. Closer to the shore, more and more waves break, until almost all the waves break in the inner surf zone. Once the waves start to break, a part of the wave energy is transformed into turbulence and heat, and wave height decreases towards the shore. Common methods to model irregular wave height transformation can be classified into four main approaches, i.e. representative wave approach, spectral approach, probabilistic approach, and parametric wave approach. For computing beach deformation, the wave model should be kept as simple as possible because of the frequent updating of wave fields to account for the change of bottom profiles. The parametric and representative wave approaches appear to be simple methods and seem to be suitable for incorporating in the beach deformation model.

[1] Associate Professor, Civil Engineering Program, Sirindhorn International Institute of Technology, Thammasat University, Pathum Thani 12121, Thailand. winyu@siit.tu.ac.th
[2] Graduate student, ditto

For the representative wave approach, the regular wave model has been directly applied to irregular waves by using representative (or equivalent) waves, while the parametric approach considers the random nature of the waves but describes the energy dissipation rate in terms of time-averaged parameters. The parametric wave models were developed based on the assumed probability density function (*pdf*) of wave height inside the surf zone. The average rate of energy dissipation is described by integrating the product of energy dissipation of a broken wave and the probability of occurrence of breaking waves. The parametric wave approach is expected to be better than the representative wave approach because it includes the random nature of the waves into the model while the other does not. Therefore, the present study focuses on the parametric wave approach.

The parametric wave models are generally based on the work of Battjes and Janssen (1978). The model relies on the macroscopic features of breaking waves and predicts only the transformation of root-mean-square (*rms*) wave height. The *rms* wave height transformation is computed from the energy flux conservation law. It is

$$\frac{\partial\left(Ec_g\cos\theta\right)}{\partial x} = -D_B \tag{1}$$

where E is the wave energy density, c_g is the group velocity, θ is the mean wave angle, x is the distance in the cross shore direction, and D_B is the energy dissipation rate due to wave breaking. The energy dissipation rate due to bottom friction is neglected. All variables are based on linear wave theory and Snell's law is employed to describe wave refraction.

From linear wave theory, the wave energy density (E) is equal to $\rho g H_{rms}^2/8$. Therefore, Eq. (1) can be written in terms of wave height as

$$\frac{\rho g}{8}\frac{\partial\left(H_{rms}^2 c_g\cos\theta\right)}{\partial x} = -D_B \tag{2}$$

where ρ is the density of water, g is the gravity acceleration, and H_{rms} is the *rms* wave height.

The *rms* wave height transformation can be computed from the energy flux balance equation [Eq. (2)] by substituting the model of energy dissipation rate (D_B) and numerically integrating from offshore to shoreline. In the offshore zone, the energy dissipation rate is set to zero. The main difficulty of Eq. (2) is how to formulate the energy dissipation rate caused by the breaking waves.

During the past decades, various energy dissipation models for the parametric wave approach have been proposed for computing H_{rms} in the surf zone. Because of the complexity of the wave breaking mechanism, most of the energy dissipation models were developed based on an empirical or semi-empirical approach. It is well known that the validity of an empirical formula may be limited according to the range of experimental conditions that were employed in the calibrations or verifications. To make an empirical formula reliable, it is necessary to calibrate or verify the formula with a large amount and wide range of experimental data. Since many energy dissipation models were developed based on data with limited experimental conditions, there is still a need for more data to confirm the underlying assumptions and to make the model more reliable. It is the purpose of this study to develop a simple energy dissipation model for the parametric wave approach based on a wide range of experimental conditions.

Experimental data of *rms* wave height transformation from 13 sources, covering 1,723 cases of wave and beach conditions, have been collected for verifying the models. The experiments cover a wide range of wave and beach conditions, including small-scale, large-scale and field experiments. The experiments cover a variety of beach conditions (i.e. plane, barred, and sandy beaches) and a range of deepwater wave steepness (H_{rmso}/L_o) from 0.001 to 0.059. A summary of the collected experimental data is given in Table 1.

Table 1 Summary of collected experimental data

Sources	**Total no. of cases**	**Total no. of data**	**Beach conditions**	H_{rmso}/L_o	**Apparatus**
Hurue (1990)	1	7	plane beach	0.026	small-scale
Smith and Kraus (1990)	12	96	plane and barred beach	0.021-0.059	small-scale
Sultan (1995)	1	12	plane beach	0.004	small-scale
Grasmeijer and Rijn (1999)	2	20	sandy beach	0.014-0.017	small-scale
Hamilton and Ebersole (2001)	1	10	plane beach	0.017	small-scale
Ting (2001)	1	7	plane beach	0.016	small-scale
Kraus and Smith (1994): SUPERTANK project	128	2,223	sandy beach	0.001-0.045	large-scale
Roelvink and Reniers (1995): LIP 11D project	95	923	sandy beach	0.004-0.028	large-scale
Dette et al. (1998): MAST III – SAFE project	138	3,559	sandy beach	0.006-0.015	large-scale
Thornton and Guza (1986)	4	60	sandy beach	0.001-0.001	field
Kraus et al. (1989): DUCK85 project	8	90	sandy beach	0.001-0.002	field
Birkemeier et al. (1997): DELILAH project	745	5,033	sandy beach	0.001-0.025	field
Herbers et al. (2006): DUCK94 project	587	6,102	sandy beach	0.001-0.029	field
Total	1,723	18,142		0.001-0.059	

This paper is divided into three main parts. The first part briefly reviews some existing dissipation models for the parametric wave approach. The second part describes the development of the present model. The last part is the verification of the present model in comparison with the existing models.

2. Existing Energy Dissipation Models

During the past decades, various energy dissipation models have been developed based on a framework of the parametric wave approach of Battjes and Janssen (1978). Brief reviews of some existing dissipation models are described below.

a) Battjes and Janssen (1978), hereafter referred to as BJ78, proposed to compute D_B as a product of the fraction of breaking waves (Q_b) and the energy dissipation of a single broken wave (D_s) as

$$D_B = Q_{b1} D_{s1} \tag{3}$$

where Q_{b1} is the fraction of breaking waves of BJ78, and D_{s1} is the energy dissipation of a single broken wave (or a possible maximum wave height) of BJ78. The energy dissipation of a single broken wave is determined from a simplified bore-type dissipation model as

$$D_{s1} = \frac{\rho g H_b^2}{4T_p} \tag{4}$$

where H_b is the breaker height or the maximum wave height, and T_p is the spectral peak period. The fraction of breaking waves (Q_{b1}) was derived based on the assumption that the probability density function (*pdf*) of wave height could be modeled with a Rayleigh distribution truncated at the breaker height (H_b) and all broken waves have a height equal to the breaker height (H_b). This was shown to imply the relation between Q_{b1} and H_{rms}/H_b as

$$\frac{1 - Q_{b1}}{-\ln Q_{b1}} = \left(\frac{H_{rms}}{H_b} \right)^2 \tag{5}$$

in which the breaker height (H_b) is determined from the formula of Miche (1951) with an additional coefficient (γ) in the tan-hyperbolic function as

$$H_b = 0.14 L \tanh(\gamma k h) \tag{6}$$

where L is the wavelength related to T_p, k is the wave number, and h is the water depth. Based on their small-scale experimental data, the coefficient γ is determined to be 0.91. As Eq. (5) is an implicit equation, it has to be solved for Q_{b1} by an iteration technique, or by a 1-D look-up table (Southgate and Nairn, 1993), or by fitting Q_{b1} with a polynomial function as

$$Q_{b1} = \sum_{n=0}^{7} a_n \left(\frac{H_{rms}}{H_b} \right)^n \tag{7}$$

where a_n is the constant of n^{th} term. A multiple regression analysis is used to determine the constants a_o to a_7. The correlation coefficient (R^2) of Eq. (7) is 0.99999999. The values of constants a_o to a_7 are shown in Table 2. Equation (7) is applicable for $0.3 < H_{rms}/H_b < 1.0$. For $H_{rms}/H_b \leq 0.3$, the value of Q_{b1} is very small and can be set at zero. The value of Q_{b1} is set to be 1.0 when $H_{rms}/H_b \geq 1.0$. The model of BJ78 has been used successfully in many applications for computing H_{rms} transformation (e.g. Abadie et al., 2006; Johnson, 2006; and Oliveira, 2007). The D_B model of BJ78 was derived based on two main assumptions, i.e. assumptions of the truncated-Rayleigh distribution of wave height and the simplified bore-type dissipation model. It should be noted that the assumption of the truncated-Rayleigh distribution (for deriving the

formula of Q_{b1}) is not supported by experimental data (Dally, 1990). Some researchers (e.g. Southgate and Nairn, 1993; and Baldock et al., 1998) demonstrated that Eq. (5) gives a large error in predicting the fraction of breaking waves (Q_b). Moreover, the simplified bore-type dissipation model for estimating energy dissipation of a broken wave is also not supported by experimental data (Rattanapitikon et al., 2003). Surprisingly, the D_B model of BJ78 seems to give good results of predicting H_{rms} and has proven to be a popular framework for estimating H_{rms} (Ruessink et al., 2003). Because the assumptions for deriving the model are not valid but the model still gives very good results, the D_B model of BJ78 may be considered as an empirical model for computing only D_B or H_{rms}.

Table 2 Values of constants a_o to a_7 for computing Q_{b1}

Constants	Values
a_0	0.2317072
a_1	-3.6095814
a_2	22.5948312
a_3	-72.5367918
a_4	126.8704405
a_5	-120.5676384
a_6	60.7419815
a_7	-12.7250603

b) Battjes and Stive (1985), hereafter referred to as BS85, used the same energy dissipation model as that of BJ78 [Eq. (3)]. They modified the model of BJ78 by recalibrating the coefficient γ in the breaker height formula [Eq. (6)]. The coefficient γ was related to the deepwater wave steepness (H_{rmso}/L_o). After calibration with small-scale and field experiments, the breaker height formula was modified to be

$$H_b = 0.14L\tanh\left\{\left[0.57 + 0.45\tanh\left(33\frac{H_{rmso}}{L_o}\right)\right]kh\right\} \tag{8}$$

where H_{rmso} is the deepwater *rms* wave height, and L_o is the deepwater wavelength. Hence, the main difference between the models of BJ78 and BS85 is only the formula for computing H_b.

c) Southgate and Nairn (1993), hereafter referred to as SN93, modified the model of BJ78 by changing the expression of energy dissipation of a single broken wave from the bore model of BJ78 (D_{s1}) to be the bore model of Thornton and Guza (1983), D_{s2}, as

$$D_B = Q_{b1}D_{s2} \tag{9}$$

in which Q_{b1} is the fraction of breaking waves of BJ78 [Eq. (5)] and D_{s2} is the energy dissipation of a single broken wave of Thornton and Guza (1983), which is expressed as

$$D_{s2} = \frac{\rho g H_b^3}{4 T_p h} \tag{10}$$

The breaker height (H_b) is determined from the formula of Nairn (1990) as

$$H_b = h\left[0.39 + 0.56 \tanh\left(33 \frac{H_{rmso}}{L_o}\right)\right] \tag{11}$$

Hence, the model of SN93 is similar to that of BJ78 except for the formulas of D_{s2} and H_b.

3. Model Development

In this study, the energy dissipation model of BJ78 is used as a framework for developing the present energy dissipation model. The D_B model is expressed as the product of fraction of breaking waves (Q_b) and energy dissipation of a single broken wave (D_s).

$$D_B = Q_b D_s \tag{12}$$

in which Q_b is a function of H_{rms}/H_b.

Since the energy dissipation of a single broken wave (D_s) is the energy dissipation of a possible maximum wave height, it may be considered as a maximum energy dissipation or a potential energy dissipation. The fraction of breaking waves (Q_b) may also be considered as a fraction of energy dissipation. The dissipation models [Eq. (12)] may be re-explained as a product of a fraction of energy dissipation and the potential energy dissipation.

The model of D_B consists of 3 main formulas, i.e. the formulas of H_b, Q_b, and D_s. The Q_b formula of BJ78 was derived based on the assumed *pdf* of wave height in the surf zone, which is not supported by the experimental data (Dally, 1990). Since the acceptable *pdf* of wave height inside the surf zone is not available (Demerbilek and Vincent, 2006), it may not be suitable to derive formula of Q_b from the assumed *pdf* of wave height. Alternatively, the formula of Q_b can be derived directly from the measured wave heights by inverting the energy dissipation model [Eq. (12)] and the wave model [Eq. (2)]. Therefore, in the present study, the formula of Q_b will be newly derived from the measured wave heights.

As Q_b is the function of H_{rms}/H_b, the formula of Q_b can be determined by plotting a relationship between measured Q_b versus H_{rms}/H_b. The required data for determining the formula are the measured data of Q_b and H_{rms}/H_b. The measured Q_b can be determined indirectly from the measured wave heights as follows.

Substituting Eq. (2) into Eq. (12), and using backward finite difference scheme to describe the differential equation, the formula for determining measured Q_b is expressed as

$$Q_{bi} = \frac{\rho g}{8 D_s} \frac{\left(H_{rmsi-1}^2 c_{gi-1} \cos\theta_{i-1} - H_{rmsi}^2 c_{gi} \cos\theta_i\right)}{x_i - x_{i-1}} \tag{13}$$

where i is the grid number. Hereafter, the variable Q_b determined from Eq. (13) is referred to as the measured Q_b.

For determining Q_b from Eq. (13), the formulas of D_s and H_b must be given. It can be seen from Sec. 2 that several formulas have been proposed for computing H_b and D_s, i.e. three formulas for H_b [Eqs. (6), (8), and (11)] and two formulas for D_s [Eqs. (4), and (10)]. It is not clear which formulas of H_b and D_s are suitable for modeling Q_b. Therefore, all of them are considered in the derivation of Q_b formula. As there are two formulas for D_s [Eqs. (4), and (10)] and three formulas for H_b [Eqs. (6), (8), and (11)], a total of six Q_b can be determined and consequently six relationships between measured Q_b versus H_{rms}/H_b are considered in this study. The required data set for deriving the formula of Q_b are the measured data of h, T, H_{rms}, θ, and x. Other related variables (e.g. H_{rmso}, L_o, L, k, and c_g) are computed based on linear wave theory. To avoid a large fluctuation in the relationships, the wave heights variation across shore should have a small fluctuation.

Because of a variety of wave conditions and a small fluctuation of wave height variation across shore, the data from Dette et al. (1998) are used for deriving the six formulas of Q_b. However, all collected data shown in Table 1 are used to verify the models for identifying the best one.

The six relationships between measured Q_b versus H_{rms}/H_b have been plotted to identify the suitable equation of the relationships. An example of a relationship between measured Q_b versus H_{rms}/H_b by using Eqs. (4) and (6) for computing D_s and H_b are shown in Fig. 1.

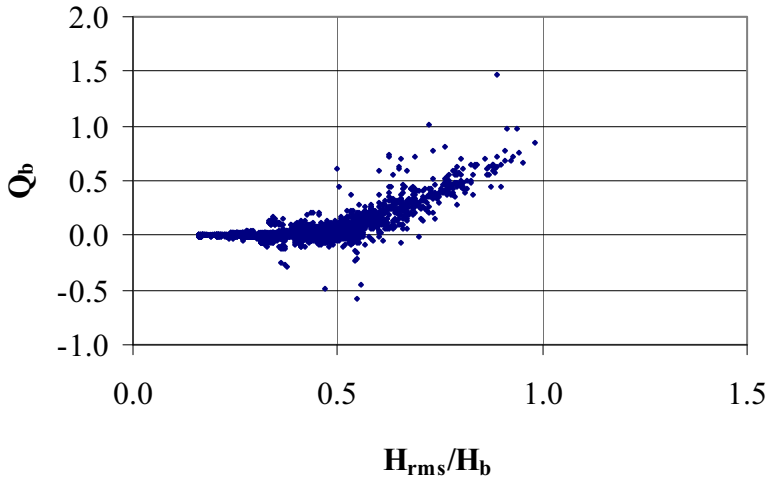

Figure 1 Relationship between measured Q_b versus H_{rms}/H_b by using Eqs. (4) and (6) for computing D_s and H_b (measured data from Dette et al., 1998)

It is found that all relationships can be fitted well with a quadratic equation as

$$Q_b = K_1 + K_2\left(\frac{H_{rms}}{H_b}\right) + K_3\left(\frac{H_{rms}}{H_b}\right)^2 \qquad \text{for} \qquad \frac{H_{rms}}{H_b} > K_4 \tag{14}$$

where K_1 to K_4 are constants. The fraction of energy dissipation (Q_b) is set to be zero when $H_{rms}/H_b \leq K_4$ (offshore zone). The constants K_1 to K_3 can be determined from multi-regression analysis between measured Q_b and H_{rms}/H_b. As the constant K_4 is the point that $Q_b = 0$ (x-intercept), it can be determined from the known constants K_1 to K_3 by solving the quadratic equation. The constants K_1 to K_4 and correlation coefficients (R^2) of the six relationships (6 formulas of Q_b) are shown in Table 3. The correlation coefficients (R^2) of the fitting vary between 0.72 to 0.77, which indicate a reasonably good fit.

Table 3 Calibrated constants (K_1 to K_4) and correlation coefficients (R^2) of Q_b formula [Eq. (14)] for difference D_s and H_b formulas

Formula No.	D_s **Formulas**	H_b **Formulas**	**Calibrated constants**				R^2
			K_1	K_2	K_3	K_4	
F1	Eq. (4)	Eq. (6)	0.189	-1.282	2.073	0.37	0.77
F2		Eq. (8)	0.293	-1.601	2.096	0.46	0.75
F3		Eq. (11)	0.309	-1.614	2.013	0.49	0.73
F4	Eq. (10)	Eq. (6)	0.240	-1.627	2.640	0.37	0.77
F5		Eq. (8)	0.465	-2.532	3.311	0.46	0.74
F6		Eq. (11)	0.544	-2.818	3.485	0.49	0.72

Substituting the six formulas of Q_b into Eq. (12), the six corresponding D_B models (MD1-MD6) can be expressed as

$$\text{MD1: } D_B = \frac{\rho g H_b^2}{4T_p}\left[0.189 - 1.282\left(\frac{H_{rms}}{H_b}\right) + 2.073\left(\frac{H_{rms}}{H_b}\right)^2\right] \qquad \text{for } \frac{H_{rms}}{H_b} > 0.37 \qquad (15)$$

in which H_b is determined from the breaker height formula of BJ78 [Eq. (6)].

$$\text{MD2: } D_B = \frac{\rho g H_b^2}{4T_p}\left[0.293 - 1.601\left(\frac{H_{rms}}{H_b}\right) + 2.096\left(\frac{H_{rms}}{H_b}\right)^2\right] \qquad \text{for } \frac{H_{rms}}{H_b} > 0.46 \qquad (16)$$

in which H_b is determined from the breaker height formula of BS85 [Eq. (8)].

$$\text{MD3: } D_B = \frac{\rho g H_b^2}{4T_p}\left[0.309 - 1.614\left(\frac{H_{rms}}{H_b}\right) + 2.013\left(\frac{H_{rms}}{H_b}\right)^2\right] \qquad \text{for } \frac{H_{rms}}{H_b} > 0.49 \qquad (17)$$

in which H_b is determined from the breaker height formula of Nairn (1990) [Eq. (11)].

$$\text{MD4: } D_B = \frac{\rho g H_b^3}{4T_p h}\left[0.240 - 1.627\left(\frac{H_{rms}}{H_b}\right) + 2.640\left(\frac{H_{rms}}{H_b}\right)^2\right] \qquad \text{for } \frac{H_{rms}}{H_b} > 0.37 \qquad (18)$$

in which H_b is determined from the breaker height formula of BJ78 [Eq. (6)].

$$\text{MD5: } D_B = \frac{\rho g H_b^3}{4 T_p h}\left[0.465 - 2.532\left(\frac{H_{rms}}{H_b}\right) + 3.311\left(\frac{H_{rms}}{H_b}\right)^2\right] \qquad \text{for } \frac{H_{rms}}{H_b} > 0.46 \qquad (19)$$

in which H_b is determined from the breaker height formula of BS85 [Eq. (8)].

$$\text{MD6: } D_B = \frac{\rho g H_b^3}{4 T_p h}\left[0.544 - 2.818\left(\frac{H_{rms}}{H_b}\right) + 3.485\left(\frac{H_{rms}}{H_b}\right)^2\right] \qquad \text{for } \frac{H_{rms}}{H_b} > 0.49 \qquad (20)$$

in which H_b is determined from the breaker height formula of Nairn (1990) [Eq. (11)].

4. Model Examination

In the beach deformation model, the wave model has to be run many times to account for the change of beach profiles. It is necessary to estimate the wave height with high accuracy because the error of the estimation may accumulate from time to time. The objective of this section is to examine the applicability of the present dissipation models (MD1-MD6) on simulating *rms* wave heights and the best one is then selected. To confirm the ability of present models, the accuracy of present models were also compared with that of three existing models (shown in Sec. 2). The measured *rms* wave heights from 13 sources (1,723 cases) of collected experimental results (shown in Table 1) are used to examine the models. The collected experiments are separated into three groups according to the experiment-scales, i.e. small-scale, large-scale, and field experiments. It is expected that a good model should be able to predict well for all experiment-scales and all collected data.

The basic parameter for determination of the accuracy of a model is the average relative error (*ER*), which is defined as

$$ER = \frac{100}{N}\sum_{j=1}^{N}\left(\frac{\left|H_{mj} - H_{cj}\right|}{H_{mj}}\right) \qquad (21)$$

where j is the wave height number, H_{cj} is the computed wave height of number j, H_{mj} is the measured wave height of number j, and N is the total number of data of measured wave heights. The small value of *ER* indicates a high level of accuracy of the model.

The *rms* wave height transformation is computed by numerical integration of the energy flux balance equation [Eq. (2)] with the energy dissipation rate of the existing and the present models [i.e. the models of BJ78, BS85, SN93, and MD1 to MD6]. A backward finite difference scheme is used to solve the energy flux balance equation [Eq. (2)]. The errors (*ER*) of each dissipation model for three experiment-scales and all collected data have been computed and shown in Table 4. The results can be summarized as follows:

a) The error (*ER*) of the models for small-scale experiments varies between 7.0% to 24.1%. The accuracy of the models for small-scale experiments in descending order are MD2, BS85, MD5, BJ78, MD3, MD6, SN93, MD4, and MD1.
b) The error (*ER*) of the models for large-scale experiments varies between 6.6% to 10.1%. The accuracy of the models for large-scale experiments in descending order are MD2, BS85, MD5, MD6, MD3, MD4, MD1, SN93, and BJ78.
c) The error (*ER*) of the models for field experiments varies between 9.8% to 18.7%. The accuracy of the models for field experiments in descending order are MD2, MD3, MD5, BS85, MD6, MD4, MD1, SN93, and BJ78.
d) The error (*ER*) of the models for all collected data, which is used to indicate the overall accuracy, varies between 8.6% to 15.4%. The overall accuracy of the models for all collected data in descending order are MD2, BS85, MD5, MD3, MD6, MD4, MD1, SN93, and BJ78.
e) Comparing the overall accuracy of the existing models (BJ78, BS85, and SN93), the model of BS85 gives the best prediction.
f) Comparing the overall accuracy of the present models (MD1-MD6), the model of MD2 gives the best prediction.
g) Considering the overall performance of all models, the model MD2 seems to be the best. Therefore, the model MD2 is recommended to use for computing the transformation of H_{rms}.

Table 4 Errors (*ER*) of the existing models and the models MD1-MD6 for 3 experiment-scales (measured data from Table 1)

Model	D_B **Formulas**	H_b **Formulas**	**Errors (*ER*)**			
			Small-scale (152 data)	Large-scale (6705 data)	Field (11285 data)	All data (18142 data)
BJ78	Eq. (3)	Eq. (6)	8.80	10.05	18.68	15.41
BS85	Eq. (3)	Eq. (8)	6.98	6.68	10.69	9.18
SN93	Eq. (9)	Eq. (11)	11.61	9.92	15.68	13.52
MD1	Eq. (15)	Eq. (6)	24.06	8.17	11.56	10.41
MD2	Eq. (16)	Eq. (8)	6.96	6.62	9.77	8.58
MD3	Eq. (17)	Eq. (11)	9.24	7.70	10.24	9.29
MD4	Eq. (18)	Eq. (6)	15.70	8.01	11.37	10.16
MD5	Eq. (19)	Eq. (8)	8.76	7.08	10.56	9.26
MD6	Eq. (20)	Eq. (11)	9.30	7.65	10.90	9.69

It can be seen that the model MD2 is similar to the model of BS85. The main difference between the models MD2 and BS85 is the formula of Q_b, which makes the model MD2 simpler than that of BS85. Although the model MD2 is simpler than that of BS85, the accuracy is better.

5. Conclusions

A simple wave model for computing the *rms* wave height transformation was developed. The *rms* wave height transformation is computed from the energy flux conservation. The energy dissipation model of Battjes and Janssen (1978) was used as a framework for developing the

present model. The model of Battjes and Janssen (1978) consists of three main formulas, i.e. the formulas of energy dissipation of a single broken wave (D_s), breaker height (H_b), and fraction of breaking waves (Q_b). The present study focuses mainly on the new derivation of Q_b formula. Unlike the common derivation, the formula of Q_b was derived directly from the measured wave heights by inverting the wave model. Based on the three existing H_b formulas and two existing D_s formulas, six Q_b formulas were developed and consequently yielded six dissipation models.

A wide range and large amount of collected experimental data (1,723 cases collected from 13 sources) were used to examine the applicability of the present models on simulating H_{rms} and select the best one. To confirm the ability of present models, the accuracy of present models were also compared with that of three existing dissipation models. The examination results were presented in terms of average relative error (*ER*). The examination shows that the model MD2 gives very good accuracy for a wide range of wave and beach conditions (with *ER* for all collected data of 8.6%) and gives better predictions than that of existing models. The model MD2 is similar to the model of BS85. The main difference between the models MD2 and BS85 is the formula of Q_b, which makes the model MD2 simpler than that of BS85. Although the model MD2 is simpler than that of BS85, the accuracy is better.

Acknowledgements

This research was sponsored by the Thailand Research Fund. The data collection of the DELILAH and DUCK94 projects were funded by the US Office of Naval Research and the US National Science Foundation.

References

Abadie, S., Butel, R., Mauriet, S., Morichon, D. and Dupuis, H. (2006). Wave climate and longshore drift on the South Aquitaine coast. *Continental Shelf Research,* 26: 1924-1939.

Baldock, T.E., Holmes, P., Bunker, S. and Van Weert, P. (1998). Cross-shore hydrodynamics within an unsaturated surf zone. *Coastal Engineering,* 34: 173-196.

Battjes, J.A. and Janssen, J.P.F.M. (1978). Energy loss and set-up due to breaking of random waves. *Proc. 16th Coastal Engineering Conf., ASCE,* pp. 569-587.

Battjes, J.A. and Stive, M.J.F. (1985). Calibration and verification of a dissipation model for random breaking waves. *J. Geophysical Research,* 90(C5): 9159-9167.

Birkemeier, W.A., Donoghue, C., Long, C.E., Hathaway, K.K. and Baron, C.F. (1997). *The DELILAH Nearshore Experiment: Summary Data Report,* US Army Corps of Engineers, Waterways Experiment Station, Vicksburg, MS.

Dally, W.R. (1990). Random breaking waves: A closed-form solution for planar beaches, *Coastal Engineering,* 14: 233-263.

Demerbilek, Z. and Vincent, L. (2006). Water wave mechanics (Part 2 – Chapter 1). *Coastal Engineering Manual,* EM1110-2-1100, Coastal and Hydraulics Laboratory – Engineering Research and Development Center, WES, US Army Corps of Engineers, pp. II-1-75.

Dette, H.H, Peters, K. and Newe, J. (1998). *MAST III – SAFE Project: Data Documentation, Large Wave Flume Experiments '96/97,* Report No. 825 and 830. Leichtweiss-Institute, Technical University Braunschweig.

Grasmeijer, B.T. and van Rijn, L.C. (1999). Transport of fine sands by currents and waves, III: breaking waves over barred profile with ripples. *J. of Waterway, Port, Coastal, and Ocean Eng., ASCE,* 125(2): 71-79.

Hamilton, D.G. and Ebersole, B.A. (2001). Establishing uniform longshore currents in a large-scale sediment transport facility. *Coastal Engineering,* 42: 199-218.

Herbers, T.H.C., Elgar, S., Guza, R.T. and O'Reilly, W.C. (2006). Surface gravity waves and nearshore circulation. *DUCK94 Experiment Data Server: SPUV Pressure Sensor Wave Height Data,* Available online at: http://dksrv.usace.army.mi/jg/dk94dir.

Hurue, M. (1990). *Two-Dimensional Distribution of Undertow due to Irregular Waves,* B.Eng. Thesis. Dept. of Civil Eng., Yokohama National University, Japan (in Japanese).

Johnson, H.K. (2006). Wave modelling in the vicinity of submerged breakwaters. *Coastal Engineering,* 53: 39-48.

Kraus, N.C., Gingerich, K.J. and Rosati, J.D. (1989). *DUCK85 Surf Zone Sand Transport Experiment,* Technical Report CERC-89-5. US Army Corps of Engineers, Waterways Experiment Station.

Kraus, N.C. and Smith, J.M. (1994). *SUPERTANK Laboratory Data Collection Project,* Technical Report CERC-94-3. US Army Corps of Engineers, Waterways Experiment Station, Vol. 1-2.

Miche, R. (1951). Le pouvoir reflechissant des ouvrages maritime exposes a l'action de la houle. *Annales Ponts et Chaussees,* 121 Annee, pp. 285-319.

Nairn, R.B. (1990). *Prediction of Cross-Shore Sediment Transport and Beach Profile Evolution,* Ph.D. thesis, Dept. of Civil Eng., Imperial College, London.

Oliveira, F.S.B.F. (2007). Numerical modeling of deformation of multi-directional random wave over a varying topography. *Ocean Engineering,* 34: 337-342.

Rattanapitikon, W., Karunchintadit, R. and Shibayama, T. (2003). Irregular wave height transformation using representative wave approach. *Coastal Engineering Journal, JSCE,* 45: 489-510.

Roelvink, J.A. and Reniers A.J.H.M. (1995). *LIP 11D Delta Flume Experiments: A Data Set for Profile Model Validation,* Report No. H 2130. Delft Hydraulics.

Ruessink, B.G., Walstra, D.J.R. and Southgate, H.N. (2003). Calibration and verification of a parametric wave model on barred beaches. *Coastal Engineering,* 48: 139-149.

Smith, J.M. and Kraus, N.C. (1990). *Laboratory Study on Macro-Features of Wave Breaking Over Bars and Artificial Reefs,* Technical Report CERC-90-12. US Army Corps of Engineers, Waterways Experiment Station.

Southgate, H.N. and Nairn, R.B. (1993). Deterministic profile modelling of nearshore processes. Part 1. Waves and currents, *Coastal Engineering,* 19: 27-56.

Sultan, N. (1995). *Irregular Wave Kinematics in the Surf Zone,* Ph.D. Dissertation. Texas A&M University, College Station, Texas, USA.

Thornton, E.B. and Guza, R.T. (1983). Transformation of wave height distribution. *J. Geophysical Research*, 88(C10): 5925-5938.

Thornton, E.B. and Guza, R.T. (1986). Surf zone longshore currents and random waves: field data and model. *J. of Physical Oceanography,* 16: 1165-1178.

Ting, F.C.K. (2001). Laboratory study of wave and turbulence velocity in broad-banded irregular wave surf zone. *Coastal Engineering,* 43: 183-208.